

Generation of Microbial Oil via a Process Engineering Approach

New generation of up- /downstream processing and a feedstock

MAHMOUD MASRI

Vollständiger Abdruck der vor der Fakultät für Chemie der Technischen Universität München
zur Erlangung des akademischen Grades eines

Doktors der Naturwissenschaften (Dr. rer. nat.)
genehmigten Dissertation

Vorsitzender: Prof. Dr. Andreas Jentys
Prüfer: 1. Prof. Dr. Thomas Brück
2. Prof. Dr. Volker Sieber
3. Prof. Dr. Rainer Buchholz

Die Dissertation wurde am 23.07.2019 bei der Technischen Universität München eingereicht und durch die Fakultät für Chemie am 29.11.2019 angenommen.

This work was performed from April 2013 to December 2016 under the supervision of Prof. Dr. T. Brück at the institute of Werner Siemens-Chair of Synthetic Biotechnology (WSSB), Department of Chemistry, Technical University of Munich.

First Reviewer *Prof. Dr. Thomas Brück*
Werner Siemens-Chair of Synthetic Biotechnology (WSSB)
Faculty in Chemistry
Technical University of Munich

Second Reviewer *Prof. Dr. Volker Sieber*
Chair of Chemistry Biogenic Raw Materials
Faculty in Chemistry
Technical University of Munich

Third Reviewer *Prof. Dr. Rainer Buchholz*
Institute of Bioprocess Engineering
Faculty in Engineering
Friederich Alexander University of Erlangen Nürnberg

Date of defense *09.12.2019*

Table of Contents

<i>Table of Contents</i>	V
<i>Declaration</i>	VII
<i>Acknowledgments</i>	IX
<i>Abstract</i>	XI
<i>List of publications (as a first-author)</i>	XV
<i>List of publications (as a co-author)</i>	XIX
<i>List of patents:</i>	XXI
PART I: SCIENTIFIC BACKGROUND	0
1 Introduction	2
2 <i>Oleaginous yeast</i>	3
2.1 <i>Terrestrial biomass as Yeast feedstock</i>	3
2.2 <i>Marine biomass as yeast feedstock</i>	4
2.3 <i>Waste biomass as feedstock</i>	5
2.1 <i>Volatile fatty acids (VFAs) as feedstock</i>	6
3 Triacylglycerol biosynthetic and lipid droplet biogenesis	7
3.1 From Sugar and acetate to a giant lipid droplet	8
3.2 Factors that influence LD size	16
4 Challenges in lipid production from oleaginosus yeast	19
4.1 Techno-economic analysis (TEA) and MO cost:	19
4.2 Technical challenges:	20
4.3 Life cycle assessment (LCA) and environmental challenges:	21
5 Work objectives	24
6 Discussion	25
7 Methods	31
7.1 Strains and precultures	31
7.2 Media	31
7.3 Bioreactors	31
7.4 Analysis and assays	32
7.5 Techno-economic analysis	33
7.6 Life-cycle for global warming potential (GWP)	34
8 References	35
PART II: PUBLICATIONS OVERVIEW	0
PART III: PUBLICATIONS FULL TEXT	0

Declaration

I hereby declare that the current dissertation has been independently written by me. All the presented results, explanations and thoughts have not been taken from any other writings analogously or literally. The sources and aids have been indicated and cited. The present work has not yet been submitted or otherwise published to another examination authority in the same or similar form.

Mahmoud Masri

Garching, dem 09.12.2019

Acknowledgments

To the First, the Last, the All-knowing, the Evident, and the Eternal Owner of Sovereignty, thank you with my full submission. It is all from your guiding, supporting, helping, and blessing. *Praise be to Allah.*

Firstly, I would like to express my sincere gratitude to my advisor **Prof. Dr. Thomas Brück** for the continuous support of my Ph.D. study and related research, for his patience, motivation, and immense knowledge. His guidance helped me in all the time of research and writing this thesis. Prof. Dr. Brück coaching was not limited to scientific aspects but it expanded to many aspects of life, planning, and leadership. I could not have imagined having a better advisor and mentor for my Ph.D. study. Thank you a lot **Prof. Dr. Thomas Brück**.

Besides my advisor, I would like to thank the rest of my thesis committee: **Prof. Dr. Andreas Jentys, Prof. Dr. Volker Sieber, and Prof. Dr. Rainer Buchholz**, not only for their insightful comments and encouragement, but also for the questions which incited me to widen my research from various perspectives.

My sincere thanks also go to **Dr. Norbert Mehlmer, Dr. Farah Qoura, Dr. Daniel Garbe, and Dr. Monika Fuchs**, who provided me the opportunity to join their team as intern. Without their precious support it would not be possible to conduct this research.

I thank my fellow lab-mates: **Samer, Pariya, Dirk, Wojciech, Johannes, Jan, Elias, Tobias, Markus, Max, Matthias, Katarina, Felix B., Wolfgang, Steven, Christian, Patrick, Dania, Nikolaus, Zora, Marion, Kevin, Nathanael, Felix M., Sophia, Michael, and Timm** for the stimulating discussions, for the sleepless nights we were working together before deadlines, and for all the fun we have had in the last years. With a special mention to **Gülnoz, Martina, Veronika, Petra, Dominik, Barbara and Tom** the pilot supporting team. It was fantastic to have the opportunity to work with all of you. What a cracking place to work! Also, I thank my friends **Abdulsalam, Ahmed, Boutheina, Martina, Eszter and Asma** for working together.

My deepest thanks to my family; my parents, my brother and sisters **Shaza, Qutaiba, and Ruba** for supporting me spiritually throughout writing this thesis and my life in general. I am proud that I am part of this family. Thanks for all your encouragement!

And finally, last but by no means least, because they are the first, they are a part of me, they are the target behind, they are the sense of all. To my beloved small family **Salam, Leen and Tala**, thank you for all support.

To the very special persons in my life:

To **my wife Salam**, to who endures difficulties with me, to who shared my concerns, sorrows as well as my joys and my happiness. Many Thanks.

To **my life-coach**, to the one who opens all the doors, and breaks the odds and hardships in my life, to my **Mom**, I owe it all to you. Many Thanks

To **my father**, I fully understand that you can't read my words. But I well know that you were looking forward to this moment and you would be fully proud of my achievements. I miss you every single day, I see you in my dreams. I ask Allah Almighty to have mercy on you.

Sincerely yours
Mahmoud Masri

Abstract

Contemporary societies heavily rely on fossil fuels as their major energy source. Renewable energy sources, such as biofuel, are desired to displace fossil fuels owing to concerns about climate change. In this respect, alternative bio-based technologies aim to supply fuels in a cost-effective and sustainable manner while contributing to the reduction of greenhouse gases. The current generation of biofuel is completely dependent upon edible crop oil, which is derived from sources such as palm oil, resulting in serious complications to universal food-chain and biodiversity. Lipids from oleaginous microorganisms have great potential for displacing crop-derived oils as biofuel substrates, but many restrictions prevent their economical and industrial application.

The current project primarily addressed the key technical and environmental constraints concerning single cell lipid production from oleaginous yeasts related to sustainable feedstock, time-effective biomass and lipid yield, low-energy-demand for downstream processing as well as solvent-free processing as well as fermentative CO₂ emission. Additional points contributing to this thesis are from collaborations with different partners.

With respect to sustainable feedstock, we attempted to utilize monosaccharides from marine macrophytes (Seagrass and Macroalgae) as feedstock for MO production. Among the studied samples, *P. oceanica* from the Mediterranean Sea and *L. digitata* from the western coast of Ireland displayed the best lipid productivity, exceeding the well-documented minimal nitrogen media.

Additionally, the non-lipid yeast biomass (the yeast cell-wall) was applied, for the first time, as a unique sugar source. The enzymatically produced yeast hydrolysate provided a sugar/nutrition rich medium for yeast fermentation, resulting in increasing biomass and lipid productivities.

Acetic acid, as a sustainable yeast feedstock, was evaluated whether solo or in conjunction with sugar. The monoauxic co-fermentation system enabled the simultaneous assimilation of sugar and acetic acid in rich-based medium. Via this co-fermentation, *C. oleaginosus* had a significantly high cell density (245 g L⁻¹), lipid content (87% w^dw_{biomass}) and lipid productivity (2.4 g L⁻¹ h⁻¹). This co-fermentation freed TG biosynthesis from nitrogen-scarce needs, which subsequently avoided the classical diauxic fermentation and paved the way to the flash (short, approximately 45 h) or continuous fermentation mode.

Microalgae, as another lipid producer, might be the optimal platform to assimilate CO₂ from yeast fermentation. In this respect, the fatty acid profile and productivity were evaluated in

wild-type and ultraviolet-C mutants of *Isochrysis sp.*, *Nannochloropsis maritima* and *Tetraselmis sp.*

Relocation of CO₂ from heterotrophic yeast to autotrophic algae was discussed in a common work with our partner at the University of Jordan. In this collaboration, chemisorption based on chitosan oligosaccharide/DMSO was used to capture CO₂. For our part, the biodegradation test justified the green sorbent consideration.

Development of downstream processing and lipid recovery was a major part of the current work. In the framework of the LIPOMAR project, a single *in-situ* enzymatic treatment process was established to achieve holistic cell lysis and lipid recovery/purification without the need for pretreatment or subsequent application of an organic solvent.

In more details, the established enzymatic downstream processing comprises a two-step enzymatic treatment. While the initial step imposes a holistic cell-wall lysis performed by a mixture of hydrolases, the second treatment requires cell emulsion systems, such proteins. The activity of mixtures of commercial hydrolases were tested in the first generation. Subsequently, an in-house yeast-selective hydrolase system was produced using the yeast cell itself induced by the filamentous fungus *T. reesei*. A commercial protease treatment, alone or in combination with the addition of DISSOLVAN® (Clariant), was successfully applied for the demulsification step.

An alkaline extracellular protease from *Yarrowia lipolytica* was isolated and characterized. This cured protease shows promising stability and activities that may allow it to be used downstream for lipid recovery in future work.

To evaluate the economic and ecological advantages of the designed MO process, a techno-economic analysis estimated a cost of \$0.95-1.6 per kg lipid according to the current process design due to the baseline productivity of 1.4 g L⁻¹ h⁻¹. Furthermore, life cycle assessment analysis assumed an emission of 3.56 kg CO₂ equivalents for every 1 kg of yeast oil produced.

List of publications (as a first-author)

The current thesis is based on the publications and patents listed below.

- I. A seagrass based biorefinery for generation of single cell oils targeted at biofuel and oleochemical production. **Masri M. A.**, Younis S., Mehlmer N., Quora F., Brück T., Energy Technol. 2018, 6, 1026–1038. **Status: Accepted**
<https://doi.org/10.1002/ente.201700919>

MM analyzed and enzymatically hydrolyzed the seagrass biomass. MM cultivated yeast on the hydrolysate. MM contributed to manuscript writing

- II. A waste free, microbial oil centered cyclic bio-refinery approach based on flexible macroalgae biomass, **M. A. Masri**, W. Jurkowski, P. Shaigani, M. Haack, N. Mehlmer and T. Brück, Applied Energy 224 (2018) 1–12 **Status: Accepted**
<https://doi.org/10.1016/j.apenergy.2018.04.089>

MM analyzed and enzymatically hydrolyzed the algal biomass. MM cultivated yeast on the hydrolysate and established the FACS based lipid assay. MM contributed to manuscript writing

- III. A sustainable, high-performance process for the economic production of waste-free microbial oils that can replace plant-based equivalents, **Masri M.A.**, Garbe D, Mehlmer N., Brück T., 2019, 12, 2717, Energy & Environmental Science, 2019 **Status: Accepted**
<https://doi.org/10.1039/C9EE00210C>

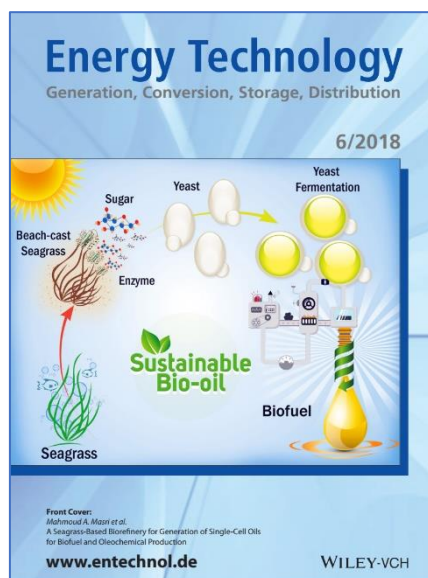
MM was responsible for the entire work.

- IV. Single Step Extraction and Purification of Renewable Triglycerides from Oleaginous Yeast *Cutaneotrichosporon oleaginous*. Using A Completely Solvent Free Enzymatic Cell Lysis, **Masri M. A.**, Schmidt Y., Mehlmer N., Brück T., 2019. **Status: In preparation**

MM was responsible for the entire work.

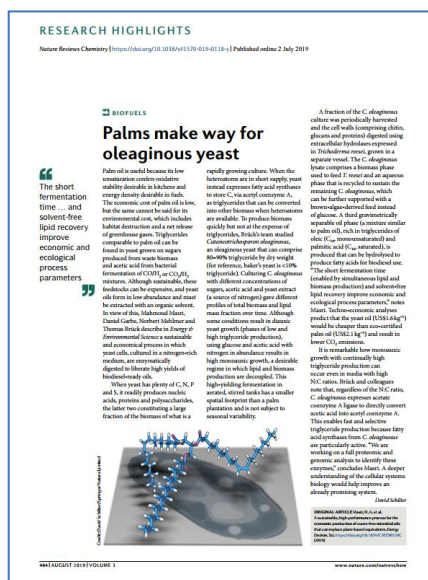
Featured work:

Front cover page: in Energy Technol,
2018,6,1026–1038



Back cover page: in Energy & Environmental
Science, EES, 2019, 12, 2717

Highlights: Nat. Rev. Chem., 3, 464, 2019



List of publications (as a co-author)

- V. Chemisorption of CO₂ by chitosan oligosaccharide/DMSO: organic carbamate–carbonate bond formation; Abdussalam K. Qaroush, Khaleel I. Assaf, Sanaa K. Bardaweel, Ala'a Al-Khateeb, Fatima Alsoubani, Esraa Al-Ramahi, **Mahmoud A. Masri**, Thomas Brück, Carsten Troll, Bernhard Rieger and Ala'a F. Eftaiha, *Green Chem.*, 2017, 19, 4305. **Status: Accepted**
<https://doi.org/10.1039/C7GC01830D>

MM performed the biodegradation test. MM contributed to the manuscript writing.

- VI. Catalytic decomposition of the oleaginous yeast *Cutaneotrichosporon oleaginosus* and subsequent biocatalytic conversion of liberated free fatty acids, Martina K. Braun, Jan Lorenzen, **Mahmoud A. Masri**, Yue Liu, Eszter Baráth, Thomas Brück, Johannes A. Lercher, *ACS Sustainable Chemistry & Engineering*. **Status: Accepted**
<https://doi.org/10.1021/acssuschemeng.8b04795>

MM analyzed the yeast biomass, produced the ethanol and TEA and contributed to the manuscript writing.

- VII. Strain selection of microalgae isolated from Tunisian coast: characterization of the lipid profile for potential biodiesel production, Asma Gnouma, Emna Sehli, Walid Medhioub, Rym Ben Dhieb, **Mahmoud A. Masri**, Norbert Mehlmer, Wissem Slimani, Khaled Sebai, Amel Zouari, Thomas Brück, Amel Medhioub, *Bioprocess and Biosystems Engineering* 41:1449–1459 (2018). **Status: Accepted**
<https://doi.org/10.1007/s00449-018-1973-5>

MM analyzed the algal biomass and lipid and contributed to the manuscript writing.

- VIII. Isolation and Screening for Protease Activity by Marine Microorganisms; Bessadok, Boutheina; **Masri A., Mahmoud**; Brück, Thomas; Sadok, Saloua; *Bull. Inst. Natn. Scien. Tech. Mer de Salammbô*, Vol. 42, (2015). **Status: Accepted**

M performed the protein extraction, DNA extraction, SDS-gel, strain identification.

- IX. Characterization of the Crude Alkaline Extracellular Protease of *Yarrowia lipolytica* YITun15, Bessadok, Boutheina; **Masri A., Mahmoud**; Brück, Thomas; Sadok, Saloua. *Journal of FisheriesSciences.com*, 11(4): 019-024 (2017). **Status: Accepted**
<https://doi.org/10.21767/1307-234X.1000137>

MM designed the assay methods and characterization experiments.

List of patents:

- X. Extraction of Renewable Triglycerides from Oleaginous Microorganisms, **Mahmoud A. Masri**, Thomas Brück. Patent No.: EP 3 536 800 A1 (2019). **Status: Published**

- XI. A method for producing microbial lipids, **Mahmoud A. Masri**, Thomas Brück. Application Patent No.: EP19157805.3 (2019). **Status: Submitted**

PART I: SCIENTIFIC BACKGROUND

Introduction

Oleaginous yeast

*Triacylglycerol biosynthetic and lipid
droplet biogenesis*

*Challenges in lipid production from
oleaginous yeast*

Work objectives

Methods

Discussion



1 Introduction

Driven by massive demands for energy, human impacts on the environment are exposing the ecosystems of Earth to increasing risk.¹⁻³ The need for low-carbon energy sources as alternatives to fossil fuel is realized by originating several generations of biofuel.^{4,5} In fact, desired carbon savings from biofuel usage is influenced by the way they are produced. First biofuels generation availing edible-crops, such as corn, sugarcane, soybeans, and palm, were associated with land-use change and habitat fragmentation, which subsequently threatened several mammal, bird, plant and other species.⁶⁻⁸ Over the last 50 years, accumulating land clearing and increasing population density have resulted in almost two-thirds of mammals that weigh 10 kg or more being threatened with extinction.⁸

Converting rainforests, peatlands, savannas, or grasslands to food crop-based biofuels is releasing massive amounts of CO₂ into the atmosphere, far exceeding those released by the fossil fuels they were created to displace. In contrast, biofuels made from waste biomass, biomass grown on degraded and abandoned agricultural lands or non-terrestrial biomass grown from direct fixation of CO₂ provide immediate and sustained greenhouse gas (GHG) advantages.

As alternative lipid producers, oleaginous microorganisms display great potential for displacing crop-derived oils due to their increased aerial and space-time productivity.⁹ Oleaginous yeast, in more specifically *Cutaneotrichosporon oleaginosus* (ATCC 20509), surpass other microbial producers due their unique biochemical characteristics of rapid growth to high cell density, harnessing a wide spectra of feedstocks and coping with a variety of cytotoxic compounds.^{10,11}

At present, microbial oil (MO) has failed to be established at industrial manufacturing, as it was below the set sustainability goals of economic and social development, as well as environmental protection.¹²

2 Oleaginous yeast

Oleaginous yeasts are characterized by their significant ability to accumulate fatty acids in the form of triglycerides,¹³ as well as their capacity to convert a broad variety of biomass feedstocks of varying quality and composition into biomass and lipids.

With respect to single cell oil (SCO) production, oleaginous yeasts have numerous advantages over other microbial producers. Yeast fermentation is less affected by climate compared to phototrophic microalgae. Yeast fermentation is even more tolerant to diverse complex sugar matrixes and it can use other simple compounds as carbon sources compared to heterotrophic microalgae cultivation.² Tolerance to metal ions and relatively low oxygen demand are yeast advantages over oleaginous fungi. Moreover, yeast's relatively large cell size simplifies harvesting and handling compared to bacteria.^{14, 15}

Of the nearly 600 known yeast species, approximately 30 are considered oleaginous species. These belong to the following genera: *Yarrowia*, *Candida*, *Cryptococcus*, *Rhodotorula*, *Rhodospiridium*, *Rhizopus*, *Trichosporon* and *Lipomyces*. Oleaginous species such as *Y. lipolytica*, *L. starkeyi*, *R. toruloides* and *C. oleagnosus* are among the most studied oleaginous yeast.^{16, 17}

In general, oleaginous yeasts have superior metabolic flexibility compared to classical yeast, such as *S. cerevisiae*. Amongst oleaginous yeasts, *C. oleagnosus* and *R. toruloides* demonstrate extensive metabolic flexibility compared to the model yeasts *Y. lipolytica* and *L. starkeyi*. In particular, *C. oleagnosus* demonstrates the most extensive capability of metabolizing diverse carbon source classes.^{10, 18}

Many feedstocks classes have been evaluated within the aim of seeking out for a sustainable carbon source. Glucose from varied matrixes is the most studied feedstock for oleaginous yeasts. Xylose, the second constituent sugar of hemicellulosic biomass, has received the most attention as an alternative carbon source.^{10, 18} Application of glycerol as a carbon source has many advantages over sugars, including lower cost (as a crude byproduct from biodiesel), better availability, a greater degree of reduction, reduced CO₂ emission during fermentation and less direct competition with food and feed production.¹⁹ Waste-fats or hydrophobic materials have been tested as a carbon source for oleaginous yeast as well.²⁰ Besides, volatile fatty acids (VFAs), such as acetic acid, propionic acid and n-butyric acid, are yet another class of potential feedstocks. Bioconversion of VFAs via oleaginous yeast to SCO can be considered a viable prospect for sustainable waste management.²¹⁻²⁴

2.1 Terrestrial biomass as Yeast feedstock

Terrestrial cellulolytic and hemicellulolytic based biomass hydrolysates may represent an economical way to provide a high concentration of sugars. Hydrolysis of microcrystalline cellulose,

which is the main component in such biomasses, requires harsh chemical pretreatment, resulting in inhibitory byproduct formation (acetic acid, furfural, and 5-hydroxymethylfurfural). *R. toruloides* and *C. oleaginosus* are capable of metabolizing hydrolysate feedstocks of various biomass sources without the need for dilution or detoxification.²⁵ In contrast, *L. starkeyi* growth was affected by these byproducts even in diluted feedstock.²⁶

High xylose content is another challenge for hemicellulolytic based biomass hydrolysates. *C. oleaginosus* metabolizes xylose without any catabolite repression or genetic modification at similar rates to glucose.^{10, 18} In contrast, *Y. lipolytica* exhibits cryptic xylose metabolism, resulting in low-rate utilization of xylose as a sole carbon source.¹¹ Interestingly, *Y. lipolytica* was able to use xylose in ammonia fiber expansion pretreated corn stover hydrolysates but not as a sole carbon source.²⁷

As third challenge, lignin is an underutilized component because of its heterogeneous structure and the toxicity of its depolymerized products. In fact, lignocellulosic biomasses, which comprise agricultural byproducts, municipal solid wastes, low input energy crops and forest residue, are the most abundant renewable organic resource, occupying half of total global biomass.²⁸

One recent publication demonstrated that *C. oleaginosus* cells showed high tolerance to high concentrations of mono-aromatic compounds (15 different compounds). Specifically, lipid accumulation reached up to 69.5% (w/w) when grown on lignin-derived aromatics.¹⁰ *C. oleaginosus* showed a unique tolerance to toxic byproducts generated during thermo-catalytic pretreatment of lignocellulose, such as acetic acid, HMF, and furfural, at concentrations that are lethal for other organisms. Interestingly, *C. oleaginosus* has the metabolic capacity to both tolerate and convert these common fermentation inhibitors into biomass.²⁹

2.2 Marine biomass as yeast feedstock

Macrophyte marine biomass (MB) comprises primarily macroalgae and seagrass and accounts up to 71% (w/w) of all biologically stored carbon.^{30, 31} MB converts solar energy into chemical energy with higher photosynthetic efficiency comparing to terrestrial biomass.³²⁻³⁵ For example, macroalgae species such as *Ulva sp.*, *Fucus sp.*, and *Laminaria sp.* can fix a 48.7, 561 and 124 $\mu\text{mol CO}_2/\text{h}$ for each 1 g dry weight biomass.³⁶ Moreover, seagrass meadows are among the ecosystems with the highest productivity on earth. Seagrass stores 27.4 million tons per year of organic carbon (C_{org}).³⁴

In fact, both high photosynthetic efficiency and aerial productivity enable the MB to generate and store sufficient carbon to comply with feedstock demands of any biorefinery concept. Additionally, MB has less risk to compete with food and energy generation compared to terrestrial energy crops, like

corn and wheat. For instance, markets for seaweed based foodstuffs are limited to East Asia, where macroalgae are used for food, hydrocolloids, fertilizer, and animal feed.³⁷

Due to unfavorable C/N/P ratio of 474:24:1, seagrass biomass shows a relatively low natural biodegradation rate (about 19%) with regard to its leafy biomass being degraded by herbivores and heterotrophs.³⁸ Therefore, detached seagrass-leaf material seasonally accumulates as banquettes on beaches and shorelines. Utilization of such biomass for biotechnology processes offers a great socioeconomic opportunity.

Taxonomically, macroalgae and seagrass are multicellular photosynthetic organisms. Seagrass belongs to higher flowering plants. These occupy four plant families; Posidoniaceae, Zosteraceae, Hydrocharitaceae, and Cymodoceaceae. By contrast, macroalgae belong to the lower plants, consisting of a leaf-like thallus instead of roots, stems, and leaves. Macroalgae are classified into; green (phylum Chlorophyta), red (Rhodophyceae), gold (Chrysophyceae) and brown algae (Phaeophyceae), according to the thallus color derived from natural pigments and chlorophylls.

In general, green algae biomass contains mannan, ulvan, starch and cellulose as polysaccharides which results in monomers of glucose, mannose, rhamnose, xylose, uronic acid, and glucuronic acid. In return, brown algae cell wall contains laminarin, mannitol, fucoidan, cellulose, and network of alginate which can be hydrolyzed to glucose, galactose, fucose, xylose, uronic acid, mannuronic acid, guluronic acid, and glucuronic acid. Red algae biomass consists of carrageenan, agar, cellulose and lignin, which correspond to glucose, galactose and agarose. Cellulose is the main polymeric sugar in seagrass, therefore, glucose is the major monomeric sugar of seagrass hydrolysates.³⁹ High sugar content (mainly glucose) is an additional reason to consider the seagrass and macroalgae as attractive, alternative feedstock for biotechnological platforms.

To that end, biomass hydrolysate of the marine microalgae *Scenedesmus sp.*⁴⁰, macroalgae and beach-cast seagrass⁴¹ have been demonstrated to be suitable fermentation substrates for yeast-based lipid production. *C. oleaginosus* was able to utilize microalgae hydrolysate (*Scenedesmus sp.*) cells, accumulating good biomass at the same lipid content.⁴⁰ Brown algae hydrolysate is a preferable carbon source over green algae hydrolysate for *C. oleaginosus*.⁴² Seven beach-cast seagrass hydrolysates were tested to produce SCO.⁴¹ In this work, *Pasadena Ocean* was shown to be superior.

2.3 Waste biomass as feedstock

Industrial byproducts could provide a carbon source for oleaginous yeasts. The biodiesel industry generates crude glycerol (80% glycerol, 10% water, 7% ash and 3% methanol) as a byproduct.^{43, 44} Methanol contamination severely inhibits microbial growth. Crude glycerol as feedstock for yeasts has been thoroughly evaluated in genera including *Candida*, *Yarrowia*, *Rhodospiridium*, *Rhodotorula*,

Cryptococcus, *Trichosporonoides*, *Lipomyces* and *Schizosaccharomyces*.⁴⁵⁻⁴⁷ *R. toruloides* showed good performance with high lipid yield and content, up to 26.7 g L⁻¹ and 70% (w/w), which was observed with the strain AS2.1389, a 5-L fermenter.⁴⁸ *C. oleaginosus* achieved the highest biomass, lipid production and lipid content on diluted crude glycerol fermentation medium to 1.4% methanol (w/v).⁴³

. Waste oil from vegetable frying was successfully applied as feedstock for *Y. lipolytica*, where a lipid content of 57.89% (w/w) was obtained.²⁰ It is noteworthy that lipid accumulation in this experiment was dependent on nitrogen content, contained in the waste oil fraction (e.g., nitrogen seeping from meat, chicken and fish into the frying oil).²⁰ In that regard, increasing nitrogen concentrations lead to lower lipids yields, as nitrogen limitation is an initiator of lipogenesis.

2.1 Volatile fatty acids (VFAs) as feedstock

VFAs, commonly, refers to acetic acid (AA), propionic acid (PA), n-butyric acid (BA), isobutyric acid (iBA), n-valeric acid (VA), and isovaleric acid (iVA). VFAs can be generated from ecologically sound starting materials, such as CO, waste gases, and CO₂/H₂,⁴⁹⁻⁵¹ using biotechnological processes (i.e., fermentation of *Clostridium acetivum* and *Acetobacterium woodii*).^{49, 50, 52, 53} Sludge, food wastes, and a variety of biodegradable organic wastes are considered as feedstock platform for VFAs production via anaerobic fermentation. It worthy to mention that acetic acid has relativity low market price,⁵² which favors economically sound production routes. Accordingly, VFAs are a promising feedstock platform for MO production with many ecological and economic advantages.

The feasibility of valorization of VFAs on some yeast strains, such as *Y. lipolytica*, *R. toruloides*, *C. oleaginosus* and *C. albidus*, has been investigated.²¹⁻²⁴ Recently, some reports have demonstrated that acetic acid can serve as the sole feedstock for *C. oleaginosus* cultivation.^{21, 23, 54-57} VFAs from rice straw hydrolysates lead to lipid content of 28% (w/w).⁵⁸ In this experiment, odd-chain fatty acids (C15, C17) was detected which was attributed to the presence of propionic acid.⁵⁸ These findings were consistent with detecting the formation of C_{15:0}, C_{17:0} and C_{17:1}, when propionic acid is used within the feed.⁵⁹ VFAs from anaerobic fermentation of brown algae have been used by the oleaginous yeast *C. oleaginosus* to produce lipids in a repeated batch system, resulting in a high lipid content of 61% (w/w).²³

Recently, some reports have demonstrated that acetic acid can serve as the sole feedstock for *Cutaneotrichosporon oleaginosus* cultivation.^{21, 23, 54-57} However, although application of acetic acid as the sole carbon source results in considerably high intracellular lipid content (60–73%, w_{lipid}/^dw_{biomass}), biomass productivity is inhibited, leading to poor overall oil yields.^{23, 54, 56} Moreover, multistep,²¹ continuous,⁵⁴ and pH-stat^{55, 56} fermentation have been tested to identify the best method for implementation of acetic acid as the sole carbon source feedstock. The pH-stat approach shows

promising lipid productivity.⁵⁵ However, constant feeding of costly yeast extract, peptone, vitamins, and other nutrients in all pH-stat trials prohibits the economic development of this process. Thus, further studies are needed to achieve optimal integration of acetic acid in the microbial oil production process.

In fact, to build a fermentation system with high lipid productivity it is essential to understand lipid formation inside yeast and to understand the current challenges that SCO production is facing.

3 Triacylglycerol biosynthetic and lipid droplet biogenesis

Cytoplasmic lipid droplets (LDs) are ubiquitous, dynamic cellular organelles serving as crucial reservoirs of energetic triacylglycerols (TGs). LDs are a central metabolic hub participating in various cellular activities, such as protein and lipid trafficking, protein degradation and cell signaling⁶⁰, LDs also supply lipids for membrane synthesis.^{61, 62} LD formation is a subsequent step to TG sequestering between the two leaflets of the endoplasmic reticulum (ER) membrane.⁶³ Therefore, understanding the proportional relationship between TG biosynthesis and LD biogenesis is essential to maximize the lipid productivity.

LDs consist of highly hydrophobic cores surrounded by a monolayer phospholipid shield. Diverse TGs, their precursor intermediates and degradation products occupy the LDs hydrophobic core. Depending on the cell type, the LD core might contain sterol esters (SEs) beside TGs, and the TG/SE ratio fluctuates among cells.⁶⁴ TGs and SEs could be colocalized within one LD or dominant in separated LDs. In colocalized LDs, TGs and SEs can be segregated in random ways or structured in concentric layers: inner dominant TG cores (Di: 350 nm) are surrounded by a concentric SE layers (Thickness: 3.7 nm) encircled by a phospholipid monolayer and end up with LD diameters of 400 nm.⁶⁵ Additionally, LD cores can also contain precursors of more complex molecules, such as sphingolipids, signaling molecules (e.g., eicosanoids), and lipophilic hormones (retinoic acid, retinyl esters and steroids) or even a wax ester.^{66, 67} Membranes, RNA, RNA-binding proteins, and ribosomal subunits beside proteins, such as eicosanoid-producing enzymes, have been previously detected in the hydrophobic core of LDs.^{68, 69}

The outer phospholipid monolayer shield seems similar across different cell types.^{66, 70} However, yeast LDs in general are primarily composed of phosphatidylcholine (PC), phosphatidylinositol (PI) and phosphatidylethanolamine (PE) with very small percentages of phosphatidylserine (PS) and phosphatidic acid (PA).⁷¹⁻⁷⁴ Bound proteins, comprising TG synthesis, N-linked glycosylation, lipolysis,

lipolytic regulators, phospholipids (PLs) metabolism, ER-associated protein organization and degradation, are localized to LD surfaces.^{75, 76}

Cells dynamically regulate LD size, number, and distribution in response to physiological cues. Therefore, LD sizes might range from very small (less than 4 nm), such as exists in wide type *Saccharomyces cerevisiae*⁶², to rich supersized LDs (approximately 1 μm) in some *S. cerevisiae* mutants,⁷⁷⁻⁷⁹ even exceeding 100 μm as giant and unilocular LD occupying the entire cytoplasm of an oleaginous yeast cell under stressed conditions (**Figure 1**).⁸⁰

LD density is inversely correlated with size, ranging from less than 0.95 g mL^{-1} , in cases of large LDs, to greater than 1.063 g mL^{-1} for small LDs, which is larger than microsomes.^{63, 81} Therefore, by density-based separation methods, only LDs larger than 1 μm will be in the top-floating LD fraction. Accordingly, smaller LDs will remain in denser fractions.⁸² Given that many factors can enhance LD size, observation has shown that such factors subsequently enhance TG production.⁷⁸ In that respect, it is critical to understand the molecular mechanisms underlying LD growth to large LDs sizes, especially where oleaginous yeasts are concerned, taking into consideration oleaginous yeast's central role as lipid sources for food, pharmaceutical and biofuel industries.

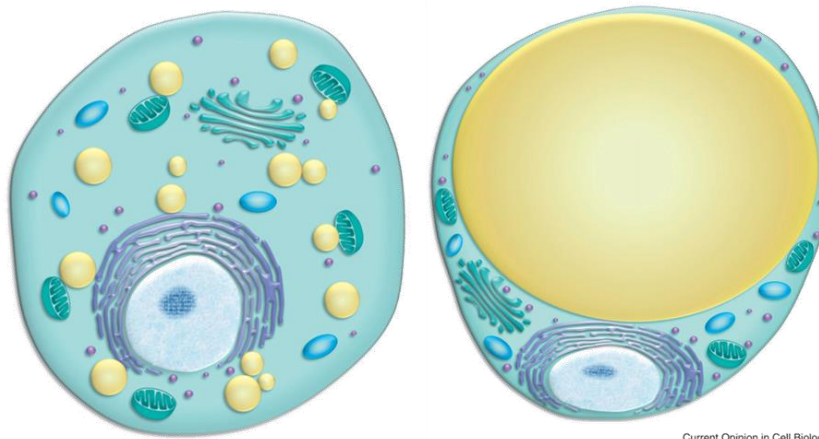


Figure 1: Lipid droplet sizes (Source: Modified from Current "Opinion in Cell Biology 2012, 24:509–516").⁸³

3.1 From Sugar and acetate to a giant lipid droplet

Acetic acid utilization as a carbon source first requires passing through the cell membrane. Carboxylate transporter proteins mediate transport of acetate ions, while direct diffusion is thought to be the mechanism for transport of the undissociated form of acetic acid at low pH.⁸⁴ Monocarboxylate transporters, such as Jen1p or Ady2p, transport acetate anions into the cytoplasm.⁸⁵ The aquaglyceroporin channel (Fps 1) facilitates the direct diffusion of undissociated form of acetic acid. Acetic acid is subsequently converted into acetyl-CoA via acetyl-CoA synthetase (ACS) or acetate-CoA

ligase (ACL).⁸⁵ This direct conversion was reported in microalgae and in non-oleaginous microorganisms, such as *Saccharomyces cerevisiae*.⁸⁶ In the case of oleaginous microorganisms, some yeast species, such *Cutaneotrichosporon oleaginosus*, demonstrate the ability to directly utilize acetate as a carbon source, resulting in high lipid content.⁵⁵ Both the monocarboxylate transporter and acetate-CoA ligase have previously been reported in a transcriptomic analysis of *Cutaneotrichosporon oleaginosus*.⁸⁷

Biomass growth inhibition associated with acetic acid usage as a carbon source is widely reported in yeast.^{23, 54, 56} All weak acids cause a growth delay or even cell death, depending on their concentrations as well as on their lipophilic properties.⁸⁸ The less lipophilic acetic acid compromises cell viability and activates acetic acid-programmed cell death (AA-PCD). At lethal concentrations of acetic acid (in *S. cerevisiae* ~80 mM), the first response (15 min) is production of reactive oxygen species (ROS), such as intracellular hydrogen peroxide and superoxide anions. Subsequently, mitochondria induce (60-150 min) cytochrome c (cyt c) release, leading to mitochondrial dysfunction. The increase of caspase-like activity eventually leads to AA-PCD.^{89, 90} Therefore, organic acid concentrations, as well as their lipophilic moiety, should be considered before the application of organic acids as feedstock.

Once acetate is converted into acetyl-CoA, fatty acid synthesis is virtually started. Acetyl-CoA is considered a universal precursor for fatty acid synthesis. In fact, overexpression of ACS in *Saccharomyces cerevisiae*, *Chlamydomonas reinhardtii* and *Schizochytrium sp.* leads to increased lipid accumulation.^{91, 92} Acetyl-CoA carboxylase (ACC) converts acetyl-CoA to malonyl-CoA. This reaction occurs in the cytosol in all general heterotrophs.⁹³ The presence of glucose in the cultivation media deactivates the ACS1 form of acetyl-CoA synthetase, encoded by the *facA*. Subsequently, co-fermentation of acetic acid and glucose in organisms process the ACS1 form of acetyl-CoA synthetase in a diauxic shift.⁹⁴ In contrast, some oleaginous yeasts show the capability to up-take glucose and acetic acid simultaneously.

Overexpression of ACC alone is insufficient to boost lipid biosynthesis. Actually, ACC overexpression needs to occur in combination with overexpression of other essential genes to increase lipid accumulation.⁸⁶ An engineered *Y. lipolytica* doubles lipid content when ACC1 is overexpressed in combination with diacylglycerol acyltransferase (DGA1).⁹⁵ In contrast, solely overexpressing ACC1 in *Y. lipolytica* and *Aspergillus oryzae* resulted in only minor changes in lipid accumulation.^{95, 96}

Fatty acid biosynthesis requires one molecule of Acetyl-CoA with 7-9 molecules of malonyl-CoA to begin 7-8 cycles of multistep chemical reactions that end with 16- and 18-carbon fatty acids.^{97, 98} Fatty acid synthase (FAS), particularly FAS I in yeast, has two subunits, α and β , which each contain six copies of four functional domains.⁹⁹ In total, six copies of eight independent functional domains catalyze the

SCIENTIFIC BACKGROUND

C_{16:0} and C_{18:0} bio synthesis via activation (phosphopantetheinyl transferase [subunit α], PPT), priming (acetyltransferase [subunit β], AT), multiple cycles of elongation (ketoacyl synthase [subunit α], KS→ malonyl transacylase [subunit β], MPT→ ketoacyl reductase [subunit α], KR→ dehydratase [subunit β], DH→ enoyl reductase [subunit β], ENR→ ketoacyl synthase [subunit α], KS...), and termination (malonyl/palmitoyl transacylase[subunit α], MPT). These reactions all occur in a limited space inside the α₆β₆ complex.^{97,98}

These C2-addition serial reactions require 1 ATP and 2 NADPH molecules and release 1 CO₂ molecule for each cycle.⁹⁸ Therefore, NADPH deficiency is considered a restricting factor. Conversion of malate into pyruvate, intermediated by the malic enzyme (ME), is one major common sources of NADPH in oleaginous yeast.¹⁰⁰ Overexpression of NADP⁺-dependent ME in *Rhodotorula glutinis* significantly enhanced lipid accumulation.¹⁰¹ The pentose phosphate pathway (PPP) is another source for NADPH that leads to improved lipid productivity when up-regulated in *Y. lipolytica*.¹⁰²

Overexpression of acyl-carrier protein (ACP) or 3-ketoacyl ACP synthase, together with fatty acyl-ACP thioesterase, in *Haematococcus pluvialis* improved FA synthesis and was significantly correlated with monounsaturated FA (MUFA) synthesis and polyunsaturated FA (PUFA) synthesis.¹⁰³ In *S. cerevisiae*, overexpression of three fatty acid biosynthesis genes, acetyl-CoA carboxylase (ACC1), fatty acid synthase 1 (FAS1) and fatty acid synthase 2 (FAS2), led to accumulated lipids of approximately 17% of the dry cell weight.¹⁰⁴

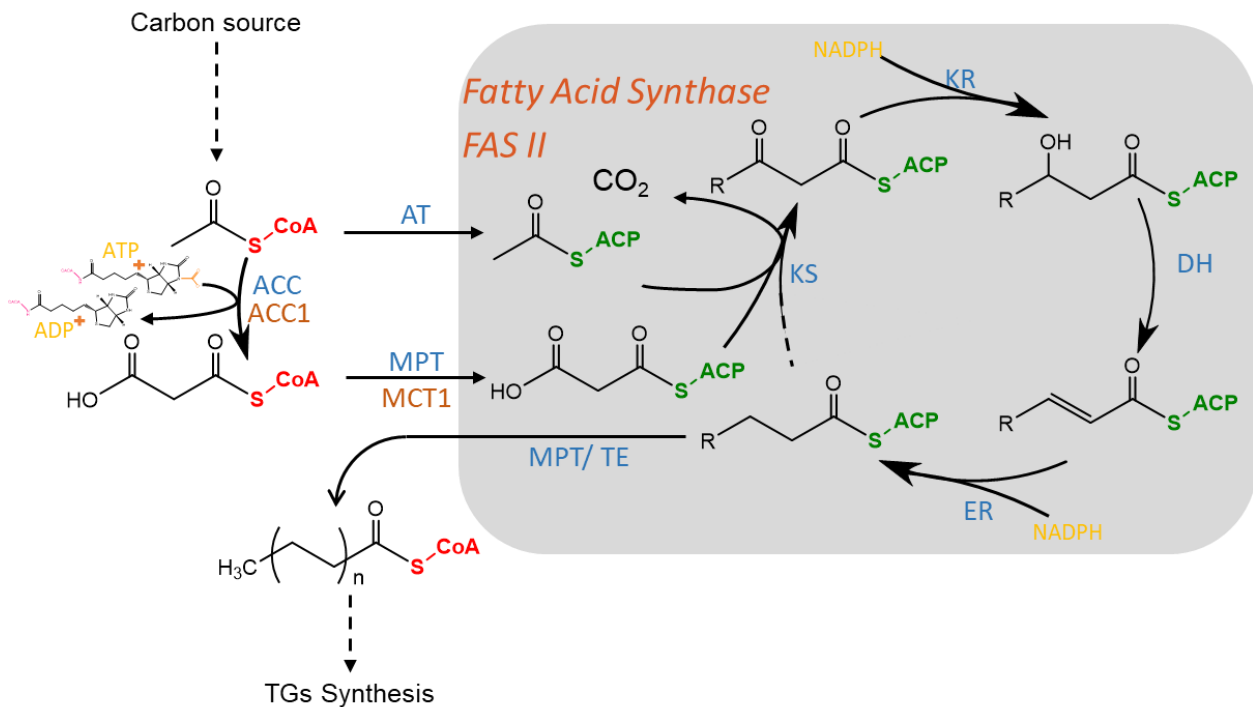


Figure 2: Fatty acid synthase FASII. Acetyl carboxylase (ACC), Acetyl transferase (AT), Ketoacyl synthase (KS), ketoacyl reductase (KR), Dehydratase (DH), Enoyl reductase (ER), malonyl/palmitoyl transferase (MPT), and domains acyl carrier protein (ACP).

Once saturated $C_{16:0}$ and $C_{18:0}$ fatty acids are initially synthesized, $C_{16:0}$ and $C_{18:0}$ are successively moved into the endoplasmic reticulum (ER) where the desaturases and elongases are located. In the ER, a series of desaturation and elongation steps begin. In general, elongase complexes have β -ketoacyl-CoA synthase (KCS), β -ketoacyl-CoA reductase, β -hydroxyacyl-CoA dehydratase and enoyl-CoA reductase activities.¹⁰⁵ The first step of these reactions is $\Delta 9$ desaturase to produce the mono-unsaturated oleic acid ($C_{18:1}$, ω -9). Oleic acid (OA) is first esterified with phospholipids, such as PC, to undergo the next desaturation step with $\Delta 12$ desaturase. Resultant linoleic acid (LA) ($C_{18:2}$, ω -6) may subsequently be converted into α -linolenic acid (ALA) ($C_{18:3}$ ω -3) via $\Delta 15$ desaturase. OA, LA and ALA separately go through sequential desaturation (by; $\Delta 6$, $\Delta 5$ and $\Delta 4$ desaturases) and elongation (various elongases) for the synthesis of all poly unsaturated fatty acids (PUFAs) (Figure 3).

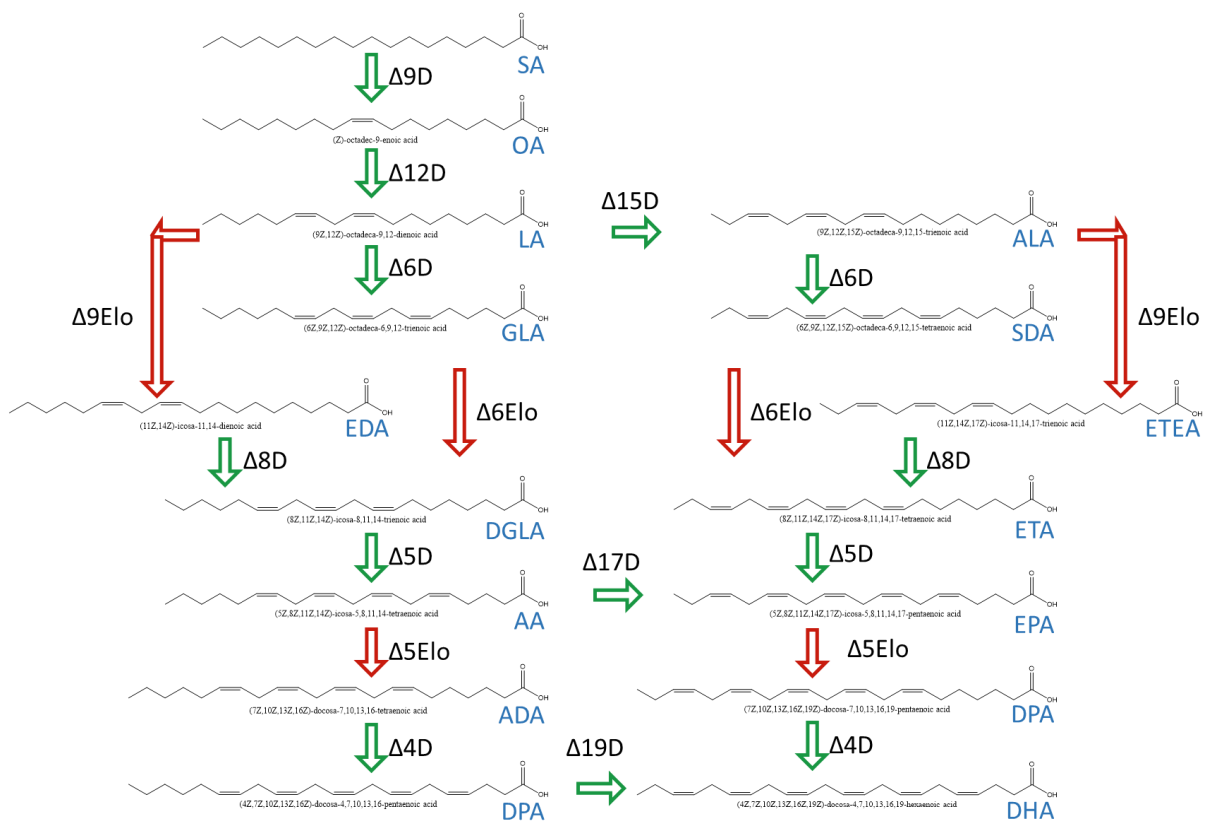


Figure 3: Biosynthesis of v-6 and v-3 PUFAs in yeasts starting from saturated stearic acid and going through successive desaturations and elongations. D: desaturases, Elo: elongases, ADA: adrenic acid, ALA: α -linolenic acid, DPA: docosapentaenoic acid, EDA: eicosadienoic acid, ETA: eicosatetraenoic acid, ETEA: eicosatrienoic acid, LA: linoleic acid, OA: oleic acid, SA: stearic acid, and SDA: stearidonic acid.

Out of five different $\Delta 5$ desaturases overexpressed in *S. cerevisiae*, $\Delta 5$ desaturases from *P. tetraurelia* were shown to be superior in arachidonic acid (ARA) and eicosapentaenoic acid (EPA) up-regulation.¹⁰⁶ PUFA production in *Y. lipolytica* has been extensively studied. GLA production was enhanced by overexpressing $\Delta 12$ and $\Delta 6$ desaturases in *M. alpine*,¹⁰⁷ while overexpressing $\Delta 4$, $\Delta 5$, $\Delta 6$ and $\Delta 17$ desaturases resulted in DHA production.^{108, 109} EPA was also produced by overexpressing $\Delta 12$, $\Delta 8$, $\Delta 17$ and $\Delta 19$ desaturases and C16-18 elongases.^{110, 111} In contrast, few reports have demonstrated

production of PUFA from *C. oleaginosus*. ALA production was improved by expression of $\Delta 9$ elongase and $\Delta 12$ desaturase in *C. oleaginosus*.¹¹²

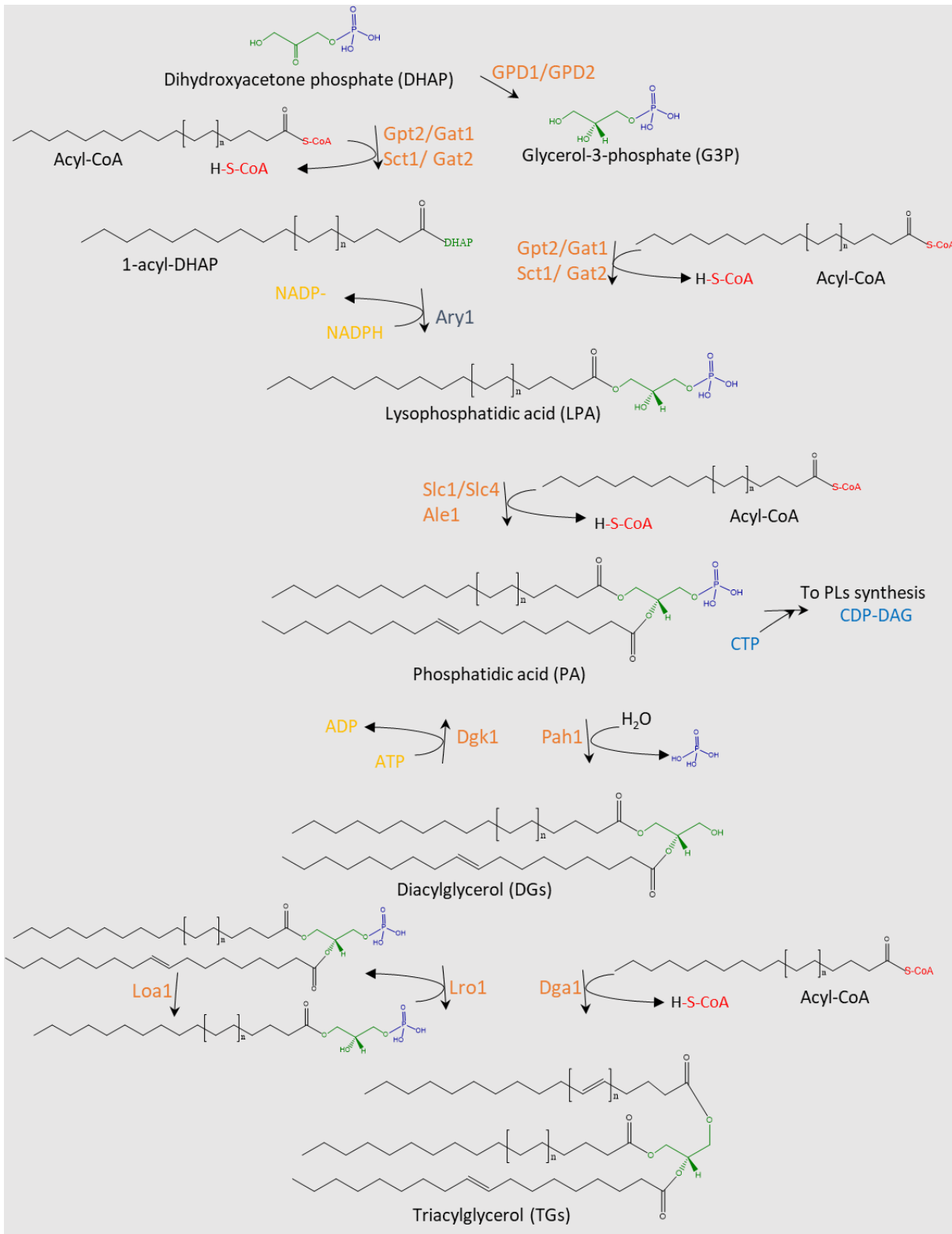


Figure 4: Triacylglycerol synthesis starting from dihydroxyacetone phosphate (DHAP) and glycerol-3-phosphate.

Fatty acids are moved into the ER endoplasmic reticulum and the outer mitochondrial membrane where they are activated by acyl CoA synthase to be attached to the glycerol backbone and form TGs.

The Kennedy pathway, which describes TG synthesis via various acyltransferases (i.e., glycerol-3-phosphate acyltransferase, GPAT; lysophosphatidic acid acyltransferase, LPAAT; diacylglycerol acyltransferase, DGAT; lysophosphatidylcholine acyltransferase, LPAT) takes place in the ER.

Sn-Glycerol-3-phosphate (G3P) has been suggested to play an important role in TAG biosynthesis as it is the glycerol backbone precursor. Glycerol can be considered a source for G3P. Glycerol first passes through the cell membrane via the glycerol/H⁺-symporter encoded by STL1.^{113, 114} Glycerol kinase (GK) catalyzes glycerol phosphorylation to G3P.¹¹⁵ Alternatively, G3P is produced during the glycolysis metabolic pathway.

Glucose is phosphorylated by hexokinase to form α -D-glucose 6-phosphate, which isomerizes to β -D-fructose 6-phosphate via glucose-6-phosphate isomerase. A second phosphorylation step by phosphofructokinase occurs on fructose 6-phosphate to synthesize fructose 1,6-bisphosphate. Fructose-bisphosphate aldolase breaks down fructose 1,6-bisphosphate into dihydroxyacetone phosphate (DHAP) and glyceraldehyde 3-phosphate (GALP). Finally, G3P is synthesized by reducing dihydroxyacetone phosphate (DHAP) performed by glycerol-3-phosphate dehydrogenase (GPDH, encoded: GPD1 and GPD2). Glycerol generated upon hydrolyzing fats with glycerol kinase can be converted to G3P by phosphorylation as an additional source of G3P. Overexpression of G3P dehydrogenase in *Y. lipolytica* results in increased G3P, which leads to increased TG accumulation.¹¹⁶

Once generated, *sn*-glycerol-3-phosphate is subsequently esterified with a long-chain acyl-CoA as the initial step of the synthesis of TGs and PLs.^{117, 118} This esterification is catalyzed by *sn*-glycerol-3-phosphate acyltransferases (GPATs, encoded: Gpt2/Gat1 and Sct1/Gat2), forming 1-acyl-*sn*-glycerol 3-phosphate (lysophosphatidic acid LPA). LPA can also be synthesized from acylation of dihydroxyacetone phosphate by a two-step reaction involving *sn*-glycerol-3-phosphate acyltransferases followed by 1-acyldihydroxyacetone-phosphate reductase (AYPR, encoded: Ayr1).¹¹⁹ LPA is subsequently acylated at position *sn*-2, making 1,2-distearoyl-*sn*-glycero-3-phosphate (phosphatidic acid PA) via lysophosphatidic acid acyltransferase (LPAAT, encoded: Slc1, Ale1/Slc4). PA hydrolysis to diacylglycerols (DGs) and phosphate is mediated by phosphatidate phosphatase (PAP, encoded: Pah1).^{120, 121} Diacylglycerol acyltransferase (DGA, encoded: Dga1 and Dga2) catalyzes the terminal reaction in the acyl-Co A Kennedy pathway and converts DGs to TGs via esterification with a FA-CoA. A second pathway for TG formation in yeast is mediated by lecithin cholesterol acyl transferase (LCAT encoded: Lor1), which is esterified by lysophospholipids, such as PC and PE, to DG.^{122, 123}

GPAT is one of the limiting factors in triacylglycerol biosynthesis.¹²⁴ While no work was performed on yeast, overexpression of GPAT in *Arabidopsis thaliana* results in increased seed oil.¹²⁵ DGA is another limiting factor that has received extended efforts and work. Lipid accumulation was enhanced in the model yeast *S. cerevisiae* when DGA1 was overexpressed alone and in combination with FAA3

(long chain fatty acid-CoA ligase 3).^{126, 127} Overexpression of DGA1 in *Y. lipolytica* yielded a 4-fold increase in lipid content.⁹⁵ Lipid accumulation of 90% (w/dw_{biomass}) was recorded in *Y. lipolytica* by overexpressing a number of genes involved in lipogenesis, i.e., ACL, AMPD MAE, DGA1 and DGA2.¹²⁸ In contrast to DGA1, Lor1 has not been tested in oleaginous yeast. In fact, Lor1 has several advantages over DGA1. Lor1 is capable of remodeling membrane phospholipids, resulting in reducing the amount of PC (converts PLs to TGs) and subsequently enhancing LD formation.^{129, 130} Secondly, Dga1 significantly contributes to TAG synthesis during the stationary phase. In contrast, Lro1 activity is more prominent in the exponential growth phase.¹³¹ This characteristic advantage could improve lipid productivity, even in a rich medium.

Up-regulation of lipogenesis genes results in deactivation of ATP-dependent citrate lyase (ATP-CL), subsequently leading to increased citrate concentration.¹²⁸ Citrate is either secreted into the growth medium or accumulated in the cytosol, causing inhibition of 6-phospho-fructokinase (Embden-Meyerhof-Parnas catabolic pathway) and leading to intracellular⁹³ or extracellular polysaccharide accumulation, causing high viscosity in the growth medium.¹³² Utilization of acetate as feedstock via ACS/ACL could also inhibit ATP-CL, as acetyl-CoA is the mutual product.

Now TGs have been synthesized, and LDs are about to emerge. Several models have described how synthesized TGs contribute to LD biogenesis. The most popular model hypothesizes that TGs, at very low concentration, are likely to be assimilated in parallel with phospholipids within the ER membrane.¹³³ As TG content exceeds the solubility limit, TGs are sequestered and oiled out between the two leaflets of the ER membrane. At this step, TG concentration is estimated at 3-7% (w/dw_{cell}) (**Figure 5**).^{134, 135} A mere accumulation, TGs coalesce to form lipid lenses through laterally diffusing within the ER leaflets. In terms of terminology, lipid lenses are called prenascent LDs. Electron microscopy has recently been used to observe lipid lens formation in yeast immediately after induction of droplet formation via overexpression of fat storage-inducing transmembrane (FIT) proteins.¹³⁶ A homo-oligomeric integral membrane protein called seipin (encoded: FLD1) destabilizes the ER PL bilayer, resulting in increased prenascent droplet stabilization that permits them to mature.^{67, 137}

As prenascent LDs are increased in size, ER membrane deformation toward the cytosol occurs. This vectorial deformation toward the cytosol could simply be explained by the slight differences in surface tension between the two ER leaflets, which are sufficient to induce vectorial budding in model systems.^{138, 139} In fact, many factors, such as phospholipids and proteins, control cytosol-oriented vectorial deformation.¹⁵ FIT2 and its orthologs in yeast, Yft2p and Scs3p, play an important role in vectorial budding. These enzymes directly bind to DGs and TGs and have weak PA activity. The results have shown that deletion of these two genes (Yft2p and Scs3p) results in the failure of LDs to emerge from

SCIENTIFIC BACKGROUND

the ER.¹³⁶ Perilipins, in yeast Pln1 p, is another protein family that contributes to ER membrane deformation.¹⁴⁰

The surface area of the ER outer leaflet then expands, as TGs are accumulated in the core of prenascent LDs, resulting in growth of the droplet, which becomes largely surrounded by phospholipids. In yeast, growth of prenascent LDs is accompanied by transmigration of Dga1p from RE to the LD surface.¹⁴¹ In the absence of LDs, Dga1p is distributed throughout the ER.¹⁴² Thus, it is possible that TGs are synthesized throughout the ER and diffuse through the bilayer to LD formation sites. Alternatively, enzyme activity for TG synthesis may occur specifically at regions of the ER where LDs form.¹⁴³

Above a certain size, depending on TG and PL composition, lipid lenses in the ER are predicted to be unstable and bud; however, it is the mechanism for how the prenascent LDs become nascent LDs has only recently been clarified.¹⁴³ In most prevailing budding modules, the mechanism of LD formation is similar to dewetting due to thermal fluctuations.¹⁴⁴ Nascent LDs could also form by transformation of ER-associated vesicles.^{145, 146}

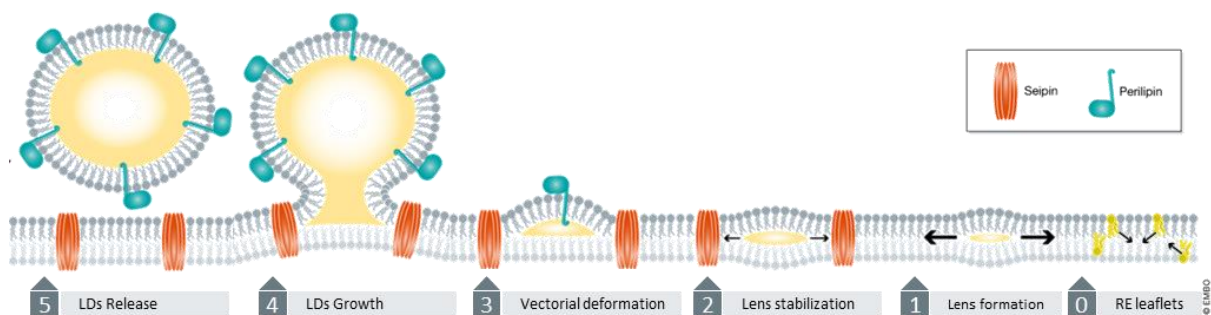


Figure 5: Lipid droplet formation (Source: modified from "The EMBO Journal (2018) 37: e98947").⁶⁷

The smallest mature cytosolic LDs have diameters in the range of 250–500 nm, which will increase in size as more TGs are continuously built.⁷⁹ LDs are often found in proximity to the ER. There is significant evidence that mature LDs are separated from the ER,⁶⁷ and in some instances, LDs build a connection to the ER through ER–LD membrane bridges.¹⁴⁷ These ER–LD connections are playing an important role in the migration of TGs from the ER to LDs, as well as in relocation of enzymes necessary for TG synthesis from the ER to the LD surface for *in situ* TG synthesis.^{148, 149} In both cases, the LDs will grow to a great size. There are other models projecting how LDs might grow, such as through LD-LD fusion.¹⁵⁰

In fact, LD-LD fusion is remarkably uncommon in normal cells under regular circumstances; however, this is not the case when cells are under extreme conditions. In this respect, prototypes based on LD surface modulation or protein-intermediate direct fusion have been suggested.¹⁵¹

Modulating the LD surface by decreasing the amount of PC and increasing the amount of PA improves homotypic LD-LD fusion.^{78, 152} Some surfactants induce LD-LD fusion as well.¹⁵³ Surfactants such as 3-(2-Ethylphenoxy)-1-[[[(1S)-1,2,3,4-tetrahydronaphth-1-yl] amino]-(2S)-2-propanol oxalate salt (SR 59230A), DMSO and N-[2-(p-Bromocinnamylamino)ethyl]-5-isoquinolinesulfonamide dihydrochloride (H-89 dihydrochloride hydrate) have been proven to enhance LD-LD fusion.¹⁵³

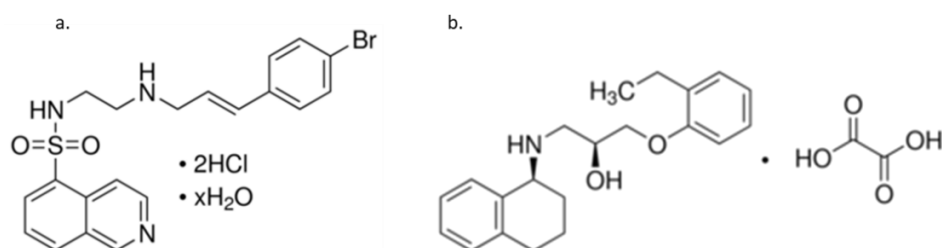


Figure 6: Surfactants can be used to enhance lipid droplet fusion. (a) N-[2-(p-Bromocinnamylamino)ethyl]-5-isoquinolinesulfonamide dihydrochloride (H-89 dihydrochloride hydrate). (b) 3-(2-Ethylphenoxy)-1-[[[(1S)-1,2,3,4-tetrahydronaphth-1-yl] amino]-(2S)-2-propanol oxalate salt (SR 59230A).

Direct fusion of LDs can be accrued either by removing phospholipids by COPI or by fat-specific protein (FSP27) mediating permeation.¹⁴³

On the LD surface, coatomer protein (COP-I) machinery plays an important role in establishing connections to the ER.^{148, 154} COPI proteins act on LD surfaces by removing phospholipids, thereby increasing LD surface tension and favoring the fusion of LDs with other membranes.¹⁵⁴ COP-I (encoded by Arf1-C159S-K181C in humans) has been produced in *E. coli* where purified protein was tested *in-vitro* (on budded Nanodroplets) and *in-vivo* (in *S. cerevisiae*). In both experiments, COP-I was able to increase the surface tension of LDs to the water, making LDs subsequently float on the top of the water phase.¹⁵⁴

The permeation module is supported by localization of FSP27 to the LD surface. FSP27 builds an LD-LD contact site where TAG can be freely exchanged through Fsp27-enriched LD contact sites.¹⁵⁵ Fsp27 directly binds to triglyceride lipase (ATGL) and inhibits lipolysis, which is considered a second mechanism that helps Fsp27 increase LD sizes.¹⁵⁶ Overexpression of FSP27 in cells leads to increased LD size, whereas depletion abolishes LDs with diameters larger than ~12 μm in adipocytes.

3.2 Factors that influence LD size

Many factors have been identified that affect LD size. Such factors include proteins that are directly involved in TG/SE synthesis/hydrolysis and LD associated proteins or phospholipids.⁸³

3.2.1 Phospholipids

Phosphatidylcholine (PC) and phosphatidylethanolamine (PE), as a general rule, are the major components of most LDs in yeast cells⁷⁴ with little phosphatidylserine (PS) and phosphatidic acid (PA) found. PC acts as a surfactant to prevent LD coalescence, resulting stunted LD growth.¹⁵² Likewise, yeast mutants with severely impaired PC synthesis (mutants with *opi3Δ*, *ino2Δ*, and *ino4Δ*) showed increasing levels of PA and synthesized supersized LDs (SLDs) and consequently enhanced TG formation.⁷⁸ In fact, a small amount of PA, ~2% of total PLs, is sufficient to trigger LD coalescence in vitro.⁷⁸ Therefore, it is believed that the size of LDs can be increased by reducing the amount of PC and/or by increasing the amount of PA. Cholesterol and sphingolipids are additional types of lipids that localize to the surface of LDs, but where they impact LD growth remains to be explored.⁷⁴

Upon starvation, yeast cells convert phospholipid intermediates and sterols to neutral lipids, which in turn can be hydrolyzed to release fatty acids and sterols for immediate membrane synthesis and cell growth when glucose becomes available.⁷⁸ Therefore, starvation might decrease PC synthesis, and consequently, an increased PE to PL ratio (or a decrease in PC/TAG) has been associated with SLD (supersized LD) formation.¹⁵⁷

3.2.2 Glycosylation proteins

Glycosylation proteins, including *anp1*, *erd1*, *mnn10*, *mnn11*, *och1*, *ost4* and *pmr1*, significantly restrict the growth of LDs.⁷⁶ In fact, glycosylation proteins remarkably impact the lipid profile and elevated TGs/SEs when compared to wild type. Mutants defective in *anp1* and *pmr1* display increased synthesis of both TGs (by 30% and 70%, respectively) and SEs (by 40% and 110%, respectively). In contrast, deletion of *erd1*, *och1* and *ost4* resulted in a 70–100% increase in TG synthesis only.⁷⁶ The same effect was noted when glycosylation inhibitors were used. Chemicals such as Tm (Tunicamycin) and BFA (Brefeldin A), which inhibit N-linked glycosylation, induce neutral lipid synthesis and LD formation at low concentrations (Tm: 10 µg/ml, BFA: 75 µg/ml).¹⁵⁸

3.2.3 Fsp27 and CIDE proteins

Two protein families are LD-associated proteins that have recently been reported to regulate lipid storage and energy homeostasis in mice and humans.¹⁵⁹ The first family is the fat-specific protein (Fsp27) and cell death-inducing DFF45-like effector (CIDE), which includes Cidea and Cideb. Fsp27 mediates LD growth by merging smaller donor LDs slowly into larger acceptor LDs.¹⁵⁵

3.2.4 Perilipin 1

The perilipin family (PLIN) is one of most extensively characterized proteins localized to LD surfaces. Perilipin1 is highly expressed in white adipocytes, where it coats giant and unilocular LD.^{160, 161} Perilipin1 is a member of the PAT family (such as perilipin, adipophilin and TIP47) and includes perilipins1-5. Perilipin1 and 2 primarily localize to the surface of normal LDs, and perilipin1 displaces

all perilipin2 when LDs become giant, implying that perilipin1 may promote the formation of giant LDs. This hypothesis was supported by findings that perilipin1-deficient mice exhibit dramatically reduced adipocyte and LD sizes.^{162, 163} Perilipin3, 4 and 5 are stable in the cytoplasm and relocate to nascent LDs upon increased TAG synthesis.¹⁶⁴

Additionally, the oleosin family is located on LDs with high lipid content. Overexpression of Oleosin and perilipin family members (PLIN1, ADRP/PLIN2 and TIP47/PLIN3) in *Saccharomyces cerevisiae* cells promotes the sequestration of neutral lipids from the ER bilayer, thereby inducing LD formation.^{165, 166} One of the suggested mechanisms for Perilipin1 to promote unilocular LD formation is through activation of Fsp27.¹⁶⁷

3.2.5 Seipin (*Fld1p*)

LD sizes were enlarged by approximately 30% in *Saccharomyces cerevisiae* lacking FLD1 (caused by the deletion of YLR404W). Moreover, small LDs from *fld1Δ* cells demonstrate significantly enhanced fusion activities of 60% both in vivo and in vitro.⁷⁷ The *fld1Δ* cells were identified, and most of the mutated genes are known to regulate synthesis of phospholipids. This effect can be explained given that Fld1/seipin may modulates PA metabolism.^{78, 168} Levels of seipin/Fld1p are also adversely correlated with TAG storage in yeast.¹⁶⁹

3.2.6 FITM1&2

Fat storage-inducing transmembrane proteins (FITM) are integral ER membrane proteins produced in yeast to human species. Overexpression of FITM2 significantly increases TAG storage and droplet size in mouse liver and in cultured cells, and this effect was enhanced when a gain of function mutant of FIT2 was expressed.¹⁷⁰

3.2.7 Acyl-CoA synthetase 3

Acyl-CoA synthetase 3 promotes lipid droplet biogenesis in ER microdomains. ACSL3 plays an important role in channeling fatty acids into nascent LDs.⁷⁵ Absence of ACSL3 was shown to significantly reduce nucleation of emerging LDs, short- and long-term accumulation of neutral lipids, and the size and number of mature LDs.⁷⁵ ACSL3's crucial interactions with scaffolding proteins, such as Spartin/SPG20 and AUP1, determine LD composition, size, and number.^{171, 172} Accordingly, ACSL3 has been found in complexes with neutral lipid synthesis enzymes.¹⁴⁹ Furthermore, ACSL3 plays a dynamic role in relocation of the enzyme between the ER and LDs, which may represent a cellular homeostatic sensor given that ACSL3 regulates the activity of key lipogenic transcription factors, such as PPAR- γ , ChREBP, SREBP1-c, and LXR- α .¹⁷³

4 Challenges in lipid production from oleaginous yeast

In the present state-of-art, several technical and environmental challenges are restricting any sustainably viable industrial manufacturing of MO. Costly feedstock procurement, extended fermentation times, complex lipid recovery, and poorly lipid titer are the major technical challenges. From the environmental perspective, application of toxic solvents, high energy demand (indirect CO₂ emission), and direct CO₂ emission during the fermentation, increases the associated GHGs emission with MO production.

Therefore, MO processes need to be improved in a way, that all technical and environmental challenges are taken into consideration. However, it is vitally important to implement keep-performance-indicators (KPIs) to continually evaluate and monitor any changes within the MO process design. Such KPIs can be; a process cost assessment (such TEA methodology) and environment impact analysis (such LCA framework).

4.1 Techno-economic analysis (TEA) and MO cost:

TEA is a methodology framework to analyze the technical and economic viability of a production process. TEA normally combines process modeling, engineering design and economic evaluation. The initial step to prepare a TEA, is to identify the mass flux through consecutive functional units and define the equations for any mass conversion. The *in-silico* process modeling is then the next step, where each functional unit is represented by; machinery, mass inputs, mass outputs, energy balance, men-power need, time, and consumables. The equipment sizing, mass- and energy fluxes need to be assessed using well known procedures and rules of thumb. Alternatively, a modeling software such SuperPro Designer (SPD) or Aspen can be applied, where an internal mathematical function is integrated. Normally, different scenarios for mass- and energy balance are taken in consideration to epitomize an optimistic, pessimistic, and an average (baseline) scenarios. Consequently, capital, operation, and raw material costs can be estimated. As last step, cost sensitivity to highest impacted parameters is calculated.

To that end, TEA offers a reliable framework for mass conversion, energy consumption, waste emission, and thus overall process efficiency.

TEA methodology was applied to estimate the cost of MO. In this respect, microbial oil expected prices from *Candida curvata* were estimated at US\$3000/ton based on lactose fermentation excluding the raw materials cost.¹⁷⁴ Recently, microbial oil from *R. toruloides* for production and biodiesel from glucose carried an estimated production cost of US\$5500/ton oil and US\$5900/ton biodiesel¹⁷⁵, which is not feasible in the current market where vegetable oil prices are around US\$500–900/ton and biodiesel is at US\$1220/ton.¹⁷⁵ In addition, waste treatment costs were not considered in these techno-economic studies. This additional cost not only extensively impacts the total lipid price but

heavily impacts the environment results in fresh water depletion and eutrophication. The microbe meal, as a coproduct, has a price of around US\$400–800/ton.¹⁷⁶ This coproduct can be considered as extra cost savings. Thus, SCO biorefinery would be slightly more encouraging (~US\$5000/ ton oil) but would still not be viable. Production of high-value FAs, such as ARA, GLA, DHA, or upgrading the lipid for high-value products, such as biolubricants or food/ pharmaceutical targeting oleochemicals, could improve the economic viability of SCO.

4.2 Technical challenges:

Improvement of lipid yield, productivity, and titer is critical for making SCO economically feasible. Diauxic growth effects are one of the major challenges that reduce productivity. Yeast grown in nutrient-rich media exhibit rapid cell growth associated with high phospholipid production and correspondingly low levels of neutral lipids.^{71,177} As nutrients become exhausted, yeast respond to this imminent starvation by decreasing their phospholipid production and shunting precursor lipids into the synthesis of TGs at the ER, corresponding to a burst of LD biogenesis. This transition phase from fermentation to respiration is defined as the diauxic shift.^{79, 178} While the first phase requires approximately 2-3 days, and biogenesis of large LDs first appear on the third to fourth fermentation day. Diauxic growth effects elongate the fermentation time where lipid productivity is decayed, operation cost is increased and substrate-to-lipid yield is reduced.

Low lipid productivity and low lipid titer are primarily associated with utilization of a complex sugar matrix, such as lignocellulosic hydrolysates.^{179, 180} This can be attributed to a limited ability to control C:N, low sugar concentration, presence of sugar mixtures and inhibitor formation during pretreatment, such as furfural, hydroxymethylfurfural (HMF), VFAs, phenolic compounds, and other chemical species.¹⁸¹ An effective fermentation system can be established once yeast growth and lipid accumulation are dissociated from the C:N ratio. Such decoupling can reduce the side effect of the sugar mixture in complex media. Managing inhibitor formation as well as developing yeast mutants that are capable of tolerating them has been the subject of considerable research. An approach toward developing biomass-specific enzyme systems offers an inhibitor-free hydrolysate ditto that minimizes processing steps, such as pretreatment/detoxification.^{179, 180}

Lipid extraction and lipid purification from intracellular compartments involves harvesting of microbial cells from broth, either by drying the cells or forcing cell disruption then lipid extraction. Frequently used cell-harvesting techniques include centrifugation, filtration, and flocculation.^{182, 183} The lower the cell density obtained, the more expensive the harvesting. Likewise, high lipid content leads to technical difficulties, restricting centrifugation and flocculation, as the cell specific gravity is less than water.

After harvesting, drying yeast cells practically improves lipid recovery during extraction compared to disrupted wet cell biomass.¹⁸⁴ Since the cell drying is a high-energy process therefore, several methods have been investigated, such as high-pressure homogenization, bead beating, ultrasonication, microwave treatment or chemical hydrolysis, to efficiently disrupt wet microbial cells.¹⁸⁴⁻¹⁸⁶ Alternatively, enzymatic hydrolysis has previously been applied to enhance cell rupture in oleaginous yeasts.^{183, 185, 187-189} Outmoded organic solvent based lipid extraction methods, such as Bligh and Dyer and the Soxhlet, are still implemented using chloroform, methanol, or even hexane even after such enzymatic treatment.^{186, 190} Supercritical liquids, such as SCCO₂, are alternatively applied in a state of organic solvents to avoid energy-intensive solvent recovery.^{184-186, 191} The high pressure applied in such alternative methods is still an energy consuming process. Hydrothermal liquefaction has been used for algae (at 300°C for 5 min) and for yeast (at 180°C for 5 min).^{192, 193} Other energy-consuming extraction methods that can be applied include pyrolysis, gasification, and direct combustion, which are reviewed by Millege *et al.*¹⁹⁴ Upscaling of such mechanical stress, temperature shock, or chemical treatment results in additional complications/cost in the downstream process.^{195, 196} It is a challenging task to apply such methods at the industrial level due to cost issues and lack of environmental sustainability.

4.3 Life cycle assessment (LCA) and environmental challenges:

4.3.1 Life cycle Assessment (LCA)

LCA or cradle to the grave analysis is a methodology framework to evaluate environmental impacts of a product's life comprising; raw material extraction, raw materials processing, manufacture, distribution, use, repair and maintenance, and later on disposal or recycling.

According to ISO 14040 guidelines, LCA is carried out in four phases which are; goal and scope, inventory analysis, impact assessment, and interpretation of a life cycle. At the initial phase (goal and scope phase), a clear system boundary and serving criteria for the in-focus part of the product-life-cycle should be defined. The inventory analysis is concerned with the description of material- and energy flux within the defined system boundary. It is very important at this stage to consider the process; interaction with environment such as; consumed raw materials and the emissions to the environment. Detailed inventory analysis data was used for impact assessment of each functional unit on all environmental impact categories. The impact assessment is evaluated by normalization and eventually also by weighting. Finally, interpretation of a life cycle involves critical review, determination of data sensitivity, and result presentation.

Attributional and consequential approaches are the main approaches to proceed with LCA. By the attributional approach, inputs and outputs are attributed to the functional unit of a product system by linking and/or partitioning the unit processes of the system under the specified normative allocation rule. In consequential approach, activities in a product system are linked so that the activities are included in the product system to the extent that they are expected to be changed as a consequence of a change in demand for the functional unit.

Many methodologies can be used to perform an LCA. The full LCA involves all functional units of specific product from resource extraction (*cradle*) to use phase and disposal phase (*grave*) so called, *cradle-to-grave* method. A partial LCA can be limited to certain part of the product life such as: *cradle-to-gate*, which focus on steps from resource extraction (*cradle*) to the factory gate(*gate*). *Gate-to-gate* is seeking at only one value-added process in the entire production chain. *Gate-to-gate* modules may also later be linked in their appropriate production chain to form a complete *cradle-to-gate* evaluation.

4.3.2 Environmental challenges for MO production

Application of organic solvents leads to contamination in the water phase, along with residual biomass and lipids. Traces of toxic organic solvents prevent recycling of side products under economic constraints. Additionally, application of organic solvents negatively affects quality of the finished product and restricts applications of the products in foods and pharmaceuticals.¹⁹⁶ Hence, the complexity of advanced solvent removal is considered an extra cost and energy squandering. Moreover, application of hydrothermal methods results in the formation of inhibitory compounds, which again restrict recycling of the water phase.¹⁹³

Carbon dioxide emission is one of the major environmental challenge for any fermentative process. In fact, 50-60% of total input carbon is converted to CO₂, where the rest is fixed within the biomass and lipid. In this respect, released CO₂ can be used as feedstock for microalgae or acetic acid producer microorganism such as *Acetobacterium woodii*. However, due to the variation in the growth rate between the yeast and microalgae, direct transformation will result in many technical problems and reduce the efficiency. Therefore, such transformation needs an intermediate step, which captures the CO₂ and released at appropriate rate.

Green sorbents for carbon dioxide (CO₂) capturing has widely been reported. These reports focused on synthesis/use bio-feedstocks,^{197,198} metal organic frameworks (MOFs)¹⁹⁸⁻²⁰⁰ and synthetic oligomers²⁰¹. In co-work with Dr. Qarousha, we exploited a sustainable oligochitosan dissolved in DMSO as a green sorbent for CO₂ capturing.

In fact, the key to an economically successful SCO platform is to shorten and simplify cultivation and downstream methods, which could significantly reduce production cost.²⁰²

5 Work objectives

In this work, we aimed to establish a new integrated process chain for production of yeast-based lipids, enabling uncoupled, monoauxic biomass growth and lipid accumulation with short fermentation time. To apply an economically feasible and environmentally sustainable process, monoauxic growth should be accomplished in a single step, *in-situ* and solvent free extraction to recover downstream lipid processing, permitting complete recycling of water and side product streams. This process permits operation in continuous or batch fermentation mode using a sustainable system that incurs no land use changes, ecosystem destruction, or biodiversity reduction that is associated with utilization of terrestrial biomass. Therefore, we aimed to utilize marine macrophyte carbon sources, such as seagrass and macroalgae, in co-fermentation with acetic acid. A comprehensive techno-economic analysis (TEA) and life cycle assessment (LCA) of the new yeast lipid production process needs to be performed to validate our findings.

6 Discussion

Contemporary societies heavily rely on fossil fuels as their major source of energy, which accompanied by high CO₂ emission and subsequent increases the average surface air temperatures on Earth. Renewable energy sources, such as biofuels, are desired to displace fossil fuels as they have a lower carbon content. In this respect, alternative bio-based technologies seek to supply fuels in a cost-effective and sustainable manner, while contributing to the reduction of greenhouse gases. Current generation biofuels are completely dependent upon crop oils, such as palm oil, resulting in serious issues for biodiversity. Lipids from oleaginous microorganisms have great potential to displace crop-derived oils as a biofuel substrate, but many restrictions prevent their economical and industrial application.

The current project primarily addressed the key technical and environmental constraints concerning single cell lipid production from oleaginous yeast related to sustainable feedstock, time-effective biomass and lipid yield, as well as low-energy-demand for downstream processing. Additionally, environmental restrictions regarding solvent needs and fermentative CO₂ emission. Moreover, publication concerning lipid production from microalgae, and screening and characterization of extracellular proteases, contributed to the thesis were performed in collaboration with different partners.

With respect to a sustainable feedstock, we used marine biomass to avoid any associated land use changes or any negative impacts to the Earth's ecosystem. Two published manuscripts discuss the conversion of monosaccharides from marine macrophytes (Seagrass⁴¹ and Macroalgae⁴²) to yeast-based lipid production. In both work, MB was liquefied via a solo enzymatic hydrolysis without any chemical treatment. Readily available beach-cast seagrass provides a potentially sustainable feedstock for cost effective bioenergy/biofuel production. Among the studied seagrass samples, *P. oceanica* from the Mediterranean Sea displays the best lipid productivity, exceeding well-documented minimal nitrogen media.⁴¹ Likewise, marine macroalgae, such as *U. lactuca* (green algae) and *L. digitata* (brown algae), offer a prospective feedstock for bio-oil production from yeast. In this work, *L. digitata* exhibited high biomass and lipid productivity.⁴²

Application of macroalgae or seagrass in biotechnological processes has been demonstrated. In previous reports, chemical hydrolysis²⁰³, chemo-enzymatic hydrolysis²⁰⁴, biological degradation²⁰⁵ and anaerobic digestion^{206,207} were applied to hydrolyze and liquefy

the macroalgae biomass. Resulted sugar- / VFAs-rich hydrolysates were introduced to be bioenergy generation, encompassing biogas (methane)²⁰⁷, bio-ethanol²⁰⁸, acetone and bio-butanol generation²⁰⁹. To the best of our knowledge, beach-cast seagrass and macroalgae hydrolysates have not been investigated in the field of MO production. Nevertheless, solid fraction, which is the residual biomass after biomass hydrolysis, has been completely ignored. There is no value adding applications for this fraction, which negatively impact the overall process cost. To present, the most widespread application for this hydrolysis residue is an application as fertilizer or animal feed^{210, 211}.

In the current work, we avoided any chemical pretreatment via establishing an efficient enzymatic hydrolysis process that can stand alone for selective seagrass, macroalgae and yeast hydrolysis.^{41, 42, 80} Even more, we have demonstrated that the solid macroalgae residue is able to recover about 0.6 mmol g⁻¹ of heavy metals per dry biomass with selectivity to Pb=Ce=Cu>Ni.

Additionally, the non-lipid yeast biomass, the yeast cell-wall, is applied for first time as a unique sugar source. The enzymatically produced yeast hydrolysate displays a sugar/nutrition rich medium for yeast fermentation, resulting in high biomass and lipid productivities 2.4 g L⁻¹ h⁻¹ (Biomass: 147 g L⁻¹, Lipid 77% (w/w), Time: 42 h).⁸⁰

To compare current work lipid productivity with previous reported one, the best lipid productivity of *Lipomyces starkeyi* was 0.12 g L⁻¹ h⁻¹ (biomass: 31.5 g L⁻¹, lipids: 55% [w_{lipid}/^dw_{biomass}]) in a co-fermentation of 90 g L⁻¹ cellobiose and xylose.²¹² Using corn stover hydrolysate as the medium, a lipid productivity of 0.23 g L⁻¹ h⁻¹ (biomass: 48 g L⁻¹, lipids: 34% [w_{lipid}/^dw_{biomass}]) was reported with *Rhodotorula graminis*.²¹³ Similarly, *Rhodospiridium toruloides* Y4, was cultivated in a 15-L stirred-tank fermenter on glucose, afforded a lipid productivity of 0.54 g L⁻¹ h⁻¹ (biomass: 106.5 g L⁻¹, lipids: 67.5% [w_{lipid}/^dw_{biomass}]).²¹⁴

A lipid productivity of 0.66 g L⁻¹ h⁻¹ (biomass: 168 g L⁻¹, lipids: 75% [w_{lipid}/^dw_{biomass}]) was recorded of *C. oleaginosus* based on pH-stat acetic acid fermentation.⁵⁵ *Yarrowia lipolytica* NS432 showed a productivity of 0.73 g L⁻¹ h⁻¹ (biomass: 110 g L⁻¹, lipids: 77% [w_{lipid}/^dw_{biomass}]) in fed-batch glucose fermentation.²¹⁵ However, the best yield reported in the literature was obtained in an oxygen-rich batch culture of *Rhodotorula glutinis*, with a productivity of 0.87 g L⁻¹ h⁻¹ (biomass: 185 g L⁻¹, lipids: 40% [w_{lipid}/^dw_{biomass}]).²¹⁶

Acetic acid, as feedstock, is another sustainable nutrient source since it can be generated from ecologically sound starting materials, such as CO, waste gases, and CO₂/H₂⁴⁹⁻⁵¹ using biotechnological processes (i.e., fermentation of *Clostridium aceticum* and *Acetobacterium woodii*).^{49, 50, 52, 53} At industrial scale, SEKAB, Sweden, demonstrates production of acetic acid

from bioethanol, which was originally a second-generation cellulosic bioethanol from forestry waste.

In fact, acetic acid fermentation has previously demonstrated as a sole feedstock for *C. oleaginosus* cultivation.^{21, 23, 54-57} In this respect, the application of acetic acid as the sole carbon source results in considerably high intracellular lipid content (60–73%, $w_{lipid}/d w_{biomass}$) with low total biomass productivity, leading to poor overall oil yields.^{23, 54, 56} Moreover, multistep,²¹ continuous,⁵⁴ and pH-stat^{55, 56} fermentations have been tested in order to identify the best implementation of acetic acid as the sole carbon source feedstock. The pH-stat approach shows promising lipid productivity.⁵⁵ However, constant feeding of costly yeast extract, peptone, vitamins, and other nutrients in all pH-stat trials prohibits the economic development of this process.

Some of the key achievements in the current work include the development of a monoauxic co-fermentation system enabling simultaneous assimilation of sugar and acetic acid in rich-based medium into yeast biomass and lipid. The co-fermentation freed TG biosynthesis from nitrogen scarcity, which subsequently avoided classical diauxic fermentation and paved the way to the flash (short, approximately 40-48 h) or continuous operation mode.⁸⁰

In return, a considerable fraction of feedstock is still converted to CO₂ by yeast respiration. Microalgae, in this respect, might be the optimal platform to assimilate released CO₂ utilized to build biomass and lipids. Our common work with Aquaculture Laboratory on *Isochrysis sp.*, *Nannochloropsis maritima* and *Tetraselmis sp* shows that *Isochrysis sp.* contains approximately 29.3% and 18.4% (w/w_{total FA}) monounsaturated and polyunsaturated fatty acids, respectively, whereas random mutagenesis using ultraviolet-C results in significantly increased C_{16:0}–C_{18:0} content compared to the wild type strain.²¹⁷

Relocation of CO₂ from heterotrophic yeast to autotrophic algae was discussed in a collaboration with our partner at the University of Jordan. In this collaboration, a CO₂ chemisorption system was created. CO₂ was captured on chitosan oligosaccharide/DMSO (CS·HCl/DMSO) system based on reversible carbamato–carbonato bonds. For our part, the biodegradation test revealed that degradation of approximately 80% of CS·HCl/DMSO was achieved after 33 days. These results indicate that established chemisorption systems can be considered as green sorbent. The CS·HCl/DMSO sorbent system has a capacity of 2.4 mmol CO₂ per g of sorbent.²¹⁸

Development of downstream processing for lipid recovery was also a focus of the current thesis. A single step catalytic cell-wall lysis via hydrothermal treatment (180°C, 10 min) was the concern of a common publication with a catalysis research center in TUM. For my contribution,

yeast biomass was analyzed, and yeast hydrolysate was evaluated as feedstock for bioethanol production.

An enzymatic based downstream processing approach was established as part of the main tasks in the LPOMAR project. A single *in situ* enzymatic treatment process was allowed holistic cell lysis and lipid recovery/purification without the need for pretreatment or subsequent application of an organic solvent. After such enzymatic treatment, moderate density-based separation forces, such as centrifugation, will be sufficient to release 90% (w/w) of lipids as the upper phase.

Enzymatic approaches have previously been applied to enhance the cell rupture of oleaginous yeasts^{185, 187-189}. A partial enzymic hydrolysis followed by ethyl acetate lipid extraction has recently been reported for *Rhodospiridium toruloides*.²¹⁹ In analogy, a process termed enzyme-assisted aqueous extraction processing (EAEP) was applied for lipid extraction in the microalgae *Chlorella vulgaris*, *Scenedesmus dimorphus*, and *Nannochloropsis sp.*²²⁰ In the EAEP, a pre-treatment by ultrasonic irradiation and post-treatment by heating at 95°C were required. These pre- / post-treatments considered as a high-energy consuming process thus it is inapplicable at industrial scale. In 2011, a mix of different enzymes; papain, pectinase, snailase, neutrase, alcalase and cellulase were optimized on the filamentous fungus *Mortierella alpina* for arachidonic acid extraction. To support the hydrolysis procedure, an addition of hexane was still required¹⁸⁷. Overall in the published processes, various pre-treatments have been applied prior to the enzymatic cell lysis. Moreover, the lipids still have to be extracted with an organic solvent to recover the triglycerides.

In the current work, the established enzymatic based downstream processing comprises two enzyme treatments, while the initial step imposes a holistic cell-wall lysis performed by a mixture of hydrolases, and second treatment inflicts cell emulsion systems, such as proteins. The hydrolase mixture can be produced either by mixing of commercial enzyme activities as it is described in our first patent filed with Clariant (related paper is still in preparation) or can be produced in single preparation by filamentous fungus *T. reesei* where a yeast-selective hydrolase system was produced using the yeast cell itself as an inducing system (the second patent filed with TUM).⁸⁰

Following hydrolase treatment, a demulsification step is still needed. In both patents/papers, a commercial protease was used. In the first patent with Clariant, we claimed that DISSOLVAN® addition (Clariant) improves lipid recovery.

In this regard, two common papers with marine biodiversity and biotechnology laboratory were concerned with isolation and characterization of alkaline extracellular proteases from *Yarrowia lipolytica*.^{221, 222} This cured protease could be considered for the demulsification step as an alternative to commercial proteases in a future work. From these publications, the purified extracellular alkaline protease extracted from *Yarrowia lipolytica* show promising stability and activities that may be used downstream for lipid recovery.

Finally, the main focus of this thesis was to establish an integrated operation for bioconversion of acetic acid and sugar to sustainable lipids at maximum productivity with minimal waste generation and energy consumption. In the suggested bioprocess, all side-products were reintegrated into the main production route.

To gain a better understanding of our designed bioprocess, a techno-economic analysis revealed that the cost gap compared to plant-based lipids was considerably reduced from \$5.5 per kg lipid (in a previous study¹⁷⁵) to an estimated cost of \$1.1-1.6 per kg lipid. Moreover, life cycle assessment analysis assumed an emission of 3.56 kg CO₂ equivalents for every 1 kg of yeast oil produced.⁸⁰

The approaches established in this work link previous efforts to a forward-thinking optimized approach. There are still many possible parameters to be optimized and metabolic modifications that can be implemented to further improve productivity or change the fatty acid profile.

Acetate-CoA ligase (ACL) directly transforms acetic acid into acetyl-CoA, which is further converted to fatty acids. Some publications have shown that propionic acid or butyric acid follow the same uptake pathway, resulting in alteration of the lipid profile and formation of nonconventional fatty acids, such C_{15:0}, C_{17:0} and C_{17:1}.⁵⁹ From this perspective, determining which lipid profile can be obtained if the volatile fatty acid contains a double bond, functional group or even side-chain is important. Moreover, manipulating this process through changes in pH, temperature, *p*O₂ content, and acetic acid concentration could enhance lipid productivity and change the lipid profile.

Lipid productivity based on co-fermentation can also be boosted, whereas tool boxes compromise process and genetic approaches. Fermentation conditions, modes, and media can all play a role in enhancing lipid productivity. Genetic approaches, however, are still an essential key. Overexpression of Acyl-CoA synthetase 3 accelerates acetate conversion to FA, promoting TG biosynthesis and LD biogenesis.⁷⁵

Enhancing yeast's ability to uptake oligosaccharides together with monosaccharides is also beneficial for improving lipid yield and reducing production cost, especially when the lignocellulosic biomass is in focus.²²³

Overexpression of Lor1 is another example that can reduce PL content and endorse TG formation.^{129, 130} In fact, Lor1 was shown to be more prominent in nutrition-rich conditions (the exponential growth phase).¹³¹ Therefore, such enzymes are more compatible with designed processes.

Modulating the PL level to reduce PC and increase PA, downregulation of glycosylation proteins and overexpression of fat storage-inducing transmembrane proteins (FITM) could be targets for future work within the same aim.

To improve lipid recovery, two directions can be followed. In the first direction, mixtures could be generated from other fungi, such as *Aspergillus niger* or *Fusarium oxysporum*.

Improving the efficacy of hydrolases can lead to enhanced lipid recovery. Therefore, screening for higher hydrolases from *Aspergillus niger*, *Fusarium oxysporum* or other hydrolase producers can be performed as a next step. Addition of surfactants, such as 3-(2-Ethylphenoxy)-1-[[[(1S)-1,2,3,4-tetrahydronaphth-1-yl] amino]-(2S)-2-propanol oxalate salt (SR 59230A), DMSO, and N-[2-(p-Bromocinnamylamino)ethyl]-5-isoquinolinesulfonamide dihydrochloride (H-89 dihydrochloride hydrate), could improve the demulsification step.¹⁵³

Coatomer protein (COP-I) machinery shows a unique and apparently intrinsic capability to work on PL monolayers and budding oil droplets. *In vivo* and at the molecular level, LP monolayers work to keep a low cytosol/oil interface tension (below 2 mN/m). Thus, the action of COPI prevents PL from completely covering LD surfaces, which provides more accessibility to TGs for binding/reacting with other components. *In vitro*, COP-I machinery clamps to the surface of the monolayer at a water/oil interface, causing increased surface tension that facilitates TG separation from water. This unique capability can be employed to improve the demulsification step of single cell lipid production.

Finally, current TEA and CLA were assumed to procure a chemical-based acetic acid from China. Alternatively, on-site fermentative acetic acid can be modeled starting from CO, waste gases, or CO₂/H₂⁴⁹⁻⁵¹ using microbial producers, such as *Clostridium acetivum* and *Acetobacterium woodii*.^{49, 50, 52, 53} This approach can reduce the cost and GHG emission via dispensing the transportation cost and GHG.

To that end, the current thesis is an unpretentious contribution to society's efforts to promote world economic sustainability and enhance the quality of life, *so help me, God*.

7 Methods

7.1 Strains and precultures

C. oleaginosus (ATCC 20509) and *Yarrowia lipolytica* YITun15 were activated from -80°C stock by sub-culturing on YPD plate (10 g L⁻¹ yeast extract, 20 g L⁻¹ peptone, 20 g L⁻¹ glucose, and 15% agar). Pre-culture was cultivated in Erlenmeyer flasks containing YPD media broth (10 g L⁻¹ yeast extract, 20 g L⁻¹ peptone, and 20 g L⁻¹ glucose) containing antibiotics (10 mg L⁻¹ ampicillin, 10 mg L⁻¹ kanamycin, and 12 mg L⁻¹ tetracycline). The yeast was incubated in a rotary shaker at 100 rpm and 28°C for 2 days and was then used as the inoculum.

Two brown algae (*Laminaria digitata*) and one green algae (*Ulva lactuca*) sample were harvested from the western coast of Ireland in March and June 2013 (North Seaweed Ltd- Netherlands). The samples were washed thoroughly (with distilled water) to eliminate salt, sand and contaminants. Subsequently, samples were dried and grind down to ≤ 0.5 mm grain size using a Planetary Ball Mill- (Fritsch, Germany).

Fresh and aged seagrass samples were collected during the summer seasons of 2013 and 2014 from six different locations worldwide: two samples from Baltic Sea (Hohenkirchen and Greifswald), two from Mediterranean Sea (Malta), one in Caribbean Sea (Isla de Mujeres, Mexico), one from Great Australian Bight (Beachport, South Australia) and one sample from North Atlantic Ocean (Bahamas). The samples were washed thoroughly to get rid of accumulated salt, sand and contaminants, dried and grinded down to ≤ 0.5 mm thickness using Planetary Ball Mill (Fritsch, Germany). For reproducibility purposes, all experiments and analysis were conducted in triplicates.

T. reesei ATCC 56765 (RUT C-30) and ATCC 13631 were activated in LB media (5 g L⁻¹ yeast extract, 10 g L⁻¹ tryptone) and was then used as inoculum for fermentation.

7.2 Media

Different media were applied for each experiment. These media contained major nutrient components (carbon and nitrogen sources) plus base medium. The composition of the base medium was as follow: 0.05 g L⁻¹ NH₄Cl, 2.4 g L⁻¹ KH₂PO₄, 0.9 g L⁻¹ Na₂HPO₄·12H₂O, 1.5 g L⁻¹ MgSO₄·7H₂O, 0.025 g L⁻¹ FeCl₃·6H₂O, 0.001 g L⁻¹ ZnSO₄·7H₂O, 0.2 g L⁻¹ CaCl₂·2H₂O, 0.024 g L⁻¹ MnSO₄·5H₂O, 0.025 g L⁻¹ CuSO₄·5H₂O, and 0.003 g L⁻¹ Co(NO₃)₂·6H₂O. The composition of the main nutrition was as follows: medium A (C/N ratio 125) was composed of 30.0 g L⁻¹ glucose and 0.5 g L⁻¹ yeast extract; medium B (C/N ratio 125) was composed of 0.5 g L⁻¹ yeast extract and 4.1 g L⁻¹ CH₃COONa; medium C (C/N ratio 130) was composed of 30.0 g L⁻¹ glucose, 0.5 g L⁻¹ yeast extract, and 4.1 g L⁻¹ CH₃COONa; medium D (C/N ratio 34) was composed of 30.0 g L⁻¹ glucose, 0.5 g L⁻¹ yeast extract, and 5.0 g L⁻¹ peptone; medium E was composed of 1.0 g L⁻¹ yeast extract, 1.0 g L⁻¹ peptone, and 4.1 g L⁻¹ CH₃COONa; and medium G (C/N ratio 28) was composed of 60.0 g L⁻¹ glucose, 5.0 g L⁻¹ yeast extract, 5.0 g L⁻¹ peptone, and 4.1 g L⁻¹ CH₃COONa.

Brown algae hydrolysate (C/N ratio 85) was prepared by enzymatic hydrolysis of *Laminaria digitata* without any chemical pretreatment. Detailed information for the enzymatic hydrolysis is presented in our previous publication.⁴²

For *T. reesei* cultivation, medium F was composed of 10 g L⁻¹ *C. oleaginosus* cell wall, 10 g L⁻¹ yeast extract, 10.0 g L⁻¹ glucose, 1.4 g L⁻¹ (NH₄)₂SO₄, 2 g L⁻¹ KH₂PO₄, 0.4 g L⁻¹ CaCl₂·2H₂O, 0.3 g L⁻¹ MgSO₄·7H₂O, 0.005 g L⁻¹ FeSO₄·7H₂O, 0.004 g L⁻¹ CoCl₂·6H₂O, 0.003 g L⁻¹ MnSO₄·H₂O, and 0.002 g L⁻¹ ZnSO₄·7H₂O. Glucose was obtained from Roth-Germany (Art. No. 6780.2), yeast extract was obtained from PanReac AppliChem- Germany (A1552,1000), peptone from casein was obtained from Roth- Germany (Art. No. 8952.2), and other chemicals were obtained from Merck-Germany.

7.3 Bioreactors

For cultivation of *C. oleaginosus*, the following bioreactor systems were used: 1) a DASGIP four parallel bioreactor system (Eppendorf, Germany) with a working volume of 1 L (4× 1 L); 2) INFORS HT three parallel System (Switzerland) with a working volume of 3 L (3× 3 L); and 3) Bio-Engineer fermentation system (Bio-Engineer, USA) with a working volume of 50 L. The temperature was set to 28°C, and the pH of the bioreactor was adjusted to pH 6.5 ± 0.02 with 3 M NaOH or 70–100% (w/w) acetic acid. Stirring (350–800 rpm), oxygen ratio (21–100%), aeration (8.0–1.5 vvm), and pressure (1.25–1.5 bar) were regulated automatically to maintain dissolved oxygen at a pO₂ of 50% or more. Foam was prevented by the addition of 0.01% (v/v) of an antifoam agent (Antifoam 204; Merck). To evaluate reproducibility, each fermentation was carried out three times. The values are presented as averages, and each point was analysed in triplicate. Error bars represent the standard deviation.

7.4 Analysis and assays

7.4.1 Sugar, lipid, and fatty acid profiles; cell counting, and dry biomass analyses

Sugars consumption and release were analysed by high-performance liquid chromatography (HPLC; Agilent 1100 series) with a Rezex ROA-Organic Acid (Aminex HPX 87H) column. Biomass growth was monitored by measuring the optical density at 600 nm, using the gravimetric method (lyophilisation of 5×2 mL washed culture for 2 days [Christ alpha 2-4 LD Plus]), and using cell counting (FACS S3 [Bio-Rad, Germany]). Lipid content was analysed using the Blich-Dyer method.¹⁹⁰ Detailed procedures are described in our previous work.⁴² To evaluate reproducibility, all experiments were repeated three times. The values are presented as averages, and error bars represent standard deviations. Fatty acid profiles were measured using GC-FID (Shimadzu, Japan) after methylation. The methylation procedure and analysis set up were reported previously.⁴²

7.4.2 On-site production of yeast-specific cell wall hydrolases

The fermentation of *T. reesei* ATCC 56765 (RUT C-30) and ATCC 13631 was carried out in the Bio-Engineer fermentation system. Fermentation parameters were set according to a previously established protocol.²²⁴ Medium F was applied as the cultivation medium.

As part of medium F, the partially purified cell wall was prepared as follows. Briefly, after lipid extraction, residual *C. oleaginosus* biomass was washed with double distilled water three times, dried by lyophilisation for 2 days, ground, and then used as a hydrolase-inducing system in the *T. reesei* fermentation.

After fermentation, *T. reesei* biomass was removed by centrifugation. The resulting water phase (50 L supernatant) contained all secreted hydrolase enzymes, which were subsequently purified and concentrated by cross-flow filtration (10 kDa polyethersulfone filter; Pall). The final volume of the resulting hydrolase enzyme system was 1 L.

7.4.3 Flow cytometry-based cell counting

Cell counting via flow cytometry was carried out with a Bio-Rad S3 FACS (BioRad, Hercules, USA) equipped with 488 nm/ 100 mW laser beam. The counting was conducted using 100 μ l of sample after 100 times dilution. The cell density diagram describes Side scatter [SSC] on "Y" axis and Forward scatter [FSC] on the "X"-axis.

7.4.4 Cerium concentration measurement

Samples were first diluted 1:99 by mixing 50 μ l with 4.95 ml of deionized water. The measurement was then performed in a multi well plate with 100 μ l diluted sample mixed with 100 μ l buffer in each well. The buffer contained 100 mM sodium acetate, 10 mM copper (II), 10 mM nickel (II), and 10 mM lead (II). The pH was adjusted to 5.0 with glacial acetic acid. For every series of measurements, a calibration curve consisting of 4 points (cerium: 2.5 mM, 5 mM, 7.5 mM and 10 mM) was prepared the same way, as the samples. For measuring luminescence, a black quartz-glass 96-well microtiter plate manufactured by Hellma Analytics (Germany) and an EnSpire 2 Multimode Plate Reader (Perkin Elmer, USA) were used.

The reliability of the luminescence-based cerium detection method in presence of other metals has also been evaluated. To that end, triplicate samples with known copper concentration (10 mM, 20 mM and 40 mM) have been measured in the cerium concentration range 2.5 mM to 10 mM. All datasets can be described by a global linear regression curve with very good coefficients of determination (R-square) of 0.985 (Cu 40 mM) 0.987 (Cu 20 mM) and 0.992 (Cu 10 mM). The data plot with regression curve is depicted in the supplementary information (AE, 224, 2018, 1–12, Supplementary Fig. 15). The applicable limit for this method is about 1 mM cerium if interfering metals are present. For model samples containing only cerium the dilution factor can be decreased (until self-quenching occurs) leading to a limit of quantification (LOQ) at about 0.62 μ M with signals at 308 RFU compared to 193 +/- 12 RFU for the blank (AE, 224, 2018, 1–12, Supplementary Table 15). Notably, all metal chelating/binding agents should be eliminated from the assay solution. This was achieved, by repeated washing of the sample to eliminate any water-soluble components.

7.4.5 Hydrolase activity assays

Multiple hydrolase activities were detected in the on-site generated enzyme system. For yeast cell wall hydrolysis, activities of cellulase, xyloglucanase, β -glucosidase, mannanase, xylanase, and laminarinase were evaluated. Therefore, 50.0 mg cellulose, xyloglucan, cellobiose, mannan, xylan, and laminarin was incubated with 1 mL buffer (Na acetate, 50 mM, pH 5.0) and 0.35% (w/w_{biomass}) enzyme solution. To test the enzyme activity of *C. oleaginosus* biomass, 50.0 mg of partially purified cell wall was incubated with 1 mL buffer (Na acetate, 50 mM, pH 5.0) and 0.35% (w/w_{biomass}) enzyme solution. All tests were incubated for 28 h at 50°C. Gravimetric /sugar analyses (HPLC) were used after hydrolysis.

To evaluate the performance of the on-site generated system, a tailored hydrolase system with regard to commercial equivalents, we conducted comparative experiments. The evaluated commercial enzyme systems were

as follows: mix 1 (mannanase [Clariant, Switzerland], Cellic Ctec2 [Novozymes, Denmark], Cellic Htec [Novozymes], and β -glucosidase [Novozymes]); mix 2 (Liquebeet [Clariant], CLA [Clariant], mannanase [Clariant], 1.3- β -glucanase [Megazyme, France], and β -glucosidase [Novozymes]). To ensure reproducibility, all experiments were conducted in triplicate. The reported values are presented as averages, and error bars represent standard deviations.

7.4.6 Determination of total dissolved solids and elemental analysis

Total dissolved solids [TDS] and element analysis was carried by drying 100.0 ml of the hydrolysate at 105°C (overnight). Resulting crystals were incinerated at 1500°C for 3 hours. Obtained ash material was subjected to scanning electron microscopy (SEM) with energy-dispersive X-ray (EDX) analysis using a JSM-7500F scanning electron microscope (JEOL, Japan). Crystals were mounted on carbon film and prepped for analysis. EDX analysis was performed on multiple areas (100 × 100 μm) in backscattered electron (BSE) mode for each ash sample. The average value was calculated to obtain the elemental composition for the ash of the hydrolysate.

7.5 Techno-economic analysis

Techno-economic analysis (TEA) was carried out to estimate the total capital investment and operating cost for process flowsheets that could be used for the production of lipids from oily yeast.

As there is a lack of major databases (such as NREL) for process design related to oleaginous yeasts oil production, process and economic data were collected from current results and those reported in the available literature,^{175, 225, 226, 227} as well as integrated mathematical functions in SuperPro Designer version 10 (Intelligen, Inc., Scotch Plains, NJ, USA).^{228, 229}

The *in-silico* process simulation created a production plant with an annual lipid production capacity of 23,000 metric tonnes. The required feedstock (i.e., acetic acid, glucose, and amino acids) and chemicals were estimated based on current media compositions and the results of the current work. The individual yeast biomass, lipid formation, and enzymatic hydrolysis are represented by respective equations in the supplementary data. The built-in material and energy balance data in SPD were applied to determine the required equipment sizing and respective purchasing prices.

Therefore, the simulated plant consisted of multiple unit operations, encompassing feed handling, fermentation, hydrolysis, product recovery, and side-product recycling. Hence, 11 fermenters (10 in use, one as standby, 250 m³ each), four stirred tank reactors for *C. oleagnosus* lysis and lipid mobilization (three in use, one as standby, 250 m³ each), five bending/storage/receiving tanks (250 m³ each), three decanter centrifuges (two in use, one as standby, 159920 L h⁻¹ each), a centrifugal compressor, an air filter, and an ultrafiltration unit were modelled in SPD (see the simplified process flow diagram in **EES, 2019, 12, 2717, Fig. S8**). The standby units were included to avoid maintenance-based downtime.

Major process parameters and assumptions applied to develop the process model and determine the required materials, energy, and costs are presented in, **EES, 2019, 12, 2717, Table S2**.

As lipid productivity had the highest impact on cost with respect to all other process parameters, the baseline scenario was established based on harvesting 4 days after initiation of the fermentation process. Thus, baseline lipid productivity was approximately 1.4 g L⁻¹ h⁻¹ (biomass: 200 g L⁻¹, lipids: 85% [$w_{\text{lipid}}/d w_{\text{biomass}}$], after 120 h). However, the optimal scenario was consistent with the best productivity reported in this study, which was 2.4 g L⁻¹ h⁻¹ (biomass: 147 g L⁻¹, lipids: 73% [$w_{\text{lipid}}/d w_{\text{biomass}}$], after 42 h). These productivity values represented the average value of six biological replications with \pm 5% relative standard deviation (**EES, 2019, 12, 2717, Fig. S13**). **EES, 2019, 12, 2717, Figs. S9–S11** show data for the sensitivity analysis during lipid productivity.

An internal SPD mathematical function adjusted the equipment purchase cost (PC) based on the required process equipment sizing with respect to the analysis year (2018).²³⁰ Relevant installation cost factors of 1.6 and 1.8, derived from the initial PC, were extracted from a very detailed biomass conversion focused TEA study.^{229, 231} Process piping, warehouse and site development were estimated as 4.5, 4.4 and 9.0% of the inside-battery-limit (ISBL) equipment costs respectively.²³¹ The indirect plant costs, including engineering and construction, were estimated as 20% and 10% of total direct cost (TDC), respectively, where TDC is defined as PC plus installation cost plus process piping.²³¹ A capital interest factor of 6% was added to the total capital investment. The annual operating cost was estimated by the facility-dependent cost (including maintenance) as 3% of TDC.²³¹ The operator cost was adjusted to German full-cost tariff TV-L 11, 13, and 14.²³² Raw material costs were estimated based on the available whole-sale market price. The cooperate insurance was calculated as 0.7% of the total capital investment (TCI).²³¹ A detailed cost analysis is presented in **EES, 2019, 12, 2717, Tables S3–S11**.

7.6 Life-cycle for global warming potential (GWP)

The life cycle and environmental analysis (LCA) for the entire process chain described in this study was investigated in order to identify environmental process hotspots that could indicate whether the yeast products were a viable alternative to conventional plant oils. An attributional cradle-to-gate assessment of a fully integrated, commercial-scale yeast lipid production unit based on the data presented in the TEA section was performed. Allocation was not applied. All side product streams were entirely recycled within a process loop. The underlying models were based on experimental data generated within the project (lab-scale) and fed into process simulation models for the initial TEA analysis; all other required datasets were complemented by literature data (e.g., transport). The environmental data are based on publicly available LCA databases, such as US LCI²³³ and the BioEnergieDat²³⁴ database. The mass balance for the functional unit of 1 kg oil is illustrated in **EES, 2019, 12, 2717, Fig. S15**. This Sankey diagram of the complete process chain highlights two aspects: the large share of acetic acid as a feedstock and the importance of medium recycling for process efficiency. *In-papyro*, the model reflected a simulated business case in North Germany near the North Sea coast, designed with minimal land requirements in order to avoid competition with food production. The model also included all processes from sourcing initial feedstocks, such as acetic acid and macroalgae carbohydrates, followed by processing steps that encompasses yeast fermentation, side-stream recycling, and subsequent downstream processing for lipid production. The algae *L. digitata* could be collected by tractor and subsequently hydrolysed. Transport of feedstocks was included in the analysis. However, like numerous other LCA studies^{235, 236}, infrastructure, such as fermenters and centrifuges, was not considered. Moreover, chemicals, such as sodium hydroxide, calcium chloride, magnesium sulphate, and other inorganic chemical components required for growth medium and process cleaning activities, were excluded from the LCA matrix because they were used in minor amounts that did not affect the overall material flow. The full system boundary is depicted in **EES, 2019, 12, 2717, Fig. S14c**. The impact analysis, as defined in the process flow diagram (**EES, 2019, 12, 2717, Fig. S14c**), was calculated based on the CML method (Faculty of Science in Leiden University method [Centrum voor Milieuwetenschappen, V4.4, 2015]); however, because of its relevance, this publication concentrates on the global warming potential. The life cycle inventory is documented in the supplementary data (**EES, 2019, 12, 2717, Tables S12–S21**).

8 References

1. W. Steffen, P. J. Crutzen and J. R. McNeill, *AMBIO: A Journal of the Human Environment*, 2007, **36**, 614-622.
2. W. Steffen, W. Broadgate, L. Deutsch, O. Gaffney and C. Ludwig, *The Anthropocene Review*, 2015, **2**, 81-98.
3. P. M. Vitousek, H. A. Mooney, J. Lubchenco and J. M. Melillo, *Science*, 1997, **277**, 494-499.
4. J. Fargione, J. Hill, D. Tilman, S. Polasky and P. Hawthorne, *Science*, 2008, **319**, 1235-1238.
5. T. Searchinger, R. Heimlich, R. A. Houghton, F. Dong, A. Elobeid, J. Fabiosa, S. Tokgoz, D. Hayes and T.-H. Yu, *Science*, 2008, **319**, 1238-1240.
6. T. Newbold, L. N. Hudson, S. L. Hill, S. Contu, I. Lysenko, R. A. Senior, L. Börger, D. J. Bennett, A. Choimes and B. Collen, *Nature*, 2015, **520**, 45.
7. I. T. I. R. L. o. T. S. V. 2016-2., <http://www.iucnredlist.org>, (accessed 2016, 2016).
8. J. K. McKee, P. W. Sciulli, C. D. Foose and T. A. Waite, *Biological Conservation*, 2004, **115**, 161-164.
9. S. Pinzi, D. Leiva, I. López-García, M. D. Redel-Macías and M. P. Dorado, *Biofuels, Bioproducts and Biorefining*, 2014, **8**, 126-143.
10. A. Yaguchi, A. Robinson, E. Mihealsick and M. Blenner, *Microbial cell factories*, 2017, **16**, 206.
11. G. M. Rodriguez, M. S. Hussain, L. Gambill, D. Gao, A. Yaguchi and M. Blenner, *Biotechnology for biofuels*, 2016, **9**, 149.
12. U. N. G. Assembly, *Journal*, 2005.
13. M. Spagnuolo, A. Yaguchi and M. Blenner, *Current opinion in biotechnology*, 2019, **57**, 73-81.
14. C. A. Santos and A. Reis, *Applied microbiology and biotechnology*, 2014, **98**, 5839-5846.
15. H. Shen, Z. Gong, X. Yang, G. Jin, F. Bai and Z. K. Zhao, *Journal of biotechnology*, 2013, **168**, 85-89.
16. I. R. Sitepu, L. A. Garay, R. Sestric, D. Levin, D. E. Block, J. B. German and K. L. Boundy-Mills, *Biotechnology advances*, 2014, **32**, 1336-1360.
17. G. Munch, R. Sestric, R. Sparling, D. B. Levin and N. Cicek, *Bioresource technology*, 2015, **185**, 49-55.
18. M. Spagnuolo, M. S. Hussain, L. Gambill and M. Blenner, *Frontiers in microbiology*, 2018, **9**.
19. C. Li, K. Lesnik and H. Liu, *Energies*, 2013, **6**, 4739-4768.
20. H. El Bialy, O. M. Goma and K. S. Azab, *World Journal of Microbiology and Biotechnology*, 2011, **27**, 2791-2798.
21. P. Fontanille, V. Kumar, G. Christophe, R. Nouaille and C. Larroche, *Bioresource technology*, 2012, **114**, 443-449.
22. X.-F. Huang, J.-N. Liu, L.-J. Lu, K.-M. Peng, G.-X. Yang and J. Liu, *Bioresource technology*, 2016, **206**, 141-149.
23. X. Xu, J. Y. Kim, H. U. Cho, H. R. Park and J. M. Park, *Chemical Engineering Journal*, 2015, **264**, 735-743.
24. S. Vajpeyi and K. Chandran, *Bioresource technology*, 2015, **188**, 49-55.
25. J. Brandenburg, J. Blomqvist, J. Pickova, N. Bonturi, M. Sandgren and V. Passoth, *Yeast*, 2016, **33**, 451-462.
26. K. V. Probst and P. V. Vadlani, *Bioresource technology*, 2015, **198**, 268-275.
27. P. J. Slininger, B. S. Dien, C. P. Kurtzman, B. R. Moser, E. L. Bakota, S. R. Thompson, P. J. O'Bryan, M. A. Cotta, V. Balan and M. Jin, *Biotechnology and bioengineering*, 2016, **113**, 1676-1690.
28. L. Qin, L. Liu, A.-P. Zeng and D. Wei, *Bioresource technology*, 2017, **245**, 1507-1519.
29. A. Yaguchi, M. Spagnuolo and M. Blenner, *Current opinion in biotechnology*, 2018, **53**, 122-129.
30. I. K. Chung, J. Beardall, S. Mehta, D. Sahoo and S. Stojkovic, *Journal of Applied Phycology*, 2011, **23**, 877-886.
31. S. Beer and E. Koch, *Marine Ecology Progress Series*, 1996, **141**, 199-204.
32. B. Subhadra and M. Edwards, *Energy Policy*, 2010, **38**, 4897-4902.
33. K. Gao and K. R. McKinley, *Journal of Applied Phycology*, 1994, **6**, 45-60.
34. J. W. Fourqurean, C. M. Duarte, H. Kennedy, N. Marbà, M. Holmer, M. A. Mateo, E. T. Apostolaki, G. A. Kendrick, D. Krause-Jensen and K. J. McGlathery, *Nature geoscience*, 2012, **5**, 505.
35. N. Wei, J. Quarterman and Y.-S. Jin, *Trends in biotechnology*, 2013, **31**, 70-77.
36. K. A. Jung, S.-R. Lim, Y. Kim and J. M. Park, *Bioresource technology*, 2013, **135**, 182-190.
37. H. J. Bixler and H. Porse, *Journal of applied Phycology*, 2011, **23**, 321-335.
38. J. Cebrián, C. M. Duarte and N. Marbà, *Journal of Experimental Marine Biology and Ecology*, 1996, **204**, 103-111.
39. M. Uchida, T. Miyoshi, M. Kaneniwa, K. Ishihara, Y. Nakashimada and N. Urano, *Journal of bioscience and bioengineering*, 2014, **118**, 646-650.
40. A. Meo, X. L. Priebe and D. Weuster-Botz, *Journal of biotechnology*, 2017, **241**, 1-10.
41. M. A. Masri, S. Younes, M. Haack, F. Qoura, N. Mehlmer and T. Brück, *Energy Technology*, 2018.
42. M. Mahmoud, Y. Samer, H. Martina, Q. Farah, M. Norbert and B. Thomas, *Energy Technology*, 2018, **6**, 1026-1038.
43. J. Chen, X. Zhang, R. D. Tyagi and P. Drogui, *Bioresource technology*, 2018, **253**, 8-15.
44. F. Bauer and C. Hulteberg, *Biofuels, Bioproducts and Biorefining*, 2013, **7**, 43-51.
45. L. Signori, D. Ami, R. Posterl, A. Giuzzi, P. Mereghetti, D. Porro and P. Branduardi, *Microbial cell factories*, 2016, **15**, 75.
46. F. Spier, J. G. Buffon and C. A. Burkert, *Indian journal of microbiology*, 2015, **55**, 415-422.
47. Y. Liang, Y. Cui, J. Trushenski and J. W. Blackburn, *Bioresource technology*, 2010, **101**, 7581-7586.
48. J. Xu, X. Zhao, W. Wang, W. Du and D. Liu, *Biochemical engineering journal*, 2012, **65**, 30-36.

49. J. H. Sim, A. H. Kamaruddin, W. S. Long and G. Najafpour, *Enzyme and microbial technology*, 2007, **40**, 1234-1243.
50. J. L. Gaddy, *Journal*, 1997.
51. M. Straub, M. Demler, D. Weuster-Botz and P. Dürre, *Journal of biotechnology*, 2014, **178**, 67-72.
52. P. Pal and J. Nayak, *Separation & Purification Reviews*, 2017, **46**, 44-61.
53. E. V. LaBelle and H. D. May, *Frontiers in microbiology*, 2017, **8**.
54. Z. Gong, H. Shen, W. Zhou, Y. Wang, X. Yang and Z. K. Zhao, *Biotechnology for biofuels*, 2015, **8**, 189.
55. Z. Chi, Y. Zheng, J. Ma and S. Chen, *international journal of hydrogen energy*, 2011, **36**, 9542-9550.
56. V. Béligon, L. Poughon, G. Christophe, A. Lebert, C. Larroche and P. Fontanille, *Bioresource technology*, 2015, **192**, 582-591.
57. Z. Gong, W. Zhou, H. Shen, Z. Yang, G. Wang, Z. Zuo, Y. Hou and Z. K. Zhao, *Bioresource technology*, 2016, **207**, 102-108.
58. G. W. Park, H. N. Chang, K. Jung, C. Seo, Y.-C. Kim, J. H. Choi, H. C. Woo and I.-j. Hwang, *Process Biochemistry*, 2017, **56**, 147-153.
59. J. Liu, M. Yuan, J.-N. Liu and X.-F. Huang, *Bioresource technology*, 2017, **241**, 645-651.
60. M. A. J. T. i. c. b. Welte, 2007, **17**, 363-369.
61. D. J. Murphy and J. J. T. i. b. s. Vance, 1999, **24**, 109-115.
62. D. Zweytick, K. Athenstaedt and G. J. B. e. B. A.-R. o. B. Daum, 2000, **1469**, 101-120.
63. Y. Ohsaki, M. Suzuki, T. J. C. Fujimoto and biology, 2014, **21**, 86-96.
64. D. J. J. P. i. l. r. Murphy, 2001, **40**, 325-438.
65. T. Czabany, A. Wagner, D. Zweytick, K. Lohner, E. Leitner, E. Ingolic and G. J. J. o. B. C. Daum, 2008, **283**, 17065-17074.
66. K. Tauchi-Sato, S. Ozeki, T. Houjou, R. Taguchi and T. J. J. o. B. C. Fujimoto, 2002, **277**, 44507-44512.
67. W. M. Henne, M. L. Reese and J. M. Goodman, *The EMBO journal*, 2018, **37**, e98947.
68. H.-C. Wan, R. C. Melo, Z. Jin, A. M. Dvorak and P. F. J. T. F. J. Weller, 2007, **21**, 167-178.
69. R. C. Melo, H. D'Avila, H.-C. Wan, P. T. Bozza, A. M. Dvorak, P. F. J. J. o. H. Weller and Cytochemistry, 2011, **59**, 540-556.
70. R. Bartz, W.-H. Li, B. Venables, J. K. Zehmer, M. R. Roth, R. Welti, R. G. Anderson, P. Liu and K. D. J. J. o. l. r. Chapman, 2007, **48**, 837-847.
71. M. Radulovic, O. Knittelfelder, A. Cristobal-Sarramian, D. Kolb, H. Wolinski and S. D. Kohlwein, *Current genetics*, 2013, **59**, 231-242.
72. K. Grillitsch, M. Connerth, H. Köfeler, T. N. Arrey, B. Rietschel, B. Wagner, M. Karas and G. Daum, *Biochimica et Biophysica Acta (BBA)-Molecular and Cell Biology of Lipids*, 2011, **1811**, 1165-1176.
73. R. Schneiter, B. Brügger, R. Sandhoff, G. Zellnig, A. Leber, M. Lampl, K. Athenstaedt, C. Hrastnik, S. Eder and G. Daum, *The Journal of cell biology*, 1999, **146**, 741-754.
74. R. Bartz, W.-H. Li, B. Venables, J. K. Zehmer, M. R. Roth, R. Welti, R. G. Anderson, P. Liu and K. D. Chapman, *Journal of lipid research*, 2007, **48**, 837-847.
75. A. Kassan, A. Herms, A. Fernández-Vidal, M. Bosch, N. L. Schieber, B. J. Reddy, A. Fajardo, M. Gelabert-Baldrich, F. Tebar and C. J. J. C. B. Enrich, 2013, **203**, 985-1001.
76. W. Fei, H. Wang, X. Fu, C. Bielby and H. J. B. J. Yang, 2009, **424**, 61-67.
77. W. Fei, G. Shui, B. Gaeta, X. Du, L. Kuerschner, P. Li, A. J. Brown, M. R. Wenk, R. G. Parton and H. J. J. C. B. Yang, 2008, **180**, 473-482.
78. W. Fei, G. Shui, Y. Zhang, N. Krahmer, C. Ferguson, T. S. Kapterian, R. C. Lin, I. W. Dawes, A. J. Brown and P. J. P. g. Li, 2011, **7**, e1002201.
79. C.-W. Wang, Y.-H. Miao and Y.-S. Chang, *J Cell Sci*, 2014, **127**, 1214-1228.
80. M. A. Masri, D. Garbe, N. Mehlmer and T. B. Brück, *Energy & Environmental Science*, 2019, **12**, 2717-2732.
81. S. R. Bartholomew, E. H. Bell, T. Summerfield, L. C. Newman, E. L. Miller, B. Patterson, Z. P. Niday, W. E. Ackerman IV, J. T. J. B. e. B. A.-M. Tansey and C. B. o. Lipids, 2012, **1821**, 268-278.
82. K. Takahashi, N. Sasabe, K. Ohshima, K. Kitazato, R. Kato, Y. Masuda, M. Tsurumaki, T. Obama, S.-i. Okudaira and J. J. J. o. l. r. Aoki, 2010, **51**, 2571-2580.
83. H. Yang, A. Galea, V. Sytnyk and M. J. C. o. i. c. b. Crossley, 2012, **24**, 509-516.
84. M. Casal, O. Queirós, G. Talaia, D. Ribas and S. Paiva, in *Yeast membrane transport*, Springer, 2016, pp. 229-251.
85. S. Giannattasio, N. Guaragnella, M. Ždravčić and E. J. F. i. m. Marra, 2013, **4**, 33.
86. S. Bellou, I.-E. Triantaphyllidou, D. Aggeli, A. M. Elazzazy, M. N. Baeshen and G. J. C. o. i. B. Aggelis, 2016, **37**, 24-35.
87. R. Kourist, F. Bracharz, J. Lorenzen, O. N. Kracht, M. Chovatia, C. Daum, S. Deshpande, A. Lipzen, M. Nolan and R. A. Ohm, *mBio*, 2015, **6**, e00918-00915.
88. P. Piper, C. O. Calderon, K. Hatzixanthis and M. Mollapour, *Microbiology*, 2001, **147**, 2635-2642.
89. N. Guaragnella, S. Passarella, E. Marra and S. J. F. I. Giannattasio, 2010, **584**, 3655-3660.
90. S. Giannattasio, N. Guaragnella, M. Ždravčić and E. Marra, *Frontiers in Microbiology*, 2013, **4**.
91. R. Ramanan, B.-H. Kim, D.-H. Cho, S.-R. Ko, H.-M. Oh and H.-S. J. F. I. Kim, 2013, **587**, 370-377.
92. J. Yan, R. Cheng, X. Lin, S. You, K. Li, H. Rong, Y. J. A. m. Ma and biotechnology, 2013, **97**, 1933-1939.
93. S. Papanikolaou and G. Aggelis, *European Journal of Lipid Science and Technology*, 2011, **113**, 1031-1051.
94. S. De Cima, J. Rúa, E. Perdiguero, P. del Valle, F. Busto, A. Baroja-Mazo and D. de Arriaga, *Research in microbiology*, 2005, **156**, 663-669.
95. M. Tai and G. J. M. e. Stephanopoulos, 2013, **15**, 1-9.
96. K. Tamano, K. S. Bruno, S. A. Karagiosis, D. E. Culley, S. Deng, J. R. Collett, M. Umemura, H. Koike, S. E. Baker, M. J. A. m. Machida and biotechnology, 2013, **97**, 269-281.
97. I. B. Lomakin, Y. Xiong and T. A. J. C. Steitz, 2007, **129**, 319-332.

98. F. LYNEN, H. Engeser, E. C. Foerster, J. L. Fox, S. Hess, G. B. Kresze, T. Schmitt, T. Schreckenbach, E. Siess and F. J. E. j. o. b. Wieland, 1980, **112**, 431-442.
99. F. Fichtlscherer, C. Wellein, M. Mittag and E. J. E. j. o. b. Schweizer, 2000, **267**, 2666-2671.
100. C. J. B. I. Ratledge, 2014, **36**, 1557-1568.
101. Z. Li, H. Sun, X. Mo, X. Li, B. Xu, P. J. A. m. Tian and biotechnology, 2013, **97**, 4927-4936.
102. T. M. Wasylenko, W. S. Ahn and G. J. M. e. Stephanopoulos, 2015, **30**, 27-39.
103. A. Lei, H. Chen, G. Shen, Z. Hu, L. Chen and J. J. B. f. B. Wang, 2012, **5**, 18.
104. W. Runguphan and J. D. J. M. e. Keasling, 2014, **21**, 103-113.
105. M. Certik, S. J. J. o. b. Shimizu and bioengineering, 1999, **87**, 1-14.
106. S. Tavares, T. Grotkjær, T. Obsen, R. P. Haslam, J. A. Napier and N. J. A. E. M. Gunnarsson, 2011, **77**, 1854-1861.
107. L.-T. Chuang, D.-C. Chen, J.-M. Nicaud, C. Madzak, Y.-H. Chen and Y.-S. J. N. b. Huang, 2010, **27**, 277-282.
108. H. G. Damude, P. J. Gillies, D. J. Macool, S. K. Picataggio, J. J. Raghianti, J. E. Seip, Z. Xue, N. S. Yadav, H. Zhang and Q. Q. Zhu, *Journal*, 2014.
109. H. G. Damude, H. Zhang, L. Farrall, K. G. Ripp, J.-F. Tomb, D. Hollerbach and N. S. J. P. o. t. N. A. o. S. Yadav, 2006, **103**, 9446-9451.
110. D. Xie, E. N. Jackson, Q. J. A. m. Zhu and biotechnology, 2015, **99**, 1599-1610.
111. Z. Xue, P. L. Sharpe, S.-P. Hong, N. S. Yadav, D. Xie, D. R. Short, H. G. Damude, R. A. Rupert, J. E. Seip and J. J. N. b. Wang, 2013, **31**, 734.
112. C. Görner, V. Redai, F. Bracharz, P. Schrepfer, D. Garbe and T. J. G. C. Brück, 2016, **18**, 2037-2046.
113. C. Ferreira, F. van Voorst, A. Martins, L. Neves, R. Oliveira, M. C. Kielland-Brandt, C. Lucas and A. Brandt, *Molecular Biology of the Cell*, 2005, **16**, 2068-2076.
114. M. Klein, S. Swinnen, J. M. Thevelein and E. Nevoigt, *Environmental microbiology*, 2017, **19**, 878-893.
115. M. Turk and C. Gostinčar, *Fungal biology*, 2018, **122**, 63-73.
116. T. Dulermo and J.-M. J. M. e. Nicaud, 2011, **13**, 482-491.
117. E. P. Kennedy, 1961.
118. S. B. Weiss and E. P. J. J. o. t. A. C. S. Kennedy, 1956, **78**, 3550-3550.
119. Z. Zheng and J. Zou, *Journal of Biological Chemistry*, 2001, **276**, 41710-41716.
120. G.-S. Han, W.-I. Wu and G. M. Carman, *Journal of Biological Chemistry*, 2006, **281**, 9210-9218.
121. G. M. Carman and G.-S. Han, *Trends in biochemical sciences*, 2006, **31**, 694-699.
122. A. Dahlqvist, U. Ståhl, M. Lenman, A. Banas, M. Lee, L. Sandager, H. Ronne and S. Stymne, *Proceedings of the National Academy of Sciences*, 2000, **97**, 6487-6492.
123. P. Oelkers, A. Tinkelenberg, N. Erdeniz, D. Cromley, J. T. Billheimer and S. L. Sturley, *Journal of Biological Chemistry*, 2000, **275**, 15609-15612.
124. A. A. Wendel, T. M. Lewin, R. A. J. B. e. B. A.-M. Coleman and C. B. o. Lipids, 2009, **1791**, 501-506.
125. R. Jain, M. Coffey, K. Lai, A. Kumar and S. MacKenzie, *Journal*, 2000.
126. Y. Kamisaka, K. Kimura, H. Uemura and M. Yamaoka, *Applied microbiology and biotechnology*, 2013, **97**, 7345-7355.
127. M. S. Greer, M. Truksa, W. Deng, S.-C. Lung, G. Chen and R. J. Weselake, *Applied microbiology and biotechnology*, 2015, **99**, 2243-2253.
128. J. Blazeck, A. Hill, L. Liu, R. Knight, J. Miller, A. Pan, P. Otoupal and H. S. J. N. c. Alper, 2014, **5**, 3131.
129. S. D. Kohlwein, *Journal of Biological Chemistry*, 2010, **285**, 15663-15667.
130. J. R. Skinner, T. M. Shew, D. M. Schwartz, A. Tzekov, C. M. Lepus, N. A. Abumrad and N. E. Wolins, *Journal of Biological Chemistry*, 2009, **284**, 30941-30948.
131. P. Oelkers, D. Cromley, M. Padamsee, J. T. Billheimer and S. L. Sturley, *Journal of Biological Chemistry*, 2002, **277**, 8877-8881.
132. M. Galiotou-Panayotou, O. Kalantzi and G. Aggelis, *Antonie Van Leeuwenhoek*, 1998, **73**, 155-162.
133. H. Gorrissen, A. P. Tulloch, R. J. J. C. Cushley and p. o. lipids, 1982, **31**, 245-255.
134. W. B. Mackinnon, G. L. May and C. E. J. E. j. o. b. Mountford, 1992, **205**, 827-839.
135. N. J. King, E. J. Delikatny and K. T. J. I. Holmes, 1994, **4**, 188-198.
136. V. Choudhary, N. Ojha, A. Golden and W. A. Prinz, *J Cell Biol*, 2015, **211**, 261-271.
137. H. Wang, M. Becuwe, B. E. Housden, C. Chitruja, A. J. Porras, M. M. Graham, X. N. Liu, A. R. Thiam, D. B. Savage and A. K. Agarwal, *Elife*, 2016, **5**, e16582.
138. A. Chorlay and A. R. Thiam, *Biophysical journal*, 2018, **114**, 631-640.
139. J. Zanghellini, F. Wodlei and H. Von Grünberg, *Journal of theoretical biology*, 2010, **264**, 952-961.
140. Q. Gao, D. D. Binns, L. N. Kinch, N. V. Grishin, N. Ortiz, X. Chen and J. M. Goodman, *J Cell Biol*, 2017, **216**, 3199-3217.
141. N. Jacquier, V. Choudhary, M. Mari, A. Toulmay, F. Reggiori and R. Schneiter, *J Cell Sci*, 2011, **124**, 2424-2437.
142. N. Jacquier, V. Choudhary, M. Mari, A. Toulmay, F. Reggiori and R. J. J. C. S. Schneiter, 2011, **124**, 2424-2437.
143. F. Wilfling, J. T. Haas, T. C. Walther and R. V. J. C. o. i. c. b. Farese Jr, 2014, **29**, 39-45.
144. A. R. Thiam, R. V. Farese Jr and T. C. J. N. r. M. c. b. Walther, 2013, **14**, 775.
145. T. Fujimoto, Y. Ohsaki, J. Cheng, M. Suzuki, Y. J. H. Shinohara and c. biology, 2008, **130**, 263-279.
146. T. C. Walther and R. V. J. A. r. o. b. Farese Jr, 2012, **81**, 687-714.
147. K. G. Soni, G. A. Mardones, R. Sougrat, E. Smirnova, C. L. Jackson and J. S. J. J. o. c. s. Bonifacino, 2009, **122**, 1834-1841.
148. F. Wilfling, A. R. Thiam, M.-J. Olarte, J. Wang, R. Beck, T. J. Gould, E. S. Allgeyer, F. Pincet, J. Bewersdorf and R. V. J. E. Farese Jr, 2014, **3**, e01607.
149. F. Wilfling, H. Wang, J. T. Haas, N. Krahmer, T. J. Gould, A. Uchida, J.-X. Cheng, M. Graham, R. Christiano and F. J. D. c. Fröhlich, 2013, **24**, 384-399.

150. C. Thiele and J. Spandl, *Current opinion in cell biology*, 2008, **20**, 378-385.
151. L. V. Chernomordik and M. M. Kozlov, *Cell*, 2005, **123**, 375-382.
152. N. Krahmer, Y. Guo, F. Wilfling, M. Hilger, S. Lingrell, K. Heger, H. W. Newman, M. Schmidt-Supprian, D. E. Vance and M. J. C. m. Mann, 2011, **14**, 504-515.
153. S. Murphy, S. Martin and R. G. Parton, 2010.
154. A. R. Thiam, B. Antonny, J. Wang, J. Delacotte, F. Wilfling, T. C. Walther, R. Beck, J. E. Rothman and F. J. P. o. t. N. A. o. S. Pincet, 2013, **110**, 13244-13249.
155. J. Gong, Z. Sun, L. Wu, W. Xu, N. Schieber, D. Xu, G. Shui, H. Yang, R. G. Parton and P. J. J. C. B. Li, 2011, **195**, 953-963.
156. T. H. M. Grahn, R. Kaur, J. Yin, M. Schweiger, V. M. Sharma, M.-J. Lee, Y. Ido, C. M. Smas, R. Zechner and A. Lass, *Journal of Biological Chemistry*, 2014, **289**, 12029-12039.
157. Y. Guo, T. C. Walther, M. Rao, N. Stuurman, G. Goshima, K. Terayama, J. S. Wong, R. D. Vale, P. Walter and R. V. J. N. Farese, 2008, **453**, 657.
158. N. E. Wolins, J. R. Skinner, M. J. Schoenfish, A. Tzekov, K. G. Bensch and P. E. J. J. o. B. C. Bickel, 2003, **278**, 37713-37721.
159. J. Gong, Z. Sun and P. J. C. o. i. l. Li, 2009, **20**, 121-126.
160. D. L. J. J. o. l. r. Brasaemle, 2007, **48**, 2547-2559.
161. D. L. Brasaemle and N. E. J. J. o. B. C. Wolins, 2012, **287**, 2273-2279.
162. J. Tansey, C. Sztalryd, J. Gruia-Gray, D. Roush, J. Zee, O. Gavrilova, M. Reitman, C.-X. Deng, C. Li and A. Kimmel, *Proceedings of the National Academy of Sciences*, 2001, **98**, 6494-6499.
163. J. Martinez-Botas, J. B. Anderson, D. Tessier, A. Lapillonne, B. H.-J. Chang, M. J. Quast, D. Gorenstein, K.-H. Chen and L. Chan, *Nature genetics*, 2000, **26**, 474.
164. N. E. Wolins, D. L. Brasaemle and P. E. J. F. I. Bickel, 2006, **580**, 5484-5491.
165. N. Jacquier, S. Mishra, V. Choudhary and R. Schneiter, *J Cell Sci*, 2013, **126**, 5198-5209.
166. N. Jacquier, S. Mishra, V. Choudhary and R. J. J. C. S. Schneiter, 2013, **126**, 5198-5209.
167. Z. Sun, J. Gong, H. Wu, W. Xu, L. Wu, D. Xu, J. Gao, J.-w. Wu, H. Yang and M. Yang, *Nature communications*, 2013, **4**, 1594.
168. W. Fei, X. Du and H. Yang, *Trends in Endocrinology & Metabolism*, 2011, **22**, 204-210.
169. W. Fei, H. Li, G. Shui, T. S. Kapterian, C. Bielby, X. Du, A. J. Brown, P. Li, M. R. Wenk and P. Liu, *Journal of lipid research*, 2011, **52**, 2136-2147.
170. D. A. Gross, E. L. Snapp and D. L. J. P. o. Silver, 2010, **5**, e10796.
171. M. Milewska, J. McRedmond and P. C. J. J. o. n. Byrne, 2009, **111**, 1022-1030.
172. E. J. Klemm, E. Spooner and H. L. J. J. o. B. C. Ploegh, 2011, **286**, 37602-37614.
173. S. Y. Bu, M. T. Mashek and D. G. J. J. o. B. C. Mashek, 2009, **284**, 30474-30483.
174. C. Ratledge and Z. Cohen, *Lipid Technology*, 2008, **20**, 155-160.
175. A. A. Koutinas, A. Chatzifragkou, N. Kopsahelis, S. Papanikolaou and I. K. Kookos, *Fuel*, 2014, **116**, 566-577.
176. M. Jin, P. J. Slininger, B. S. Dien, S. Waghmode, B. R. Moser, A. Orjuela, L. da Costa Sousa and V. Balan, *Trends in biotechnology*, 2015, **33**, 43-54.
177. D. F. Markgraf, R. W. Klemm, M. Junker, H. K. Hannibal-Bach, C. S. Ejsing and T. A. Rapoport, *Cell reports*, 2014, **6**, 44-55.
178. A. D. Barbosa, H. Sembongi, W.-M. Su, S. Abreu, F. Reggiori, G. M. Carman and S. Sinioglou, *Molecular biology of the cell*, 2015, **26**, 3641-3657.
179. B. S. Dien, J. Zhu, P. J. Slininger, C. P. Kurtzman, B. R. Moser, P. J. O'Bryan, R. Gleisner and M. A. Cotta, *RSC Advances*, 2016, **6**, 20695-20705.
180. S. Harde, Z. Wang, M. Horne, J. Zhu and X. Pan, *Fuel*, 2016, **175**, 64-74.
181. E. Palmqvist and B. Hahn-Hägerdal, *Bioresource technology*, 2000, **74**, 25-33.
182. A. Ahmad, N. M. Yasin, C. Derek and J. Lim, *Environmental technology*, 2014, **35**, 2244-2253.
183. Z. Li, L. Zhang, X. Shen, B. Lai and S. Sun, *Wei sheng wu xue tong bao*, 2000, **28**, 72-75.
184. J. Kim, G. Yoo, H. Lee, J. Lim, K. Kim, C. W. Kim, M. S. Park and J.-W. Yang, *Biotechnology advances*, 2013, **31**, 862-876.
185. G. Jin, F. Yang, C. Hu, H. Shen and Z. K. Zhao, *Bioresource technology*, 2012, **111**, 378-382.
186. K. de Boer, N. R. Moheimani, M. A. Borowitzka and P. A. Bahri, *Journal of Applied Phycology*, 2012, **24**, 1681-1698.
187. J.-Y. You, C. Peng, X. Liu, X.-J. Ji, J. Lu, Q. Tong, P. Wei, L. Cong, Z. Li and H. Huang, *Bioresource technology*, 2011, **102**, 6088-6094.
188. K. Liang, Q. Zhang and W. Cong, *Journal of agricultural and food chemistry*, 2012, **60**, 11771-11776.
189. C.-C. Fu, T.-C. Hung, J.-Y. Chen, C.-H. Su and W.-T. Wu, *Bioresource Technology*, 2010, **101**, 8750-8754.
190. E. G. Bligh and W. J. Dyer, *Canadian journal of biochemistry and physiology*, 1959, **37**, 911-917.
191. X. Zhang, S. Yan, R. D. Tyagi, R. Y. Surampalli and J. R. Valéro, *Bioresource technology*, 2014, **169**, 175-180.
192. L. Garcia Alba, M. P. Vos, C. Torri, D. Fabbri, S. R. Kersten and D. W. Brilman, *ChemSusChem*, 2013, **6**, 1330-1333.
193. M. Braun, J. Lorenzen, M. Masri, Y. Liu, E. Baráth, T. B. Brück and J. A. Lercher, *ACS Sustainable Chemistry & Engineering*, 2019.
194. J. J. Milledge and S. Heaven, *Reviews in Environmental Science and Bio/Technology*, 2014, **13**, 301-320.
195. A. L. Colombo, A. C. B. Padovan and G. M. Chaves, *Clinical microbiology reviews*, 2011, **24**, 682-700.
196. J. M. Ageitos, J. A. Vallejo, P. Veiga-Crespo and T. G. Villa, *Applied microbiology and biotechnology*, 2011, **90**, 1219-1227.
197. H. Xie, S. Zhang and S. Li, 2006.
198. K. Pohako-Esko, M. Bahlmann, P. S. Schulz and P. Wasserscheid, *Industrial & Engineering Chemistry Research*, 2016, **55**, 7052-7059.
199. Y. Lin, Q. Yan, C. Kong and L. Chen, *Scientific reports*, 2013, **3**, 1859.

200. Z. Hu, M. Khurana, Y. H. Seah, M. Zhang, Z. Guo and D. Zhao, *Chemical Engineering Science*, 2015, **124**, 61-69.
201. A. K. Qaroush, D. A. Castillo-Molina, C. Troll, M. A. Abu-Daibes, H. M. Alsayouri, A. S. Abu-Surrah and B. Rieger, *ChemSusChem*, 2015, **8**, 1618-1626.
202. F. Santamauro, F. M. Whiffin, R. J. Scott and C. J. Chuck, *Biotechnology for biofuels*, 2014, **7**, 34.
203. J.-H. Yeon, S.-E. Lee, W.-Y. Choi, D.-H. Kang, H.-Y. Lee and K.-H. Jung, *Journal of microbiology and biotechnology*, 2011, **21**, 323-331.
204. N.-J. Kim, H. Li, K. Jung, H. N. Chang and P. C. Lee, *Bioresource technology*, 2011, **102**, 7466-7469.
205. J.-S. Jang, Y. Cho, G.-T. Jeong and S.-K. Kim, *Bioprocess and biosystems engineering*, 2012, **35**, 11-18.
206. T. N. Pham, W. J. Nam, Y. J. Jeon and H. H. Yoon, *Bioresource technology*, 2012, **124**, 500-503.
207. S. Gupta, N. Abu-Ghannam and A. G. Scannell, *Food and Bioproducts Processing*, 2011, **89**, 346-355.
208. S. Horn, I. Aasen and K. Østgaard, *Journal of Industrial Microbiology & Biotechnology*, 2000, **25**, 249-254.
209. H. van der Wal, B. L. Sperber, B. Houweling-Tan, R. R. Bakker, W. Brandenburg and A. M. López-Contreras, *Bioresource technology*, 2013, **128**, 431-437.
210. M. Soleymani and K. A. Rosentrater, *Bioengineering*, 2017, **4**, 92.
211. R. P. John, G. Anisha, K. M. Nampoothiri and A. Pandey, *Bioresource technology*, 2011, **102**, 186-193.
212. Z. Gong, Q. Wang, H. Shen, C. Hu, G. Jin and Z. K. Zhao, *Bioresource technology*, 2012, **117**, 20-24.
213. S. Galafassi, D. Cucchetti, F. Pizza, G. Franzosi, D. Bianchi and C. Compagno, *Bioresource technology*, 2012, **111**, 398-403.
214. Y. Li, Z. K. Zhao and F. Bai, *Enzyme and microbial technology*, 2007, **41**, 312-317.
215. J. Friedlander, V. Tsakraklides, A. Kamineneni, E. H. Greenhagen, A. L. Consiglio, K. MacEwen, D. V. Crabtree, J. Afshar, R. L. Nugent and M. A. Hamilton, *Biotechnology for biofuels*, 2016, **9**, 77.
216. J. G. Pan, M. Y. Kwak and J. S. Rhee, *Biotechnology letters*, 1986, **8**, 715-718.
217. A. Gnouma, E. Sehli, W. Medhioub, R. B. Dhieb, M. Masri, N. Mehlmer, W. Slimani, K. Sebai, A. Zouari and T. Brück, *Bioprocess and biosystems engineering*, 2018, **41**, 1449-1459.
218. A. K. Qaroush, K. I. Assaf, S. K. Bardaweel, F. Alsoubani, E. Al-Ramahi, M. Masri, T. Brück, C. Troll, B. Rieger and F. E. Ala'a, *Green Chemistry*, 2017, **19**, 4305-4314.
219. Z. Li, L. Zhang, X. Shen, B. Lai and S. Sun, *Wei sheng wu xue tong bao*, 2001, **28**, 72-75.
220. Y. Ohsaki, M. Suzuki and T. Fujimoto, *Chemistry & biology*, 2014, **21**, 86-96.
221. B. Bessadok, M. Masri, T. Breuck and S. Sadok, *Bull. Ins. Natn. Scien. Tech. Mer de Salammbô*, 2015, **42**, 21-23.
222. B. Bessadok, M. Masri, T. Breuck and S. Sadok, *Journal of FisheriesSciences. com*, 2017, **11**, 019-024.
223. Z. Gong, Q. Wang, H. Shen, L. Wang, H. Xie and Z. K. Zhao, *Biotechnology for biofuels*, 2014, **7**, 13.
224. A. Ahamed and P. Vermette, *Biochemical Engineering Journal*, 2008, **40**, 399-407.
225. N. R. Baral, O. Kavvada, D. Mendez-Perez, A. Mukhopadhyay, T. S. Lee, B. A. Simmons and C. D. Scown, *Energy & Environmental Science*, 2019, **12**, 807-824.
226. F. Xu, J. Sun, N. Konda, J. Shi, T. Dutta, C. D. Scown, B. A. Simmons and S. Singh, 2015.
227. J. Sun, N. M. Konda, J. Shi, R. Parthasarathi, T. Dutta, F. Xu, C. D. Scown, B. A. Simmons and S. Singh, *Energy & Environmental Science*, 2016, **9**, 2822-2834.
228. D. P. Petrides, *Computers & chemical engineering*, 1994, **18**, S621-S625.
229. D. Petrides, *Bioseparations science and engineering*, 2000.
230. S. Designer, User's Guide V10, http://www.intelligen.com/downloads/SuperPro_ManualForPrinting_v10.pdf, (accessed Intelligen, Inc.,).
231. D. Humbird, R. Davis, L. Tao, C. Kinchin, D. Hsu, A. Aden, P. Schoen, J. Lukas, B. Olthof and M. Worley, *Process design and economics for biochemical conversion of lignocellulosic biomass to ethanol: dilute-acid pretreatment and enzymatic hydrolysis of corn stover*, National Renewable Energy Lab.(NREL), Golden, CO (United States), 2011.
232. F. government, public service information, <https://oeffentlicher-dienst.info/tv-l/west/>).
233. National Renewable Energy Laboratory (NREL), U.S. Life Cycle Inventory Database,, <https://www.nrel.gov/lci/>).
234. L. Schebek, The open source data platform for bio-energy in Germany, <http://www.bioenergiedat.de/>, 2018).
235. C. Liptow, A.-M. Tillman, M. Janssen, O. Wallberg and G. A. Taylor, *The International Journal of Life Cycle Assessment*, 2013, **18**, 1071-1081.
236. J. H. Schmidt, *Journal of Cleaner Production*, 2015, **87**, 130-138.

PART II: PUBLICATIONS OVERVIEW

Seagrass

Macroalgae

Co-fermentation

Downstream Processing

Chemo-sorption

Macroalgae

Hydrothermal

Extracellular protease



A seagrass based biorefinery for generation of single cell oils targeted at biofuel and oleochemical production

Masri M. A., Younis S., Mehler N., Quora F., Brück T.
Energy Technology, 2018,6,1026–1038.

<https://doi.org/10.1002/ente.201700919>

Status: Accepted

Contribution: MM analyzed and enzymatically hydrolyzed the seagrass biomass. MM cultivated yeast on the hydrolysate. MM contributed to manuscript writing.

Summary

The increasing use of plant-based lipids for sustainable energy and biofuels applications does compromise food security and results in reduced biodiversity. Currently, more than two times the globally available arable land would be required to meet the global market demand of biodiesel. Consequently, searching for alternative starting materials that offer renewability and sustainability is of vital importance.

78 million tons of residual seagrass deposits accumulate annually on shorelines worldwide. These represent an untapped feedstock for fermentative single-cell oil production, targeted at biofuel and oleochemical generation, without affecting the sensitive marine environment or compromising food security. Seven beach-cast samples of seagrass (related to *Z. marina*, *Z. noltii*, *S. filiforme*, *P. australis*, *P. oceanica*, and *T. testudinum*) were collected from marine ecosystems around the world. A combination of 18S rRNA phylogenetic, structural, and comprehensive biomass analyses of seagrass leaves were applied. The carbohydrate content ranged from 73 to 81% (w/dw_{biomass}). Single-step enzymatic hydrolysis was developed to efficiently release the monomeric sugars contained in seagrasses biomass without any pretreatment. *P. oceanica* hydrolysate allowed for higher lipid yields (6.8 g L^{-1}) compared to the synthetic minimal medium (5.1 g L^{-1}) in shake flasks, and was subsequently utilized as the sole fermentation medium for oleaginous yeast *T. oleaginosus* at a technical scale using a fed-batch bioreactor, which provided 24.5 g L^{-1} lipids ($0.35 \text{ g L}^{-1} \text{ h}^{-1}$). Moreover, the sugar/lipid conversion ratio was 0.41 (w/w). Cumulative data indicates that by exploiting only half of the global beach-cast seagrass, approximately 4 million tons of microbial oils could be generated.

Produced from readily available beach-cast waste materials, this simplified enzyme-treated seagrass media, provides a potential route to cost-effective sustainable bioenergy/biofuel production. Out of seven samples of seagrasses, *P. oceanica* (Mediterranean Sea) displays the best lipid productivity exceeding the well-optimized minimal nitrogen media. Generally, marine biomass does not affect terrestrial agricultural activity. Moreover, in this study we only employ aged seagrass banquettes that are washed ashore and do not affect the marine ecosystem. Therefore, the process presented in this study offers a biorefinery model for sustainable generation of microbial lipids with no impact on agricultural security or sensitive marine ecosystems.

A waste-free, microbial oil centered cyclic bio-refinery approach based on flexible macroalgae biomass

M. A. Masri, W. Jurkowski, P. Shaigani, M. Haack, N. Mehlmer and T. Brück.

Applied Energy, 224 (2018) 1–12

<https://doi.org/10.1016/j.apenergy.2018.04.089>

Status: Accepted

Contribution: MM analyzed and enzymatically hydrolyzed the algal biomass. MM cultivated yeast on the hydrolysate and established the FACS based lipid assay. MM contributed to manuscript writing.

Summary

Biofuels and the oleochemical industry are highly dependent on plant oils for the generation of renewable product lines. Consequently, production of plant lipids, such as palm and rapeseed oil, for industrial applications competes with agricultural activity and is associated with a negative environmental impact. Additionally, established chemical routes for upgrading bio-lipids to renewable products depend on metal-containing catalysts. Metal leaching during oil processing results in heavy metal contaminated process wastewater. This water is difficult to remediate and leads to the loss of precious metals. Therefore, the biofuels and chemical industry requires sustainable solutions for production and upgrading of bio-lipids. With regard to the former, a promising approach is the fermentative conversion of abundant, low-value biomass into microbial, particularly yeast-based lipids. This study describes the holistic, value-adding conversion of underexploited, macroalgae feedstocks into yeast oil, animal feed and biosorbents for metal-based detoxification of process wastewater. The initial step comprises a selective enzymatic liquefaction step that yields a supernatant containing 62.5% and 59.3% (w/dw_{biomass}) fermentable sugars from *L. digitata* and *U. lactuca*, respectively. By dispensing with chemical pretreatment constraints, we achieved a 95% (w/w) glucose recovery. Therefore, the supernatant was qualified as a cultivation media without any detoxification step or nutrition addition. Additionally, the hydrolysis step provided 27–33% (w/dw_{biomass}) of a solid residue, which was qualified as a metal biosorbent. Cultivation of the oleaginous yeast *C. oleaginosus* on the unprocessed hydrolysis supernatant provided 44.8 g L⁻¹ yeast biomass containing 37.1% (w/dw_{biomass}) lipids. The remaining yeast biomass after lipid extraction is targeted as a performance animal feed additive.

To facilitate the integration of our technology in existing chemical and biotechnological production environments, we have devised simple, rapid and cost-efficient methods for monitoring both lipogenesis and metal sorption processes. The application of the new optical monitoring tools is essential to determine yeast cell harvesting times and biosorption capacities respectively. For the first time we report on a waste-free bioprocess that combines sustainable, microbial lipid production from low value marine biomass with in-process precious metal recycling options. Our data allowed for a preliminary economic analysis, which indicated that each product could be cost competitive with current market equivalents. Hence, the synaptic nature of the technology platform provides for the economic and ecologic viability of the overall process chain.

A sustainable, high-performance process for the economic production of waste-free microbial oils that can replace plant-based equivalents

Mahmoud A. Masri, Daniel Garbe, Norbert Mehlmer, and Thomas Brück.

Energy and Environmental Science, 2019, 12, 2717

Patent Application No.: EP19157805.3 (2019)

<https://doi.org/10.1039/C9EE00210C>

Status: Paper: Accepted

Contribution: MM was responsible for the entire work.

Summary

Globally, biofuel and oleochemical production based on plant oils negatively affects biodiversity. As an alternative triglyceride source, lipid production from oleaginous yeasts faces numerous challenges in feedstock availability, lipid productivity, downstream processing, and waste treatment, prohibiting the design of a cost-competitive process with regard to plant equivalents.

In this study, we present a fully integrated operation for microbial oil production, which consolidates upstream and downstream processing with side-stream recycling. Co-fermentation of sugar and acetic acid was successfully implemented in fed-batch, semi-continuous, and continuous fermentation modes. Process validation was conducted at a 25-L scale with a lipid productivity of $1.2 \text{ g L}^{-1} \text{ h}^{-1}$. *Cutaneotrichosporon oleaginosus* cell debris was used as an inducer in *Trichoderma reesei* fermentation for on-site generation of yeast-specific cell-wall hydrolases. *In situ* hydrolase application allowed for efficient *C. oleaginosus* cell lysis (85% w/w) and simultaneous lipid release. A subsequent centrifugation step yielded 90% (w/w) recovery of intracellular lipids without the need for any organic solvent. The nutrient-rich water phase was applied as an internal sugar source for yeast subsequent fermentation cycles. With this yeast hydrolysate, the lipid productivity was considerably increased to $2.4 \text{ g L}^{-1} \text{ h}^{-1}$.

A techno-economic analysis of the current lipid production processes estimated costs at \$1.6/kg lipid. Moreover, life cycle assessment analysis assumed an emission of 3.56 kg CO₂ equivalents for every 1 kg produced yeast oil. Accordingly, we established an integrated operation for bioconversion of acetic acid and sugar to sustainable lipids at maximum productivity coupled with minimal waste generation and energy consumption.

In this study, we established an integrated operation for bioconversion of acetic acid and sugar to sustainable lipids at maximum productivity with minimal waste generation and energy consumption; the cost gap compared with plant-based lipids was considerably reduced.

The approach established in this report links previous efforts to a forward-thinking optimized approach. Thus, we believe there are still many possible parameters to be optimized and metabolic modifications that can be implemented to further improve productivity. Moreover, proteomic and metabolomics analyses could further guide process development.

Extraction of Renewable Triglycerides from Oleaginous Microorganisms.

Masri M. A., Brück T.

Patent No. EP 3 536 800 A1 (2019)

Status: Published

Contribution: *MM was responsible for the entire work*

Summary

In the past decade, the global demand for plant- and animal-based lipids as platform for pharmaceutical, food, biofuel and oleochemical industry increased by 65%. To meet the increase of market demand with taking into consideration the environmental aspects as to mitigate the CO₂ emissions motivate industry to develop novel sustainable bioprocesses.

With an ability to accumulate up to 70% lipids of their dry weight, oleaginous microorganisms are poised to be the next generation for host lipid production. The conversion of microorganism's lipids into bio-kerosene, bio-diesel and bio-lubricants as well pharmaceutical and food applications has been well documented.

Conventional triglyceride extraction procedures require two discrete consecutive steps: The initial step comprises cell-wall lysis either via temperature shocks, chemical treatment or high-pressure homogenization. In the second step triglycerides are extracted with organic solvent such as petroleum ether, methanol, or chloroform. None of these methods are easily scaled to industrial level due to cost issues and lack of environmental sustainability. Moreover, the latter application of organic solvents negatively impacts the quality of the finished product. Hence, the complexity of solvent removal is considered as extra cost and energy squandering.

The design of a specific enzyme system is essential for cell lysis and oil recovery, encompassing; cellulase, polygalacturonase, mannanase, laminarinase and beta-glucosidase activities. The enzyme system was optimized on an artificial biomass in order to carry out a complete cell lysis into monosaccharides. In the first stage of optimization, the biochemical components of a partially purified cell-wall of the well-established oleaginous yeasts, *T. oleaginosus* was analyzed. Data resulting from biomass analysis was used for the selection of required enzyme activates for selective cell lysis of *T. oleaginosus*. Subsequently, the optimized enzyme system was tested directly on harvested culture of living cells without any pretreatment. Process conditions of pH, incubation temperature, enzyme concentration and space-time conversion yields were evaluated in order to minimize the process cost and duration. For the demulsification of the cell lysate, a protease activity was added to the enzyme system to accomplish a direct release of single cellular lipid. FACS cell counting in combination with fluoresce-/ electron- microscope and gravimetric analysis was used to evaluate the efficiency of the newly established process. Finally, lipids extraction at scale of 2 liters was performed to verify the scalability of the suggested downstream process.

Chemisorption of CO₂ by chitosan oligosaccharide/DMSO: organic carbamato–carbonato bond formation

Abdussalam K. Qaroush, Khaleel I. Assaf, Sanaa K. Bardaweel, Ala'a Al-Khateeb, Fatima Alsoubani, Esraa Al-Ramahi, **Mahmoud A. Masri**, Thomas Brück, Carsten Troll, Bernhard Rieger and Ala'a F. Eftaiha.

Green Chem., 2017, 19, 4305

<https://doi.org/10.1039/C7GC01830D>

Status: Accepted

Contribution: *MM performed the biodegradation test. MM contributed to the manuscript writing.*

Summary

One of the efficient approaches for climate change mitigation is carbon capture and sequestration (CCS). It is considered as an important technology to minimize CO₂ emission from flue gas in order to adhere to emission regulations imposed by several governmental agencies in leading industrial countries, viz., China, USA, and countries in the EU. To overcome problems associated with the mature technology of monoethanolamine (MEA) wet scrubbing agent, 'Green sorbents for carbon dioxide (CO₂) capturing' is a new addition in sustainable chemistry that was introduced very recently by our research group, although others have also reported significant contributions.

A newly formed bond of organic carbamato–carbonato emerged upon bubbling CO₂ in a low molecular weight chitosan hydrochloride oligosaccharide CS·HCl/DMSO binary mixture. The aforementioned bond was detected and confirmed using attenuated total reflectance-Fourier transform Infrared (ATR-FTIR) spectroscopy, with two prominent peaks at 1551 cm⁻¹ and 1709 cm⁻¹ corresponding to ionic organic alkylcarbonate (RCO₃⁻) and carbamate (RNH–CO₂⁻ NH₃⁺–R), respectively. ¹H–, ¹³C–, and ¹H–¹⁵N heteronuclear single quantum coherence (HSQC) NMR experiments were also employed. According to ¹³C NMR, two newly emerged peaks at 157.4 ppm and 161.5 ppm attributed for the carbonyl carbon within the sequestered species RCO₃⁻ and RNH–CO₂⁻ NH₃⁺–R, respectively. Upon CO₂ bubbling, cross peaks obtained from ¹H–¹⁵N HSQC at 84.7 and 6.8 ppm correlated to the ammonium counterpart chemical shift bound to the proton resonances. Volumetric uptake of CO₂ was measured using an ATR-FTIR autoclave equipped with a silicon probe. The equilibrium sorption capacity was 0.6 and 0.2 bars through the formation of RCO₃⁻ and RNH–CO₂⁻ NH₃⁺–R, respectively. Moreover, physisorption by the dried DMSO contributed to additional 0.4 bars. Density functional theory (DFT) calculations supported the occurrence of the suggested dual mechanisms and confirmed the formation of carbonate at **C-6** of the glucosamine co-monomer.

Moreover, CS·HCl/DMSO showed a slight impact on cell proliferation after 48 hours; this was a clear evidence of its non-toxicity. The biodegradation test revealed that a degradation of about 80% of CS·HCl/DMSO was achieved after 33 days; these results indicated that this method is suitable for green industry. CS·HCl/DMSO showed modest activities against *Staphylococcus aureus* and *Escherichia coli*. In addition, CS·HCl/DMSO demonstrated a significant antifungal activity against *Aspergillus flavus* in comparison with Fluconazole.

Catalytic decomposition of the oleaginous yeast *Cutaneotrichosporon oleaginosus* and subsequent biocatalytic conversion of liberated free fatty acids.

Martina K. Braun, Jan Lorenzen, **Mahmoud A. Masri**, Yue Liu, Eszter Baráth, Thomas Brück, Johannes A. Lercher.
ACS Sustainable Chem, Eng.2019, 7, 7

<https://doi.org/10.1021/acssuschemeng.8b04795>

Status: Accepted

Contribution: *MM analyzed the yeast biomass, produced the ethanol and TEA and contributed to the manuscript writing.*

Summary

A single step catalytic cell wall lysis and triglyceride hydrolysis combined with the enzymatic conversion of lipids using the oleaginous yeast *Cutaneotrichosporon oleaginosus* (ATCC 20509) as a model is described. Catalytic decomposition of yeast cells resulted in hydrolysis of about a third of cellular polysaccharides and all triglycerides. Enzymatic processing of the lipid fraction with an oleate hydratase from *Stenotrophomonas maltophilia* led to conversion of oleic acid to 10-hydroxystearic acid (10-HSA) (50%) without additional purification. Cell wall polysaccharides were depolymerized by in situ formed amino acids from cell protein fragments. The activity of the in situ generated, free amino acids was higher compared to that of additionally added acids. Studies with the cellobiose and β -(1 \rightarrow 3)-glucan indicated that glutamic and aspartic acids, which are the dominant amino acids in yeast cells, are surprisingly more effective in hydrolysis in aqueous phase than sulfuric acid. This points to a concerted mechanism of glycosidic ether bond cleavage catalyzed by amino acids rather than to a pathway catalyzed by hydronium ions. The overall yield of the presented downstream process at 453 K resulted in the release of 80% of total lipids.

Following our zero-waste strategy, the yeast hydrolysate after the hydrothermal treatment was tested as cultivation media for ethanol production, as alternative for terrestrial biomass. The hydrolysate was used without further nutrient addition or optimization. *S. cerevisiae* showed ability to metabolize the sugar contained in the hydrolysate and convert it to ethanol. The ethanol titer (7.5 g L⁻¹) was comparable to other ethanol production procedures, using thermochemical processed biomass hydrolysates with wild type baker's yeast as the fermentation organism.

This work offers a green and economic way for the utilization of yeast and a new insight into the conversion of biomass in the presence of endogenous catalysts. This present study shows the synergy between chemical and biotechnological techniques to develop industrially relevant processes.

Strain selection of microalgae isolated from Tunisian coast: characterization of the lipid profile for potential biodiesel production

Asma Gnouma, Emna Sehli, Walid Medhioub, Rym Ben Dhieb, **Mahmoud A. Masri**, Norbert Mehlmer, Wissem Slimani, Khaled Sebai, Amel Zouari, Thomas Brück, Amel Medhioub.
Bioprocess and Biosystems Engineering 41:1449–1459 (2018).

<https://doi.org/10.1007/s00449-018-1973-5>

Status: Accepted

Contribution: *MM analyzed the algal biomass and lipid and contributed to the manuscript writing.*

Summary

In the marine ecosystem, photosynthetic microalgae constitute an important component of the marine flora since they form the basis of the aquatic food chain. These tiny plants have attracted a lot of attention as sustainable producers of bioactive compounds and lipid-containing biomass for food, animal feed and for biofuels.

Microalgae could be of importance for future biodiesel production as an alternative for a third generation of biofuels. To select the most appropriate strain for biodiesel production, three microalgae species, namely *Isochrysis* sp., *Nannochloropsis maritima* and *Tetraselmis* sp., isolated from Tunisian coast, were biochemically characterized. Initially, gas chromatography analysis showed that *Isochrysis* sp. and *N. maritima* contained 5- and 10-fold total fatty acids, respectively, more than *Tetraselmis* sp. Then, the two microalgae *Isochrysis* sp. and *N. maritima* were subject to random mutagenesis using ultraviolet-C radiation. Subsequently, a total of 18 mutants were obtained from both species. The neutral lipid evaluation on said 18 mutants allowed the retention of only 7 to further fatty acid characterization. Finally, gas chromatography revealed that the mutant 5c *Isochrysis* sp. was characterized by a high level of saturated fatty acids (52.3%), higher amount of monounsaturated fatty acids (29.3%), lower level of polyunsaturated fatty acids (18.4%) and a significant 1.3-fold increase in its C16–C18 content compared to the wild-type strain, which would make it an interesting candidate for biofuel production.

To summarize, the mutant 5c *Iso.* sp. has shown the highest FI value among all the samples analyzed by FCM reflecting a twofold increase of NL content compared to WT *Iso.* sp. Furthermore, considering its higher SFA and MUFA levels, its lower PUFA levels and its significant 1.3-fold increase of C16–C18 content compared to WT *Iso.* sp., it could be indicated that the mutant 5c *Iso.* sp. has a good combination of different parameters which would make it an interesting candidate for an eventual biodiesel production. The contribution of this work lies in the possibility to select candidate microalgae strains which could be interesting for biodiesel production without formally resorting to many mutation-selection procedures or to many types of expensive equipment.

Isolation and Screening for Protease Activity by Marine Microorganisms

Bessadok, Boutheina; **Masri A., Mahmoud**; Brück, Thomas; Sadok, Saloua.

Bull. Inst. Natn. Scien. Tech. Mer de Salammbô, Vol. 42, (2015)

<https://www.oceandocs.org/bitstream/handle/1834/9040/11.pdf?sequence=1>

Status: Accepted

Contribution: *MM performed the protein extraction, DNA extraction, SDS-gel, strain identification.*

Summary

The aim of this study was to isolate and identify marine yeast strains from seawater, sediments seaweed, and fish/shrimp coproducts. Over six-different identified species of marine yeast, *Yarrowia lipolytica* strain having a proteolytic activity. Enzyme extracts showed that the relative optimal enzymatic activity was reached at pH = 9.0 and temperature of 45.0°C.

Characterization of the Crude Alkaline Extracellular Protease of *Yarrowia lipolytica* YITun15.

Bessadok, Boutheina; **Masri A., Mahmoud**; Brück, Thomas; Sadok, Saloua.
Journal of FisheriesSciences.com, 11(4): 019-024 (2017)

<https://doi.org/10.21767/1307-234X.1000137>

Status: Accepted

Contribution: *MM designed the assay methods and characterization experiments.*

Summary

Yarrowia lipolytica YITun15 (GeneBank Acc. N MF327143), isolated from farmed *Dicentrarchus labrax*'s gills, secretes an alkaline extracellular protease, which exhibited the highest activity at pH 9 and temperature 45°C. The enzyme activity extracted was tested in the presence of different ion metal and protein inhibitors. The enzyme activity increased in the presence of both Cu²⁺ (1 mM) and Mn²⁺ (5mM) in the medium. K⁺, Na²⁺, Mg²⁺ and Ca²⁺ had no effect on the enzyme activity while Ni⁺, Hg⁺, Zn²⁺ and Fe²⁺ decreased significantly its relative activity to 43.63%, 66.25%, 30.75% and 19.48% respectively at the 5 mM level. The enzyme was almost (activity=1.47%) inhibited by phenylmethylsulfonyl fluoride at the concentration of 5 mM. However, the protease activity was relatively constant in the presence of EDTA and SDS that may conclude that this enzyme was not a metalloprotease and belong to the serine protease category. After 18 months-storage at -20°C, the enzyme activity has decreased to 23.17%. This protease may have a potential application in food and detergent activity.

The purified extracellular alkaline protease extracted from *Yarrowia lipolytica* YITun15 shows promising proprieties of stability and activities that may be used in profile various applications. Further, this study will be completed with proteomic analysis to sequence and well characterization.

PART III: PUBLICATIONS FULL TEXT

A seagrass based biorefinery for generation of single cell oils targeted at biofuel and oleochemical production

A waste free, microbial oil centered cyclic bio-refinery approach based on flexible macroalgae biomass

A sustainable, high-performance process for the economic production of waste-free microbial oils that can replace plant-based equivalents

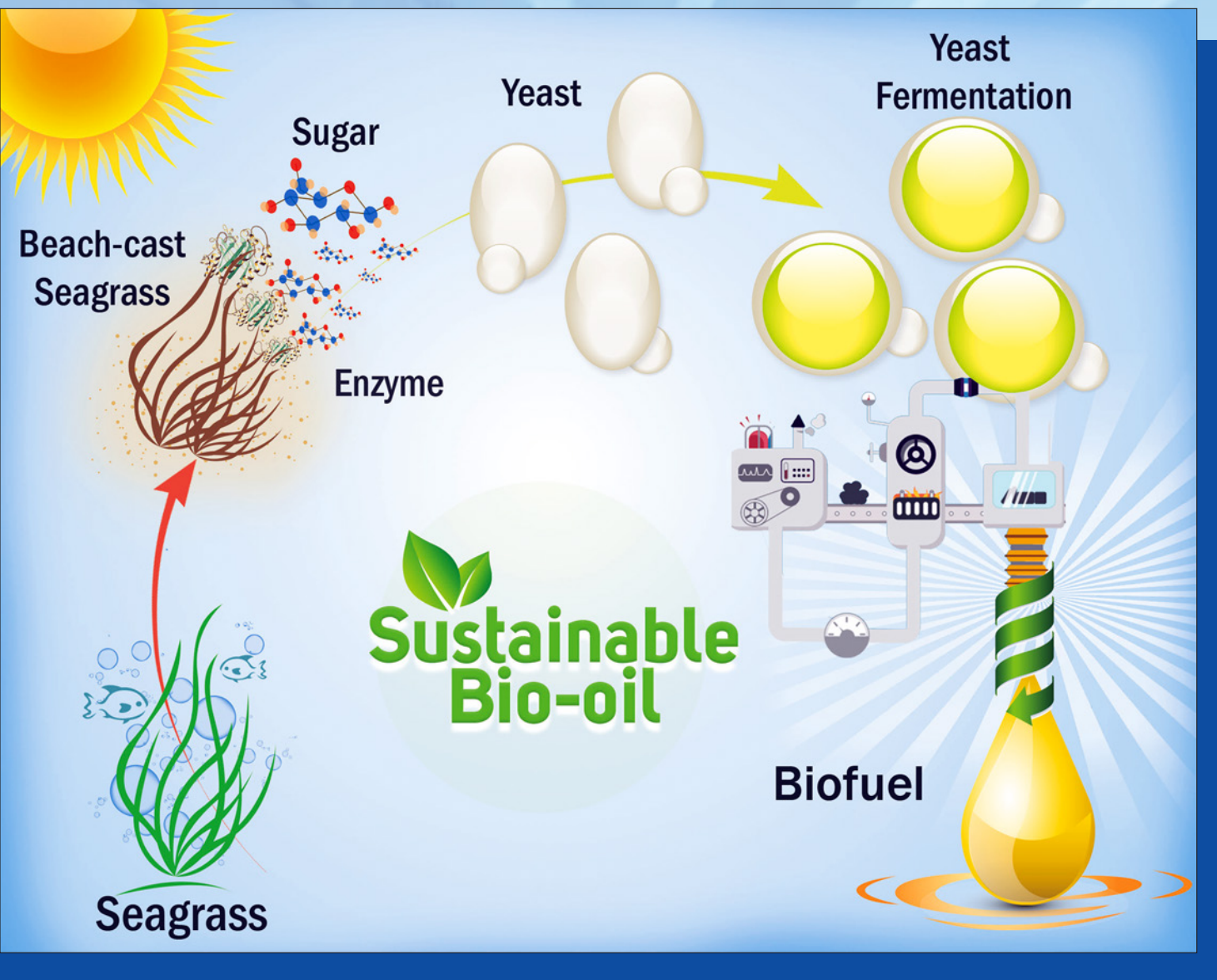
Chemisorption of CO₂ by chitosan oligosaccharide/DMSO: organic carbamato–carbonato bond formation

*A seagrass based biorefinery for generation of single cell oils
targeted at biofuel and oleochemical production*

Energy Technology

Generation, Conversion, Storage, Distribution

6/2018



Front Cover:

Mahmoud A. Masri et al.

A Seagrass-Based Biorefinery for Generation of Single-Cell Oils for Biofuel and Oleochemical Production

www.entechinol.de

WILEY-VCH



A Seagrass-Based Biorefinery for Generation of Single-Cell Oils for Biofuel and Oleochemical Production

Mahmoud A. Masri⁺, Samer Younes⁺, Martina Haack, Farah Qoura, Norbert Mehlmer,^{*} and Thomas Brück^{*[a]}

78 million tons of residual seagrass deposits accumulate annually on shorelines worldwide. These represent an untapped feedstock for fermentative single-cell oil production, targeted at biofuel and oleochemical generation, without affecting the sensitive marine environment or compromising food security. Seven beach-cast samples of seagrass (related to *Z. marina*, *Z. noltii*, *S. filiforme*, *P. australis*, *P. oceanic*, and *T. testudinum*) were collected from marine ecosystems around the world. A combination of 18S rRNA phylogenetic, structural, and comprehensive biomass analyses of seagrass leaves were applied. The carbohydrate content ranged from 73 to 81% (w^d/w_{biomass}). Single-step enzymatic hydrolysis was developed

to efficiently release the monomeric sugars contained in seagrasses biomass without any pretreatment. *P. oceanica* hydrolysate allowed for higher lipid yields (6.8 g L^{-1}) compared to the synthetic minimal medium (5.1 g L^{-1}) in shake flasks, and was subsequently utilized as the sole fermentation medium for oleaginous yeast *T. oleaginosus* at a technical scale using a fed-batch bioreactor, which provided 24.5 g L^{-1} lipids ($0.35 \text{ g L}^{-1} \text{ h}^{-1}$). Moreover, the sugar/lipid conversion ratio was 0.41 (w/w). Cumulative data indicates that by exploiting only half of the global beach-cast seagrass, approximately 4 million tons of microbial oils could be generated.

Introduction

The increasing use of plant-based lipids for sustainable energy and biofuels applications does compromise food security and results in reduced biodiversity.^[1] Currently, more than two times the globally available arable land would be required to meet the global market demand of biodiesel.^[2] Consequently, searching for alternative starting materials that offer renewability and sustainability is of vital importance.

Single-cell oil (SCO) production as a platform for biofuel production has been investigated with microorganisms encompassing *Aspergillus awamori*,^[3] *Scenedesmus sp.*,^[4] *Yarrowia lipolytica*,^[5] *Cryptococcus sp.*,^[6] and *Trichosporon oleaginosus*.^[7] *T. oleaginosus* (ATCC 20509), a recently isolated oleaginous yeast,^[8] is able to convert different monomeric carbon sources (C5 and C6 sugars), as well as complex waste feedstock materials, into triacylglycerol lipids stored in sub-cellular compartments,^[9] with cellular lipid yields of up to 70% of the cell dry weight.^[8] Palmitic acid, stearic acid, and oleic acid are the major fatty acids of the accumulated triglycerides. Moreover, the biodiesel B20 derivative from *T. oleaginosus* lipid has been shown to meet the ASTM certification.^[7a] Therefore, the SCO fatty acid composition offers a potent alternative to vegetable oils, by alleviating competition with food resources. Nevertheless, feeding these oleaginous microorganisms with a suitable carbon source, which allows for cost-effective biodiesel production, remains a considerable challenge.

Marine biomass as a carbon source, accounts for up to 71% (w/w) of all biologically stored carbon globally.^[10] At present, macroalgae and seagrass are the most abundant

marine macrophytes available.^[11] With relatively high photon conversion efficiency,^[12] seagrass meadows are among the highest productivity ecosystems on earth. This productivity is estimated to be approximately 27.4 million tons per year of organic carbon (C_{org}).^[13] Seasonally, detached seagrass-leaf material accumulates as banquettes on beaches and shorelines. This phenomenon is enhanced by the relatively low natural biodegradation rate ($\approx 19\%$) of this leafy biomass by herbivores and heterotrophs.^[14] For instance, in the south coast of Australia (Beachport, South Australia), seagrass accumulated at a height of 1.5 m extending along the shoreline with a length in excess of 50 km (Figure S1, Supporting Information). Seagrass biomass contains an unfavorable C/N/P ratio of 474:24:1 which hampers its biological degeneration.^[15] Factoring in that approximately 50% of the available seagrass biomass is degraded, buried on the ocean seabed, or

[a] M. A. Masri,⁺ S. Younes,⁺ M. Haack, Dr. F. Qoura, Dr. N. Mehlmer, Prof. Dr. T. Brück
Department of Chemistry—Professorship of Industrial Biocatalysis
Technical University of Munich (Germany)
E-mail: brueck@tum.de

[*] These authors contributed equally to this work.

Supporting information and the ORCID identification number(s) for the author(s) of this article can be found under:
<https://doi.org/10.1002/open.201700604>.

© 2017 The Authors. Published by Wiley-VCH Verlag GmbH & Co. KGaA. This is an open access article under the terms of the Creative Commons Attribution Non-Commercial NoDerivs License, which permits use and distribution in any medium, provided the original work is properly cited, the use is non-commercial and no modifications or adaptations are made.

consumed by herbivores, simple calculations indicate that 40 million tons of dry seagrass biomass remain available for biotechnological applications. To that end, efficient enzymatic hydrolysis of seagrass leaf microfibril could provide a sustainable stream of monomeric hexose and pentose sugars that could be used as a fermentation medium. In general, the resulting sugar-rich hydrolysate as well low nitrogen and phosphor content may actually be beneficial for cultivation of selected oleaginous yeasts, as these organisms initiate lipogenesis only when the nitrogen or phosphate concentration is low. However, according to published data, enzymatic hydrolysis and fermentation steps were successful only when pretreatment stages were used in advance. These pretreatment processes present additional costs and usually release inhibitory compounds that hinder the fermentation.^[16]

Few studies have evaluated the utilization of fresh seagrasses biomass as a feedstock platform for the production of bioethanol.^[17] In the available reports, the utilization of beach-cast seagrass residue has not been considered. To the best of our knowledge, the production of SCO by microbial fermentation on hydrolysates derived from beach-cast seagrass biomass has not been investigated.

The aim of this work was to investigate the feasibility of utilizing seagrass hydrolysate for the fermentation of oleaginous yeast with the focus on biodiesel production, in addition to other industrial applications.^[9] Seven seagrass samples from six different seagrass eco-regions were collected, and a phylogenetic classification of each sample was established using ITS1 and 18S rRNA sequencing. To further elucidate the structure of the samples, electron microscopy analysis of the leaves was performed. Biomass analysis of each seagrass sample was also conducted in a detailed manner. Subsequently, an optimized enzyme system was devised that allowed efficient hydrolysis and liquefaction of the seagrass biomass without the need for chemical pretreatment. Without further nutrient addition, the resulting seagrass hydrolysate was utilized as the sole cultivation medium for the oleaginous yeast *Trichosporon oleaginosus*. Hydrolysates derived from aged-seagrass samples proved to be an excellent cultivation media, comparable to conventional defined synthetic media. Lipid production was scaled to fed-batch fermentation using the best performing seagrass hydrolysate to evaluate the potential for biodiesel generation. Finally, the fatty acid profile of the produced lipid was characterized to test its suitability for biodiesel production. This study demonstrated for the first time that residual seagrass biomass, accumulating in massive deposits on beaches and shorelines, can be applied as a new feedstock for the production of biogenetic fats and oils. With downstream processing, the resulting plant oil-like lipids could be upgraded by using well-known processes into high-value biokerosene, biodiesel, and biolubricants.^[6,7,9]

Results and Discussion

Previous reports demonstrated that oleaginous yeasts such as *Yarrowia lipolytica* and *Lipomyces starkeyi* can produce lipids from sources such as pure glucose, xylose, and sucrose

in batch fermenters.^[18] Further studies investigated the use of renewable feedstocks such as glycerol and molasses as carbon sources for lipid accumulation in oleaginous yeasts.^[18a] *Trichosporon oleaginosus* (ATCC 20509) has the capacity to metabolize a variety of carbon sources including hexoses and pentoses.^[8] Under nitrogen- or phosphate-limiting conditions, this yeast can accumulate up to 70% of its dry weight as lipids, composed mainly of C₁₆ and C₁₈ fatty acids.^[19]

Regarded as nuisance, especially in resorts and touristic destinations, beach-cast seagrass deposits are exclusively disposed of without valorization.^[20] In this study, we have examined the value-added use of aged seagrass waste as a readily available, low-cost, raw feedstock for production of microbial lipids in *T. oleaginosus*. Nevertheless, neither a comprehensive biomass analysis nor an optimized enzymatic treatment system have yet been established.

Identification of seagrass samples

The different seagrass strains and their corresponding locations are shown in Table 1. These identified seagrasses are related to the four genera (out of eleven total known Genera) *Zostera*, *Syringodium*, *Posidonia*, and *Thalassia* sp., which cluster in the four seagrass families *Zosteraceae*, *Cymodoceaceae*, *Posidoniaceae*, and *Hydrocharitaceae*, respectively.

Table 1. Selected seagrass samples, locations, and identification based on ITS1 and 18S rRNA sequencing.

Strain	Location ^[a]
<i>Z. marina</i> (1)	Baltic Sea (Hohenkirchen)
<i>S. filiforme</i>	Caribbean Sea (Mexico)
<i>P. australis</i>	South Australia
<i>T. testudinum</i>	North Sea (Bahamas)
<i>Z. marina</i> (2)	Baltic Sea (Greifswald)
<i>Z. noltii</i>	Mediterranean Sea (Malta1)
<i>P. oceanica</i>	Mediterranean Sea (Malta2)

[a] GPS Data is given in the Supporting Information (Table S1).

In this study, the standard 18S sequence information was employed, for the first time for phylogenetic analysis of seagrass. The data was subsequently assembled to generate a maximum-likelihood phylogenetic tree (Figure S2). This tree identified two major groups: *Posidonia australis* is resolved in the smaller one, basal to the group containing *Zostera* spp., *Syringodium filiforme*, *Thalassia testudinum*, and *Posidonia oceanica*, all species with complex phyllotaxy. All sequences are available in the Supplementary Information.

The *Zostera* clade was resolved based solely on strain level (*Z. noltii* and *Z. marina*) and not into different geographically distinct groups. *Posidonia oceanica* and *Syringodium filiforme* are resolved in a third clade within two lineages of species and the forth clade harbored *Thalassia testudinum*.

Unexpectedly, *Posidonia oceanica* and *Posidonia australis* showed a considerable genetic divergence in the 18S rDNA-based phylogenetic tree. In contrast, previous reports apply-

ing an rbcL cladogram showed that these two *Posidonia* strains are closely related.^[21] However, the present study is the first using conventional 18S rDNA sequences to assemble a phylogenetic relatedness of global seagrass populations. Consequently, more work should be conducted towards the choice of genetic markers that can be reproducibly used to construct the seagrass phylogeny, as it is predicted that 91 % of the entire seagrass diversity is still unknown.^[22] Possible candidates that could complement the current phylogenetic marker are phyB and the plastidial matK.^[22]

Comprehensive biomass analysis

The overall biochemical composition of the seven seagrass samples is summarized in Table 2. As expected, all samples

Seagrass	Content in seagrass [% ($w^d w_{\text{biomass}}$)]			ash
	lipid	protein	sugar	
<i>Z. marina</i> (1)	2.6 ± 0.13	13.4 ± 0.13	73.4 ± 1.17	10.6 ± 0.94
<i>S. filiforme</i>	1.8 ± 0.09	07.6 ± 0.08	77.3 ± 0.87	13.3 ± 1.03
<i>P. australis</i>	2.1 ± 0.19	07.5 ± 0.06	78.7 ± 1.17	11.7 ± 0.04
<i>T. testudinum</i>	2.4 ± 0.34	05.3 ± 0.11	79.1 ± 0.74	13.2 ± 0.66
<i>Z. marina</i> (2)	3.0 ± 0.25	10.4 ± 0.11	73.3 ± 0.57	13.3 ± 0.03
<i>Z. noltii</i>	7.2 ± 0.46	11.9 ± 0.14	73.9 ± 0.91	07.0 ± 0.41
<i>P. oceanica</i>	2.3 ± 0.41	05.1 ± 0.06	80.8 ± 0.57	11.8 ± 0.68

display a high carbohydrate content of 73–81 % ($w^d w_{\text{biomass}}$) of total dry weight. Interestingly, the protein content differs widely among the various seagrasses. *P. oceanica* and *T. testudinum* 5 % ($w^d w_{\text{biomass}}$) contained less protein than *Z. marina* (14 % $w^d w_{\text{biomass}}$ Baltic Sea, Hohenkirchen, Germany). Interestingly, the lipid content of 2–3 % ($w^d w_{\text{biomass}}$) was relatively low for all seagrass samples, except for *Z. noltii*, which showed a lipid content of 7 % ($w^d w_{\text{biomass}}$). The fatty acid analysis data for each lipid sample is reported in the Supporting Information (Table S2). Ash constituted 12–13 % ($w^d w_{\text{biomass}}$) of the dry weight for most seagrass samples. *Z. noltii* and *Z. marina* (Baltic Sea- Hohenkirchen, Germany) were the exception with lower-than-average ash contents of 7 and 10 % ($w^d w_{\text{biomass}}$), respectively. The subtle differences in the biochemical compositions of all seven examined seagrass strains may be attributed to different climate conditions, the

composition of the ocean water, the time of the year, or the composition of marine sediments.

Moreover, as most samples were collected as beach-cast residues, sun bleaching and exposure to the weather is an essential factor that will influence the biomass composition of all seagrass samples. The state of the biomass is also reflected by its color as in the case of the *Z. marina* sample, collected from the Baltic Sea- Hohenkirchen, which was fresh, relatively pure, and had a dark green color. Conversely, the second *Z. marina* sample collected from Baltic Sea, Greifswald was aged and characterized by a light-yellowish color.

Finally, biomass analysis showed water contents of the various seagrass samples ranging between 8 and 10 % (w/w_{biomass}) (data not shown).

Carbohydrate compositional content

The biomass analysis indicates that conventional chemical biomass hydrolysis with single acid treatment will result in an underestimation of the actual sugar content.^[23] Consequently, we have developed and optimized a combined approach involving both a chemical and an enzymatic biomass treatment, which improved the determination of the total and differential carbohydrate contents (optimization data is not shown). The results are presented in Table 3 as a percentage of the total dry biomass weight.

As expected, glucose is the dominant monomeric carbohydrate, most likely derived from cellulosic leaf fibers. Hence, glucose contributes approximately 67 % ($w^d w_{\text{biomass}}$) of the total biomass in *Z. noltii*, whereas it only accounts for about 40 % ($w^d w_{\text{biomass}}$) of *P. australis*. All seven strains contain various neutral pentose (rhamnose and xylose) and hexose (glucose and galactose) sugars as well as some sugar acids (glucuronic and galacturonic acid). Glucose is the dominant sugar in all samples, whereas all other sugar types have been detected at concentrations <10 % ($w^d w_{\text{biomass}}$). This data makes seagrass biomass a potentially suitable source for the fermentation of various microorganisms, as glucose is the preferred carbon source for a diverse array of pro- and eukaryotic microorganisms.

Chemical composition of biomass ash

Minerals contained in the ash are important for yeast fermentation as some trace elements play an essential role in

Seagrass	Carbohydrate in seagrass [% ($w^d w_{\text{biomass}}$)]				
	galacturonic acid	glucose	xylose, mannose, fructose	rhamnose	fucose
<i>Z. marina</i> (1)	6.46 ± 0.26	58.13 ± 0.11	4.27 ± 0.16	3.82 ± 0.39	0.99 ± 0.06
<i>S. filiforme</i>	5.73 ± 0.10	56.08 ± 0.19	3.67 ± 0.19	3.05 ± 0.17	1.19 ± 0.03
<i>P. australis</i>	5.18 ± 0.15	51.53 ± 0.15	7.31 ± 0.51	7.79 ± 0.07	1.31 ± 0.05
<i>T. testudinum</i>	8.81 ± 0.08	56.09 ± 0.22	2.77 ± 0.05	3.91 ± 0.27	1.01 ± 0.03
<i>Z. marina</i> (2)	6.54 ± 0.12	54.06 ± 0.01	3.87 ± 0.16	5.54 ± 0.13	1.12 ± 0.01
<i>Z. noltii</i>	4.11 ± 0.24	66.36 ± 0.02	2.48 ± 0.35	3.31 ± 0.07	0.56 ± 0.02
<i>P. oceanica</i>	6.61 ± 0.10	55.99 ± 0.17	3.67 ± 0.09	7.17 ± 0.12	1.23 ± 0.02

lipid production.^[24] At present, this is the first report on the ash composition from banquettes of various seagrass species.^[25] Elemental analysis of ash from each seagrass sample was performed using SEM and energy-dispersive X-ray spectroscopy (EDX). The main inorganic elements constituting the ash structure are Ca and Mg, followed by smaller amounts of Al and S. The concentrations of these elements vary extensively between the seagrass species; this is largely dependent on the availability of nutrients in the specific marine ecosystem. Minute concentrations of Sr, W, Cr, and Mo were detected among the various samples. Interestingly, phosphate was completely absent from both *P. oceanica* and *T. testudinum*. The detailed elemental analysis is presented in Supporting Information (Table 4).

Structural analysis

For industrial applications, high biomass density offers an economical advantage concerning the cost of handling and transportation of the materials. To gain detailed insight into the seagrass structural characteristics, fiber location, and quantity, SEM was applied to examine cross sections of each type of seagrass leaf. As depicted, *Z. marina* leaves (Figure 1) are organized in closed cell structures located only at the outer surfaces of the leaf. They appear to reinforce a central hollow matrix, which leads to a low density of leaves. Conversely, a dense non-hollow structure is observed in *P. oceanica*, with fiber bundles interspersed within the leaf matrix (Figure 1). This observation might explain the fact that, throughout the handling of the seagrass samples, *P. oceanica* had the highest density, which presents it as the most advantageous material for processing and transportation.

Treatment of seagrass biomass

The production of biomass hydrolysates for microbial biofuel production can be conducted using complete chemical hydrolysis (H_2SO_4 or solid acid catalysts).^[26] Moreover, mild chemical processing can be also implemented as pretreatment for subsequent enzymatic hydrolyses. However both methods often generate inhibitory substances, thereby necessitating a complex detoxification step preceding fermentation.^[27] To circumvent these difficulties, a purely enzymatic-

based approach was applied in the current study, which efficiently releases the carbohydrate monomers without any pretreatment. Sterilization of the various seagrass samples was performed in a laboratory-scale autoclave at 120 °C for 15 min. This step was performed to eliminate microbial contaminants that could be present within the seagrass residues. Sterilization opens up the cell wall to allow access for the hydrolytic enzymes; however, this step is not really considered as pretreatment (such as chemical pretreatment and hydrolysis of carbohydrates), as saccharification of hemicellulose and cellulose starts at temperatures above 150 °C.^[16] Nitsos et al., (2012) implemented optimization procedures of hydrothermal pretreatment of lignocellulosic biomass with temperatures varying within 130–220 °C over 15–180 min,^[28] which still generated—although to a lower extent—unwanted inhibitory chemicals. The main structural constituents of seagrass are cellulose and hemicellulose with no lignin present, alleviating the harsh pretreatment that lignocellulosic biomass would have required.

A mixture of seagrass-specific hydrolases, including cellulolytic, hemicellulolytic, pectinolytic, laminarolytic enzymes and a β -glucosidase, was formulated to provide an optimum hydrolase system. The corresponding activities were obtained from four commercial enzyme products: Cellic CTec 2 (C), Cellic HTec (H), Pectinex (P), and Novozymes 188 (B), which are all products of Novozymes. The optimization of the required enzymes system extended over 35 different enzyme mixtures at varied concentrations. Briefly, the optimization process was performed using *Z. marina* as a model substrate. Biomass-to-glucose conversion ratios from various mixtures of Cellic CTec 2 with Cellic HTec at a fixed total concentration of 1.0% (w/dw_{biomass}) are presented in Figure S3 (Supporting Information). The ratio ranges 2:3 and 1:4 (C/H w/w) showed the highest conversion ratios at 36.1 to 37.8% (w/dw_{biomass}), respectively. The ratio 1:4 (C/H w/w) was used at different concentrations starting from 0.2 to 2.0% (w/dw_{biomass}) (2–20 mg g^{-1} biomass). Addition of the β -glucosidase activity to the previous mix increased the glucose recovery from 37.8 to 47.5% (Figure S4).

The optimum activity was obtained at a commercially relevant concentration (1.5% w/dw_{biomass} , 15 mg g^{-1} biomass), temperature of 50.0 °C, and pH 5.0 (50.0 mM, Sodium acetate) for 72 h. All seven seagrass samples were subjected to the

Table 4. Mineral composition of seagrass ash samples.

Seagrass	Elemental content [% (w/dw_{ash})]																
	O	Na	Mg	Al	Si	P	S	Cl	K	Ca	Mn	Fe	Cu	Sr	W	Cr	Mo
<i>Z. marina</i> (1)	67.4 ^[a]	1.4	10.3	1.4	7.3	0.7	1.8	0.0	0.6	8.5	0.2	0.2	0.1	n.d.	n.d. ^[b]	n.d.	n.d.
<i>S. filiforme</i>	65.8	n.d.	8.9	0.7	n.d.	0.9	6.1	n.d.	n.d.	17.2	n.d.	n.d.	n.d.	0.5	n.d.	n.d.	n.d.
<i>P. australis</i>	63.0	n.d.	9.8	1.1	0.1	0.3	1.5	n.d.	n.d.	23.7	n.d.	0.2	n.d.	n.d.	0.1	n.d.	n.d.
<i>T. testudinum</i>	73.1	n.d.	6.0	0.6	n.d.	n.d.	5.3	n.d.	n.d.	15.0	n.d.	n.d.	n.d.	n.d.	n.d.	n.d.	n.d.
<i>Z. marina</i> (2)	66.4	2.6	8.4	1.3	6.3	0.8	1.8	n.d.	2.1	9.1	0.5	0.3	0.3	n.d.	n.d.	0.0	n.d.
<i>Z. noltii</i>	65.0	2.3	10.6	1.3	2.6	3.2	1.3	0.5	0.5	11.9	0.1	0.2	0.1	n.d.	n.d.	n.d.	0.5
<i>P. oceanica</i>	69.3	n.d.	12.7	1.0	n.d.	n.d.	2.6	n.d.	n.d.	14.1	n.d.	n.d.	n.d.	0.3	n.d.	n.d.	n.d.

[a] Relative STDV for all given numbers is $\leq \pm 2\%$. [b] n.d.: Not detectable

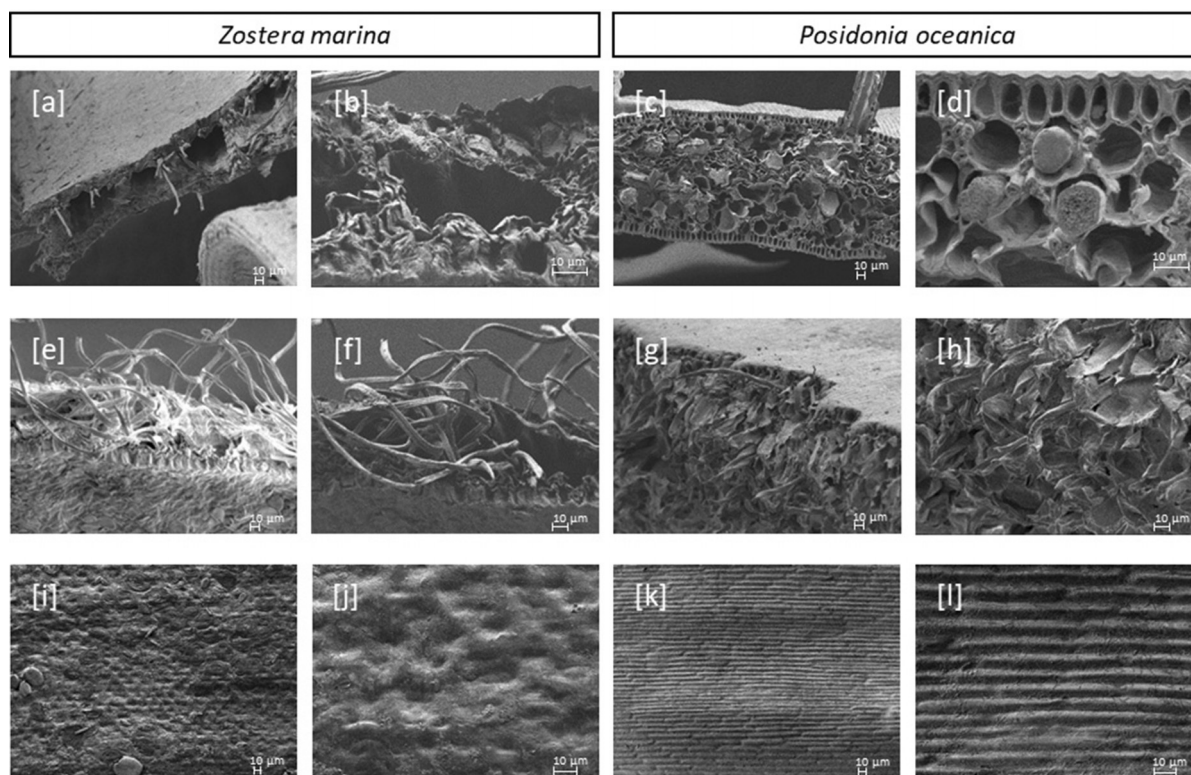


Figure 1. Electron microscopy image. Applied energy: 1.00 kV, LEI, detector: SEM/LM. *Zostera marina*: (A, B) show the leaf transverse section at 300 and 1500 times magnification, respectively, (C, D) show the leaf fibers at 430 and 600 times magnification, respectively and (E, F) show the surface of leaf at 300 and 1000 times magnification, respectively. *Posidonia oceanica*: (G, H) show the leaf transverse section at 300 and 1500 times magnification, respectively, (I, J) show the leaf fibers at 430 and 600 times magnification, respectively; and (K, L) show the surface of leaf at 300 and 1000 times magnification, respectively. Scale bars correspond to 10 μm .

same enzymatic treatment for three days. Glucose release as the controlling process indicator was monitored by HPLC (Figure 2). Hydrolysate from *Z. noltii* contained the highest amount of glucose with 32 g L^{-1} followed by *P. oceanica* with almost 28.5 g L^{-1} . As expected, glucose was the major sugar in the hydrolysate. However, other monosaccharides have been generated as well. The sugar composition of the final hydrolysates is presented in Supporting Information (Table S3).

The remainder of the organic-bound nitrogen in the final hydrolysate (following 10 kDa cross filtration) was determined by using the Kjeldahl method. For all samples, the nitrogen content was measured in g L^{-1} and a Kjeldahl nitrogen-to-protein conversion factor of 6.25 was used (Table 5). Consistent with the biomass analysis results prior to the cross filtration, *T. testudinum* and *P. oceanica* hydrolysates exhibited the lowest nitrogen contents with 0.6 and 0.5 g L^{-1} , respectively, whereas *Z. marina* (North Sea) hydrolysate contained the highest amount (3.5 g L^{-1}). It is also worth mentioning that the Kjeldahl method applied here measured the nitrogen bound in organic substances only (total Kjeldahl nitrogen was not determined). However, it is acceptable to consider that nitrogen as ammonia (NH_3) and ammonium (NH_4^+) are negligible and the total nitrogen in the hydrolysates was not appreciably underestimated. Factoring in glucose as the main carbon source, *T. testudinum* and *P. oceani-*

ca hydrolysates hold the highest C/N ratios with approximate values of 48 and 52, respectively.

Utilization of hydrolysates as sole media for bio-oil production

The potential use of seagrass hydrolysate as sole carbon source for lipid production was evaluated. This assessment was conducted without any nutritional addition to the hydrolysate. The well-documented oleaginous yeast *Trichosporon oleaginosus* was cultivated in each of the seven hydrolysates. The resulting data are compared to the cultivation data obtained in nitrogen-limiting medium A, optimized to promote high lipid accumulation.^[29] To evaluate the *T. oleaginosus* growth rate, the optical density (OD_{600}) was recorded every 24 h with an initial optical density of 0.5 (Figure 3). Cultures grown in *P. oceanica* hydrolysate as the sole cultivation medium, reached $\text{OD}_{600}=45$ at day 5, which was faster than any other cultivation medium.^[29] Most interestingly, no growth was observed in hydrolysates from *Z. noltii* and *Z. marina* (North Sea).

By contrast, *T. oleaginosus* grew very well in *Z. marina* hydrolysate from the Baltic Sea. This is due to the former hydrolysates originating from fresh seagrass samples, whereas the latter hydrolysates were all derived from aged seagrass samples that were previously exposed to sunlight.

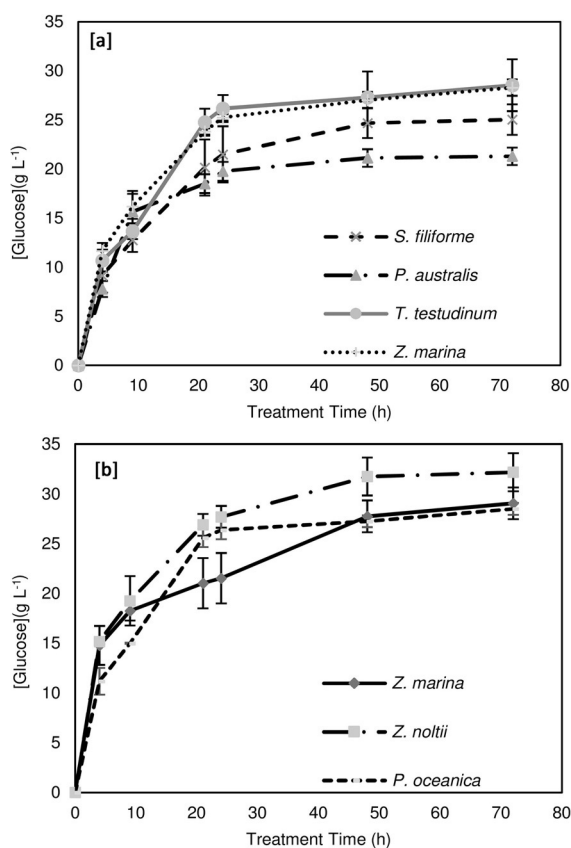


Figure 2. Time dependent release of glucose during enzymatic treatment of the seagrass samples. [a] *S. filiforme*, *P. australis*, *T. testudinum*, and *Z. marina* (2); [b] *Z. marina* (1), *Z. noltii* and *P. oceanica*.

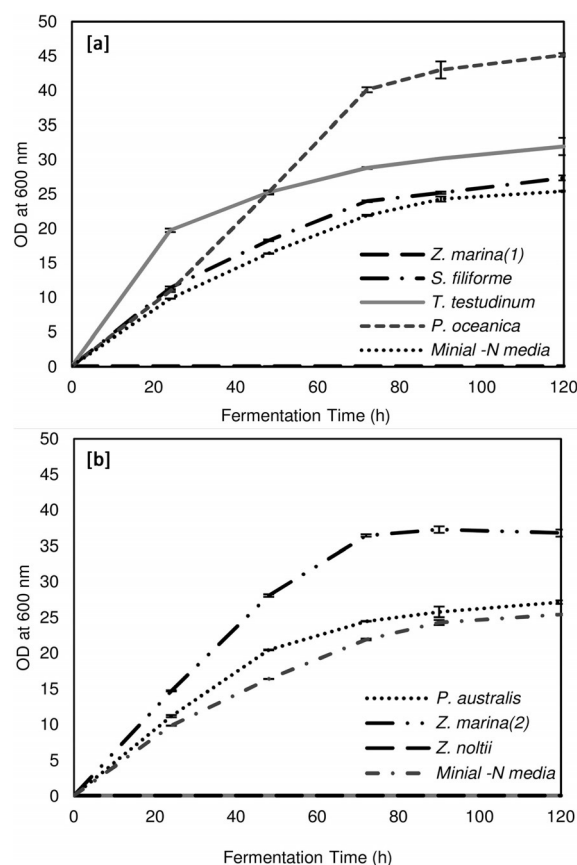


Figure 3. *T. oleaginosus* growth by the time during shake flask fermentation using the seagrass hydrolysates as a sole medium. [a]: hydrolysate of *Z. marina* (1), *S. filiforme*, *T. testudinum* and *P. oceanica*; [b] hydrolysate of *Z. marina* (2), *Z. noltii* and *P. australis*.

Table 5. Kjeldahl nitrogen content in the hydrolysate after 10 kDa cross filtration. ^[a]			
Hydrolysate	Protein content [% (w ^d w)]	Nitrogen content [% (w ^d w)] [g L ⁻¹]	
<i>Z. marina</i> (1)	2.10	0.34	3.54
<i>S. filiforme</i>	0.43	0.07	0.72
<i>P. australis</i>	0.47	0.07	0.76
<i>T. testudinum</i>	0.38	0.06	0.59
<i>Z. marina</i> (2)	0.55	0.09	0.90
<i>Z. noltii</i>	1.60	0.26	2.56
<i>P. oceanica</i>	0.36	0.06	0.55

[a] All relative standard deviation are less than 5%.

Certain inhibitory compounds, including phenolic acids,^[30] bacteriostatic agent,^[31] and rosmarinic acid,^[32] could be still present in fresh samples from *Z. noltii* and *Z. marina* (North Sea). Interestingly, yeast grown in *T. testudinum*, *Z. marina* (Baltic Sea), and *P. oceanica* reached OD₆₀₀ values of 29, 39, and 40, respectively, in just 3 days, whereas *T. oleaginosus* cultivated in medium A (Minimal-N medium) was only able to reach OD₆₀₀=15 in the same time period. The presence of various nutrients and trace elements in the respective seagrass hydrolysates could account for this high growth rate.

Gravimetric analysis was performed to determine the total lipid content in *T. oleaginosus* after 5 days of fermentation

(Figure 4). The yeast produced nearly 55% (w^dw_{biomass}) lipids while growing in minimal-N medium. Amongst the seagrasses, *P. australis* and *S. filiforme* hydrolysates enabled the highest lipid accumulation of approximately 50% (w^dw_{biomass}). *T. oleaginosus* cultivated in *P. oceanica* hydrolysate accumulated approximately 45% (w^dw_{biomass}) lipid content.

These aforementioned results show the total lipid content (C) as percent of cell dry weight. Measuring lipid production (P)—expressed as grams per liter of culture—produced differing results (Figure 5). After 5 days fermentation, the lipid productivity of *T. oleaginosus* reached its peak of 6.8 g L⁻¹ in *P. oceanica* hydrolysate. *T. testudinum* hydrolysate allowed for a 5.7 g L⁻¹ lipid accumulation, whereas yeast grown in medium A produced roughly 5.1 g L⁻¹ of SCO.

Lipid accumulation in oleaginous microorganisms is usually initiated upon nutrient deprivation (nitrogen, phosphate, or sulfur).^[33] Minimal-N medium is known to induce lipid biosynthesis in *T. oleaginosus* as it contains low nitrogen content. Nitrogen-limitation is considered to be essential for induction of lipogenesis in oleaginous yeasts and other organisms. Consequently, it was implemented for large-scale (15-L stirred-tank) fed-batch fermentation and biofuel production in yeast.^[34]

The results of biomass analysis of *P. oceanica* and *T. testudinum* may explain the high lipid accumulation in *T. oleagi-*

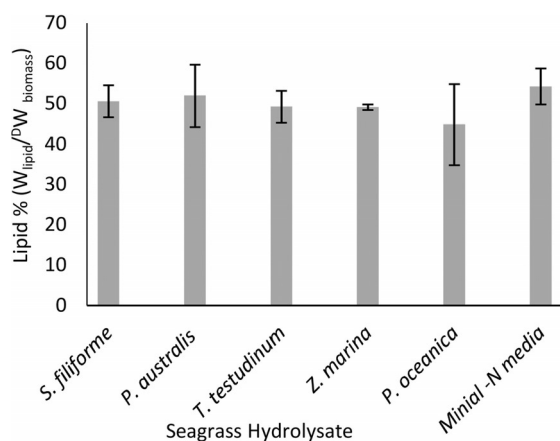


Figure 4. Lipid production of *T. oleaginosus* cultivated in various seagrass hydrolysates after 5 days shake flask fermentation as percent dry weight % ($w_{\text{lipid}}/d_{w_{\text{biomass}}}$).

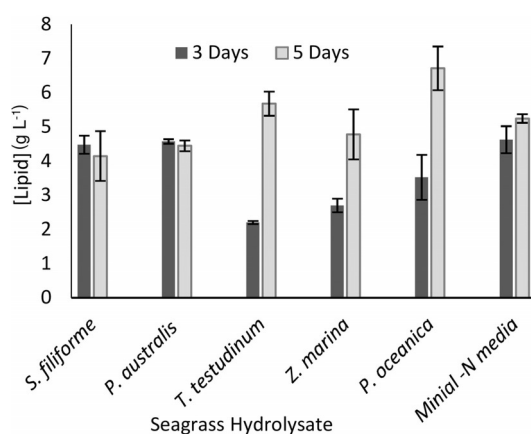


Figure 5. Lipid production of *T. oleaginosus* cultivated in various seagrass hydrolysates after 3 and 5 days as lipid g L^{-1} culture.

nosus cultivated in their corresponding hydrolysates. Protein content in these two samples was the lowest amongst all seagrasses with only 5% ($w_{\text{lipid}}/d_{w_{\text{biomass}}}$) of total dry weight. Following 10 kDa cross-filtration, *P. oceanica* and *T. testudinum* hydrolysates contained the least amount of nitrogen and exhibited the highest C/N ratios (52 and 48 respectively) among all other samples. However, the C/N ratio of medium A is approximately 150; thus, other factors besides nitrogen-limitation may be driving the lipogenesis in *T. oleaginosus* grown in these two samples. In the ash analysis, phosphate from *P. oceanica* and *T. testudinum* strains was not detectable. The effect of phosphate limitation on the lipid production in yeast strains has been previously examined.^[35] Exemplary, lipid accumulation in *Rhodospiridium toruloides* was directly associated with a high carbon/phosphorus (C/P) ratio, and it was maintained even in the presence of excess nitrogen.^[36] *P. oceanica* and *T. testudinum* hydrolysates with both high C/N and high C/P ratios allowed for higher lipid accumulation compared to minimal-N medium exhibiting only nitrogen limitation. The deficiency of phosphate and exhaustion of nitrogen allowed rapid lipid accumulation from

less than 2.4 g L^{-1} at day 3 (*T. testudinum* hydrolysate) to a maximum of 6.8 g L^{-1} at day 5 (*P. oceanica* hydrolysate). Furthermore, the relatively high nitrogen content in the hydrolysates compared to medium A allowed for higher yeast biomass production. Following 5 days culture, *T. oleaginosus* cultivated in *T. testudinum* and *P. oceanica* reached cell dry masses of approximately 11.6 and 15.5 g L^{-1} , respectively. Conversely the yeast only achieved approximately 9.8 g L^{-1} of dry biomass when grown in medium A (Figure S5, Supporting Information). The Seagrass hydrolysates exhibited rather optimal C/N/P content, thereby allowing simultaneous high cell biomass and high lipid production. C/N and C/P ratios might not be the only reason behind the high lipid yields. Chemical nutrition and the presence of various trace elements in the hydrolysates could also explain the clear advantage over the synthetic medium A. Further investigation would help to elucidate the factors contributing to lipogenesis in *T. oleaginosus* grown in seagrass hydrolysates.

In this study, the hydrolysates from seagrass were used as the sole carbon source for yeast growth and lipid production in aerated shake flasks. Optimization of fermentation can help to enhance the obtained lipids yield. This is achieved by adding further nutrition to the media or using bioreactors.

Lipid production in fed-batch bioreactor

Based on the data from previous shake flask cultures, *P. oceanica* from Malta was chosen as biomass feedstock for fermentation at liter scale. *T. oleaginosus* was cultivated in controlled fed-batch with *P. oceanica* hydrolysate as the sole carbon source and without any nutrients addition. The hydrolysate contained $28.5 \pm 0.59 \text{ g L}^{-1}$ glucose and $5.53 \pm 0.26 \text{ g L}^{-1}$ pentose. 1 L of undiluted hydrolysate was employed as the main fermentation medium with another 100 mL of concentrated *P. oceanica* hydrolysate used as feed for the fermentation. The highest yeast dry cell weight (DCW) of approximately 42 g L^{-1} was obtained from 70 h batch culture (Figure 6). Lipid accumulation was initiated after 24 h upon depletion of nitrogen as nutrient. Yeast lipid content peaked at 54.4% ($w/d_{w_{\text{biomass}}}$) triglycerides ($0.35 \text{ g L}^{-1} \text{ h}^{-1}$) after 96 h of fermentation (Figure 7), with the total lipid concentration reaching 24.5 g L^{-1} of hydrolysate at the same time point (Figure 8).

Bioconversion of cellulosic biomass by microbial fermentation usually necessitates an acidic/alkaline thermochemical pretreatment step to facilitate the subsequent enzymatic hydrolysis of cellulose.^[37] Lipid production from corn stover by the oleaginous yeast *Cryptococcus curvatus* required a pretreatment of the biomass with 0.5M NaOH at 80°C for 75 min.^[38]

Moreover, pretreatment could generate substances that inhibit the enzymatic hydrolysis step and disrupt the microbial fermentation. Furfural was found to elongate the lag-phase, whereas benzoic acid negatively affected the microbial growth rate and biomass yield.^[39] A complex chemical detoxification phase would be required, and all these extra steps present additional costs and diminish the eco-friendly aspect

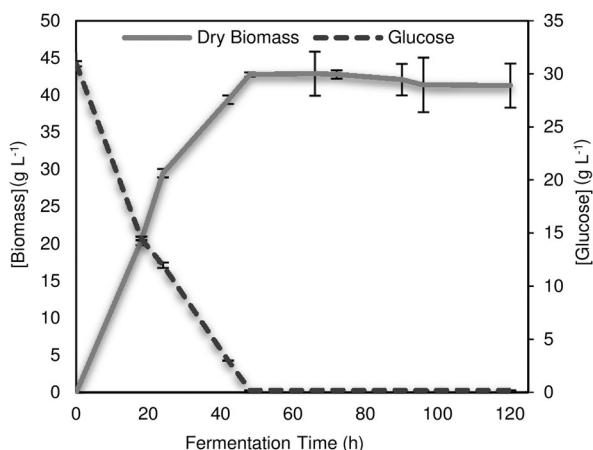


Figure 6. Increase of biomass and substrate consumption of *T. oleaginosus* during fermentation time using *P. oceanica* hydrolysate in a 1 L stirred tank bioreactor.

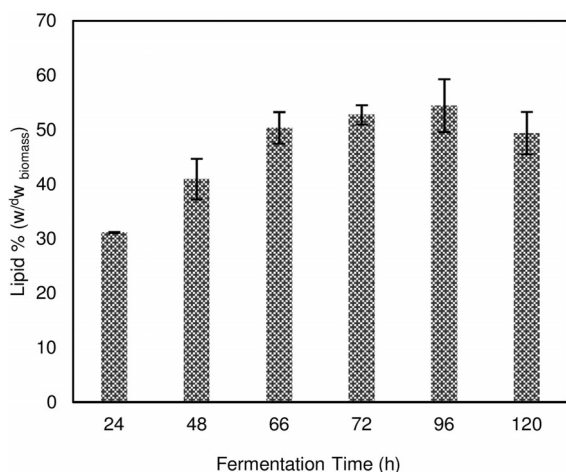


Figure 7. *T. oleaginosus* fermentations on *P. oceanica* hydrolysate conducted in 1 L stirred tank bioreactors. Lipid yield expressed as percentage of the dry cell weight.

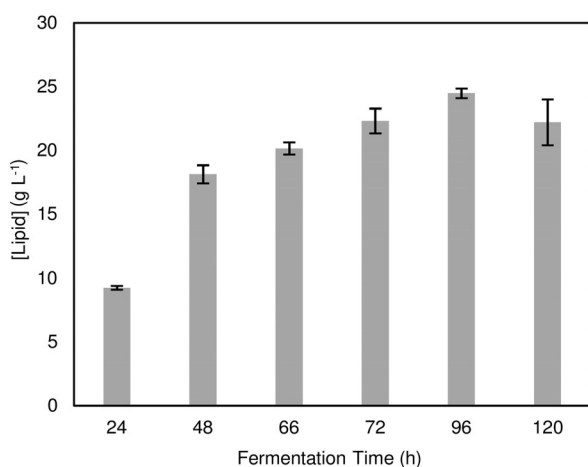


Figure 8. *T. oleaginosus* fermentations on *P. oceanica* hydrolysate conducted in 1 L stirred tank bioreactors. Lipid productivity as g L⁻¹.

of the process. In our upscaling experiment, neither dilution nor detoxification of the hydrolysate medium was necessary given that no inhibitory effect on the yeast was detected. This fact highlights the importance of using a purely enzymatic-based hydrolysis approach, and the viability of seagrass biomass as feedstock for microbial oil production.

Following fermentation, seagrass biomass (120 g) was converted to 25 g of microbial lipids with a lipid coefficient of 208.4 mg g⁻¹. In comparison, Meo et al., 2017 used *T. oleaginosus* in a bioreactor to convert 250 g of microalgae biomass into 30 g of lipids with a lipid coefficient of only 120 mg g⁻¹. Furthermore, the researchers supplemented 126 g pure glucose as feed,^[40] whereas in our experiment, seagrass hydrolysate was used as the sole carbon source for both the main and the feeding fermentation media. Additionally, the microalgae biomass was disrupted (to open the cell and facilitate the subsequent hydrolysis) with a high-pressure homogenizer—an energy consuming process—and required additional pretreatment. Therefore, our result demonstrate that seagrass is a superior feedstock compared to microalgae hydrolysate. Finally, the yeast fatty acid profile, measured by gas chromatography with flame ionization detection (GC-FID), shows high percentages of C_{16:0}, C_{18:0}, and C_{18:1}, which are suitable for subsequent high-quality biodiesel production (Table 6).

Table 6. Comparison of the *T. oleaginosus* fatty-acid profile cultivated in medium A and *P. oceanica* hydrolysate.

Media	Fatty acid content [% (w/w)]			
	C _{16:0} ^[a]	C _{18:0}	C _{18:1}	other
medium A	31.6 ^a	9.5	51.0	7.9
<i>P. oceanica</i>	34.7	6.2	51.2	7.9

[a] Relative STDV for all given numbers is $\leq \pm 1\%$.

With no need for pretreatment or expensive additives, lack of environmental impact, and universal availability, seagrass biomass can be a cost-effective feedstock for microbial lipid production—a particularly valuable factor in advancing and achieving the sustainable production of biodiesel.

Material balance and techno-economic evaluation

Every 1 ton of seagrass could theoretically generate approximately 17000 L of hydrolysate (60 g L⁻¹). After centrifugation and separation, 16000 L of hydrolysate can be recovered, which contain an average of 0.510 ton of fermentable sugars (34 g L⁻¹). Moreover, the hydrolysate contains various organic materials, such as proteins, which represent nitrogen and carbon sources in addition to carbohydrates. To liquefy the seagrass, approximately 14 kg of enzyme and 83 kg of chemicals (buffer solution) are required per ton of seagrass feedstock. The hydrolysis step would generate 0.370 tons of solid residual biomass, which can be utilized in further applications such as animal feed or plant fertilizers. According to current results, 0.21 tons of oil can be produced.

In 2014, a techno-economic evaluation for microbial oil production estimated the costs to be $\$5.5 \text{ kg}^{-1}$.^[41] The study was based on pure glucose as feedstock with an annual production capacity of 10000 tons of oil. To achieve targeted capacity, 12 fermenters each having a volume of 250 m^3 , would be required, and these fermenters each would run 47 times per year. The total volume of culture media would amount to 140850 m^3 , with a total glucose content of 42081 tons. In the reported evaluation, the glucose-to-SCO conversion yield was 0.23 g g^{-1} .^[41]

Based on the current study, supplying the previous unit with seagrass hydrolysate as alternative and sole fermentation media requires two times a volume of 140850 m^3 (first as main media and second as feeding after 10 times concentration). To produce the required volume, 18.78 tons of seagrass are required (0.06 ton m^{-3}). In addition, 12 vessels each with a volume of 250 m^3 would be necessary to run about 104 times per year. Taking into consideration that each run requires approximately 7 h loading and 70 h operation, the total process time would be 7500 hours per year.

Following hydrolysis, a solid/liquid disk separator should be installed in combination with a hydrolysate concentration unit. Furthermore, sterilization of raw materials is always required prior to hydrolysis. As the techno-economic evaluation has already included the sterilization step, it would be redundant to re-include it in the hydrolysate production process.

The installed equipment costs, fixed capital investment (FCI) calculations, operations (C_{OL}) costs, and utility costs (C_{UT}) of the previously mentioned process steps can be estimated using a similar unit equivalent to the study from Koutinas et al.^[41] Hence, the costs of the bioreactor (R-101), solid/liquid disk separator (VE-101), filtration (D-201), and condenser (V-202) can be used to estimate the cost of the hydrolysate manufacturing process.^[41] Additionally, heating units (E-101 and E-102)^[41] will be included. Overall aforementioned items and their respective costs are listed in Tables 7 and 8.

Material	Unit costs	Amount per Year [ton]	Cost per Year [\\$]
seagrass	$\$1 \text{ ton}^{-1}$	18 779	$\$18 779$
enzyme	$\$10 \text{ kg}^{-1}$	262.9	$\$2 629 000$
chemical	$\$1.5 \text{ kg}^{-1}$	524.2	$\$7 863 000$
total			$\\$10 510 779$

Category	Description	Cost per year [M\\$]
FCI cost	sum of (R-101, VE-101, D-201 V-202 E-101 and E-102) $\times 1.2$ ^[41]	54.6
operational cost (C_{OL})	sum of worker count $\times 4.5 = 20$	0.50
utility cost (C_{UT})	sum of (R-101, VE-101, D-201 V-202 E-101 and E-102) ^[41]	3.912
material cost (C_{RM})	from Table 7	10.5

Finally the estimated annual cost of hydrolysate manufacture (COM) can be calculated by applying the Turton equation:^[42]

$$\text{COM} = 0.28\text{FCI} + 2.73C_{OL} + 1.23(C_{RM} + C_{UT} + C_{WT})$$

Therefore, the COM of hydrolysate will be $\$34.38$ million to generate $281 690 \text{ m}^3$ hydrolysate, which corresponds to $\$0.112$ per liter.

Based on the calculation following Koutinas et al., after replacing the glucose with seagrass hydrolysate, the cost of microbial oil from seagrass hydrolysate is estimated to be $\$7.3 \text{ kg}^{-1}$. It is worth mentioning that the glucose-to-SCO conversion yield was 0.23 g g^{-1} ,^[34,41] whereas the seagrass biomass and the contained sugar-to-SCO conversion yields were 0.21 and 0.41 g g^{-1} , respectively.

Contrary to plant-derived oil, microbial oil production is not affected by seasonal or climate changes. Moreover, microbial oil (MO) production does not affect agricultural activity and food security. However, due to the low biomass production costs, vegetable oil costs are lower than MO ranging between 1.1 and $\$2.1 \text{ kg}^{-1}$ for soybean and peanut oil, respectively.^[41] Despite the availability of cheap raw materials, the challenge of SCOs production remains in the hydrolysis and biomass formation steps, which represent a significant part of the overall process costs.

Discussion

Seasonally, piles of seagrass residues accumulate on beaches and shores all over the globe. In excess of 80% of this biomass is not degraded biologically. This undesirable "waste" is constantly being removed or buried, especially in touristic destinations. In this work, we assessed the application of this waste material as a feedstock for SCO and subsequent bio-fuel/biolubricant production. This assessment presents seagrass biomass as a new starting material for biodiesel production, alternative to edible plant-based lipids.

Electron microscopy and comprehensive biomass analysis were performed on the various seagrass samples. The acquired data facilitated the optimization of enzymatic hydrolysis and offered insights regarding the hydrolysate compositions, trace elements content, and C/N/P ratios. An enzymatic-based hydrolysis method was optimized that efficiently released the carbohydrate monomers and allowed the production of seagrass hydrolysate without the need for energy-intensive thermochemical pretreatment. This single-step method prevented the generation of inhibitory compounds

that normally required complex detoxification steps prior to fermentation. This approach is both cost-effective and eco-friendly.

Low density and high moisture content in feedstock materials are the main limitations for energy-efficient biomass-based processes, generating increased transport and operational costs.^[16] Biomass analysis of the collected samples showed low water content. Furthermore, structural analysis, in particular that of *P. oceanica*, revealed a dense (non-hollow) structure. Seagrass biomass, exhibiting high density and minimal water content, is an advantageous raw material for cost-effective industrial applications. However, the biomass composition of seagrass might vary depending on the environment (location) and time of harvest. Furthermore, not all seagrass species offer the same industrial advantages as *P. oceanica*.

Previous reports used pure sucrose,^[7a] synthetic media,^[43] pre-treated secondary wastewater sludge,^[7b] and pre-treated microalgae hydrolysate fed with pure glucose^[40] as cultivation media for oily yeasts. Conversely, *T. oleaginosus* was successfully cultivated in all hydrolysates of aged-seagrass as the sole carbon source, without expensive additives such as yeast extract and biotin. *T. oleaginosus* cultivated in *P. oceanica* hydrolysate in a bioreactor accumulated a substantial amount of lipids ($\approx 25 \text{ g L}^{-1}$). The produced lipid, mainly in the form of triglycerides, is a preferred feedstock for chemo-catalytic conversion into green jet fuels,^[44] thermochemical (pyrolysis) conversion into biogas and biosolids,^[45] and ultrasonic cavitation to make clean biodiesel.^[46] McCurdy et al., showed that lipids from *T. oleaginosus* can be converted into biodiesel with a recovery of 98.9%. Furthermore, flash point, viscosity, sulfur content, and acid number of the corresponding B20 meet the ASTM requirement and it is comparable to Soybean B20.^[7a]

Based on the data presented in this study, 120 g of seagrass could be converted fermentatively to 25.0 g of lipids. Accordingly, by exploiting only half of the available residual seagrass biomass from around the globe, approximately 3.915 million tons of triglyceride-type lipids could theoretically be produced (with a process efficiency 85%). Enzymatic transesterification of these lipids with methanol or ethanol would yield 6.24 million tons (5.6 billion liters) of B100 biodiesel and 0.48 million tons glycerol [based on a conversion factor of 80% (*w/w*)]. Interestingly, this potential biodiesel yield from seagrass residues is comparable to the entire B100 production of USA in 2015 (4.8 billion liters),^[1] which adds up to 26% of the global B100 production volume (21.6 billion liters) in that same year.^[47] Moreover, the USA predominantly (53%) generated this B100 production volume through conversion of edible oils, such as corn and soybean oil.^[1] The generation of these edible oil feedstocks required approximately 6.4 and 11.8 million hectares of agricultural land, respectively, for corn and soybean cultivation.^[1,48]

The use of seagrass residues for the production of equivalent volumes of B100 biodiesel would not affect any agricultural activity or have any effect on sensitive marine ecosystems. Therefore, seagrass biomass would represent a real sus-

tainable alternative to the application of edible plant oils particularly. However, despite its many industrial advantages, the use of seagrass as feedstock for SCO production might suffer from logistical drawbacks, such as collection and transportation of feedstocks from around the globe. The use of seagrass residue for renewable fuel production would require a significant alteration in the production logistics of the centralized processing of biofuels. As seagrasses are available only at scattered locations, which commonly are not close to human populations, its effective utilization as a biofuels feedstock would argue for a small decentralized production network. It is conceivable, that small, decentralized fermentation/chemical upgrading units could be installed at seagrass collection sites, which would convert only the relevant biomass amounts locally available. The resulting biofuel volumes could either be collected and then brought to centralized logistic hubs, or more preferably be utilized by nearby human settlements or industrial facilities that require a self-sustaining energy source. This study offers fundamental knowledge that can be used in future work to optimize oil production in large-scale bioreactors, investigate mechanisms of substrate-to-lipid conversion, and further assess the economics of biofuel and biodiesel production before commercialization of this technology.

Conclusions

Produced from readily available beach-cast waste materials, this simplified enzyme-treated seagrass media, provides a potential route to cost-effective sustainable bioenergy/biofuel production. Out of seven samples of seagrasses, *P. oceanica* (Mediterranean Sea) displays the best lipid productivity exceeding the well-optimized minimal nitrogen media. Generally, marine biomass does not affect terrestrial agricultural activity. Moreover, in this study we only employ aged seagrass banquettes that are washed ashore and do not affect the marine ecosystem. Therefore, the process presented in this study offers a biorefinery model for sustainable generation of microbial lipids with no impact on agricultural security or sensitive marine ecosystems.

Experimental Section

Samples

Fresh and aged seagrass samples were collected during the summer seasons of 2013 and 2014 from six different locations worldwide: two samples from the Baltic Sea (Hohenkirchen and Greifswald), two from the Mediterranean Sea (Malta), one in the Caribbean Sea (Isla de Mujeres, Mexico), one from the Great Australian Bight (Beachport, South Australia), and one sample from the North Atlantic Ocean (Bahamas). The samples were washed thoroughly to remove accumulated salt, sand and contaminants, dried, and ground down to $\leq 0.5 \text{ mm}$ thickness using a planetary ball mill (Fritsch, Germany). For reproducibility purposes, all experiments and analyses were conducted in triplicate.

Sequence determination, phylogeny

Genomic DNA was isolated from seagrass samples using the innuPREP Plant DNA Kit (Analytik Jena, Germany). Extracted DNA was then run on 1% agarose gel (100 mA, 120 V) for 10 min. A gel area corresponding to 8000–10000 kilobase (kb) size was cut. DNA was purified from the cut gel using innuPREP DOUBELepure Kit (Analytik Jena, Germany). Two sets of primers were used for DNA amplification from all samples. The first set EukA (5'- AACCTGGTTGATCCTGCCAGT-3') and EukB (5'-TGATCCTTCTGCAGGTTACCTAC-3') amplify the entire 18S rRNA region (almost 950 bp).^[49] Primers ITS1 (5'-TCCGTAGGTGAACCTGCGG-3') and NL4 (5'-GGTCCGTGTTTCA AGACGG-3')^[50] bind to entire intervening ITS1, 5.8S, ITS2 rRNA, and the D1/D2 domain (a portion of the 26S rRNA gene).

Biomass analysis

HPLC analysis

Sugar composition was analyzed by an Agilent 1100 series HPLC with a Refractive Index (RI) detector (Shodex, RI101) and Ultraviolet Index (Sedere-France, Sedex 75). The sugars were separated by using two different methods. In the first, a Rezex ROA-Organic Acid column (Aminex HPX 87H) was used with the eluent (5.0 mM H₂SO₄) at a flow rate of 0.5 mL min⁻¹. The column heater was set at 70 °C, and the detector was set at 40 °C. In the second method, sugars were separated using an Aminex HPX-87P column. An isocratic mobile phase of double distilled H₂O was pumped at a rate of 0.6 mL min⁻¹. The column temperature was 70 °C with the detector set at 50 °C.

GC-FID analysis

Lipids were extracted according to the Folch procedure.^[51] The fatty acids were converted into fatty acid methyl esters (FAMES) as described in Griffiths et al.^[52] Glyceryl trionadecanoate (C_{19:0}-TAG, 1.00 mg) was added prior to the reaction as an internal standard. FAMES was analysed using GC-FID [Zebtron Capillary GC column (Phenomenex, Germany)]. The column was 30.0 m in length with an internal diameter of 0.32 mm and a film thickness of 0.25 µm. The column operated at a temperature of 150 °C for 1 min before increasing to 240 °C at a rate of 5 °C min⁻¹. The injector injected a sample amount of 1.0 µL at a temperature of 240 °C with a split ratio of 10 and hydrogen was used as the carrier gas at a flow rate of 3 mL min⁻¹. Before injection, FAME (C_{12:0}) was added to the samples as an internal standard for quantitation.

Electron microscope and EDX

Scanning electron microscopy (SEM) was performed using a JSM-7500F scanning electron microscope (JEOL, Japan) with an accelerating voltage of 1, 2, or 5 kV and a secondary electron detector.

The ash profile was determined using SEM with energy-dispersive X-ray (EDX) analysis. Ash samples were mounted on a carbon film and prepped for analysis. EDX analysis was performed on multiple areas (100 × 100 µm²) in backscattered electron (BSE) mode for each ash sample. The average value was calculated to obtain the elemental composition of the ash.

Kjeldahl analysis

The protein amount was determined using the standard operating procedure by Kjeldahl et al. Dry seagrass biomass (2.00 g) was digested (InKjel M, behr Labor technik GmbH-Germany) and distilled (Vapodest 10, Gerhardt- Germany).

Seagrass treatment

Enzymatic hydrolysis of each of the seagrass samples was conducted using 2 L glass bottles (Schott) containing 1.0 L of acetate buffer solution (50.0 mM, pH 5.0) and 60.0 g of biomass. Reactions were initiated by adding an enzyme solution and incubating at 50 °C while stirring at 400 rpm using magnetic stirrer for 72 h. The used enzymes include Cellic CTec 2 (Novozymes- Denmark), Cellic HTec (Novozymes- Denmark), Pectinex (Novozymes- Denmark), and Novozymes 188 (Novozymes- Denmark). In parallel, two controls were included: control one contained a substrate without the enzyme solution and control two contained an enzyme solution without a substrate. The controls were conducted in 50 mL falcon tubes containing 25.0 mL of acetate buffer solution (50.0 mM, pH 5.0) and 500.0 mg of biomass.

Hydrolysate preparation

The samples were then centrifuged for 30 min at 8000 g, followed by cross-filtration (10 kDa membrane made from regenerated cellulose was used with the following parameters: inlet pressure (P1) 2 bar, repellant pressure (P2) 0.3–0.5 bar, and the permeate was open to atmospheric pressure. The flow rates of repellant and permeate were approximately 2 L min⁻¹ and 0.1 L min⁻¹, respectively. 0.2 µm filter capsules were installed at the outlet to sterilize the resulted hydrolysate. A sexokinase assay kit (Megazyme- Ireland), was used to measure the glucose concentration of each sample at 340 nm, repeated four times. For the standard curve, five calibration points were measured at concentrations: 0.5, 1.0, 2.0, 3.0, and 4.0 g L⁻¹. The final sugar analysis was performed by using HPLC as described above. A subsample from each hydrolysate was analyzed to detect reduced nitrogen using the Kjeldahl method.

Utilization of hydrolysates as sole medium for bio-oil production

For observation of its growth rate and lipid accumulation, the yeast *Trichosporon oleaginosus* (ATCC 20509) was cultivated in 1 L Erlenmeyer flasks containing 300 mL of the different enzymatic hydrolysates. The flasks were supplemented with an aeration system supplying the cultures with 0.2 L min⁻¹ pre-filtered air. Nitrogen-limited medium (medium A) as previously described,^[53] was used as a positive control. With an initial seeding OD₆₀₀ = 0.5, all cultures were incubated in a rotary shaker at 120 rpm at 28 °C for 5 days. OD₆₀₀ was measured every day, and liquid cultures were divided for subsequent gravimetric analysis. A technical draw for aerated flasks is available in the Supporting Information (Figure S6).

Lipid at fed-batch bioreactor

Dried grinded *P. oceanica* (120 g) was subjected to enzymatic hydrolysis followed by 10 kDa cross-filtration (as previously described) generating 2 L of hydrolysate. For fed-batch cultivation, 1 L served as the main fermentation medium and the remaining

1 L was concentrated 10 times by using a rotary evaporator and used as feed for the bioreactor. *T. oleaginosus* was cultured in the seed medium YPD (10 gL⁻¹ yeast extract, 20 gL⁻¹ peptone, and 20 gL⁻¹ glucose) at 28 °C and 120 rpm for 24 h. 10% of the culture was inoculated into the seagrass hydrolysate. Fed-Batch cultivation of *T. oleaginosus* was performed in a 2 L bioreactor (INFORS HT system, Switzerland) with a working volume of 1 L in *P. oceanica* hydrolysate with an approximate C/N ratio of 52. The temperature was maintained at 28 °C, and the pH of the bioreactor was adjusted to pH 6.5 ± 0.2 with 1 M NaOH by the system. Stirring (200–400 rpm) and aeration (1.0–2.0 normal liters per minute of air) were regulated automatically to maintain the dissolved oxygen at above 50%. Foam was prevented by the addition of 0.01% (v/v) of an antifoam agent (Antifoam 204, Sigma Aldrich). Substrate feeding was initiated at day 1. Samples were withdrawn manually at 24 h intervals for 6 days, and were used for subsequent determination of OD₆₀₀, the dry cell weight, and lipid content.

Dry biomass determination/ gravimetric analysis lipids

Dry biomass was processed by lyophilization for 2 days at -80 °C and 0.04 mbar (Christ alpha 2–4 LD plus). Gravimetric quantification of the lipid was performed using the Bligh–Dyer method.^[54] Briefly, a high-pressure homogenizer (Avestin emulsiflex C3) was used followed by three times solvent extraction using Folch solution.

Fatty acid profile

GC–FID, see the procedure as described above.

Acknowledgements

M.M., F.Q., and T.B. acknowledge financial support by the German Federal Ministry of Education and Research for supporting the “LIPOMAR” (grant number: 031A261) and “Advanced Biomass Value” (grant number: 03SF0446A) projects. Information concerning the Advanced biomass projects can be obtained at: <http://www.ibbnetzwerk-gmbh.com/de/service/pressebereich/pm-06052013-advanced-biomass-value/>. S.Y., N.M., and T.B. also acknowledge financial support for the project “Resource efficient production processes for polyhydroxybutyrate based biopolymers” of the Bavarian State Ministry for Environment and Consumer Protection (StMUV, grant number TLKO1U-69045).

Conflict of interest

The authors declare no conflict of interest.

Keywords: bioenergy • biofuels • enzymatic treatment • fermentation • seagrass

- [1] U.S.E.I. Administration, U.S. Energy Information Administration, 2016.
 [2] V. H. Smith, B. S. Sturm, S. A. Billings, *Trends Ecol. Evol.* **2010**, *25*, 301–309.

- [3] G. V. Subhash, S. V. Mohan, *Fuel* **2014**, *116*, 509–515.
 [4] a) L. Chng, K. Lee, D. Chan; b) A. Guldhe, B. Singh, I. Rawat, K. Ramluckan, F. Bux, *Fuel* **2014**, *128*, 46–52.
 [5] Y. A. Tsigie, L. H. Huynh, P. L. T. Nguyen, Y.-H. Ju, *Fuel Process. Technol.* **2013**, *115*, 50–56.
 [6] Y.-H. Chang, K.-S. Chang, C.-L. Hsu, L.-T. Chuang, C.-Y. Chen, F.-Y. Huang, H.-D. Jang, *Fuel* **2013**, *105*, 711–717.
 [7] a) A. T. McCurdy, A. J. Higham, M. R. Morgan, J. C. Quinn, L. C. Seefeldt, *Fuel* **2014**, *137*, 269–276; b) X. Zhang, S. Yan, R. D. Tyagi, R. Y. Surampalli, J. R. Valéro, *Fuel* **2014**, *134*, 274–282.
 [8] P. Gujjari, S.-O. Suh, K. Coumes, J. J. Zhou, *Mycologia* **2011**, *103*, 1110–1118.
 [9] a) P. Akhtar, J. Gray, A. Asghar, *J. Food Lipids* **1998**, *5*, 283–297; b) P. Meesters, G. Huijberts, G. Eggink, *Appl. Microbiol. Biotechnol.* **1996**, *45*, 575–579; c) Y. Liang, T. Tang, T. Siddaramu, R. Choudhary, A. L. Umagiliyige, *Renewable Energy* **2012**, *40*, 130–136.
 [10] I. K. Chung, J. Beardall, S. Mehta, D. Sahoo, S. Stojkovic, *J. Appl. Phycol.* **2011**, *23*, 877–886.
 [11] S. Beer, E. Koch, *Mar. Ecol. Prog. Ser.* **1996**, *141*, 199–204.
 [12] B. Subhadra, M. Edwards, *Energy Policy* **2010**, *38*, 4897–4902.
 [13] J. W. Fourqurean, C. M. Duarte, H. Kennedy, N. Marbà, M. Holmer, M. A. Mateo, E. T. Apostolaki, G. A. Kendrick, D. Krause-Jensen, K. J. McGlathery, *Nat. Geosci.* **2012**, *5*, 505–509.
 [14] J. Cebrián, C. M. Duarte, N. Marbà, *J. Exp. Mar. Biol. Ecol.* **1996**, *204*, 103–111.
 [15] S. Enriquez, C. M. Duarte, K. Sand-Jensen, *Oecologia* **1993**, *94*, 457–471.
 [16] M. H. L. Silveira, A. R. C. Morais, A. M. D. C. Lopes, D. N. Olekszyzen, R. Bogel-Lukasik, J. Andreaus, L. P. Ramos, *ChemSusChem* **2015**, *8*, 3366–3390.
 [17] a) M. Uchida, T. Miyoshi, M. Kaneniwa, K. Ishihara, Y. Nakashimada, N. Urano, *J. Biosci. Bioeng.* **2014**, *118*, 646–650; b) M. Pilavtepe, M. S. Celiktas, S. Sargin, O. Yesil-Celiktas, *Ind. Crops Prod.* **2013**, *51*, 348–354.
 [18] a) M. Rakicka, Z. Lazar, T. Dulermo, P. Fickers, J. M. Nicaud, *Bio-technol. Biofuels* **2015**, *8*, 1; b) R. Wang, J. Wang, R. Xu, Z. Fang, A. Liu, *BioResources* **2014**, *9*, 7027–7040.
 [19] R. Kourist, F. Bracharz, J. Lorenzen, O. N. Kracht, M. Chovatia, C. Daum, S. Deshpande, A. Lipzen, M. Nolan, R. A. Ohm, *mBio* **2015**, *6*, e00918-15.
 [20] a) E. P. Green, F. T. Short, *World atlas of seagrasses*, University of California Press, **2003**; b) G. De Falco, S. Simeone, M. Baroli, *J. Coastal Res.* **2008**, *24*, 69–75.
 [21] a) D. H. Les, M. A. Cleland, M. Waycott, *Syst. Bot.* **1997**, *22*, 443–463; b) Y. Kato, K. Aioi, Y. Omori, N. Takahata, Y. Satta, *Genes Genet. Syst.* **2003**, *78*, 329–342.
 [22] B. H. Daru, K. Yessoufou in *DNA Barcoding in Marine Perspectives*, Springer, Switzerland, **2016**, pp. 313–330.
 [23] D. W. Templeton, M. Quinn, S. Van Wychen, D. Hyman, L. M. Laurens, *J. Chromatogr. A* **2012**, *1270*, 225–234.
 [24] J. M. Ageitos, J. A. Vallejo, P. Veiga-Crespo, T. G. Villa, *Appl. Microbiol. Biotechnol.* **2011**, *90*, 1219–1227.
 [25] a) M. Yamamuro, A. Chirapart, *J. Oceanogr.* **2005**, *61*, 183–186; b) J. L. Siegal-Willott, K. Harr, L.-A. C. Hayek, K. C. Scott, T. Gerlach, P. Sirois, M. Reuter, D. W. Crewz, R. C. Hill, *J. Zoo Wildlife Med.* **2010**, *41*, 594–602; c) G. Brudecki, R. Farzanah, I. Cybulska, J. E. Schmidt, M. H. Thomsen, *Energy Procedia* **2015**, *75*, 760–766.
 [26] a) Y. A. Tsigie, C.-Y. Wang, N. S. Kasim, Q.-D. Diem, L.-H. Huynh, Q.-P. Ho, C.-T. Truong, Y.-H. Ju, *BioMed Res. Int.* **2012**, *2012*, 378384; b) S. Morales-delaRosa, J. M. Campos-Martin, J. L. Fierro, *Cellulose* **2014**, *21*, 2397–2407.
 [27] H. Huang, X. Guo, D. Li, M. Liu, J. Wu, H. Ren, *Bioresour. Technol.* **2011**, *102*, 7486–7493.
 [28] C. K. Nitsos, K. A. Matis, K. S. Triantafyllidis, *ChemSusChem* **2013**, *6*, 110–122.
 [29] L. Yong-Hong, L. Bo, Z. Zong-Bao, B. Feng-Wu, *Chin. J. Biotechnol.* **2006**, *22*, 650–656.
 [30] P. Davies, C. Morvan, O. Sire, C. Baley, *J. Mater. Sci.* **2007**, *42*, 4850–4857.
 [31] Y. Liu, G. Jiang, Z. Wu, *J. Ocean Univ. China* **2010**, *9*, 68–70.

- [32] J. Wang, X. Pan, Y. Han, D. Guo, Q. Guo, R. Li, *Mar. Drugs* **2012**, *10*, 2729–2740.
- [33] S. Papanikolaou, G. Aggelis, *Eur. J. Lipid Sci. Technol.* **2011**, *113*, 1031–1051.
- [34] Y. Li, Z. K. Zhao, F. Bai, *Enzyme Microb. Technol.* **2007**, *41*, 312–317.
- [35] G. Zhang, W. T. French, R. E. Hernandez, J. Hall, D. Sparks, W. E. Holmes, *J. Chem. Technol. Biotechnol.* **2011**, *86*, 642–650.
- [36] S. Wu, C. Hu, G. Jin, X. Zhao, Z. K. Zhao, *Bioresour. Technol.* **2010**, *101*, 6124–6129.
- [37] L. J. Jönsson, B. Alriksson, N.-O. Nilvebrant, *Biotechnol. Biofuels* **2013**, *6*, 16.
- [38] Z. Gong, H. Shen, X. Yang, Q. Wang, H. Xie, Z. K. Zhao, *Biotechnol. Biofuels* **2014**, *7*, 158.
- [39] Y. Zha, B. Muilwijk, L. Coulier, P. J. Punt, *J. Bioprocess. Biotech.* **2012**, *2*, 112–122.
- [40] A. Meo, X. L. Priebe, D. Weuster-Botz, *J. Biotechnol.* **2017**, *241*, 1–10.
- [41] A. A. Koutinas, A. Chatzifragkou, N. Kopsahelis, S. Papanikolaou, I. K. Kookos, *Fuel* **2014**, *116*, 566–577.
- [42] R. Turton, R. C. Bailie, W. B. Whiting, J. A. Shaeiwitz, *Analysis, synthesis and design of chemical processes*, Pearson Education, **2008**.
- [43] Y. Wei, V. Siewers, J. Nielsen, *Appl. Microbiol. Biotechnol.* **2017**, *101*, 3577–3585.
- [44] C. Zhao, T. Brück, J. A. Lercher, *Green Chem.* **2013**, *15*, 1720–1739.
- [45] N. Muradov, A. Gujar, J. Baik, T. Ali, *Fuel Process. Technol.* **2015**, *140*, 236–244.
- [46] S. Asif, L. F. Chuah, J. J. Klemeš, M. Ahmad, M. M. Akbar, K. T. Lee, A. Fatima, *J. Cleaner Prod.* **2017**, *161*, 1360–1373.
- [47] S. GmbH, <https://www.statista.com>, **2016**.
- [48] T. J. t. F. Project, **2016**.
- [49] B. Díez, C. Pedrós-Alió, R. Massana, *Appl. Environ. Microbiol.* **2001**, *67*, 2932–2941.
- [50] C. Kurtzman, C. Robnett, *J. Clin. Microbiol.* **1997**, *35*, 1216–1223.
- [51] J. Folch, M. Lees, G. S. Stanley, *J. Biol. Chem.* **1957**, *226*, 497–509.
- [52] M. Griffiths, R. Van Hille, S. Harrison, *Lipids* **2010**, *45*, 1053–1060.
- [53] M. Suutari, P. Priha, S. Laakso, *J. Am. Oil Chem. Soc.* **1993**, *70*, 891–894.
- [54] E. G. Bligh, W. J. Dyer, *Can. J. Biochem. Physiol.* **1959**, *37*, 911–917.

Manuscript received: August 23, 2017

Revised manuscript received: September 24, 2017

Accepted manuscript online: September 27, 2017

Version of record online: December 11, 2017

Energy Technology

Supporting Information

A Seagrass-Based Biorefinery for Generation of Single-Cell Oils for Biofuel and Oleochemical Production

Mahmoud A. Masri⁺, Samer Younes⁺, Martina Haack, Farah Qoura, Norbert Mehlmer,^{*} and Thomas Brück^{*[a]}

ente_201700604_sm_miscellaneous_information.pdf



Figure 1S: Accumulated seagrass at the south coast of Australia (the photo has taken from Beachsport, South Australia, Australia in 2013). These deposits can exceed a height of 1.5 meter extending along the shoreline and beyond the range of vision.

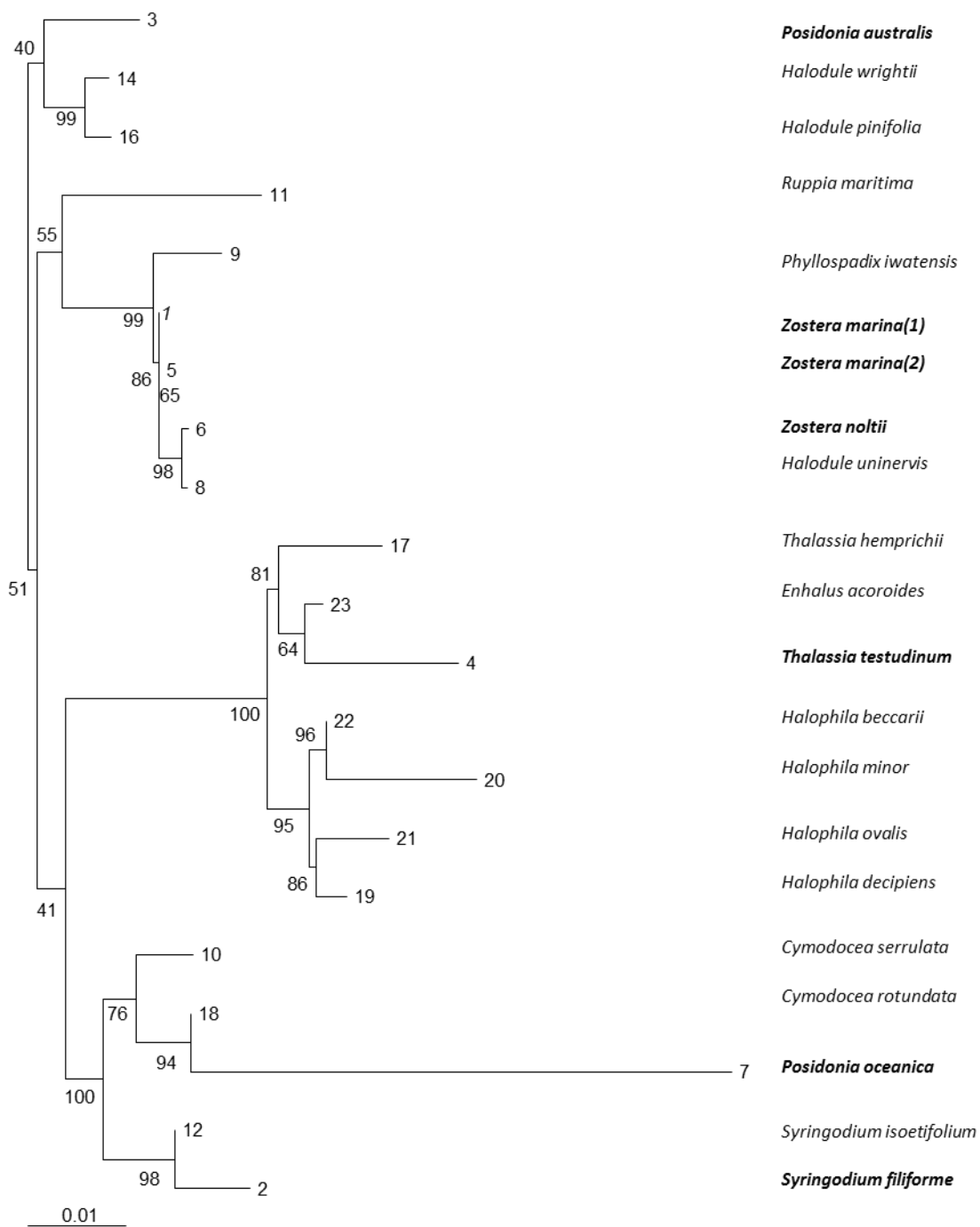


Figure 2S: Phylogenetic dendrogram based on nucleic acids sequences of 18S rRNA. Performed by the neighbour-joining method using software from PHYLIP, version 3.57c; the PRODIST program with Kimura-2 factor was used to compute the pairwise evolutionary distances for the above aligned sequences, the topology of the phylogenetic tree was evaluated by performing a bootstrap (algorithm version 3.6 b) with 1000 bootstrapped trials. The tree was drawn using Tree View 32 software. Bar corresponds to 1 nucleic acid substitutions per 10 nucleic acids.

Table 1: Selected seagrass samples, locations and identification based on ITS1 and 18S rRNA sequencing.

Strain	Location	GPS Data
<i>Zostera marina</i> (1)	Baltic Sea (Hohenkirchen)	53°56'36.4"N 11°19'01.5"E
<i>Syringodium filiforme</i>	Caribbean Sea (Mexico)	21°14'41.5"N 86°44'18.0"W
<i>Posidonia australis</i>	South Australia	37°29'26.9"S 140°00'51.9"E
<i>Thalassia testudinum</i>	North Sea (Bahamas)	25°04'19.5"N 77°57'55.0"W
<i>Zostera marina</i> (2)	Baltic Sea (Greifswald)	54°05'26.1"N 13°27'31.0"E
<i>Zostera noltii</i>	Mediterranean Sea (Malta1)	35°52'06.2"N 14°34'26.2"E
<i>Posidonia oceanic</i>	Mediterranean Sea (Malta2)	35°49'15.4"N 14°33'32.1"E

Table 2S: Lipid analysis of seagrass using GC-MS with C_{19:0} TAG as internal standard for methylation.

Fatty Acid	% (w/dW _{Biomass})						
	<i>Z. marina</i> (1)	<i>S. filiforme</i>	<i>P. australis</i>	<i>T. testudinum</i>	<i>Z. marina</i> (2)	<i>Z. noltii</i>	<i>P. oceanica</i>
C_{12:0}	0.00±0.000	0.00±0.000	0.00±0.000	0.023±0.004	0.012±0.001	0.029±0.004	0.021±0.001
C_{14:0}	0.033±0.002	0.050±0.004	0.083±0.014	0.125±0.016	0.090±0.019	0.131±0.007	0.061±0.038
C_{14:1}	0.06±0.001	0.070±0.001	0.040±0.0007	0.045±0.008	0.046±0.002	0.054±0.005	0.045±0.027
C_{16:0}	0.634±0.026	0.602±0.018	0.580±0.063	0.789±0.125	0.818±0.059	1.616±0.099	0.471±0.308
C_{16:1}	0.282±0.022	0.057±0.003	0.115±0.012	0.058±0.007	0.102±0.003	0.084±0.008	0.051±0.021
C_{16:3} (Ω4)	0.033±0.004	0.023±0.001	0.021±0.002	0.020±0.001	0.031±0.001	0.040±0.002	0.010±0.002
C_{18:0}	0.243±0.032	0.330±0.023	0.326±0.031	0.357±0.066	0.344±0.037	0.321±0.044	0.152±0.125
C_{18:1} (Ω9)	0.106±0.011	0.109±0.010	0.195±0.023	0.343±0.047	0.389±0.056	0.375±0.017	0.206±0.196
C_{18:1} (Ω7)	0.065±0.007	0.054±0.006	0.111±0.013	0.054±0.008	0.128±0.004	0.059±0.004	0.076±0.032
C_{18:2} (Ω6)	0.204±0.012	0.057±0.004	0.073±0.010	0.057±0.009	0.203±0.025	1.506±0.072	0.085±0.037
C_{18:3} (Ω3)	0.417±0.004	0.040±0.002	0.032±0.004	0.019±0.002	0.152±0.007	2.689±0.030	0.076±0.027
C_{18:4} (Ω3)	0.055±0.009	0.073±0.010	0.089±0.006	0.020±0.001	0.020±0.000	0.060±0.007	0.040±0.008
C_{20:0}	0.060±0.002	0.070±0.002	0.030±0.001	0.023±0.004	0.086±0.002	0.035±0.003	0.035±0.016
C_{20:1} (Ω9)	0.020±0.003	0.030±0.002	0.040±0.001	0.024±0.010	0.030±0.002	0.030±0.008	0.042±0.011
C_{20:2} (Ω6)	0.010±0.005	0.01±0.005	0.010±0.006	0.022±0.016	0.009±0.000	0.019±0.001	0.023±0.027
C_{20:4} (Ω6)	0.010±0.002	0.02±0.003	0.010±0.004	0.006±0.001	0.006±0.000	0.008±0.000	0.029±0.024
C_{20:3} (Ω3)	0.010±0.002	0.01±0.001	0.020±0.002	0.012±0.004	0.017±0.002	0.016±0.001	0.025±0.029
C_{20:5} (Ω3)	0.017±0.01	0.013±0.002	0.024±0.01	0.073±0.006	0.055±0.007	0.107±0.008	0.064±0.016
C_{22:0}	0.110±0.000	0.03±0.001	0.100±0.005	0.029±0.002	0.142±0.004	0.086±0.005	0.034±0.025
C_{22:1} (Ω9)	0.05±0.001	0.01±0.0008	0.030±0.004	0.010±0.001	0.006±0.002	0.038±0.003	0.025±0.034
C_{24:0}	0.110±0.005	0.12±0.008	0.120±0.004	0.07±0.004	0.152±0.004	0.125±0.008	0.435±0.606
C_{22:6} (Ω6)	0.022±0.001	0.038±0.002	0.046±0.007	0.012±0.001	0.075±0.003	0.193±0.023	0.052±0.027

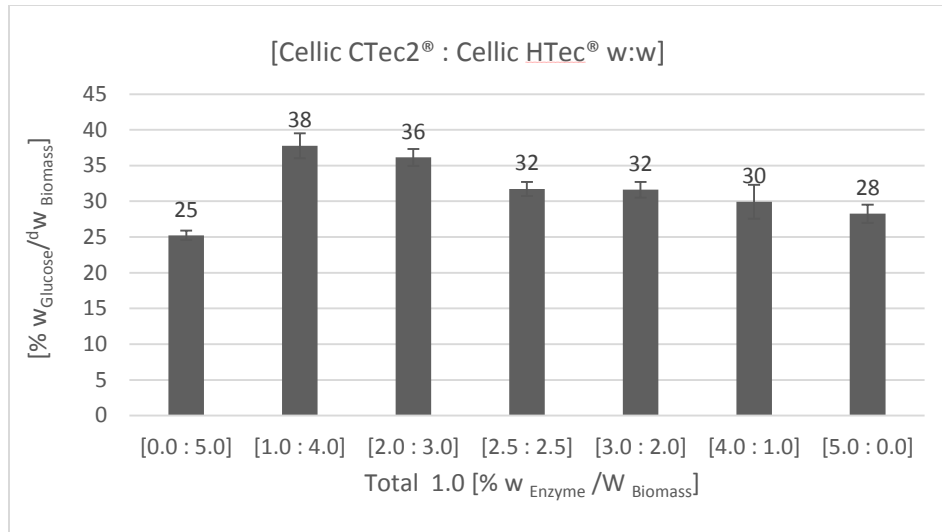


Figure 3S: Glucose concentration in the *Zostera marina* hydrolysate obtained with different combination of Cellic CTec2® : Cellic HTec® at total concentration of 1.0 [% w_{Enzyme} / W_{Biomass}]. The enzymatic hydrolysis was conducted in acetate buffer (pH 5.0, 50mM), at 50°C, 250 rpm for 3 days.

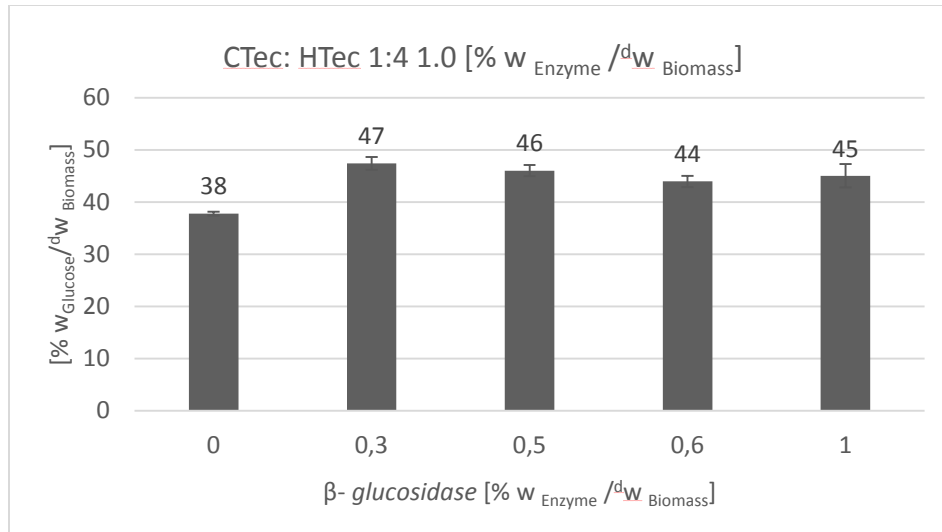


Figure 4S: Glucose concentration in the *Zostera marina* hydrolysate obtained with different concentration of β -glucosidase with Cellic CTec2® : Cellic HTec® 1:4 at total concentration of 1.0 [% w_{Enzyme} / W_{Biomass}]. The enzymatic hydrolysis was conducted in acetate buffer (pH 5.0, 50mM), at 50°C, 250 rpm for 3 days.

Table 3S: The sugar analysis of the final hydrolysates.

Seagrass	g.L ⁻¹						
	<i>Z. marina</i> (1)	<i>S. filiforme</i>	<i>P. australis</i>	<i>T. testudinum</i>	<i>Z. marina</i> (2)	<i>Z. noltii</i>	<i>P. oceanica</i>
Glucose	29.1±1.59	25.1±3.1	21.3± 0.89	28.5±2.64	28.3±0.83	32.2±1.91	28.5±0.59
Galacturonic Acid	2.9±0.66	0.81±0.067	0.27±0.01	0.87±0.05	0.6±0.02	2.88±0.1	0.63±0.02
Xyl, Man, Gal, Fruc	4.21±1.02	4.07±0.51	4.02±0.00	5.25±0.3	5.42±0.08	8.09±0.39	5.53±0.26
Rhamnose	0.53±0.09	n.d.	n.d.	n.d.	n.d.	n.d.	n.d.
Arabinose	n.d ^[a] .	0.1±0.01	n.d.	n.d.	n.d.	n.d.	0.15±0.01
Fucose	0.28±0.04	0.16±0.01	0.18±0.01	0.2±0.01	0.18±0.01	0.37±0.02	0.2±0.01

[a] n.d.: Not detectable.

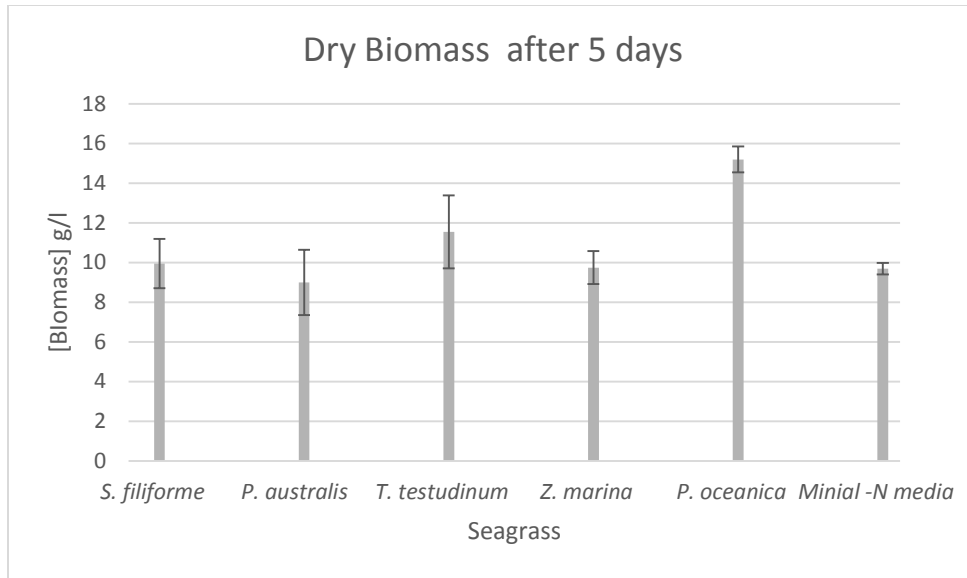


Figure 5S: Dry biomass after 5 days fermentation of *T. oleaginosus* using seagrass hydrolysates comparing to minimal nitrogen media.

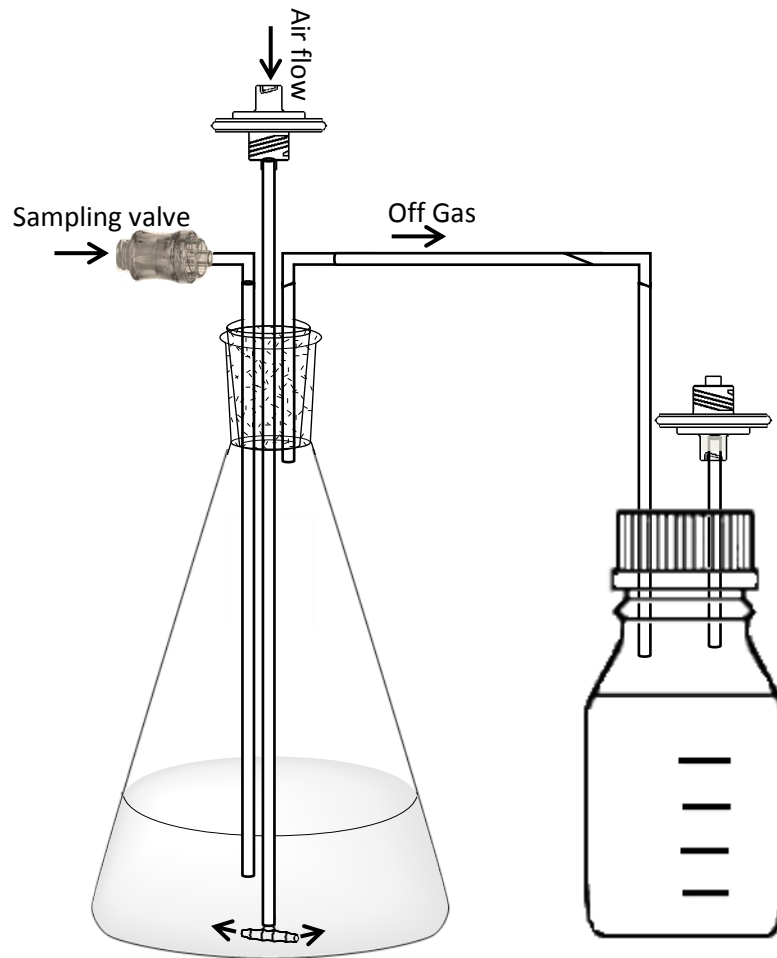


Figure 6S: The flasks were supplemented with an aeration system supplying the cultures with 0.2 L/min pre-filtered air.

The Used 18s-rRNA Sequences for the phylogenetic relatedness:

> *Zostera marina*

GATAACTTGACGGATCGCATGGCCTTTGTGCCGGCGACGCATCATTCAAATTTCTGCCCTATCAACT
TTCGATGGTAGGATAGGGGCCTACCATGGTGGTGACGGGTGACGGAGAATTAGGGTTTCGATTCCGG
AGAGGGAGCCTGAGAAACGGCTACCACATCCAAGGAAGGCAGCAGGCGCGCAAATTACCCAATCCT
GACACGGGGAGGTAGTGACAATAAATAACAATACCGGGCTCTTTGAGTCTGGTAATTGGAATGAGTA
CAATCTAAATCCCTTAACGAGGATCCATTGGAGGGCAAGTCTGGTGCCAGCAGCCGCGGTAATTCCA
GCTCCAATAGCGTATATTTAAGTTGTTGCAGTTAAAAAGCTCGTAGTTGGACTTTGGGTTGGGTCCG
CCGGTCCGCCTTTTGGTGTGCACCGACTGTCTTGTCCCTTCTGCTGGTGATGCGTTCTGTCTTAG
TTGGTCCGGTCTGCTCCGGCGCTGTTACTTTGAAGAAATTAGAGTGCTCAAAGCAAGCCTACGCT
CTGTATACATTAGCATGGGATAACATCACAGGATTTTCGATCCTATTTTGTGGCCTTCGGGATCCGGAG
TAATGATTAAGAGGGACAGTCGGGGGCATTTCGATTTTCATAGTCAGAGGTGAAATTCTTGGATTTATG
AAAGACGAACAACCTGCGAAAGCATTTCGAAGGATGTTTTTATTAAATCAAGAACGAAAGTTGGGGGC
TCGAAGACGATCAGATACCGTCTAGTCTCAACCATAAACGATGCCGACCAGGGATTGGCGGATGTT
GCTTTTAGGACTCTGCCAGCACCTTATGAGAAATCAAAGTTTTTGGGTTCCGGGGGGAGTATGGTCCG
CAAGGCTGAACTTAAAGGAATTGACGGAAGGGCACCACCAGGAGTGGAGCCTGCGGCTTAATTTG
ACTCAACACGGGGAACTTACCAGGTCCAGACATAGTAAGGATTGACAGATTGAGAGCTCTTTCTTG
ATTCTATGGGTGGTGGTGCATGGCCGTTCTTAGTTGGTGGAGCGATTTGTCTGGTTAATTCCGTTAA
CGAACGAGACCTCAGCCTGCTAACTAGCTATGCGGAGGATACCCTTCGTGGCCAGCTTCTTAGAGG
GACTATGGCCGCCTAGGCCACGGAAGTTTGGAGCAATAACAGGTCTGTGATGCCCTTAGATGTTCTG
GGCCGCACGCGCGCTACACTGATGTATTCAACGAGTTTATAACCTTAGTTGATAGGCTTGGGTAATC
TTTGAAAATTTTCATCGTGATGGGGATAGATCATTGCAATTGTTGGTCTTCAACGAGGAATTCCTAGTA
AGCGTGAGTCATCAGCTCGCGTTGACTACGTCCCTGCCCTTTGTACACACCCGCCCCGCTCGCTCCTA

> *Syringodium filiforme*

TCATATGCTTGTCTCAAAGATTAAGCCATGCATGTGCAAGTATGAACAGAATCATATTGTGAAACTGC
GAATGGCTCATTAAATCAGTTATAGTTTGTGGTATCACCTTACTCGGATAACCGTAGTAATTCT
AGAGCTAATACGTGCACCCAAGTCCCAACTTCCGGAAGGGACGCATTTGTTAGATAAAAGGTCGATG
CGGGCTTTGCCCGTTTCTCGGATGAATCATGATAACTTGACGGATCGCATGGCCGTTGTGCTGGCG
ACGCATCATTCAAATTTCTGCCCTATCAACTTTTCGATGGTAGGATAGGGGCCTACCATGGTGTGAC
GGGTGACGGAGAATTAGGGTTTCGATTCCGGAGAGGGAGCCTGAGAAACGGCTACCACATCCAAGG
AAGGCAGCAGGCGCGCAAATTACCCAATCCTGACACGGGGAGGTAGTGACAATAAATAACAATACC
GGGCTCTTAGAGTCTGGTAATTGGAATGAGTACAATCTAAATCCCTTAAACGAGGATCCATTGGAGGG
CAAGTCTGGTGCCAGCAGCCGCGGTAATTCCAGCTCCAATAGCGTATATTTAAGTTGTTGCAGTTAA
AAAGCTCGTAGTTGGACCTTGGGTTGGGCCGGCCGGTCTGCCTTGGGTGTGTATCGGCCGTCTCGT
CCCTTCTGCCGGAGACGCGCTCCTGTCTTTCATTGGTTCGGGTCGTGCTTCTGGCGCTGTTACTTTGA
AGAAATTAGAGTGCTTAAAGCAAGCCTATGCTCTGTATACATCAGCATGGGATAACATCATAGGATTT
CGGTCCTATTGTGTTGGCCTTCCGGATCGGAGTAATGATTAAGAGGGACAGTCGGGGGCATTTCGTA
TTTCATAGTCAGAGGTGAAATTCTTGGATTTATGAAAGACGAACAACCTGCGAAAGCATTTCGAAGGA
TGTTTTTCATTAATCAAGAACGAAAGTTGGGGGCTCGAAGACGATCAGATACCGTCTAGTCTCAACC
ATAAACGATGCCGACCAGGGATTGGCGGATGTTGCTTTTAGGACTCTGCCAGCACCTTATGAGAAAT
CAAAGTTTTTGGGTTCCGGGGGGAGTATGGTCGCAAGGCTGAAACTTAAAGGAATTGACGGAAGGG
CACCACCAGGAGTGGAGCCTGCGGCTTAATTTGACTCAACACGGGGAACTTACCAGGTCCAGACA
TAGTAAGGATTGACAGATTGAGAGCTCTTTCTTGATACTATGGGTGGTGGTGCATGGCCGTTACTTA
GTTGGTGGAGCGATTTGTCTGGTTAATTCCGTTAACGAACGAGACCTCAGCCTGCTAACTAGCTATG
CGGAGGTGACCCTTCGTGGCCAGCTTCTTAGAGGGACTATGGCCGCTTAGGCCACGGAAGTTTGGAG
GCAATAACAGGTCTGTGATGCCWWWRAYGTTNNYGGCCGCACGCGCGCTACACTGATGTATTC
AACGAGTTTATAACCTTGACCGACAGTTTGGGTAATCTTCGAAAATTTTCATCGTGATGGGGATAGAT
CATTGCAATTGTTGGTCTTCAACGAGGAATTCCTAGTAAGCGCGAGTCATCAGCTCGCGTTGACTAC
GTCCCTGCCCTTTGTACACACCCGCCCCGCTCGCTCCTACCGATTGAATGGTCCGGTGAAGTGCTCGGA
TCGTGGCGACGTTGGTGGTCTGCCGCTGACGACGCTGCGAGAAGTCCATTGAACCTTATCATTTAGA
GGAAGGAGAAT

> *Posidonia australis*

GTAGTCATATGCTTGTCTCAAAGATTAAGCCATGCATGTGCAAGTATGAACTAATTCAGACTGTGAAA
CTGCGAATGGCTCATTAAATCAGTTATAGTTTGTGGTATCTTGCTACTCGGATAACCGTAGTA
ATTCTAGAGCTAATACGTGCACCAAACCCCGACTTCANGGAAGGGATGCATTTGTTAGATAAAAAGG
CCGACGCGGGCTTTGCCCGTTGCTCTGATGATACATGATAACTTGACGGATCGCATGGCCATTGTGC
CGGCGACGCATCATTCAAATTTCTGCCCTATCAACTTTTCGATGGTAGGATCGGGGCCTACCATGGTG
GTGACGGGTGACGGAGAATTAGGGTTCGATTCCGGAGAGGGAGCCTGAGAAACGGCTACCACATC
CAAGGAAGGCAGCAGGCGCGCAAATTACCCAATCCTGACACGGGGAGGTAGTGACAATAAATAACA
ATACCGGGCTCATTGAGTCTGGTAATTGGAATGAGTACAATCTAAATCCCTAACGAGGATCCATTGG
AGGGCAAGTCTGGTGCCAGCAGCCGCGGTAATTCCAGCTCCAATAGCGTATATTTAAGTTGTTGCAG
TTAAAAGCTCGTAGTTGGACCTTGGGTTGGGTGCGTCTGCCTATNGGTGTGCACCGGCCGT
CTCGTCCCTNNNNNNNNNCTGCTGGTGACGCGCTCCTGTCTTAAGTGGTCCGGTCTGCCTCCG
GCGCTGTTACTTTGAAGAAATTAGAGTGTCAAAGCAAGCCTATGCTCNATATACATTAGCATGGGAT
AACGCCATAGGATTTCCGTCCTATTGTGTTGGCCTTCGGGATCGGAGTAATGATTAAGAGGGACAGT
CGGGGGCATTTCGTATTTTCATAGTCAGAGGTGAAATTTGGATTTATGAAAGACGAACGACTGCGAA
AGCATTGCCAAGGATGTTTTCAATCAAGAACGAAAGTTGGGGGCTCGAAGACGATCAGATACC
GTCCTAGTCTCAACCATAAACGATGCCGACCAGGATTGGCGGATGTTGCTTTAAGGACTCCGCCA
GCACCTTATGAGAAATCAAAGTCTTTGGGTTCCGGGGGAGTATGGTCGCAAGGCTGAAACTTAAAG
GAATTGACGGAAGGGCACCACCAGGAGTGGAGCTGCGGCTTAATTTGACTCAACACGGGGAAACT
TACCAGGTCCAGACATAGTAAGGATTGACAGATTGAGAGCTCTTTCTTGATTCTATGGGTGGTGGTG
CATGGCCGTTCTTAGTTGGTGGAGCGATTTGTCTGGTTAATTCCGTTAACGAACGAGACCTCASCCT
GCTAACTAGCTATGCGGAGGTGACCCTTCGTGSCCAGCTTCTTAGAGGGACTATGGCCGCTTAGGC
CACGGAAGTTTGAGGCAATAACAGGTCTGTGATGCCCTTAGATGTTCTGGGCCGCACGCGCGCTAC
ACTGATGTATTCAACGAGTTTATAACCTTGCCGATAGGCTTGGGTAATCTTGAAAATTTTCATCGTG
ATGGGGATAGATCATTGCAATTGTTGGTCTTCAACGAGGAATTCCTAGTAAGCGTGAGTCATCAGCT
CGCGTTGACTACGTCCCTGCCCTTTGTACACACCGCCCGTCCGCTCCTACCGATTGAATGGTCCGGT
GAAGTGCTCGGATCGTGACGACGTGAGTGGTCTGCCGCTGGCGACGTTGCGAGAAGTCCATTGAAC
CTTATCATTTAGAGGAAGGAGAAGTCTGTAACAAGGTTTCCGTAGGTGAACCTGCGGAAGGATCAA

> *Thalassia testudinum*

TGTTTCCCAGAATAAACCATGCATGTGCAAGTATGAACTAATTCGGACTGTGAACTGCGAATGGCTC
ATTAATCAGTTATAGTTTGTGGTACTTACTACTCGGATAACCGTAGTAATTCTAGAGCTAATA
CGTGCTCCAAGCCCCGACTTCTGGAAGGGCTGCATTTATTAGGTAAAAGGCCAATGTGGGCTTTGCC
CGCTTYTCGGATGACACATGGTAACTCGGCGGATCGCACGGCCCTCGTGCTGGCGACGCATCATT
AAATTTCTGCCCTATCAACTTTTCGATGGTAGGATAGGGGCTTACCATGGTGGTGACGGGTGACGGAG
AATTAGGGTTCGATTCCGGAGAGGGAGCCTGAGAAACGGCTACCACATCCAAGGAAGGCAGCAGGC
GCGCAAATTACCCAATCCTGACACGGGGAGGTAGTGACAATAAATAACAATACCGGGCTCTACGAGT
CTGGTAATTGGAATGAGTACAATCTAAATCCCTAACGAGGATCCATTGGAGGGCAAGTCTGGTGCC
AGCAGCCGCGGTAATTCCAGCTCCAATAGCGTATATTTAAGTTGTTGCAGTTAAAAGCTCGTAGTTG
GACTTTGGGTTGGGCCGGCCGTCCTTTGGTGTGCACCGGTCGTCTCGTCCCTTTCCGCCGGG
GGCGCGCTCCTGGTCTTAATTGGCCGGGTCGTGCCTTCGGCGCTGTTACTTTGAAGAAATTAGAGT
GCTCAAAGCAAGCCCAAGCTCTGCATACATTAGCATGGGATAACATCACAGGATTTCCGTCCTATTG
TGTTGGCCTTCGGGATCGGAGTAATGATTAAGAGGGACAGTCGTGGGCATTTCGTATTTTCATAGTCAG
AGGTGAAATTTGGATTTATGAAAGACGAACAACCTGCGAAAGCATTTCGCAAGGATGTTTTTCATTAA
TCAAGAACGAAAGTTGGGGGCTCGAAGACGATCAGATACCGTCCCTAGTCTCAACCATAAACGATGCC
GACCAGGGATCGGCGGATGTTGCTTGTACGACATCGCCGGCACCTTATGAGAAATCAGAGTTTTTG
GTTCCGGGGGGAGTATGGTCGCAAGGCTGAACTTAAAGGAATTGACGGAAGGGCACCACCAGG

AGTGGAGCCTGCGGCTTAATTTGACTCAACACGGGGAAACTTACCAGGTCCAGACATAGTAAGGATT
GACAGACTGAGAGCTCTTTCTTGATTCTATGGGTGGTGGTGCATGGCCGTCTTAGTTGGTGGAGC
GATTTGTCTGGTTAATTCCGATAACGAACGAGACCTCAGCCTGCTAACTAGCTATGCGGAGGCGACC
CTCCGTGGCCAGCTTCTTAGAGGGACTATGGCCGTTGAGGCCACGGAAGTTTGAGGCAATAACAGG
TCTGTGATGCCCTTAGATGTTCTGGGCCGACGCGCGCTACACTGATGTATTCAACGAGTTTATAAC
CTTGGCTGACAGGCCCGGTAATCTTGCAAATTTTCATCGTGATGGGGATAGATCATTGCAACTGTTG
GTCTTCAACGAGGAATCCTAGTAAGCGCGAGTCATCAGTTCGCGTTGACTACGTCCCTGCCCTTTG
TACACACCGCCCGTCGCTCCTACCGATTGAATGGTCCGGTGAAGTGCCCGGATCGCGGCGACGCC
GGCGGTCTGCCGCTGGTGACGTCGCGAGAAGTCCACTGAACCTTATCATTAGAGGAAGGAG

> *Zostera marina*

GATAACTTGACGGATCGCATGGCCTTTGTGCCGGCGACGCATCATTCAAATTTCTGCCCTATCAACT
TTCGATGGTAGGATAGGGGCCTACCATGGTGGTGACGGGTGACGGAGAATTAGGGTTCGATTCCGG
AGAGGGAGCCTGAGAAACGGCTACCACATCCAAGGAAGGCAGCAGGCGCGCAAATTACCCAATCCT
GACACGGGGAGGTAGTGACAATAAATAACAATACCGGGCTCTTTGAGTCTGGTAATTGGAATGAGTA
CAATCTAAATCCCTAACGAGGATCCATTGGAGGGCAAGTCTGGTGCCAGCAGCCGCGGTAATTCCA
GCTCCAATAGCGTATATTTAAGTTGTTGCAGTTAAAAAGCTCGTAGTTGGACTTTGGGTTGGGTCCG
CCGGTCCGCTTTTTGGTGTGCACCGACTGTCTTGTCCCTTCTGCTGGTGATGCGTTCCTGTCCTTAG
TTGGTCCGGTCGTGCCTCCGGCGCTGTTACTTTGAAGAAATTAGAGTGCTCAAAGCAAGCCTACGCT
CTGTATACATTAGCATGGGATAACATCACAGGATTTTCGATCCTATTTTGTGGCCTTCGGGATCGGAG
TAATGATTAAGAGGGACAGTCGGGGGCATTTCGATTTTCATAGTCAGAGGTGAAATTCCTGGATTTATG
AAAGACGAACAACCTGCGAAAGCATTGGCCAAGGATGTTTTCAATTAATCAAGAACGAAAGTTGGGGGC
TCGAAGACGATCAGATACCGTCCTAGTCTCAACCATAAACGATGCCGACCAGGGATTGGCGGATGTT
GCTTTTAGGACTCTGCCAGCACCTTATGAGAAATCAAAGTTTTTGGGTTCCGGGGGGAGTATGGTCCG
CAAGGCTGAAACTTAAAGGAATTGACGGAAGGGCACCACCAGGAGTGGAGCCTGCGGCTTAATTTG
ACTCAACACGGGGAAACTTACCAGGTCCAGACATAGTAAGGATTGACAGATTGAGAGCTCTTTCTTG
ATTCTATGGGTGGTGGTGCATGGCCGTTCTTAGTTGGTGGAGCGATTTGTCTGGTTAATTCCGTTAA
CGAACGAGACCTCAGCCTGCTAACTAGCTATGCGGAGGATACCCTTCGTGGCCAGCTTCTTAGAGG
GACTATGGCCGCCTAGGCCACGGAAGTTTGAGGCAATAACAGGTCTGTGATGCCCTTAGATGTTCTG
GGCCGCACGCGCGCTACACTGATGTATTCAACGAGTTTATAACCTTAGTTGATAGGCTTGGGTAATC
TTTGAAAATTTTCATCGTGATGGGGATAGATCATTGCAATTGTTGGTCTTCAACGAGGAATTCCTAGTA
AGCGTGAGTCATCAGCTCGCGTTGACTACGTCCCTGCCCTTTGTACACACCGCCCGTCGCTCCTA

> *Zostera noltii*

AGTCATATGCTTGTCTCAAAGATTAAGCCATGCATGTGCAAGTATGAACTAATTCAGACTGTGAACT
GCGAATGGCTCATTAAATCAGTTATAGTTTGTGGTGGTACCTTGCTACTCGGATAACCGTAGTAAT
TCTAGAGCTAATACGTGCACCAAACCCCAACTTCTGGAAGGGATGCATTTGTTAGATAAAAGGTTGA
CACGGCTTTGTTGCTTCTGATGATTGATAACTTACGGATCGCACGGCCTTTGTGCCGGCG
ACGCATCATTCAAATTTCTGCCCTATCAACTTTTCGATGGTAGGATAGGGGCCTACCATGGTGGTGC
GGGTGACGGAGAATTAGGGTTCGATTCCGGAGAGGGAGCCTGAGAAACGGCTACCACATCCAAGG
AAGGCAGCAGGCGCGCAAATTACCCAATCCTGACACGGGGAGGTAGTGACAATAAATAACAATACC
GGGCTCTTTGAGTCTGGTAATTGGAATGAGTACAATCTAAATCCCTAACGAGGATCCATTGGAGGG
CAAGTCTGGTGCCAGCAGCCGCGGTAATTCCAGCTCCAATAGCGTATATTTAAGTTGTTGCAGTTAA
AAAGCTCGTAGTTGGACCTTGGGTTGGGTCCGGCCGGTCCGCCTTTTGGTGTGCACCGACTGTCTTG
TCCCTTCTGCTGGTGCCTTCTGTCCTTAGTTGGTCCGGTTCGCTCCGCGCTGTTACTTTG
AAGAAATTAGAGTGCTCAAAGCAAGCCTATGCTCTGTATACATTAGCATGGGATAACATCACAGGATT
TCGATCCTATTTTGTGGCCTTCGGGATCGGAGTAATGATTAAGAGGGACAGTCGGGGGCATTTCGTA
TTTCATAGTCAGAGGTGAAATTCCTGGATTTATGAAAGACGAACAACCTGCGAAAGCATTTCGAAGGA

TGTTTTCATTAATCAAGAACGAAAGTTGGGGGCTCGAAGACGATCAGATACCGTCCTAGTCTCAACC
ATAAACGATGCCGACCAGGGATTGGCGGATGTTGCTTTTAGGACTCTGCCAGCACCTTATGAGAAAT
CAAAGTTTTTGGGTTCCGGGGGGAGTATGGTCGCAAGGCTGAAACTTAAAGGAATTGACGGAAGGG
CACCACCAGGAGTGGAGCCTGCGGCTTAATTTGACTCAACACGGGGAAACTTACCAGGTCCAGACA
TAGTAAGGATTGACAGATTGAGAGCTCTTTCTTGATTCTATGGGTGGTGGTGCATGGCCGTTCTTAGT
TGGTGGAGCGATTTGTCTGGTTAATTCCGTTAACGAACGAGACCTCAGCCTGCTAACTAGCTATGCG
GAGGATACCCTTCGTGGCCAGCTTCTTAGAGGGACTATGGCCGCCTAGGCCACGGAAGTTTGAGGC
AATAACAGGTCTGTGATGCCCTTAGATGTTCTGGGCCGCACGCGCGCTACACTGATGTATTCAACGA
GTTTATAACCTTAGCTGATAGGCTTGGGTAATCTTTGAAAATTTTCATCGTGATGGGGATAGATCATTG
CAATTGTTGGTCTTCAACGAGGAATTCCTAGTAAGCGTGAGTCATCAGCTCGCGTTGACTACGTCCC
TGCCCTTTGTACACACCGCCCGTGCCTCCTACCGATTGAATGGTCCGGTGAAGTGCTCGGATTGTG
GCGACGTTTGTGGGTCTGCCGCTGGCGACGTGCTGAGAAGTCCACTGAACCTTATCATTGAGAGGA
AGGAG

> *Posidonia oceanica*

GTTTGTCTTTAAGATTAGCCATGCATGTGCAAGTATGAACTAAATCATATTGTGAAACTGCGAATGGC
TCATTAATCAGTTATAGTTTGTGGTATCATTACTCGGATAACCGTAGTAATTCTAGAGCTA
ATACGTGCACCGAAGTCCCAACTTCCGGAAGGGACGCATTTGTTAGATAAAAGGTCGATGCGGGCC
TAGCCCGTTGCTCTGATGATTCATGATAACTTGACGGATCGCATGGCCATCGTGCTGGCGACGCATC
ATTCAAATTTCTGCCCTATCAACTTTTCGATGGTAGGATAGGGGCCTACCATGGTGGTGGGAGGAC
GGAGAATTAGGGTTCGATTCCGGAGAGGGAGCCTGAGAAACGGCTACCACATCCAAGGAAGGCAG
CAGGCGCGCAAATTACCCAATCCTGACACGGGGAGGTAGTGACAATAAATAACAATACCGGGCTCTT
GGAGTCTGGTAATTGGAATGAGTACAATCTAAATCCCTAACGAGGATCCATTGGAGGGCAAGTCTG
GTGCCAGCAGCCGCGTAATTCCAGCTCCAATAGCGTATATTTAAGTTGTTGCAGTAAAAAGCTCG
TAGTTGGACCTTGGGTTGGGTCGGCCGGTCCGCCTATGGTGTGCATCGGCCGTCTCGTCCCTTCTG
CTGGAGACGCGTTCCTGTCTTGATTGGTCCGGTCTGCTTCTGGCGCTGTTACTTTGAAGAAATTA
GAGTGCTTAAAGCAAGCCTATGCTCTGGATACATCAGCATGGGATAACATCATAGGATTTCCGTCCCT
ATTGTGTTGGCCTTCGGGATCGGAGTAATGATTAAGAGGGACAGTCGGGGGCATTCGTATTTCATAG
TCAGAGGTGAAATTCCTGGATTTATGAAAGACGAACAACCTGCGAAAGCATTGCCAAGGGATGTTTTC
ATTAATCAGAACGAAAGTTGGGGGCTCGAAGACGATCAGATACCGTCCTAGTCTCAACCATAAACGA
TGCCGGACAGGATTGCGGGATGTGCTTTTAGGACTCTGCAAGCAACTTATGAGAATCAAGGTTTTTG
GAATCGGGGGGAAGTATGGTTCGCAGCTGGAACATAATGATTGACGACGGACTACAGATGAGCCTGG
CGTCCGTAGCTTAATTTGACTCAACACGGGGAAACTTACCAGGTCCAGACATAGTAAGGATTGACAG
ATTGAGAGCTCTTTCTTGATTCTATGGGTGGTGGTGCATGGCCGTTCTTAGTTGGTGGAGCGATTTG
TCTGGTTAATTCCGTTAACGAACGAGACCTCAGCCTGCTAACTAGCTATGCGGAGGTGACCCTTCGT
GGCCAGCTTCTTAGAGGGACTATGGCCGCTTAGGCCACGGAAGTTTGAGGCAATAACAGGTCTGTG
ATGCCCTTAGATGTTCTGGGCCGCACGCGCGCTACACTGATGTATTCAACGAGTTTATAACCTTGAC
CGATAGGTTTGGGTAATCTTCGAAAATTTTCATCGTGATGGGGATAGATCATTGCAATTGTTGGTCTTC
AACGAGGAATTCCTAGTAAGCGCGAGTCATCAGCTCGCGTTGACTACGTCCCTGCCCTTTGTACACA
CCGCCCGTCGCTCCTACCGATTGAATGGTCCGGTGAAGTGCTCGGATCGTGGCGACGTGGGTGGT
CTGCCGCTGACGACGCTGCGAGAAGTCCATTGAACCTTATCATTTAGAGAAGGAAGAAGTCATAACC
ATTGCC

>Halodule uninervis

GTAAC TAATTCAGACTGTGAAACTGCGAATGGCTCATTAAATCAGTTATAGTTTGTTTGATGGTACCTT
GCTACTCGGATAACCGTAGTAATTCTAGAGCTAATACGTGCACCAAACCCCAACTTCTGGAAGGGAT
GCATTTGTTAGATAAAAAGGTTGACACGGGCTTTGTTGCTTCTGATGATTCATGATAACTTGACGGA
TCGCATGGCCTTTGTGCCGGCGACGCATCATTCAAATTTCTGCCCTATCAACTTTTCGATGGTAGGAT
AGGGGCCTACCATGGTGGTGACGGGTGACGGAGAATTAGGGTTCGATTCCGGAGAGGGAGCCTGA
GAAACGGCTACCACATCCAAGGAAGGCAGCAGGCGCGCAAATTACCCAATCCTGACACGGGGAGGT
AGTGACAATAAATAACAATACCGGGCTCTTTGAGTCTGGTAATTGGAATGAGTACAATCTAAATCCCT
TAACGAGGATCCATTGGAGGGCAAGTCTGGTGCCAGCAGCCGCGTAATTCCAGCTCCAATAGCGT
ATATTTAAGTTGTTGCAGTTAAAAAGCTCGTAGTTGGACCTTGGGTTGGGTCCGGCCGGTCCGCCTTT
TGGTGTGCACCGACTGTCTTGCCCTTCTGCTGGTGTGCGTTCCTGTCCTTAGTTGGTCCGGTCTGT
GCTTCCGGCGCTGTTACTTTGAAGAAATTAGAGTGCTCAAAGCAAGCCTATGCTCTGTATACATTAGC
ATGGGATAACATCACAGGATTTTCGATCCTATTTTTGTTGGCCTTCGGGATCGGAGTAATGATTAAGAG
GGACAGTCCGGGGCATTTCGTATTTTCATAGTCAGAGGTGAAATCCTTGATTTATGAAAGACGAACAA
CTGCGAAAGCATTTCGCAAGGATGTTTTTCATTAATCAAGAACGAAAGTTGGGGGCTCGAAGACGATC
AGATACCGTCTAGTCTCAACCATAAACGATGCCGACCAGGGATTGGCGGATGTTGCTTTTAGGACT
CTGCCAGCACCTTATGAGAAATCAAAGTTTTTGGGTTCCGGGGGGAGTATGGTCGCAAGGCTGAAA
CTTAAAGGAATTGACGGAAGGGCACCACCAGGAGTGGAGCCTGCGGCTTAATTTGACTCAACACGG
GGAAACTTACCAGGTCCAGACATAGTAAGGATTGACAGATTGAGAGCTCTTTCTTGATTCTATGGGT
GGTGGTGCATGGCCGTTCTTAGTTGGTGGAGCGATTTGTCTGGTTAATTCCGTTAACGAACGAGACC
TCAGCCTGCTAACTAGCTATGCGGAGGATACCCTTCGTGGCCAGCTTCTTAGAGGGACTATGGCCG
CCTAGGCCACGGAAGTTTGAGGCAATAACAGGTCTGTGATGCCCTTAGATGTTCTGGGCCGCACGC
GCGCTACACTGATGTATTCAACGAGTTTATAACCTTAGCTGATAGGCTTGGGTAATCTTTGAAAATTT
CATCGTGATGGGGATAGATCATTGCAATTGTTGGTCTTCAACGAGGAATTCCTAGTAAGCGTGAGTC
ATCAGCTCGCGTTGACTACGTCCCTGCCCTTTGTACACACCGCCCGTTCGCTCCTACCGATTGAATGG
TCCGGTGAAGTGCTCGGATTGTGGCGACGTTAGTGGGTCTGCCGCTGGCGACG

>Phyllospadix iwatensis

CAACCTGGTTGATCCTGCCAGTAGTCATATGCTTGTCTCAAAGATTAAGCCATGCATGTGCAAGTATG
AACTAATTCAGACTGTGAAACTGCGAATGGCTCATTAAATCAGTTATAGTTTGTTTGATGGTACCTTG
CTACTCGGATAACCGTAGTAATTCTAGAGCTAATACGTGCACCAAACCCCGACTTCTGGAAGGGATG
CATTTGTTAGATAAAAAGGTTGACACGGGCTTGTGCTGTTGCTCTGATGATTCATGATAACTTGACG
GATCGCATGGCCTTTGTGCCGGCGACGCATCATTCAAATTTCTGCCCTATCAACTTTTCGATGGTAGG
ATAGGGGCCTACCATGGTGGTGACGGGTGACGGAGAATTAGGGTTCGATTCCGGAGAGGGAGCCT
GAGAAACGGCTACCACATCCAAGGAAGGCAGCAGGCGCGCAAATTACCCAATCCTGACACGGGGA
GGTAGTGACAATAAATAACAATACCGGGCTCTTTGAGTCTGGTAATTGGAATGAGTACAATCTAAATC
CCTAACGAGGATCCATTGGAGGGCAAGTCTGGTGCCAGCAGCCGCGTAATTCCAGCTCCAATAG
CGTATATTTAAGTTGTTGCAGTTAAAAAGCTCGTAGTTGGACCTTGGGTTGGGTCCGGCCGGTCCGCC
TTATGGTGTGCACCGACCGTCTCGTCCCTTCTGCTGGTGTGCGTTCCTGTCCTTAGTTGGTCCGGT
CGTGCCTCCGGCGCTGTTACTTTGAAAGAAATTAGAGTGCTCAAAGCAAGCCTATGCTCTGTATACA
TTAGCATGGGATAACATCACAGGATTTTCGATCCTATTTTTGTTGGCCTTCGGGATCGGAGTAATGATTA
AAAGGGACAGTCGGGGGCATTTCGTATTTTCATAGTCAGAGGTGAAATCCTTGATTTATGAAAGACGA
ACAACGCGAAAGCATTTCGCAAGGATGTTTTTCATTAATCAAGAACGAAAGTTGGGGGCTCGAAGAC
GATCAGATACCGTCTAGTCTCAACCATAAACGATGCCGACCAGGGATTGGCGGATGTTGCTTTTAG
GACTCCGCCAGCACCTTATGAGAAATCAAAGTTTTTGGGTTCCGGGGGGAGTATGGTCGCAAGGCT
GAAACTTAAAGGAATTGACGGAAGGGCACCACCAGGAGTGGAGCCTGCGGCTTAATTTGACTCAAC
ACGGGGAAACTTACCAGGTCCAGACATAGTAAGGATTGACAGATTGAGAGCTCTTTCTTGATTCTAT
GGGTGGTGGTGCATGGCCGTTCTTAGTTGGTGGAGCGATTTGTCTGGTTAATTCGGTTAACGAACGA
GACCTCAGCCTGCTAACTAGCTATGCGGAGGTGACCCTTCGTGGCCAGCTTCTTAGAGGGACTATG
GCCGCTAGGCCACGGAAGTTTGAGGCAATAACAGGTCTGTGATGCCCTTAGATGTTCTGGGCCGC
ACGCGCGCTACACTGATGTATTCAACGAGTTTATAACCTTAGCTGATAGGCTTGGGTAATCTTTGAAA

ATTCATCGTGATGGGGATAGATCATTGCAATTGTTGGTCTTCAACGAGGAATTCCTAGTAAGCGTGA
GTCATCAGCTCGCGTTGACTACGTCCCTGCCCTTTGTACACACCGCCCGTCGCTCCTACCGATTGAA
TGGTCCGGTGAAGTGCTCGGATTGTGGCGACGTTAGTGGTCTGCCGCTGGCGACGTCGTGAGAAGT
CCACTGAACCTTATCATTTAGAGGAAGGAGAAGTCGTAACAAGGTTTCCGTAGGTGAACCTGCAGAA
GGATCAG

>*Cymodocea serrulata*

GATAACTTGACGGATCGCATGGCCATTGTGCTGGCGACGCATCATTCAAATTTCTGCCCTATCAACTT
TCGATGGTAGGATAGGGGCTACCATGGTGTGACGGGTGACGGAGAATTAGGGTTCGATTCCGGA
GAGGGAGCCTGAGAAACGGCTACCACATCCAAGGAAGGCAGCAGGCCGCGCAAATTACCCAATCCTG
ACACGGGGAGGTAGTGACAATAAATAACAATACCGGGCTCTTGGAGTCTGGTAATTGGAATGAGTAC
AATCTAAATCCCTTAACGAGGATCCATTGGAGGGCAAGTCTGGTGCCAGCAGCCGCGGTAATTTCCA
GCTCCAATAGCGTATATTTAAGTTGTTGCAGTTAAAAAGCTCGTAGTTGGACCTTGGGTTGGGCCGG
CCGGTCCGCCTATGGTGTGCATCGGCCGTCTCGTCCCTTCTGCCGGAGATACGTTCCCGTCCTTTT
GTTGGTCCGGTTCGTGCTTCCGGGCGCTGTTACTTTGAAGAAATTAGAGTGCTTAAAGCAAGCCTATG
CTCTGTATACATCAGCATGGGATAACATCATAGGATTTCCGGTCTATTGTGTTGGCCTTCGGGATCG
GAGTAATGATTAAGAGGGACAGTCGGGGGCATTTCRTATTTTCATAGTCAGAGGTGAAATTCCTGGATT
TATGAAAGACGAACAACACTGCGAAAGCATTGCGCAAGGATGTTTTTCATTAATCAAGAACGAAAGTTGGG
GGCTCGAAGACGATCAGATACCGTCTAGTCTCAACCATAAACGATGCCGACCAGGGATTGGCGGA
TGTTGCTTTTAGGACTCTGCCAGCACCTTATGAGAAATCAAAGTTTTTGGGTTCCGGGGGGAGTATG
GTCGCAAGGCTGAAACTTAAAGGAATTGACGGAAGGGCACCACCAGGAGTGAGAGCCTGCGGCTTAA
TTTACTCAACACGGGGAAACTTACCAGGTCCAGACATAGTAAGGATTGACAGATTGAGAGCTCTTT
CTTGATTCTATGGGTGGTGGTGCATGGCCGTTCTTAGTTGGTGGAGCGATTTGTCTGGTTAATTCGG
TTAACGAACGAGACCTCAGCCTGCTAACTAGCTATGCCGGAGGTGACCCTTCGTGGCCAGCTTCTTAG
AGGGACTATGGCCGCTTAGGCCACGGAAGTTTGGAGCAATAACAGGTCTGTGATGCCCTTAGATGTT
CTGGGCCGACGCGCGCTACACTGATGTATTCAACGAGTTTATAACCTTGACCGATAGGTTTGGGTA
ATCTTCGAAAATTTTCATCGTGATGGGGATAGATCATTGCAATTGTTGGTCTTCAACGAGGAATTCCTA
GTAAGCGCGAGTCATCAGCTCGCGTTGACTACGTCCCTGCCCTTTGTACACACCGCCCGTCGCTCC
TA

>*Ruppia maritima*

TGTGAAACTGCGAATGGCTCATTAAATCAGTTATAGTTTTGTTTGATGGTATTTGCTACTCGGATAACC
GTAGTAATTCTAGAGCTAATACGTGCACCGAAACCCCGACTTTTTGGAAGGGATGCATTTGTTAGATAA
AAGGCTGACGCGGGCTTTGCTCGTTGTTCCGATGATTCATGATAACTTGACGGATCGCATGGCCATA
GTGCCGCGCAGCATCATTCAAATTTCTGCCCTATCAACTTTTCGATGGTAGGATATTTGCCTACCATG
GTGGTGACGGGTGACGGAGAATTAGGGTTCGATTCCGGAGAGGGAGCCTGAGAAACGGCTACCAC
ATCCAAGGAAGGCAGCAGGCGCGCAAATTACCCAATCCTGACACGGGGAGGTAGTGACAATAAATA
ACAATACCGGGCTCTTCGAGTCTGGTAATTGGAATGAGTACAATCTAAATCCCTTAACGAGGATCCAT
TGGAGGGCAAGTCTGGTGCCAGCAGCCGCGGTAATTCCAGCTCCAATAGCGTATATTTAAGTTGTTG
CAGTTAAAAGCTCGTAGTTGGACCTTGGGTTGGTTCGATCGGTCTGCTTGGTGTGCATCGGTCCGT
TCGTCCCTTCTGCTGGTGTGCGGTTTCTGTCTTAATTGGTCCGGTTCGTGCCTCTGGCGCTGTTACT
TTGAAGAAATTAGAGTGCTCAAAGCAAGCCTATGCTCTGCATACATTAGCATGGGATAACATCACAG
GATTTCCGGTCTATTTTGTGGCCTTCGGGATCGGAGTAATGATTAAGAGGGACAGTCGGGGGCATT
CGTATTTTCATAGTCAGAGGTGAAATTCCTGGATTTATGAAAGACGAACAACCTGCGAAAGCATTGCGCA
AGGATGTTTTTCATTAATCAAGAACGAAAGTTGGGGGCTCGAAGACGATCAGATACCGTCTAGTCTC
AACCATAAACGATGCCGACCAGGGATTGGCGGATGTTGCTTTTAGGACTTCGCCAGCACCTTTTGGAG
AAATCAAAGTTTTTGGGTTCCGGGGGGAGTATGGTCGCAAGGCTGAAACTTAAAGGAATTGACGGAA
GGGCACCACCAGGAGTGGAGCCTGCGGCTTAATTTGACTCAACACGGGGAAACTTACCAGGTCCAG
ACATAGTAAGGATTGACAGATTGAGAGCTCTTTCTTGATTCTATGGGTGGTGGTGCATGGCCGTTCTT
AGTTGGTGGAGCGATTTGTCTGGTTAATTCGGTTAACGAACGAGACCTCAGCCTGCTAACTAGCTAT
GCGAAGGTAACCCTTCGTGGCCAGCTTCTTAGAGGGACTATGGCCGCTTAGGCTACGGAAGTTTGA

GGCAATAACAGGTCTGTGATGCCCTTAGATGTTCTGGGCCGCACGCGCGCTACACTGATGTATTCAA
CGAGTTTATAACCTTAGCCGATAGGCTTGGGTAATCTTTGAAAATTTTCATCGTGATGGGGATAGATCA
TTGCAACTGTTGGTCTTCAACGAGGAATTCCTAGTAAGCGTGAGTCATCAGCTCGCGTTGACTACGT
CCCTGCCCTTTGTACACACCGCCCGTCGCTCCTACCGATTGAATGGTCCGGTGAAGTGCTCGGATC
GTGATGA

>*Syringodium isoetifolium*

GATAACTTGACGGATCGCATGGCCGTTGTGCTGGCGACGCATCATTCAAATTTCTGCCCTATCAACT
TTCGATGGTAGGATAGGGGCCTACCATGGTGTGACGGGTGACGGAGAATTAGGGTTTCGATTCCGG
AGAGGGAGCCTGAGAAACGGCTACCACATCCAAGGAAGGCAGCAGGCGCGCAAATTACCCAATCCT
GACACGGGGAGGTAGTGACAATAAATAACAATACCGGGCTCTTGGAGTCTGGTAATTGGAATGAGTA
CAATCTAAATCCCTAACGAGGATCCATTGGAGGGCAAGTCTGGTGCCAGCAGCCGCGGTAATTCCA
GCTCCAATAGCGTATATTTAAGTTGTTGCAGTTAAAAAGCTCGTAGTTGGACCTTGGGTTGGGCCGG
CCGGTCTGCCTTTGGTGTGTATCGGCCGTCTCGTCCCTTCTGCCGGAGACGCGCTCCTGTCCTTCA
CTGGTCCGGTTCGTGCTTCTGGCGCTGTTACTTTGAAGAAATTAGAGTGCTTAAAGCAAGCCTATGCT
CTGTATACATCAGCATGGGATAACATCATAGGATTTCCGGTCCATTGTGTTGGCCTTCCGGGATCGGA
GTAATGATTAAGAGGGACAGTCGGGGGCATTCGTATTTTCATAGTCAGAGGTGAAATTCCTGGATTTAT
GAAAGACGAACAACCTGCGAAAGCATTTGCCAAGGATGTTTTTCATTAATCAAGAACGAAAGTTGGGGG
CTCGAAGACGATCAGATACCGTCCAGTCTCAACCATAAACGATGCCGACCAGGGATTGGCGGATG
TTGCTTTTAGGACTCTGCCAGCACCTTATGAGAAATCAAAGTTTTTGGGTTCCGGGGGGAGTATGGT
CGCAAGGCTGAAACTTAAAGGAATTGACGGAAGGGCACCACCAGGAGTGGAGCCTGCGGCTTAATT
TGACTCAACACGGGGAAACTTACCAGGTCCAGACATAGTAAGGATTGACAGATTGAGAGCTCTTTCT
TGATTCTATGGGTGGTGGTGCATGGCCGTTCTTAGTTGGTGGAGCGATTTGTCTGGTTAATTCCGTT
AACGAACGAGACCTCAGCCTGCTAACTAGCTATGCGGAGGTGACCCTTCGTGGCCAGCTTCTTGA
GGGACTATGGCCGCTTAGGCCACGGAAGTTTGAGGCAATAACAGGTCTGTGATGCCCTTAGATGTT
CTGGGCCGCACGCGCGCTACACTGATGTATTCAACGAGTTTATAACCTGGACCAGAGTTTGGGT
AATCTTCGAAAATTTTCATCRTGATGGGGATAGATCATTGCAATTGTTGGTCTTCAACGAGGAATTCCT
AGTAAGCGTGAGTCATCAGCTCGCGTTGACTACGTCCCTGCCCTTTGTACACACCGCCCGTCGCTC
CTA

>*Potamogeton zosteriformis* normal grass

CTGGTTGATCCTGCCAGTAGTCATATGCTTGTCTCAAAGATTAAGCCATGCATGTGCAAGTATGAACT
AATTCAACTGTGAAACTGCGAATGGCTCATTAAATCAGTTATAGTTTGTGGATGGTATACCTTGCTAC
TCGGATAACCGTAGTAATTCTAGAGCTAATACGTGCACCAAATCCCGACTTCTGGAAGGGATGCATT
TGTTAGATAAAAGGCTGACGCGGGTTTTCCCGTTGCTCTGAGGAATCATGATAACTTGACCGATCGC
ATGGTCTTTGTGCCGGCGACACATCATTCAAATTTCTGCCCTATCAACTTTTCGACGGTAGGATAGGG
GCCTACCGTGGTTTTGACGGGTGACGGAGAATTAGGGTTCGATTCCGGAGAGGGAGCCTGAGAGAC
GGCTACCACATCCAAGGAAGGCAGCAGGCCGCGCAAATTACCCAATCCTGACACGGGGAGGTAGTGA
CAATAAATAACAATACCGGGCTCTTTTGTAGTCTGGTAATTGGAATGAGTACAATCTAAATCCCTAAC
GAGGATCCATTGGAGGGCAAGTCTGGTGCCAGCAGCCGCGGTAATTCCAGCTCCAATAGCGTATAT
TTAAGTTGTTGCAGTTAAAAAGCTCGTAGTTGGACCTTGGGATGGGTCCGGTCCGGTCTGCCTATGGTG
TGTACCGCCGTCTCGTCCCTTTTGTGGTACGCGTTCCTGTCCTTAGTTGGTCCGGTCTGCTTC
CGGCGCTGTTACTTTGAAGAAATTAGAGTGCTCAAAGCAGGCCTTTGCTCTGAATATAATTAGCATGG
GATAACGTCATAGGATTTCCGGTCCATTCTGTTGGCCTTCGGGACCGGAGTAATGATTAAGAGGGAC
AGTCGGGGGCATTTCGTATTTTCATAGTCAGAGGTGAAATTCCTGGATTTATGAAAGACGAACAACCTGC
GAAAGCATTTGCCAAGGATGTTTTTCATTAATCAAGAACGAAAGTTGGGGGCTCGAAGACGATCAGAT
ACCGTCCAGTCTCAACCATAAACGATGCCGACCAGGGATTGGCGGATGTTACTTTAAGGACTCCGC
CAGCACCTTATGAGAAATCAAAGTTTTTGGGTTCCGGGGGGAGTATGGTCGCAAGGCTGAAACTTAA
AGGAATTGACGGAAGGGCACCACCAGGAGTGGAGCCTGCGGCTTAATTTGACTCAACACGGGGAAA
CTTACCAGGTCCAGACATAGTAAGGATTGACAGATTGAGAGCTCTTCTTGATTCTATGGGTGGTGG

TGCATGGCCGTTCTTAGTTGGTGGAGCGATTTGTCTGGTTAATTCCGTTAACGAACGAGACCTCAGC
CTGCTAACTAGCTATGCGGAGGTGATCCTCCGTGGCCAGCTTCTTAGAGGGACTATGGCCGCTTAG
GCCAAGGAAGTTTGAGGCAATAACAGGTCTGTGATGCCCTTAGATGTTCTGGGCCGCACGCGCGCT
ACACTGATGTATTCAACGAGTTTATAACCTGGGCCGACAGGCTTGGGTAATCTTTGAAAATTTTCATCG
TGATGGGGATAGATCATTGCAATTGTTGGTCTTCAACGAGGAATTCCTAGTAAGCGTGAGTCATCAG
CTCGCGTTGACTACGTCCCTGCCCTTTGTACACACCGCCCGTCGCTCCTACCGATTGAATGGTCCG
GTGAAGTGCTCGGATCGTGGCGACGTGAGTGGTTTCCCGCTCACGACGTCGTGAGAAGTTCACTGA
ACCTTATCATTTAGAGGAAGGAGAAGTCGTAACAAGGTTTCCGTA

>Halodule wrightii

GATAACTTGACGGATCGCATGGCCTCTGTGCTGGCGACGCATCATTCAAATTTCTGCCCTATCAACT
TTCGATGGTAGGATAGGGGCCTACCATGGTGTGGACGGGTGACGGAGAATTAGGGTTCGATTCCGG
AGAGGGAGCCTGAGAAACGGCTACCACATCCAAGGAAGGCAGCAGGCGCGCAAATACCCAATCCT
GACACGGGGAGGTAGTGACAATAAATAACAATACCGGGCTCGTTGAGTCTGGTAATTGGAATGAGTA
CAATCTAAATCCCTAACGAGGATCCATTGGAGGGCAAGTCTGGTGCCAGCAGCCGCGGTAATTCCA
GCTCCAATAGGCGTATATTTAAGTTGTTGCAGTAAAAAGCTCGTAGTTGGACCTTGGGTGGGTGCG
GCCGGTCTGCCTATAGGTGTGCATCGGCCGCTCGTCCCTTCTGCTGGTGACGCGTTCCTGTCCTTT
ATTGGTCCGGTTCGTGCCTCCGGCGCTGTTACTTTGAAGAAATTAGAGTGCTCAAAGCAGGCCTGTG
CTTGTATACATTAGCATGGGATAACGTCATAGGATTTTCGATCCTATTGTGTTGGCCTTCGGGATCGGA
GTAATGATTAAGAGGGACAGTCGGGGGCATTCTGATTTTCATAGTCAGAGGTGAAATTCCTGGATTTAT
GAAAGACGAACGACTGCGAAAGCATTGCCAAGGATGTTTTCAATTAATCAAGAACGAAAGTTGGGGG
CTCGAAGACGATCAGATACCGTCTAGTCTCAACCATAACGATGCCGACCAGGGATTGGCGGATG
TTGCTTTTAGGACTCTGCCAGCACCTTATGAGAAATCAAAGTTTTTGGGTTCCGGGGGGAGTATGGT
CGCAAGGCTGAAACTTAAAGGAATTGACGGAAGGGCACCACCAGGAGTGAGCCTGCGGCTTAATT
TGACTCAACACGGGGAAACTTACCAGGTCCAGACATAGTAAGGATTGACAGATTGAGAGCTCTTTCT
TGATTCTATGGGTGGTGGTGCATGGCCGTTCTTAGTTGGTGGAGCGATTTGTCTGGTTAATTCCGTT
AACGAACGAGACCTCAGCCTGCTAACTAGCTATGCGGAGGTGACCCTTCGTGGCCAGCTTCTTAGA
GGGACTATGGCCGCTCAGGCCATGGAAGTTTGAGGCAATAACAGGTCTGTGATGCCCTTAGATGTT
CTGGGCCGCACGCGCGCTACACTGATGTATTCAACGAGTTTATAACCTGGGCCGATAGGCTTGGGT
AATCTTCGAAAATTTTCATCGTGATGGGGATAGATCATTGCAATTGTTGGTCTTCAACGAGGAATTCCT
AGTAAGCGTGAGTCATCAGCTCGCGTTGACTACGTCCCTGCCCTTTGTACACACCGCCCGTCGCTC
CTA

>Ruppia cirrhosa

TTTCCGTAGGTGAACCTGCGGAAGGATCATTGTGCGAGATGGATAGCAATAGACGAACACGTCACCGA
ATTATTTTGGAAAAGTGTGTTTTTGTACACTATGTCCTAGCAGAAATGCTATGCTCCCTTTGGGCGT
GTGTGCATTTGTGCTCAACAACCAACCCTGGCACAACCTGTGTCAAGCAAAAAGTAGCTTGTGGTTT
GTCTCCTTCATCGTATTGAGAGGATCGCGAGTCTCACAGAATTAATTAATGCACGACTCCCGTCA
ACGGATATCTTGGCCCTTGCATCGATGAAGAACGTAGCAAAATGCGATACTTGTGATGTGAATTGTAGA
ATCCCGTGAACCATCGAGTCTTTGAATGCAAGTTGCGCCCGAAGTTGTTAGACGGACGGCATGCCT
GCCTGGGCGTCATTAATTGAGTCGCTCATTAAAGTATGATCTTCATGGTTGATGAAGCGGATTATGGC
CTTCTGGGAATTATCCGGTAGGCTTAAATGGGCGTGACCTGCTGTGTGGAGATGCACGATGGGTGG
TGAACTTTTGTGGATTGTAGTCGATCCCATCATTAGCGAATAGCACGTCGTGCCTCCCTCAACATCTT
CTTTACGTGCTTACCCTTTGCATAAGGTGTCTCGTTGGTGCCTTAATTGAAAAGTAGAGAATCTGAT
TGGGACCTCAGGTCAGGCAAGACCACCTGCTGAGTTTAA

Halodulepinifolia

GATAACTTGACGGATCGCATGGCCTCTGTGCTGGCGACGCATCATTCAAATTTCTGCCCTATCAACT
TTCGATGGTAGGATAGGGGCCTACCATGGTGTGGACGGGTGACGGAGAATTAGGGTTCGATTCCGG

AGAGGGAGCCTGAGAAACGGCTACCACATCCAAGGAAGGCAGCAGGCGCGCAAATTACCCAATCCT
GACACGGGGAGGTAGTGACAATAAATAACAATACCGGGCTCGTTGAGTCTGGTAATTGGAATGAGTA
CAATCTAAATCCCTTAACGAGGATCCATTGGAGGGCAAGTCTGGTGCCAGCAGCCGCGGTAATTCCA
GCTCCAATAGCGTATATTTAAGTTGTTGCAGTTAAAAAGCTCGTAGTTGGACCTTGGGTTGGGTCGG
CCGGTCTGCCTATAGGTGTGCATCGGCCGTCTCGTCCCTTCTGCTGGTGACGCGTTCCTGTCCTTTA
TTGGTCCGGTCTGCCTCCGGCGCTGTTACTTTGAAGAAATTAGAGTGCTCAAAGCAGGCCTGTGCT
CGTATACATTAGTATGGGATAACGTCATAGGATTTGATCCTATTGTGTTGGCCTTCGGGATCGGAGT
AATGATTAAGAGGGACAGTCGGGGGCATTTCGTATTTTCATAGTCAGAGGTGAAATTCCTGGATTTATGA
AAGACGAACGACTGCGAAAGCATTTCGCAAGGATGTTTTTCATTAATCAAGAACGAAAGTTGGGGGCT
CGAAGACGATCAGATACCGTCTAGTCTCAACCATAAACGATGCCGACCAGGGATTGGCCGGATGTT
GCTTTTAGGACTCTGCCAGCACCTTATGAGAAATCAAAGTTTTTGGGTTCCGGGGGGAGTATGGTCG
CAAGGCTGAAACTTAAAGGAATTGACGGAAGGGCACCACCAGGAGTGGAGCCTGCGGCTTAATTTG
ACTCAACACGGGGAAACTTACCAGGTCCAGACATAGTAAGGATTGACAGATTGAGAGCTCTTTCTTG
ATTCTATGGGTGGTGGTGCATGGCCGTTCTTAGTTGGTGGAGCGATTGTCTGGTTAATTCCGTTAA
CGARCGAGACCTCAGCCTGCTAACTAGCTATGCGGAGGTGACCCTTCGTGGCCAGCTTCTTAGAGG
GACTATGGCCGCTCAGGCCATGGAAGTTTGRGGCAATAACAGGTCTGTGATGCCCTTAGATGTTCTG
GGCCGCACGCGCGCTACACTGATGTATTCAACGAGTTTATAACCTGGGCCGATAGGCTTGGGTAAT
CTTCGAAAATTTTCATCGTGATGGGGATAGATCATTGCAATTGTTGGTCTTCAACGAGGAATTCCTAGT
AAGCGTGAGTCATCAGCTCGCGTTGACTACGTCCCTGCCCTTGTACACACCGCCCGTCGCTCCTA

>Thalassia hemprichii

AATTCAGACTGTGAAACTGCGAATGGCTCATTACATCAGTTATAGTTTTGTTTGATGGTACCTACTACT
CGGATAACCGTAGTAATTCTAGAGCTAATACGTGCACCGAACCCCGACTTCTGGAAGGGTTGCATTT
ATTAGATAAAAGGCCAATGTGGGCTCTGCTCACCTTTCGGATGATACATGATAACTCGACGGATCGC
ACGGCCTTCGTGCCGGCGACGCATCATTCAAATTTCTGCCCTATCAACTTTCGATGGTAGGATAGGG
GCCTACCATGGTGGTACGGGTGACGGAGAATTAGGGTTCGATTCCGGAGAGGGAGCCTGAGAAA
CGGCTACCACATCCAAGGAAGGCAGCAGGCGCGCAAATTACCCAATCCTGACACGGGGAGGTAGT
GACAATAAATAACAATACCGGGCTCTACGAGTCTGGTAATTGGAATGAGTACAATCTAAATCCCTTAA
CGAGGATCCATTGGAGGGCAAGTCTGGTGCCAGCAGCCGCGGTAATTCAGCTCCAATAGCGTATA
TTTAAGTTGTTGCAGTTAAAAAGCTCGTAGTTGGACTTTGGGTTGGGTCGGCCGGTCCGCCTTTGGT
GTGCACCGGTCGTCTCGTCCCTTTTCCGGCGACGCGCTCCTGGTCTTAATTGGCCGGGTTTCGTGC
CTTCGGCGTTGTTACTTTGAAGAAATTAGAGTGCTCAAAGCAAGCCCAAGCTCTGCATACATTAGCAT
GGGATAACATCACAGGATTTCCGGTCTATTGTGTTGGCCTTCGGGATCGGAGTAATGATTAAGAGGG
ACAGTCGTGGGCATTTCGTATTTTCATAGTCAGAGGTGAAATTCCTGGATTTATGAAAGACGAACAAC
CGAAAGCATTTCGCAAGGATGTTTTTCATTAATCAAGAACGAAAGTTGGGGGCTCGAAGACGATCAGA
TACCGTCTAGTCTCAACCATAAACGATGCCGACCAGGGATCGGCCGGATGTTGCTTGTGCGACATC
GCCGGCACCTTATGAGAAATCAAAGTTTTTGGGTTCCGGGGGGAGTATGGTCGCAAGGCTGAAACT
TAAAGGAATTGACGGAAGGGCACCACCAGGAGTGGAGCCTGCGGCTTAATTTGACTCAACACGGGG
AAACTTACCAGGTCCAGACATAGTAAGGATTGACAGACTGAGAGCTCTTTCTTGATTCTATGGGTGGT
GGTGCATGGCCGTTCTTAGTTGGTGGAGCGATTGTCTGGTTAATTCCGTTAACGAACGAGACCTCA
GCCTGCTAACTAGCTATGCGGAGGCGACCCTCCGTGGCCAGCTTCTTAGAGGGACTATGGCCGTTT
AGGCCACGGAAGTTTGGAGGCAATAACAGGTCTGTGATGCCCTTAGATGTTCTGGGCCGCACGCGCG
CTACACCGATGTATTCAACGAGTTTATAACCTTGGCTGACAGGCCCGGGTAATCTTGCAATTTTCATC
GTGATGGGGATAGATCATTGCAATTGTTGGTCYCAACGAGGAATTCCTAGTAAGCGCGAGTCATCA
GCTCGCGTTGACTACGTCCCTGCCCTTGTACACACCGCCCGTCGCTCCTACCGATTGAATGGTCC
GGTGAAGTGCTCGGATCGCGGC

>Cymodocearotundata

GATAACTTGACGGATCGCATGGCCATCGTGCTGGCGACGCATCATTCAAATTTCTGCCCTATCAACT
TTCGATGGTAGGATAGGGGCCTACCATGGTGTGACGGGTGACGGAGAATTAGGGTTCGATTCCGG
AGAGGGAGCCTGAGAAACGGCTACCACATCCAAGGAAGGCAGCAGGCGCGCAAATTACCCAATCCT
GACACGGGGAGGTAGTGACAATAAATAACAATACCGGGCTCTTGGAGTCTGGTAATTGGAATGAGTA
CAATCTAAATCCCTTAACGAGGATCCATTGGAGGGCAAGTCTGGTGCCAGCAGCCGCGGTAATTCCA
GCTCCAATAGCGTATATTTAAGTTGTTGCAGTTAAAAAGCTCGTAGTTGGACCTTGGGTTGGGTCCG
CCGGTCCGCCTATGGTGTGCATCGGCCGTCTCGTCCCTTCTGCCGGAGACGCGTTCCTGTCCTTCA
CTGGTCGGGTCTGTGCTTCTGGCGCGCTGTTACTTTGAAGAAATTAGAGTGCTTAAAGCAAGCCTATG
CTCTGCATACATCAGCATGGGATAACATCATAGGATTTCCGGTCTATTGTGTTGGCCTTCGGGATCG
GAGTAATGATTAAGAGGGACAGTCGGGGGCATTTCGATTTTCATAGTCAGAGGTGAAATTCTTGGATT
TATGAAAGACGAACAACACTGCGAAAGCATTTCGCAAGGATGTTTTTCAATTAATCAAGAACGAAAGTTGG
GGCTCGAAGACGATCAGATACCGTCTAGTCTCAACCATAAACGATGCCGACCAGGGATCGGCGGA
TGTTGCTTTTAGGACTCTGCCAGCACCTTATGAGAAATCAAAGTTTTTGGGTTCCGGGGGGGGTATG
GTCGCAAGGCTGAAACTTAAAGGAATTGACGGAAGGGCACCACCAGGAGTGGAGCCTGCGGCTTAA
TTTGACTCAACACGGGGAAACTTACCAGGTCCAGACATAGTAAGGATTGACAGATTGAGAGCTCTTT
CTTGATTCTATGGGTGGTGGTGCATGGCCGTTCTTAGTTGGTGGAGCGATTTGTCTGGTTAATTCCG
TTAACGAACGAGACCTCAGCCTGCTAACTAGCTACGCGGAGGTGACCCTTCGTGGCCAGCTTCTTA
GAGGGACTATGGCCGCTTAGGCCACGGAAGTTTGAGGCAATAACAGGTCTGTGATGCCCTTAGATG
TTCTGGGCCGCACGCGCGCTACACTGATGTATTCAACGAGTTTATAACCTTGACCGATAGGTTTGGG
TAATCTTCGAAAATTCATCGTGATGGGGATAGATCATTGCAATTGTTGGTCTTCAACGAGGAATTCC
TAGTAAGCGCGAGTCATCAGCTCGCGTTGACTACGTCCCTGCCCTTTGTACACACCGCCCGTCGCT
CCTA

>*Halophiladecipiens*

AATTCAGACTGTGAAACTGCGAATGGCTCATTAAATCAGTTATAGTTTGTGGTACTTTCTACTC
GTATAACCGTAGTAATTCTAGAGCTAATACGTGCACCAAACCCCGACTTCTGGAAGGGATGCATTTAT
TAGATAAAAGGCCAATGCGGGCTTCGATCGCTTCTCGGATGATTCATGATAACTCGACGGATCGCAC
GGCCCTCGTGCCGGCGACGCACCATTCAAATTTCTGCCCTATCAACTTTTCGATGGTAGGATAGGGG
CCTACCATGGTGGTGACGGGTGACGGAGAATTAGGGTTCGATTCCGGAGAGGGAGCCTGAGAAAC
GGCTACCACATCCAAGGAAGGCAGCAGGCCGCGCAAATTACCAATCCTGACATGGGGAGGTAGTGA
CAATAAATAACGATACCGGGCTCTACGAGTCTGGTAATTGGAATGAGTACAATCTAAATCCCTTAACG
AGGATCCATTGGAGGGCAAGTCTGGTGCCAGCAGCCGCGGTAATTCCAGCTCCAATAGCGTATATTT
AAGTTGTTGCAGTTAAAAAGCTCGTAGTTGGACTTTGGGTTGGGTCCGGCCGGTCCGCCTTTGGTGTG
CACCGGTCGTCTCGTCCCTTTGCCGGTGACGCGCTCCTGGACTTAATTGGCCGGGTCTGTCCTTC
GGCGCTGTTACTTTGAAGAAATTAGAGTGCTCAAAGCAAGCCCAAGCTCTGCATATATTAGCATGGG
ATAACATCACAGGATTTCCGGTCTATTGTGTTGGCCTTCGGGATCGGAGTAATGATTAAGAGGGATA
GTCGTGGGCATTCGTATTTTCATAGTCAGAGGTGAAATTCCTGGATTTATGAAAGACGAACAACACTGCGA
AAGCATTTGCCAAGGATGTTTTTCAATTAATCAAGAAACGAAAGTTGGGGGCTCGAAGACGATCAGATA
CCGTCTAGTCTCAACCATAAACGATGCCGACCAGGGATCGGCGGATGTTGCTTGTACGACATCGC
CGGCACCTTATGAGAAATCAAAGTTTTTGGGTTCCGGGGGGAGTATGGTTCGCAAGGCTGAAACTTAA
AGGAATTGACGGAAGGGCACCACCAGGAGTGGAGCCTGCGGCTTAATTTGACTCAACACGGGGGAAA
CTTACCAGGTCCAGACATAGTAAGGATTGACAGACTGAGAGCTCTTTCTTGATTCTATGGGTGGTGG
TGCATGGCCGTTCTTAGTTGGTGGAGCGATTTGTCTGGTTAATTCCGTTAACGAACGAGACCTCAGC
CTGCTAACTAGCTATGCGGAGGCAACCCTCCGTGGCCAGCTTCTTAGAGGGACTATGGCCGCTTAG
GCCACGGAAGTTTGAGGCAATAACAGGTCTGTGATGCCCTTAGATGTTCTAGGCCGCACGCGCGCT
ACACTGATGTATTCAACGAGTTTATAACCTTGGCTGACAGGCCCGGGTAATCTTTGAAAATTTTCATCG
TGATGGGGATAGATCATTGCAATTGTTGGTCTTCAACGAGGAATTCCTAGTAAGCGCGAGTCATCAG
CTCGCGTTGACTACGTCCCTGCCCTTTGTACACACCGCCCGTCGCTCCTACCGATTGAATGGTCCG
GTGAAGTGCTCGGATCGCGGC

>*Halophila minor*

CCATAAATTTGGGGCCTGTGGGGAAACCCCAACCCCGGGTTTTATTGGCCCTCAGGGGGTCTTT
CCCCCTAAGGCGCGAAATTTGGGAAGGCGACTGGGGGCGCCTTCTTTTTTATCCCACCGTGGGAAG
GGGAGGTTTTCAAAGCGGATTAATTGGTGTACCCCCAGGTTTTCCAGTTCAGGAGGGTGA AACG
GAGGCCAGGAATTGTTAATCGATTCCCTATAGGCGGAATTGGGCCGGAGTTGCAAGTTTCCCGCC
CCCAATGCCGCGGGGTTAATTCAGACTTGAAACTGGGAAGGGTCCATAAATCCAGTTTAAGTTTGT
TGGAGGTAATTTCTACTCGGATAACCGTAGTAATTCTAGAGCTAATACGTGCACCAAACCCCGACTTC
TGGAAGGGATGCATTTATTAGATAAAAAGGCCAATGCGGGCTTCGCTCGSTTYTCGGATGATTCATGA
TAACTCGACGGATCGCACGGCCCTCGTGCCGGCGACGCATCATTCAAATTTCTGCCCTATCAACTTT
CGATGGTAGGATAGGGGCCTACCATGGTGGTGACGGGTGACGGAGAATTAGGGTTTCGATTCCGGA
GAGGGAGCCTGAGAAACGGCTACCACATCCAAGGAAGGCAGCAGGCGCGCAAATTACCCAATCCTG
ACACGGGGAGGTAGTGACAATAAATAACGATACCGGGCTCTACGAGTCTGGTAATTGGAATGAGTAC
AATCTGAATCCCTTAACGAGGATCCATTGGAGGGCAAGTCTGGTGCCAGCAGCCGCGGTAATTCCA
GCTCCAATAGCGTATATTTAAGTTGTTGCAGTTAAAAAGCTCGTAGTTGGACTTTGGGTTGGGTCCG
CCGGTCCGCTTTGGTGTGCACCGGTCTGCTCGTCCCTTTTGCCGGTGACGCGCTCCTGGACTTAA
TTGGCCGGGTCTGTCCTTCGGCGCTGTTACTTTGAAGAAATTAGAGTGCTCAAAGCAAGCCCAAGCT
CTGCATATATTAGCATGGGATAACATCACAGGATTTCCGTCCCTATTGTGTTGGCCTTCGGGATCGGA
GTAATGATTAAGAGGGACAGTCGTGGGCATTCGTATTTCATAGTCAGAGGTGAAATTCCTGGATTTAT
GAAAGACGAACAACACTGCGAAAGCATTGGCCAAGGATGTTTTCAATTAATCAAGAACGAAAGTTGGGG
CTCGAAGACGATCAGATACCGTCCCTAGTCTCAACCATAAACGATGCCGACCAGGGATCGGCGGATG
TTGCTCATACGACATCGCCGGCACCTTATGAGAAATCAAAGTTTTTTGGGTTCCGGGGGGAGTATGGT
CGCAAGGCTGAAACTTAAAGGAATTGACGGAAGGGCACCACCAGGAGTGGAGCCTGCGGCTTAATT
TGACTCAACACGGGGAAACTTACCAGGTCCAGACATAGTAAGGATTGACAGACTGAGAGCTCTTTCT
TGATTCTATGGGTGGTGGTGCATGGCCGTTCTTAGTTGGTGGAGCGATTTGTCTGGTTAATTCCGTT
AACGAACGAGACCTCAGCCTGCTAACTAGCTATGCGGAGGCAACCCTCCGTGGCCAGCTTCTTAGA
GGGACTATGGCCGCTTAGGCCACGGAAGTTTGAGGCAATAACAGGTCTGTGATGCCCTTAGATGTT
CTGGGCCGCGACGCGCTACACTGATGTATTCAACGAGTTTATAACCTTGCGTACAGGCCCGGGT
AATCTTTGAAAATTTTCATCGTGATGGGGATAGATCATTGCAATTGTTGGTCTTCAACGAGGAATTCCT
AGTAAGCGCGAGTCATCAGCTCGCGTTGACTACGTCCCTGCCCTTTGTACACACCGCCCGTCTGCTC
CTACCGATTGAATGGTCCGGTGAAGTGCTCGGATCGCGGC

>*Halophila ovalis*

AATTCAGACTGTGAAACTGCGAATGGCTCATTAAATCAGTTATAGTTTGTGGTGGTACTTTCTACTC
GGATAACCGTAGTAATTCTAGAGCTAATACGTGCACCAAACCCCGACTTCTGGAAGGGATGCATTTA
TTAGATAAAAAGGCCAATGCGGGCTTCGCTCGCTTCTCGGATGATTCATGATAACTCGACGGATCGCA
CGGCCCTCGTGCCGGCGACGCATCATTCAAATTTCTGCCCTATCAACTTTTCGATGGTAGGATAGGGG
CCTACCATGGTGGTGACGGGTGACGGAGAATTAGGGTTTCGATTCCGGAGAGGGAGCCTGAGAAAC
GGCTACCACATCCAAGGAAGGCAGCAGGCGCGCAAATTACCCAATCCTGACACGGGGAGGTAGTGA
CAATAAATAACGATACCGGGCTCTACGAGTCTGGTAATTGGAATGAGTACAATCTAAATCCCTTAACG
AGGATCCATTGGAGGGCAAGTCTGGTGCCAGCAGCCGCGGTAATTCCAGCTCCAATAGCGTATATTT
AAGTTGTTGCAGTTAAAAAGCTCGTAGTTGGACTTTGGGTTGGGTCCGGCCGGTCCGCCTTTGGTGTG

CACCGGTCGTCTCGTCCCTTTTGCCGGTGACGCGCTCCTGGACTTAATTGGCCGGTTCGTGCCTTC
GGCGCTGTTACTTTGAAGAAATTAGAGTGCTCAAAGCAAGCCCAAGCTCTGCATATATTAGCATGGG
ATAACATCACAGGATTTTCGGTCCTATTGTGTTGGCCTTCGGGATCGGAGTAATGATTAAGAGGGACA
GTCGTGGGCATTCGTATTTTCATAGTCAGAAGGTGAAATTCCTTTGGATTTATGAAAGACGAACCAACTG
GCGAAAGCATTTCGCAAGGATGTTTTTCATTAATCAAGAACGAAAGTTGGGGGCTCGAAGACGATCAG
ATACCGTCTAGTCTCAACCATAAACGATGCCGACCAGGGATCGGCCGGATGTTGCTCATACGACATC
GCCGGCACCTTATGAGAAATCAAAGTTTTTTGGGTTCCGGGGGGAGTATGGTCGCAAGGCTGAAACT
TAAAGGAATTGACGGAAGGGCACCACCAGGAGTGGAGCCTGCGGCTTAATTTGACTCAACACGGGG
AAACTTACCAGGTCCAGACATAGTAAGGATTGACAGACTGAGAGCTCTTTCTTGATTCTATGGGTGGT
GGTGCATGGCCGTTCTTAGTTGGTGGAGCGATTTGTCTGGTTAATTCCGTTAACGAACGAGACCTCA
GCCTGCTAACTAGCTATGCGGAGGGCAACCCTCCGTGGCCAGCTTCTTAGAGGGACTATGGCCGCTT
AGGCCACGGAAGTTTGAGGCAATAACAGGTCTGTGATGCCCTTAGATGTTCTGGGTGCGACGCGCG
CTACACTGATGTATTCAACGAGTTTATAACCTTGGCTGACAGGCCCGGGTAATCTTTGAAAATTTTCAT
CGTGATGGATAGATCATTGCAATTGTTGGTCTTCAACGAGGAATTCCTAGTAAGCGCGAGTCATCAG
CTCGCGTTGACTACGTCCCTGCCCTTTGTACACACCGCCCGTCGCTCCTACCGATTGAATGGTCCG
GTGAAGTGCTCGGATCGCGGC

>*Halophila beccarii*

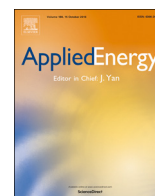
AATTCAGACTGTGAAACTGCGAATGGCTCATTAAATCAGTTATAGTTTTGTTTGATGGTACTTTCTACTC
GGATAACCGTAGTAATTCTAGAGCTAATACGTGCACCAAACCCCGACTTCTGGAAGGGATGCATTTA
TTAGATAAAAGGCCAATGCGGGCTTCGCTCGCTTCTCGGATGATTCATGATAACTCGACGGATCGCA
CGGCCCTCGTGCCGGCGACGCATCATTCAAATTTCTGCCCTATCAACTTTCGATGGTAGGATAGGGG
CCTACCATGGTGGTGACGGGTGACGGAGAATTAGGGTTCGATTCCGGAGAGGGAGCCTGAGAAAC
GGCTACCACATCCAAGGAAGGCAGCAGGCGCGCAAATACCCAATCCTGACACGGGGAGGTAGTGA
CAATAATAACGATACCGGGCTCTACGAGTCTGGTAATTGGAATGAGTACAATCTAAATCCCTTAACG
AGGATCCATTGGAGGGCAAGTCTGGTGCCAGCAGCCGCGGTAATTCAGCTCCAATAGCGTATATTT
AAGTTGTTGCAGTTAAAAGCTCGTAGTTGGACTTTGGGTTGGGTGCGCCGGTCCGCCTTTGGTGTG
CACCGGTCGTCTCGTCCCTTTTGCCGGTGACGCGCTCCTGGACTTAATTGGCCGGTTCGTGCCTTC
GGCGCTGTTACTTTGAAGAAATTAGAGTGCTCAAAGCAAGCCCAAGCTCTGTATATATTAGCATGGG
ATAACATCACAGGATTTTCGGTCCTATTGTGTTGGCCTTCGGGATCGGAGTAATGATTAAGAGGGACA
GTCGTGGGCATTCGTATTTTCATAGTCAGAGGTGAAATTCCTTTGGATTTATGAAAGACGAACAACTGCGA
AAGCATTTGCCAAGGATGTTTTTCATTAATCAAGAACGAAAGTTGGGGGCTCGAAGACGATCAGATAC
CGTCCTAGTCTCAACCATAAACGATGCCACCAGGGATCGGCCGGATGTTGCTTGTACGACATCGCC
GGCACCTTATGAGAAATCAAAGTTTTTTGGGTTCCGGGGGGGAGTATGGTCGCAAGGCTGAAACTTAA
AGGAATTGACGGAAGGGCACCACCAGGAGTGGAGCCTGCGGCTTAATTTGACTCAACACGGGGGAAA
CTTACCAGGTCCAGACATAGTAAGGATTGACAGACTGAGAGCTCTTTCTTGATTCTATGGGTGGTGG
TGCATGGCCGTTCTTAGTTGGTGGAGCGATTTGYCTGGTTAATTCCGTTAACGAACGAGACCTCAGC
CTGCTAACTAGCTATGCGGAGGGCACCCTCCGTGGCCAGCTTCTTAGAGGGACTATGGCCGCTTAG
GCCACGGAAGTTTGAGGCAATAACAGGTCTGTGATGCCCTTAGATGTTCTGGGCCGACGCGCGCY
ACACTGATGTATTCAACGAGTTTATAACCTTGGCTGACAGGCCCGGGTAATCTTTGAAAATTTTCATCG
TGATGGGGATAGATCATTGCAATTGTTGGTCTTCAACGAGGAATTCCTAGTAAGCGCGAGTCATCAG

CTCGCGTTGACTACGTCCCTGCCCTTTGTACACACCGCCCGTCGCTCCTACCGATTGAATGGTCCG
GTGAAGTGCTCGGATCGCGGC

>*Enhalus acoroides*

AATTCAGACTGTGAAACTGCGAATGGCTCATTAAATCAGTTATAGTTTGTGGTACTTACTACTC
GGATAACCGTAGTAATTCTAGAGCTAATACGTGCACCAAACCCCGACTTCTGGAAGGGATGCATTTA
TTAGATAAAAGGCCAATGCGGGCTTTGCTCGCTTTTCGGATGATACATGATAACTCGACGGATCGCA
CGGCCTTCGTGCTGGCGACGCATCATTCAAAGTTCTGCCCTATCAACTTTCGATGGTAGGATAGGGG
CCTACCATGGTGGTGACGGGTGACGGAGAATTAGGGTTCGATTCCGGAGAGGGAGCCTGAGAAAC
GGCTACCACATCCAAGGAAGGCAGCAGGCGCGCAAATTACCCAATCCTGACACGGGGAGGTAGTGA
CAATAAATAACAATACCGGGCTCTACGAGTCTGGTAATTGGAATGAGTACAATCTAAATCCCTTAACG
AGGATCCATTGGAGGGCAAGTCTGGTGCCAGCAGCCGCGGTAATTCCAGCTCCAATAGCGTATATTT
AAGTTGTTGCAGTTAAAAGCTCGTAGTTGGACTTTGGGTTGGGTCGGCCGGTCCGCCTTTGGTGTG
CACCGGTCGTCTCGTCCCTTTTGCCGGTGACGCGCTCCTGGACTTAATTGGCCGGGTGCTGCCTTC
GGCGCTGTTACTTTGAAGAAATTAGAGTGCTCAAAGCAAGCCCAAGCTCTGCATACATTAGCATGGG
ATAACATCACAGGATTTTCGGTCTATTGTGTTGGCCTTCGGGATGGGAGTAATGATTAAGAGGGACA
GTCGTGGGCATTCGTATTTCATAGTCAGAGGTGAAATTCCTGGATTTATGAAAGACGAACAACCTGCGA
AAGCATTTGCCAAGGATGTTTTTATTAATCAAGAACGAAAGTTGGGGGCTCGAAGACGATCAGATAC
CGTCCTAGTCTCAACCATAAACGATGCCGACCAGGGATCGGCGGATGTTGCTTGTACGACATCGCC
GGCACCTTATGAGAAATCAAAGTTTTTGGGTTCCGGGGGGAGTATGGTCGCAAGGCTGAAACTTAAA
GGAATTGACGGAAGGGCACCACCAGGAGTGGAGCCTGYGGCTTAATTTGACTCAACACGGGGAAAC
TTACCAGGTCCAGACATAGTAAGGATTGACAGACTGAGAGCTCTTTCTTGATTCTATGGGTGGTGGT
GCATGGCCGTTCTTAGTTGGTGGAGCGATTTGTCTGGTTAATTCCGTTAACGAACGAGACCTCAGCC
TGCTAACTAGCTATGCGGAGGCAACCCTCCGTGGCCAGCTTCTTAGAGGGACTATGGCCGTTTAGG
CCACGGAAGTTTGAGGCAATAACAGGTCTGTGATGCCCTTAGATGTTCTGGGCCGCACGCGCGCTA
CACTGATGTATTCAACGAGTTTATAACCTTGGCTGACAGGCCCGGGTAATCTTATAAATTTTCATCGTG
ATGGGGATAGATCATTGCAATTGTTGGTCTTCAACGAGGAATTCCTAGTAAGCGCGAGTCATCAGCT
CGCGTTGACTACGTCCCTGCCCTTTGTACACACCGCCCGTCGCTCCTACCGATTGAATGGTCCGGT
GAAGTGCTCGGATCGCGGC

*A waste free, microbial oil centered cyclic bio-refinery
approach based on flexible macroalgae biomass*



A waste-free, microbial oil centered cyclic bio-refinery approach based on flexible macroalgae biomass



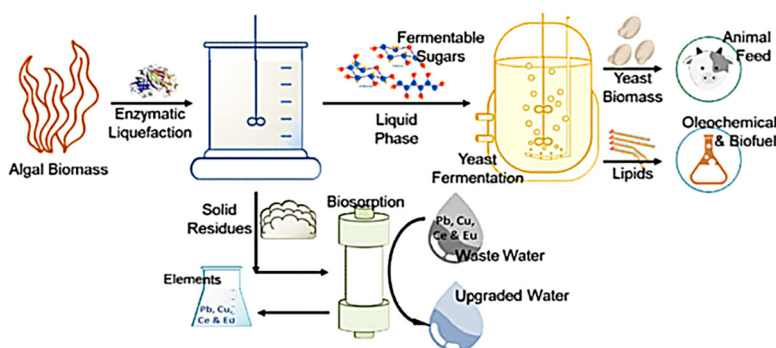
Mahmoud A. Masri, Wojciech Jurkowski, Pariya Shaigani, Martina Haack, Norbert Mehlmer*, Thomas Brück*

Department of Chemistry – Chair of Synthetic Biotechnology, Technical University of Munich, Lichtenbergstraße 4, 85748 Garching, Germany

HIGHLIGHTS

- Holistic valorization of unexploited marine biomass.
- Integrated production of plant like yeast lipids, animal feed and biosorbents.
- Enzymatic macroalgae liquefaction to obtain yeast cultivation media.
- Utilization of hydrolysis residues as precious metal biosorbent.
- New, simple and rapid analysis tools for industrial lipid/ biosorption monitoring.

GRAPHICAL ABSTRACT



ARTICLE INFO

Keywords:

Cyclic biorefinery
Macroalgae
Laminaria digitata
Cutaneotrichosporon oleaginosus
Microbial oil
Biosorbent

ABSTRACT

Biofuels and the oleochemical industry are highly dependent on plant oils for the generation of renewable product lines. Consequently, production of plant lipids, such as palm and rapeseed oil, for industrial applications competes with agricultural activity and is associated with a negative environmental impact. Additionally, established chemical routes for upgrading bio-lipids to renewable products depend on metal-containing catalysts. Metal leaching during oil processing results in heavy metal contaminated process wastewater. This water is difficult to remediate and leads to the loss of precious metals. Therefore, the biofuels and chemical industry requires sustainable solutions for production and upgrading of bio-lipids. With regard to the former, a promising approach is the fermentative conversion of abundant, low-value biomass into microbial, particularly yeast-based lipids. This study describes the holistic, value-adding conversion of underexploited, macroalgae feedstocks into yeast oil, animal feed and biosorbents for metal-based detoxification of process wastewater. The initial step comprises a selective enzymatic liquefaction step that yields a supernatant containing 62.5% and 59.3% ($w^A w_{\text{biomass}}$) fermentable sugars from *L. digitata* and *U. lactuca*, respectively. By dispensing with chemical pretreatment constraints, we achieved a 95% (w/w) glucose recovery. Therefore, the supernatant was qualified as a cultivation media without any detoxification step or nutrition addition. Additionally, the hydrolysis step provided 27–33% ($w^A w_{\text{biomass}}$) of a solid residue, which was qualified as a metal biosorbent. Cultivation of the oleaginous yeast *C. oleaginosus* on the unprocessed hydrolysis supernatant provided 44.8 g L^{-1} yeast biomass containing 37.1% ($w^A w_{\text{biomass}}$) lipids. The remaining yeast biomass after lipid extraction is targeted as a performance animal feed additive. Selectivity and capacity of solid macroalgae residues as biosorbents were assessed for removal and recycling of rare and heavy metals, such as Ce^{+3} , Pb^{+2} , Cu^{+2} and Ni^{+2} from model wastewater. The biosorption capacity of the macroalgae residues (sorption capacity $\sim 0.7 \text{ mmol g}^{-1}$) exceeds

* Corresponding authors.

E-mail address: brueck@tum.de (T. Brück).

that of relevant commercially available adsorption resins and biosorbents. To facilitate the integration of our technology in existing chemical and biotechnological production environments, we have devised simple, rapid and cost-efficient methods for monitoring both lipogenesis and metal sorption processes. The application of the new optical monitoring tools is essential to determine yeast cell harvesting times and biosorption capacities respectively. For the first time we report on a waste-free bioprocess that combines sustainable, microbial lipid production from low value marine biomass with in-process precious metal recycling options. Our data allowed for a preliminary economic analysis, which indicated that each product could be cost competitive with current market equivalents. Hence, the synaptic nature of the technology platform provides for the economic and ecologic viability of the overall process chain.

1. Introduction

The biofuels (i.e. biodiesel and biokerosene), oleochemicals (i.e. lubricants, surfactants and polymers) and the cosmetic sector are highly dependent on plant-derived triglyceride feedstocks to generate renewable product lines [1]. Due to their high areal yields, favorable chemical composition and low cost, palm and rapeseed oil are most desirable feedstocks for these processes [2]. However, the production of these plant-based lipids is associated with a negative ecological impact. More specifically, production of these chemical feedstocks competes with food production, accelerates land use change in sensitive ecosystems and thereby negatively impacts biodiversity [3]. By contrast, microbial oils generated from waste biomass streams within a bio-refinery setting potentially enable the generation of a diversified and sustainable product portfolio that is not associated with a negative environmental impact.

More recently, residual marine biomass, such as algae and seagrass, receives increasing attention as feedstock in bio-refinery processes to substitute the limited availability of residual terrestrial biomass in

specific regions of the globe with dense populations and limited agricultural land (i.e. Germany, UK, Ireland, France, Japan, India, Malaysia, China) [4,5]. In this regard, macroalgae can expeditiously generate biomass from carbon dioxide, sunlight and inorganic nutrients by efficient photosynthesis [6,7]. With their high photon conversion efficiency [7], seaweeds like *Laminaria japonica* can reach a productivity of $1300 \text{ t ha}^{-1} \text{ year}^{-1}$ biomass, which is 6.5 times higher than the productivity of sugarcane [8]. Furthermore, macroalgae are able to grow in a wide diversity of environments including fresh-, salt-, temperate- and municipal wastewater [9]. However, the use of macroalgae in biotechnological processes – much like terrestrial biomass feedstocks – requires the chemical or biological hydrolysis of polymeric carbohydrates that constitute the cellular matrix to release fermentable, monomeric carbohydrates. Previously, hydrolysis and liquefaction of macroalgae biomass has been demonstrated using chemical hydrolysis [10], chemo-enzymatic hydrolysis [11], biological degradation [12] and anaerobic digestion [13,14]. The resulting liquid hydrolysate has been reported to be enriched in fermentable sugars or volatile fatty acids [13], to be used in bioenergy generation, encompassing biogas

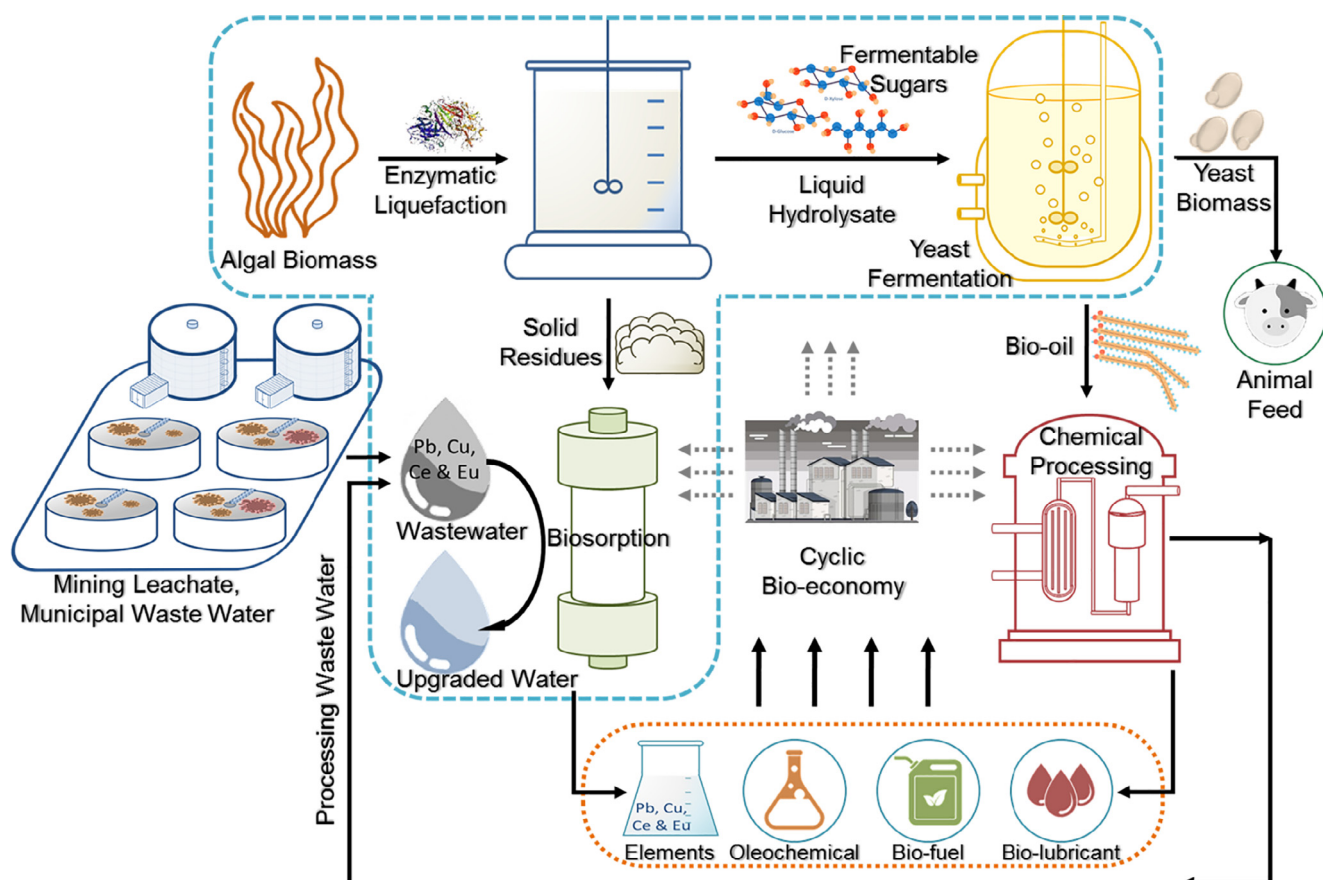


Fig. 1. The cyclic bio-refinery concept based on flexible macroalgae biomass feedstocks. The processes shown within the blue dashed line represent the focus of this study. All other processes are established at industrial scale and referenced throughout the text.

(methane) [14], bio-ethanol [15], acetone and bio-butanol generation [16]. In contrast, there are no value adding applications for the residual biomass fraction, which remains after biomass hydrolysis. At present, the most widespread application for this hydrolysis residue is application as fertilizer [9,17].

The utilization of the sugar rich liquid fraction as a fermentation base for generation of microbial oils has received increasing consideration [18,19]. In this application, designer bio-oils can be generated, that depending on the fatty acid profile could provide a sustainable resource for the production of high value pharmaceuticals, food additives, cosmetics, bio-lubricants or biofuels [20,21]. In that respect, microbial oils could directly substitute plant equivalents, such as palm oil, whose production is associated with land use change having a negative impact on biodiversity and food production [22]. Finally, biomass-hydrolysate of the marine microalgae *Scenedesmus* sp. [23] and beach-cast seagrass [5] have been demonstrated to be suitable fermentation substrates for yeast-based lipid production. The suitability of macroalgae hydrolysates for the fermentative generation of yeast oils has not been demonstrated.

This high value outlet of the liquid fraction contrasts the low value energetic use of the solid fraction remaining after enzymatic biomass hydrolysis. Therefore, the development of alternative high value applications for the solid residues that can be integrated in the bio-refinery work flow is highly desirable. One such application is biosorption, defined as passive uptake of molecules by biological matrices such as non-living cells as opposed to bioaccumulation involving active metabolism [24]. Marine macroalgae have been among the first biomass sources capable of binding high amounts of heavy metals, reaching capacities of 1.5 mmol g^{-1} [25]. Particularly, brown algae containing high amounts of alginate belong to the most studied biosorbing organisms [26]. Due to their growth performance and abundance (up to 16 million tons per year), brown algae are proposed to be a promising biosorbent [27]. Consequently, the development of biosorbents has to follow a “low-tech” and “low-price” philosophy, which can only be achieved by using inexpensive and abundant biomass residues. In a simplified model-process, desorption of biosorbents is not required since the loaded biomass can serve for energy generation as well.

In this context, process water containing heavy metals, found in the electronic, metal and chemical processing industries, poses a significant challenge for purification and recycling processes [28]. In general, heavy metal contaminants are difficult to remove by conventional technologies and potentially accumulate in the water column, where they are toxic to aquatic life [29]. Therefore, sustainable techniques for the removal and recycling of heavy metal contaminants that may contribute value to a bio-refinery set-up are in demand.

As chemo-catalytic processing of yeast triglycerides to end products, such as biolubricant and oleochemicals, potentially results in heavy metal (Ni, Cu, W, Pb, Pt, etc.[30]) contaminated wastewater streams, the solid residue was evaluated for its capacity to bind these metal toxins. Surprisingly, we could demonstrate that hydrolysis residues are excellent biosorbents, capable of opening avenues for in-process recycling of precious catalytic metals and simultaneous wastewater up-cycling. Moreover, the residual solid fraction could be a separate value-adding product stream, which can be employed in the recovery and recycling of precious metals from mining waters or municipal waste leachates respectively (Fig. 1). An important group among these metals used in modern electronics are the lanthanides. Due to rising demand and unsustainable mining practices, they currently belong to the class of critical materials [31]. Rare earth metal recycling from waste streams is rather poor amounting to only 1% in 2011 [32]. However, there are some accessible resources, such as phosphogypsum leachate [33] and red mud [34] as the most prominent examples. As biosorbents are available at very low cost, it might be possible to process these residue streams. To quantify the specific sorption capacity, we use cerium, treated here as a model for the lanthanide group. Our simple and rapid luminescence-based approach also allows to measure kinetics and

competitive biosorption in synthetic multicomponent solutions necessary for a reliable scale-up.

This study presents an entirely new cyclic bio-refinery concept based on flexible macroalgae biomass feedstocks. The assembly of value adding unit operations demonstrated herein are highly interconnected and interdependent, thereby eliminating any waste streams (Fig. 1). For the first time, we disclose optimized enzyme systems that enable selective, low energy hydrolysis of marine brown (*Laminaria digitata*) and green (*Ulva lactuca*) macroalgae biomass in the absence of physico-chemical pretreatment steps. The resulting liquid fraction, which is enriched in fermentable, monomeric sugars is applied as a fermentation base for the high yield production yeast oil triglycerides using the oleaginous yeast *Cutaneotrichosporon oleaginosus* (ATCC 20509). Fermentations carried out in aerated Erlenmeyer flasks (250 ml) and controlled stirred tank bioreactors (1L), demonstrated that *C. oleaginosus* can efficiently transform the chemically diverse macroalgae-derived sugar matrix into triglycerides, when a nutritional stressor was applied. In this context, a new staining-free flow cytometry-based method has been developed, which indicates the exact onset and extent of lipogenesis in *C. oleaginosus*. This method is generally applicable to time onset of lipid biosynthesis in oil-forming yeasts and allows for the exact determination of harvesting times, which are essential for process optimization in microbial oil-centered bio-refinery settings. While resulting yeast triglycerides are a “drop-in” feedstock for generation of bioactive agents, oleochemical building blocks and biofuels, the residual protein and carbohydrate rich yeast biomass can be used as animal feed. To close the mass balance of our cyclic bio-refinery concept we developed a new value-adding outlet for the solid residue fraction remaining after enzymatic macroalgae hydrolysis.

In summary, we present a completely new cyclic bio-refinery concept based on macroalgae biomass residues that has yeast oils as a primary outlet coupled with animal feed and biosorbent production. The bio-refinery process does not compete with agricultural activity, is not associated with land use change, is waste free and allows for in-process wastewater upgrading and metal recycling. Therefore, this set-up significantly contributes to the economic and ecologic efficiency of oleochemical generation.

2. Materials and methods

2.1. Macroalgae sample sourcing

Two brown algae (*Laminaria digitata*) and one green algae (*Ulva lactuca*) sample were harvested from the western coast of Ireland in March and June 2013 (North Seaweed Ltd – Netherlands). The samples were washed thoroughly (with distilled water) to eliminate salt, sand and contaminants. Subsequently, samples were dried and grind down to $\leq 0.5 \text{ mm}$ grain size using a Planetary Ball Mill – (Fritsch, Germany).

2.2. Enzymatic liquefaction of brown algae biomass

Enzymatic liquefaction of each *L. digitata* and *U. lactuca* samples was conducted in acetate buffer (50.0 mM, pH 5.0) containing 7–8% (w/v) biomass. Hydrolysis parameters were maintained at: 50 °C, stirring at 400 rpm for 72 h. Enzymatic hydrolysis was conducted at 1 L for lab scale. For technical scale, *L. digitata* was hydrolyzed at 30 L scale.

In this study, an admixture of the commercial hydrolase enzyme preparations Cellic CTec 2[®], Cellic HTec[®], Novozymes 188[®], (Novozymes, Denmark), *exo*-Laminarase (Megazyme-France) and α -Amylase[®] (Sigma, Germany) was used for biomass liquefaction. In the case of *U. lactuca* hydrolysis, the optimal enzyme admixture comprised a w/w ratio of 1.2: 0.3: 0.2: 0.0: 0.3 of the above enzyme preparations respectively. Analogously, the *L. digitata*, targeted hydrolase system was adjusted to a w/w admixture of 0.3:1.3:0.2:0.2:0.0, respectively. The respective enzyme admixture was dosed at total concentration of 2.0% (w/^dw_{biomass}) for brown and green algae respectively.

After biomass hydrolysis, the solid residue phase was separated by centrifugation at 8000g for 15 min. The liquid phase was purified by 10 kDa cross-flow. The filtrate was then sterilized with 0.2 μm filter and subjected to yeast fermentation. The retentate was pooled with the solid residue phase and subsequently used as a biosorbent for metal removal from dilute aqueous solutions.

2.3. Utilization of hydrolysis residues as a biosorption matrix

All biosorption experiments were conducted by incubating 20 mg air dried biosorbent in 2 ml of a defined metal solution for 3 h at room temperature. Subsequently, this suspension was centrifuged at 10,000g for 10 min and the cerium concentration was measured in supernatant. The cerium concentration ratio before and after the sorption process was used to calculate the binding capacity per gram biosorbent. Experiments were conducted as follows:

(1) Fresh biomass from March, fresh biomass from June, the mixture of both charges before and after hydrolysis. (2) Hydrolysis residue in solutions containing only cerium, and additionally nickel, copper and lead respectively as the second metal in the solution. The purpose was to determine the selectivity for cerium in presence of other metals. (3) Sorption kinetics with hydrolyzed biomass, for wet and dried samples.

2.4. Algae hydrolysates as cultivation media for yeast lipid production

2.4.1. Laboratory scale lipid production in aerated Erlenmeyer flasks

For yeast growth rate and lipid accumulation experiments, *Cutaneotrichosporon oleaginosus* (ATCC 20509) was cultivated in 1 L Erlenmeyer flasks containing 300 ml of the different enzymatic hydrolysates. The flasks were supplemented with an aeration system supplying the cultures with 0.2 L min⁻¹ filtered air. Incubation was done at 28 °C, 120 rpm for 5 days with starting OD of 0.1. All experiments and analyses were conducted in triplicates.

2.4.2. Technical scale batch lipid production in controlled stirred tank bioreactors

C. oleaginosus was inoculated in the *L. digitata* hydrolysate. Batch cultivation of *C. oleaginosus* was performed in a 2 L bioreactor (INFORS HT system, Switzerland) with a working volume of 1.5 L in *L. digitata* hydrolysate with an approximately C/N ratio of 85. The temperature was kept constant at 28 °C, and the pH of the bioreactor was fixed at 6.5 \pm 0.05 with 1 M NaOH by the system. Stirring (200–800 rpm) and aeration (air: 1.0–2.0 vvm) were regulated automatically to maintain dissolved oxygen above 50%. Foam formation was prevented by the addition of 0.01% (v/v) antifoam agent (Antifoam 204, Sigma Aldrich).

2.5. Analysis

2.5.1. Biomass analysis

Sugar analysis was sequentially carried out by chemical hydrolysis and HPLC analysis as previously published [5]. Lipid analysis was performed via GC-FID [35]. Protein content was measured according to the Kjeldahl Standard operating procedure [36]. Finally, the ash content was determined gravimetrically after 1000 °C biomass incineration for 3 h [5].

2.5.2. Determination of total dissolved solids and elemental analysis

Total dissolved solids [TDS] and element analysis was carried by drying 100.0 ml of the hydrolysate at 105 °C (overnight). Resulting crystals were incinerated at 1500 °C for 3 h. Obtained ash material was subjected to scanning electron microscopy (SEM) with energy-dispersive X-ray (EDX) analysis using a JSM-7500F scanning electron microscope (JEOL, Japan). Crystals were mounted on carbon film and prepped for analysis. EDX analysis was performed on multiple areas (100 \times 100 μm) in backscattered electron (BSE) mode for each ash sample. The average value was calculated to obtain the elemental composition for the ash of the hydrolysate.

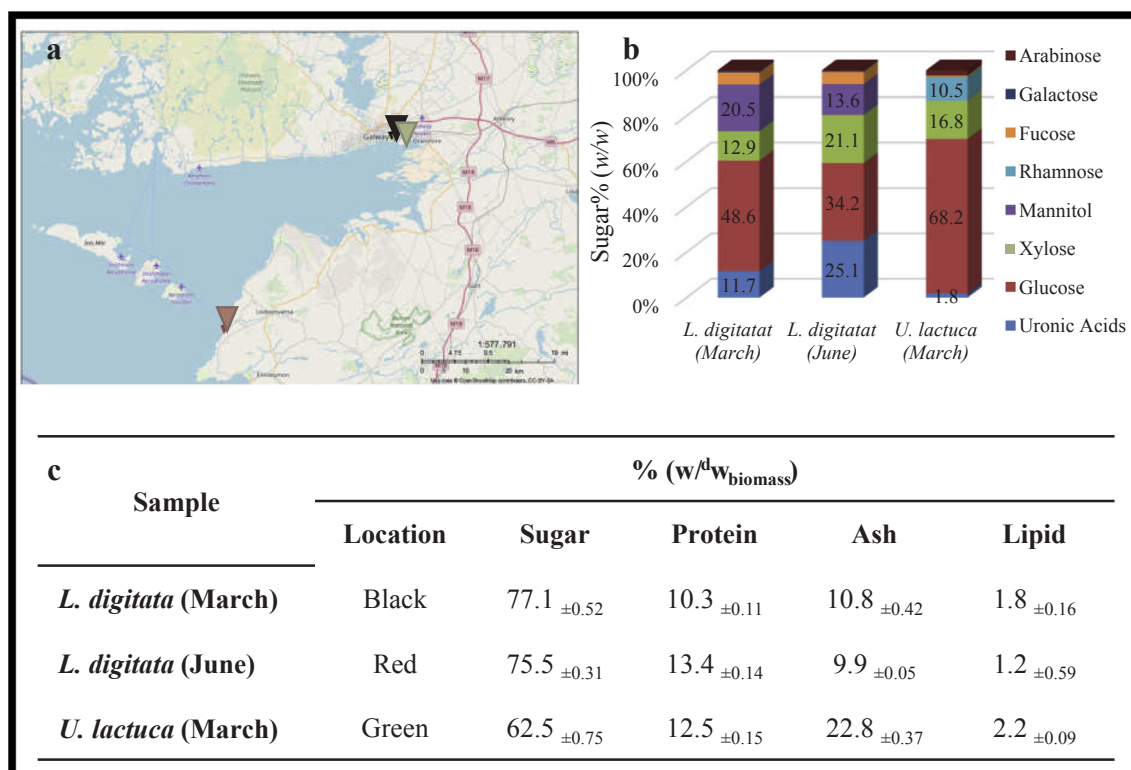


Fig. 2. (a) An image of western coast of Ireland showed the location of selected samples; *L. digitata* [1] (black rectangle), *L. digitata* [2] (red rectangle) and *U. lactuca* (green rectangle). (b) Sugar profile of macroalgae samples; *L. digitata* [1], *L. digitata* [2] and *U. lactuca*, the relative standard deviation of all value is less than \pm 4%. (c) The biomass balance of three samples; *L. digitata* [1] (harvested in March), *L. digitata* [2] (harvested in June) and *U. lactuca* (harvested in March). (For interpretation of the references to color in this figure legend, the reader is referred to the web version of this article.)

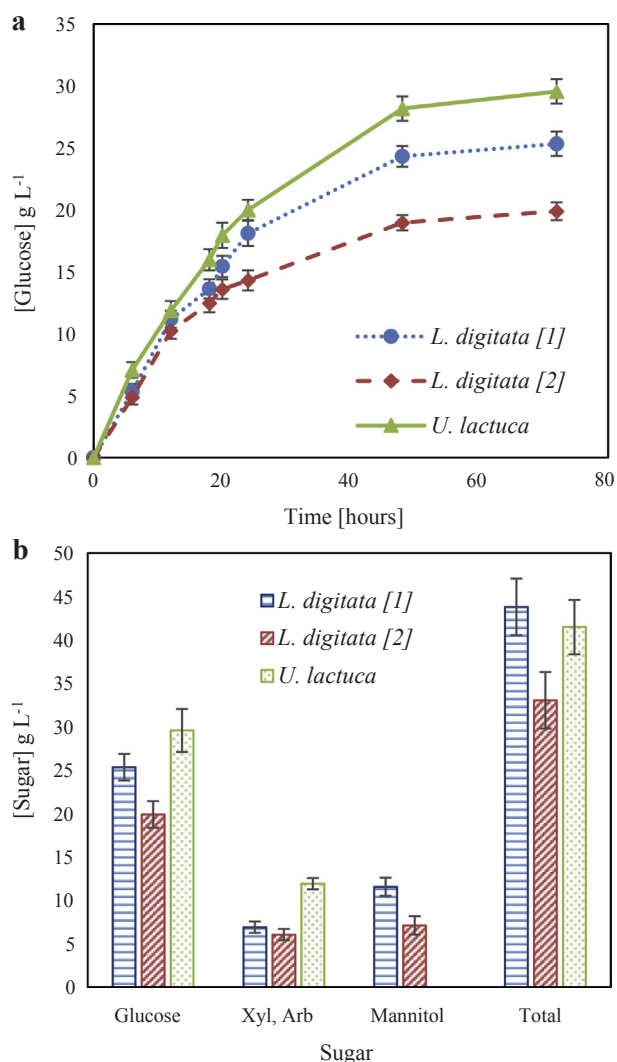


Fig. 3. (a) The proportional increase of glucose over the enzymatic hydrolysis time of *L. digitata* [1] (blue), *L. digitata* [2] (red) and *U. lactuca* (green). (b) The total sugar concentration at the final hydrolysate of *L. digitata* [1] (blue), *L. digitata* [2] (red) and *U. lactuca* (green). (For interpretation of the references to color in this figure legend, the reader is referred to the web version of this article.)

2.5.3. Gravimetric analysis of yeast biomass and lipids

Lyophilization was used to obtain dried yeast biomass. Lyophilization was carried out for 2 days at -80°C and 0.04 mbar (Christ alpha 2–4 LD plus). For lipid extraction, cell destruction was performed with a high-pressure homogenizer (Mulsiflex C3, Avestine, Canada). After lyophilization, three times solvent extraction with Folch solution was sequentially carried out. Then gravimetric lipid quantification was carried out using the Bligh-Dyer method [37]. The lipid profile was assessed via GC-FID as described previously [5].

2.5.4. Flow cytometry-based cell counting

Cell counting via flow cytometry was carried out with a Bio-Rad S3 FACS (BioRad, Hercules, USA) equipped with 488 nm/ 100 mW laser beam. The counting was conducted using 100 μl of sample after 100 times dilution. The cell density diagram describes Side scatter [SSC] on “Y” axis and Forward scatter [FSC] on the “X”-axis.

2.5.5. Cerium concentration measurement

Samples were first diluted 1:99 by mixing 50 μl with 4.95 ml of deionized water. The measurement was then performed in a multi well

plate with 100 μl diluted sample mixed with 100 μl buffer in each well. The buffer contained 100 mM sodium acetate, 10 mM copper (II), 10 mM nickel (II), and 10 mM lead (II). The pH was adjusted to 5.0 with glacial acetic acid. For every series of measurements, a calibration curve consisting of 4 points (cerium: 2.5 mM, 5 mM, 7.5 mM and 10 mM) was prepared the same way, as the samples. For measuring luminescence, a black quartz-glass 96-well microtiter plate manufactured by Hellma Analytics (Germany) and an EnSpire 2 Multimode Plate Reader (Perkin Elmer, USA) were used.

The reliability of the luminescence-based cerium detection method in presence of other metals has also been evaluated. To that end, triplicate samples with known copper concentration (10 mM, 20 mM and 40 mM) have been measured in the cerium concentration range 2.5 mM to 10 mM. All datasets can be described by a global linear regression curve with very good coefficients of determination (R-square) of 0.985 (Cu 40 mM) 0.987 (Cu 20 mM) and 0.992 (Cu 10 mM). The data plot with regression curve is depicted in the [supplementary information \(Supplementary Fig. 1S\)](#). The applicable limit for this method is about 1 mM cerium if interfering metals are present. For model samples containing only cerium the dilution factor can be decreased (until self-quenching occurs) leading to a limit of quantification (LOQ) at about 0.62 μM with signals at 308 RFU compared to 193 ± 12 RFU for the blank ([Supplementary Table 1S](#)). Notably, all metal chelating/binding agents should be eliminated from the assay solution. This was achieved, by repeated washing of the sample to eliminate any water-soluble components.

3. Results and discussion

3.1. Liquefaction of macroalgae biomass

Samples of brown macroalgae *Laminaria digitata* were harvested from the western coast of Ireland in March (black rectangle) and June 2013 (red rectangle), respectively ([Fig. 2a](#)). An additional sample of the green macroalgae (*Ulva lactuca*) was harvested in March (green rectangle) from the same location. The overall chemical composition of the algal samples was analyzed using a detailed biomass analysis ([Fig. 2c](#)).

While the brown algae displayed a carbohydrate content of up to 75–77% (w^d/w_{biomass}), the green algae samples showed a 62% (w^d/w_{biomass}) carbohydrate content. Conversely, brown algae have less inorganic ash in relation to green algae. Protein and lipid content show convergent values in all samples. In spite of higher total sugar content in the brown algae, the glucose content was higher in the green algae ([Fig. 2b](#)). It should be taken into consideration, that glucose content is important for fermentation since it is the most preferable sugar for microorganisms.

Seasonal sugar analysis of the *L. digitata* samples showed that the total sugar content is lower in June compared to the March batch. Moreover, the sugar profile showed considerable seasonal changes. In June the *L. digitata* batch contains less glucose and mannitol, which may be correlated with a decrease in the cellulosic fiber and laminarin. On the contrary, an increase in uronic acids was detected in the June batch, which could indicate an increase of alginate in the cell wall ([Fig. 2b](#)). Interestingly, the fucose concentration remained constant in both samples. In the case of *U. lactuca* glucose and xylose are the major sugars. In addition, a considerable amount of rhamnose was detected which could originate mainly from ulvan [38].

Independent of seasonal changes, glucose is the major carbohydrate monomer in the macroalgae hydrolysis supernatant. Therefore, glucose was used as indicator of hydrolysis efficiency. The glucose concentration was convergent in the first day of macroalgae hydrolysis ([Fig. 3a](#)). Thereafter, the difference in glucose release between samples is more pronounced. *U. lactuca* displays the highest glucose concentration followed by the March batch of *L. digitata* [1]. The synergistic effect of the optimized enzyme system facilitates cell wall lysis within the first 24 h,

which enhanced the sugar release over the remaining two days of hydrolysis. However, the total sugar composition showed different trends. The high amount of free mannitol in the brown algae samples, results in an overall higher concentration of total fermentable sugar in the *L. digitata* hydrolysate (Fig. 3b). The measured glucose and total fermentable sugar concentrations in the enzymatic hydrolysate were consistent with the biomass analysis. While, the glucose amount corresponds to almost 95% (w/w) of theoretical glucose content in the respective biomass sample, the total fermentable sugar concentrations indicate yields of 62.5, 47.1 and 59.3% (w/dw_{biomass}) for dried *L. digitata* [1], *L. digitata* [2] and *U. lactuca* biomass respectively. The cumulative results indicate that with the exception of alginate and fucoidan, the synergistic enzyme activities result in an almost holistic lysis of the cellulosic and laminarin biomass components.

Our current data on recoverable fermentable sugars exceeds previous reports, where *Laminaria japonica* and *Ulva lactuca* were treated chemically prior to the enzymatic hydrolysis, resulting in relatively low glucose recovery compared to the theoretical yield [11]. Another report describes a single enzyme treatment that also lead to a low hydrolysis efficiencies and sugar yields with green and brown macroalgae biomass [39]. Most interestingly, our enzymatic hydrolysis process was so efficient for recovery of fermentable sugars, that no thermochemical pretreatment was required. To that end, the addition of laminarase, amylase and β -glucosidase significantly increased the sugar release. More generally, macroalgae are more amenable to enzymatic hydrolysis compared to terrestrial, lignocellulosic biomass resources (i.e. cereal straw or forestry waste), as they do not contain lignin and most sugar polymer are present in an amorphous and not a crystalline state [40]. The lack of lignin and crystalline polymeric carbohydrates circumvents the necessity of thermo-chemical pretreatments (i.e. steam explosion), which is associated with high energy expenditure and formation of fermentation inhibitors [41].

In addition to the fermentable supernatant, enzymatic hydrolysis also generates solid residue, which represent 27% and 32.5% (w/dw_{biomass}) for *L. digitata* [1] and *U. lactuca* respectively. The analysis of the solid residue indicated, that it contained significant amounts of uronic acids, which are the main building blocks of alginate in addition to protein and inorganic components (i.e. CaCO_3) (Supplementary Fig. 2S).

Prior to using the liquid hydrolysis phase for fermentation, a 10 kDa cross-filtration step was conducted. The processed liquid phase was a light yellow clear liquid, which was used for downstream yeast fermentation without further processing. The highly viscous fraction that was retained after the cross-filtration step was subjected to component analysis. The resulting data indicated that this retentate was composed of glucose, mannitol and fucose respectively (Supplementary Fig. 2S). Based on the significant concentrations of fucose and glucose, the main sugar polymer remaining in the retentate was identified as fucoidan, which much like alginate is not accessible by commercial enzyme systems. Hence, alginate-rich solid hydrolysis residue and the fucoidan rich cross-filtration retentate was pooled and subsequently used as a biosorbent for metal removal from dilute aqueous solutions.

3.2. A cyclic biorefinery concept based on macroalgal biomass

3.2.1. Fermentative conversion of the liquid macroalgae hydrolysates to yeast oils

Sustainable bio-oil production from yeast is considered as the next generation source for triglycerides replacing plant-base lipids, in renewable chemical, cosmetic and pharmaceutical processes [21]. The application of oleaginous yeasts, such as *C. oleaginosus*, in a biorefinery setting has significant advantages over alternative microorganisms as they can rapidly grow to high cell density cultures with a biomass productivity of $2.18 \text{ g L}^{-1} \text{ h}^{-1}$ [42]. Moreover, oleaginous yeasts have the metabolic capacity to accumulate in excess of 75% ($w_{\text{triglycerides}}/dw_{\text{biomass}}$) intracellularly, when nitrogen limiting

conditions are applied [43]. The significant advantage of yeast oils over their plant equivalents is that they can be produced at the same yield and quality without seasonal variation. In contrast to industrial palm oil, microbial oil production does not negatively impact agricultural activity, food production or biodiversity as it does not induce land use change [22].

To test the suitability of macroalgae hydrolysates as feedstock, the oleaginous yeast *C. oleaginosus* was cultivated in each of the macroalgae hydrolysates as the sole fermentation medium. Results were compared to growth experiments conducted with artificial control media, whose chemical composition resembled the respective macroalgae hydrolysates.

The artificial control media were classified based on the nitrogen content into two categories; model complete hydrolysate and nitrogen-limited hydrolysate. The designed complete hydrolysates (model green algae and model brown algae hydrolysates) contained the C/N, C/S and C/P ratios as measured in the original brown or green macroalgae hydrolysates. By contrast, the nitrogen-limited hydrolysates (minimal green algae and minimal brown algae hydrolysates) featured a high C/N ratio (130–150) to induce lipogenesis. All components of nitrogen-limited hydrolysates were equivalent to earlier reports [44] with the exception of the sugar content. To ensure comparison of the artificial media to the original algae hydrolysates, the sugar profile was comparable to original algae hydrolysates.

During the first two days, the biomass formation and growth rate in all artificial media was comparable to typical cultivation in minimal media [5]. At the same time interval, the growth on real macroalgae hydrolysates was rather low. Unexpectedly by the third day, the growth rate in real hydrolysates showed a sharp increase, which exceeded that of all other media. At the end of the fermentation, the biomass yield of the real hydrolysate was considerably higher than in artificial media (Fig. 4a).

More specifically, *L. digitata* showed a growth inhibiting activity against four various bacterial or fungal species [45,46]. Interestingly, the antimicrobial natural product furaltadone was recently isolated from *U. lactuca*. To that end, changes in the yeast growth tendency over the first five day of fermentation using real and model hydrolysates could be attributed to an adaptive process of *C. oleaginosus* towards potentially cytotoxic hydrolysate compounds. The efficient adaptation of *C. oleaginosus* to these toxic components is then reflected in the rapid exponential growth phase observed from day three onwards. To that end, it is well documented that microorganism, such as oleaginous yeasts can adapt to toxic compounds contained in fermentation broth in a time dependent manner by switching on expression of detoxifying enzyme systems [47,48].

Yeast growth in model green algae hydrolysate has shown a slight superiority compared to model brown algae hydrolysate. This could be attributed to the high glucose content in model green algae hydrolysate, which is a most preferable sugar source for *C. oleaginosus*. By contrast, the real *L. digitata* hydrolysate (March batch, [sample 1]) showed a significantly higher biomass production (35.4 g L^{-1}) than the corresponding *U. lactuca* hydrolysate (28.9 g L^{-1}). In contrast, the *L. digitata* hydrolysate [2] (June batch [sample 2]) showed even lower biomass productivity (25.9 g L^{-1}).

Gravimetric lipid analysis showed 34 and 22% (w/dw_{biomass}) produced biomass in *L. digitata* [1] and *U. lactuca* hydrolysates respectively (Fig. 4b). It is noteworthy that this difference in lipid accumulation by yeast cells on different algae hydrolysates could additionally be confirmed by the microscopic imaging (Supplementary Fig. 3S). In that respect, intracellular lipids bodies could be detected in cells grown on brown algae hydrolysates. Specifically, yeast cells grown on original algae hydrolysate displayed an enlarged vacuole (Supplementary Fig. 3S). These results display the superiority of *L. digitata* [1] over *U. lactuca* hydrolysate as feedstock for oleaginous yeast *C. oleaginosus*.

With regard to the inhibited lipogenesis on *U. lactuca* hydrolysate, we suggest that the effect may be due to the presence of biologically

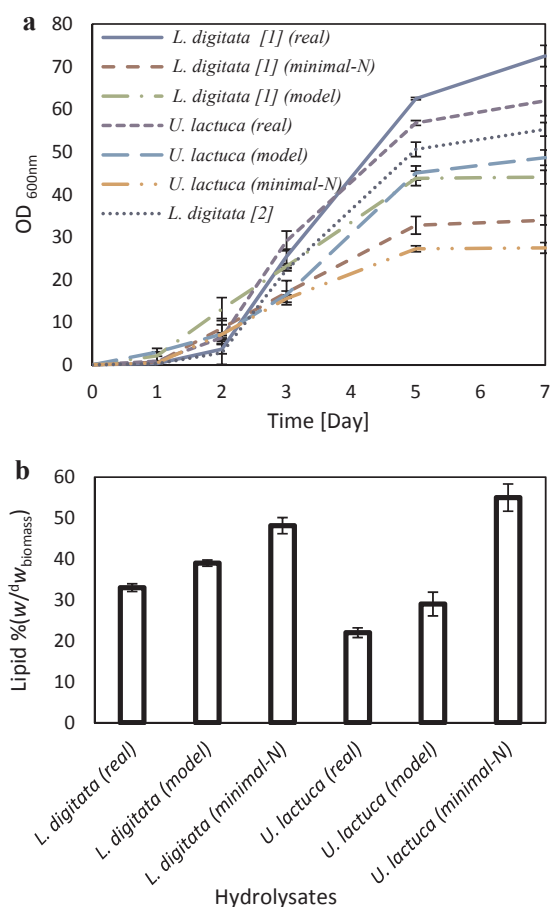


Fig. 4. (a) The increase of the optical density over the fermentation time of Real *L. digitata* [1], *L. digitata* [2] and *U. lactuca* and Model *L. digitata* [1] and *U. lactuca* and Minimal *L. digitata* [1] and *U. lactuca*. (b) The percentage of accumulated lipid by the dry biomass after 120 h of fermentation of real *L. digitata* [1] and *U. lactuca* and model *L. digitata* [1] and *U. lactuca* and minimal *L. digitata* [1] and *U. lactuca*.

active steroids in the green algae biomass such as 3-*O*- β -D glucopyranosyl-stigmasta-5,25-dien. This compound has been reported to have antimicrobial activity in the yeasts *Saccharomyces cerevisiae* and *Kluyveromyces lactis* [49].

In 2014, alginate from *Laminaria japonica* was fermented under anaerobic conditions to obtain volatile fatty acids [50]. The volatile fatty acids were consequently used as a carbon source for *C. oleaginosus*, for production of yeast triglycerides. In this set-up, a very low lipid productivity [Biomass: 4 g L⁻¹, contains lipid 48% (w/w)] was recorded [50]. Therefore, the data obtained in this study supersedes all previous data for biomass formation and total lipid yield with respect to oleaginous yeast fermentation. This can be attributed to the direct use of sugar rich liquid hydrolysates instead of volatile fatty acids as the yeast carbon source.

Based on the initial flask cultivations, *L. digitata* hydrolysate was deemed the best candidate for biomass and lipid production at 30 L scale. Hence, the brown algae hydrolysate was produced in scale of 30 L by enzymatic hydrolysis of *L. digitata*. The used biomass [2.4 kg–8.0% (w/v)] was a mixture of 1.9 kg from the March batch *L. digitata* [1] and 0.5 kg of June batch *L. digitata* [2]. After 72 h of incubation with the optimized enzyme solution, centrifugation followed by 10 KDa cross-flow filtration was performed in order to obtain a clarified liquid hydrolysate. The remaining solid residues were subjected to downstream biosorption assays. The resulting brown algae hydrolysate contained total 52 g L⁻¹ fermentable sugars and 0.45 g L⁻¹ total nitrogen resulting in a C/N ratio of 76.5 (Table 1). This C/N ratio is within the

reported limits for lipid induction in oleaginous yeasts [21,51].

Without any nitrogen supplementation or external glucose feeding, the *L. digitata* hydrolysate was used in a 2 L scale fermentation of *C. oleaginosus*. As reported previously, respiration activity represented in *pO*₂ value was used as an indicator for the end of the fermentation. To that end, the fermentation was stopped at 120 h, when the *pO*₂ returned back to the saturation value. Biomass dry weight and cell count were used to monitor the growth. According to OD₆₀₀ and dry weight, the exponential phase was terminated after 48 h of fermentation but flow cytometry measurements indicated that the cell saturation phase was already reached 20 h earlier (Fig. 5a). Lipid analysis showed an increase in the rate of lipid accumulation in the last two days of the fermentation (Fig. 5b). Under the applied conditions, 44.8 g L⁻¹ yeast biomass containing 37.1% (w^d/w_{biomass}) lipids was obtained. Therefore, our total lipid of 16.5 g L⁻¹ obtained with macroalgae hydrolysate is slightly higher than lipid yields obtained with *Cutaneotrichosporon* fermentations using corn cob (12.3 g L⁻¹ lipids) and rice straw (11.5 g L⁻¹) hydrolysate respectively [52,53]. Moreover, our previous work reported an equivalent *C. oleaginosus* fermentation using a crude hydrolysate of the seagrass *P. oceanica* as feedstock. In this context, we calculated a biomass-to-lipid conversion of 0.20 g g⁻¹, which is exactly the same as with brown algae in the current study [5].

The yeast triglycerides obtained in the current study have a similar composition to plant derived rape and palm oils, with oleic and palmitic acid being the dominant fatty acids (Supplementary Fig. 4S). Therefore, the yeast oil obtained in this study can be regarded as a direct substitute for plant oils in chemical processes [54]. In contrast to the plant equivalents, the yeast oils would have no impact negative on land use change, biodiversity or food production per-se. Moreover, they can be produced at consistent qualities, as their production process is not affected by environmental factors.

Detailed biomass analysis indicates that the residual yeast after lipid extraction contains about 15% (w/w) proteins and 85% (w/w) carbohydrates. Supplementary Fig. 5S depicts the sugar profile of the yeast residual biomass, mainly contains glucose and mannose. In addition, rhamnose and glucuronoxylomannan have been reported to be the main carbohydrate polymers of the *Cutaneotrichosporon* sp. [55]. Notably, previous studies confirm that mannan oligosaccharides contained biomass are excellent performance additives in weanling pigs feed formulations. In fact, MOS is considered as an alternative to an antimicrobial agent carbadox [56]. Therefore, we suggest that yeast cell residues obtained after oil extraction could be used as a performance additive in animal feed.

3.2.2. High through put monitoring of yeast lipogenesis by flow cytometry

Rapid measurements of the onset and extent of yeast lipogenesis is essential of in-process monitoring of yeast oil production and determination of harvesting times. Current methods either rely on gravimetric measurements or are depend on differential staining of lipid

Table 1
The chemical analysis of *L. digitata* hydrolysate.

Material	Concentration (g L ⁻¹)	Material	Concentration (g L ⁻¹)
Glucose	32.1	Nitrogen as NO ₃ /NO ₂	0.15
Mannitol	12.2	Protein	1.56
Xylose	7.6	Phosphate (as PO ₃ ⁻³)	0.6–2
Total Carbon	34.4	Total Sulfate (as S)	0.23
Total Nitrogen	0.45	Metal Ions	Na ⁺ , K ⁺ , Fe ⁺² , Ca ⁺² , Mg ⁺² , Mn ⁺² , Sr ⁺²
Nitrogen as NH ₄	0.25		

^aThe relative standard deviation of all value is less than $\pm 5\%$.

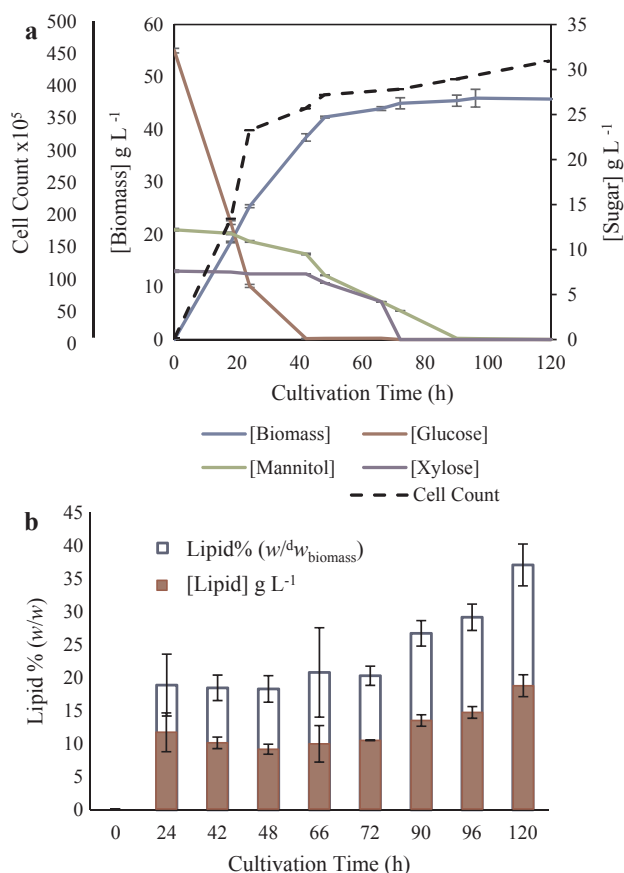


Fig. 5. Fermentation profile and lipid accumulation during 120 h of cultivation in 2 L bioreactor. (a) The cell count, dry biomass, optical density and consuming of fermentable sugar of the mixed *L. digitata* biomass. (b) The percentage of accumulated lipid and lipid productivity over the fermentation time in the mixed *L. digitata* hydrolysate.

bodies inside the yeast cells. Both methods are destructive, time consuming and they do not offer sufficient and information about cellular state of the culture. Additionally, many factors, such as cell size variation with phase of growth (lag, log, stationary), dead cell, shape of the cell, high cell density, chemicals and hydrophobic metabolites, can overlapped with obtained data causing under- or overestimation of biomass and lipids.

Therefore, rapid optical methods that could accurately determine these critical process parameters without destroying the sample would be a critical advantage when focusing on microbial oil centered biorefinery settings.

To that end, flow cytometry is an electro-optical-based technology able to analyze thousands of particles per second. Forward scatter [FSC] and side scatter [SSC] provides analysis of detailed cell features such as cell size and cell granularity respectively [57]. Previously, flow cytometry in combination with the Nile Red staining, has been used to quantify the intracellular lipid content of different microalgae [58,59] and the oil forming in some yeast like *Rhodotorula glutinis* [60]. Practically, we noted that lipid body staining in yeast cells by hydrophobic dyes such as Nile Red or Sudan black can be significantly affected by staining time, yeast type, lipid content and growth phase. Additionally, this effect significantly increased when the yeast cell has a rigid wall as in the case of *C. oleaginosus* [61]. Therefore, staining procedures do not offer reproducible assay results.

It is essential for any fermentative process to have an instantaneous assay method capable of monitoring the biomass, growth and lipid accumulation to gain instant feedback on the fermentation status.

During our microscopic assessments of the culture progress, we

noted that both size and granularity of the yeast cells increased proportionally with the intracellular lipid content. Based these observations, flow cytometry-based parameters FSC and SSC vs lipid content were measured at same time intervals.

Fig. 6 shows the cell density plot integrated with the histogram of the FSC and SSC on X and Y axes respectively. At the starting point of the fermentation, the FSC histogram showed a wide cell distribution. At time point of 42 h, this distribution increasingly focused and moved towards a larger cell size. At the same time point, the cell count and biomass formation reached the saturation phase due to nitrogen depletion. Moreover, two populations could be distinguished in our flow cytometry experiments: A small population (P2) which newly appeared at the higher FSC and SSC in addition to the main plot (P1). With progressing fermentation, the FSC histogram of P1 was shifted towards higher size value. Later on, a third population (P3) was generated at the lower FSC and SSC.

With respect to the side scatter [SSC] values started sharp as the *C. oleaginosus* has an oval cell shape. With time; the SSC values became progressively boarder and moved to higher values, which indicated an increase in the cellular granularity. Most interestingly, this data indicated that cell granularity increases proportionally with increasing lipid content. This suggests, that the cell granularity is a direct indicator of the cellular lipid content.

According to the gravimetric assay, the changes in lipid content were about 19% from 18 to 37 ($w/d w_{biomass}$). These changes could remarkably be measured instantly by monitoring the FSC and SSC in our flow cytometry experiments. Additional experiments have demonstrated, that the FSC and SSC can exceed the value 10^{+3} of the logarithmic FSC, if the lipid content rose to about 75% ($w/d w_{biomass}$). Moreover, microscopy confirmed that cells with 75% ($w/d w_{biomass}$) lipid have remarkably larger sizes and almost a spherical shape (Supplementary Fig. 6S). In summary, flow cytometry-based on FSC and SSC data can be used for the rapid, non-invasive determination of the onset and extend of yeast lipogenesis. For the first time, this method provides for the rapid in-process monitoring of key parameters controlling oleaginous yeast cultivation progress and harvesting points. In addition, flow cytometry data provides information about possible culture contaminations and cell integrity.

In conclusion, flow cytometry presents on-time dynamic information for the vitality of the yeast. Nevertheless, gravimetric analysis and optical density are still necessary to quantitatively evaluate the overall fermentation but in conjunction with flow cytometry results and these data sets become more accurate and versatile. Moreover, the new flow cytometry-based method presented herein could enhance rapid and non-invasive lipid quantification. However, this process would require more monitoring for the yeast cultures at different conditions. Finally, this flow cytometry method allows fast evaluation in the case of media optimization or screen for best lipid producer from a mutation library. This high throughput methodology for monitoring in-process yeast lipogenesis is generally transferrable to other oleaginous organisms including lipid forming bacteria and other yeast species.

3.2.3. Solid residue as metal sorbent

To enable rapid screening of biosorbent metal binding capacities we developed a new luminescence-based method, which is reported in the context of this manuscript for the first time. The new screening methodology developed herein is based on the concentration dependent broadband cerium luminescence at approx. 365 nm when excited at 269 nm. The cerium luminescence is quenched when its concentration is in high concentrations (auto-quenching mechanism) or when some other metal ions are present in the solution. The latter quenching mechanism depends on the concentration as well as species of the respective metals. However, small changes of heavy metal concentrations do not have a measurable effect on the cerium luminescence. The method developed herein applies this observation. Therefore, diluted samples in a buffer containing high and defined concentrations of heavy

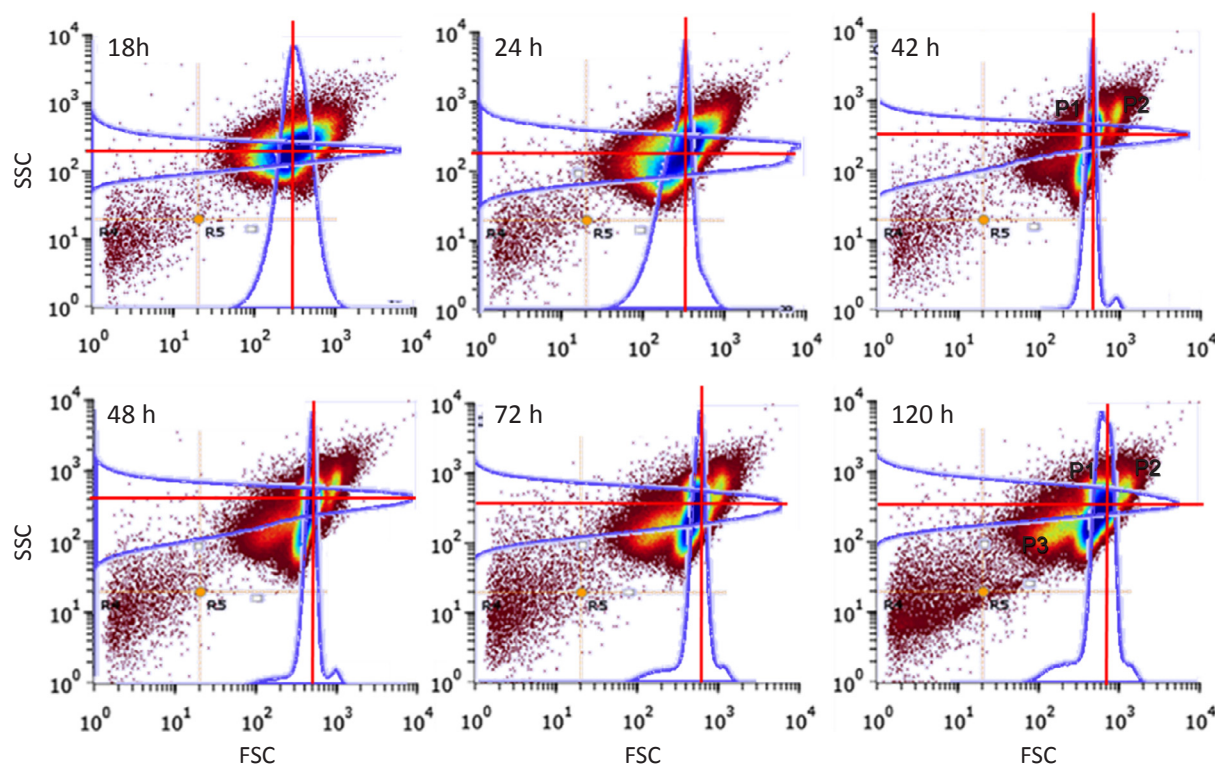


Fig. 6. Flow cytometry-based characterization of *C. oleaginosus* during 120 h of cultivation from samples of the 2 L bioreactor with mixed *L. digitata* hydrolysate. The cell density plot diagrams are showing intensity of the forward scatter [FSC] and side scatter [SSC].

metals are used to gain high fluorescence photo efficiency with controlled quenching. The molarities were chosen so, that a slight change of cerium concentration proportionally affects the luminescence, while a slight change in the alternative heavy metal concentration (if the sample contains metals other than cerium) only has marginal effects on the cerium luminescence. Furthermore, buffering with sodium acetate ensures a constant pH value for the measurement and stable complexation of heavy metal ions independent of the sample. The current methodology allows for the first time a rapid determination of the metal sorption capacity of any biological material.

The most important parameter of every sorbent is its loading (or sorption) capacity, indicating how much sorbate can be accumulated per gram of the sorbent. All four tested samples of *L. digitata* showed a very similar cerium sorption capacity at a fairly high level of about 0.60 mmol g^{-1} (84 mg g^{-1}). The raw biomass without hydrolysis performed only insignificantly better reaching 0.67 mmol g^{-1} (Table 2a). This suggests that the concept of residue valorization through bio-sorption is valid. In addition to a pooled and standardized brown algae residue, charges from different seasonal samples used for the hydrolysis were tested. In that respect, the batch harvested in March showed less cerium sorption capacity (sorption capacity: 0.58 mmol g^{-1}) than the second batch (sorption capacity: 0.67 mmol g^{-1}) harvested in June. As alginate is well characterized metal biosorbent [62] and the alginate was higher in the June than in the March batch (Fig. 2b), the higher cerium sorption capacity of the former may be related to the higher alginate content (Fig. 2b). This was supported by our control experiment where we determined the cerium sorption capacity of pure sodium alginate to be approximately 0.85 mmol g^{-1} . The data indicates that alginate may contribute the majority of sorption capacity in the macroalgae residue, while fucoidan has a minor role in this respect.

An ideally selective sorbent would bind its preferred metal up to its full sorption capacity regardless of the complexity of the solution it is used for. In reality, other ions generally hold influence on the sorption capacity of the metal in question – in this case cerium. A completely unselective sorbent (i.e. with binding spots suitable for all ions equally)

would sequester metal ions proportionally to their concentration. Therefore, we measured the sorption capacity for cerium in the presence of potentially competing ions, including copper, lead and nickel (Table 2b). Compared to the control (only cerium in solution) a significant loss of cerium binding capacity was observed, when other metals were present in solution. Mechanistically, the competing ions are likely to occupy similar binding positions on the brown algae bio-sorbent thereby limiting the specific cerium sorption. With respect to lead the specific cerium binding capacity decreases to about one half. Interestingly, this situation is observed for the solid brown algae residue as well fresh unhydrolysed brown algae biomass.

However, the unhydrolysed biomass displays a higher selectivity, when nickel or copper instead of lead are present. By contrast, the solid hydrolysis residue appears to be less selective towards cerium sorption when competing metals are present in solution. Considering that equimolar amounts of both metals were present in each assay, we can conclude, that fresh biomass shows following selectivity: $\text{Pb} = \text{Ce} > \text{Cu} > \text{Ni}$. The hydrolysis residue is less selective having an

Table 2

(a) Sorption selectivity: comparison of raw *L. digitata* and residual biomass after hydrolysis. Shown is the sorption capacity for Ce when a second metal (Cu, Ni, Pb) is present in the solution (b) Sorption capacity of *L. digitata* raw biomass from both batches and of the hydrolysate.

(a) Sorption selectivity of $[\text{Ce}^{+3}]$ as mmol g^{-1} for <i>L. digitata</i> [Mixed] in the present of:				
	$[\text{Cu}^{+2}]$	$[\text{Ni}^{+2}]$	$[\text{Pb}^{+2}]$	No Addition
Original Biomass	0.36 ± 0.053	0.51 ± 0.019	0.27 ± 0.008	0.68 ± 0.009
Hydrolysis residues	0.25 ± 0.011	0.38 ± 0.063	0.26 ± 0.019	0.62 ± 0.041
(b) Total sorption capacity of $[\text{Ce}^{+2}]$ of Hydrolysis residues:				
Hydrolysis residues	March Batch	June Batch	Mixed Biomass	Original Biomass
$[\text{Ce}^{+3}]$ as mmol g^{-1}	0.59 ± 0.025	0.67 ± 0.005	0.62 ± 0.041	0.68 ± 0.009

apparent metal selectivity series of: $Pb = Ce = Cu > Ni$. Therefore, the hydrolysis residue is not usable for selective biosorption of cerium or other lanthanides from complex solutions. However, the hydrolysis residue represents a cost effective biosorbent for the general removal of metals from dilute solutions. A performance comparison between pure alginate and the brown algae hydrolysis residue (Supplementary Fig. 7S) indicates, that the loss of this component is probably responsible for lower selectivity towards cerium. In that respect, the sorption selectivity of the pure sodium alginate control has been determined as: $Ce > Cu > Pb > Ni$. In conclusion, the brown algae hydrolysis residue may serve as an effective sorption material for the general removal of heavy metals from aqueous solution and therefore could serve for process water upgrading in a cyclic biorefinery setting discussed here.

The second most important parameter to assess biosorption performance is the determination of sorption kinetics. This parameter provides a quantitation of the biomass contact time in metal containing solutions. From a technical perspective, the sorption kinetics is essential for the determination of required size and cost of respective biosorption reactors. To that end, we have tested both air dried (60 °C) and wet biomass samples originating directly from the hydrolysis step (Fig. 7). Slight differences in sorption kinetics were observed only within first three minutes. After that time the dried biomass completely resembled the wet samples, and no further points were measured.

The wet biomass bound the metals immediately after submersion and has a lag phase for the subsequent 10 min. Thereafter, a more stable binding period was observed, where the maximum loading capacity was reached between 30 and 100 min. By contrast, the dry brown algae hydrolysate residue required more time for the first phase, while it soaked with water, and began biosorption. In general the sorption rate (about $9.2 \mu\text{mol g}^{-1} \text{min}^{-1}$) is fairly slow, as compared to green microalgae reaching 90% of maximum capacity already after few minutes [63]. Although, the maximum capacity of hydrolysis residue is significantly higher.

More generally, the cerium-based method for characterizing the metal sorption behavior of macroalgae residues is directly applicable to other bio-based metal sorption materials, such as microalgae biomass [64].

3.3. Economic evaluation of the *L. digitata* biorefinery system

Currently, the biofuels and oleochemical industry predominantly relies on the use of rapeseed and palm oil for biofuels and renewable chemical production. Particularly, production processes of palm oil have significant negative impact on the ecosystem, leading to deforestation and an associated reduction in biodiversity. As an alternative, the generation of microbial oils from terrestrial or marine waste biomass represents a scalable route for production of renewable oils targeted at the biofuels and chemicals industry without impacting the environment [65]. In that regard, the fermentative conversion of waste biomass hydrolysates via oleaginous yeasts, such as *C. oleaginosus* is economically most promising [5]. However, hydrolysis of chemically complex waste biomass often results in solid residues (i.e. lignin or unhydrolyzed sugar polymers) with limited technical applicability, which are either burned to generate process energy or used as simple fertilizer [9,17]. Therefore, these residues do not contribute to the economic viability of the bioprocess. Moreover, chemical yeast oil upgrading to fuels and chemicals may result in the environmental release of heavy metal contaminated process water, which negatively impacts the ecological footprint of the process [30]. To address the issue of economic and ecologic viability this study presents a new, waste-free, cyclic bio-refinery process focusing on the holistic conversion of marine macroalgae biomass for the generation of yeast based lipids and a biological metal sorbent that is capable to extract heavy metals from process water.

We have developed a selective liquefaction of macroalgae biomass

using an optimized enzyme system, which provided a liquid phase that contained fermentable sugars. The liquid phase was used for cultivation of the oleaginous yeast *C. oleaginosus*, which achieved high biomass yields compared to artificial control media. The obtained microbial lipids can be converted to a variety of high value platform chemicals for the renewable manufacturing of oleochemicals, bio-lubricant or bio-fuels by established chemical procedures [20]. After lipid extraction, analysis showed that residues yeast biomass can be used as animal feed (Fig. 1).

Most recently, a techno-economic evaluation of a macroalgae-based biogas and bioethanol production facility has been reported [17]. In this process, the biogas digestate was applied for thermic electricity production or it can be used as animal feed. This study demonstrated that due to the low price for bioethanol and biogas, a scale of $680,000 \text{ t year}^{-1}$ of dry macroalgae biomass would be required to render the process economically viable [17]. However, we have applied our previous calculations that demonstrated that a fermentation medium based on marine biomass hydrolysates would cost about $\$0.11 \text{ L}^{-1}$ [5]. Whereas, the crude yeast oil product could reach costs $\$5.5\text{--}7.3 \text{ kg}^{-1}$ [5,66] based on the applied process. However, the crude yeast oil could be processed to high-value products, such as performance oleochemical ingredients targeting biolubricant, cosmetic and pharmaceutical industries [67]. These applications would justify the relatively high-cost of the fermentative processes. Moreover, this cost will be partially recovered, if the profits generated by utilizing the yeast biomass as animal feed and solid macroalgae residues as biosorbents are taken in consideration.

We have demonstrated that the solid macroalgae residue is able to recover about 0.6 mmol g^{-1} of heavy metals per dry biomass. For example, if lead is used as metal to be removed from wastewater, the binding capacity would be 124 mg g^{-1} dry biomass. This impressive capacity exceeds commercially available resins such as Amberlite® IRC-718 with a capacity of only 20 mg g^{-1} [68] at a cost of approx. $\$92 \text{ kg}^{-1}$ (<http://en.chemmerce.com/chemicals/21312-54423/>). Nevertheless, a direct comparison might be misleading, because synthetic resins offer greater long-term stability and no variability of binding capacities as opposed to products of biological origin. All this has been considered when marketing a similar algae based product, the AlgaSORB®, which is sold for approx. $\$1.5 \text{ kg}^{-1}$. Although the sorption capacity of this product is not published, it is based on *Chlorella* sp. (eukaryotic green algae) and *Arthrospira* sp. (cyanobacteria) cells. To that end, it is reported, that the biosorption potential of brown algae is more than double of both green microalgae and cyanobacteria respectively. Therefore, brown macroalgae derived biosorbents could be marketed at an even higher price.

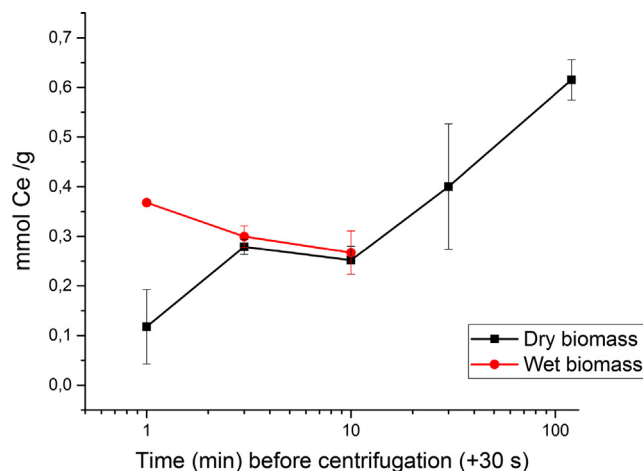


Fig. 7. Sorption kinetics of *L. digitata* residual biomass after hydrolysis for dry and wet biomass.

4. Conclusion

In this study we have selected marine green (*U. lactuca*) and brown (*L. digitata*) macroalgae biomass as process feedstocks, as their production has no negative impact on agricultural activity or the environment but provides higher biomass yields than the most favorable terrestrial crops. For the first time, we established a highly efficient enzymatic hydrolysis process that converts 62.5% (*L. digitata*) and 59.3% (*U. lactuca*) of the total biomass into soluble fermentable sugar monomers. In addition to the total sugar yield, we focused on the overall glucose yield as this sugar is most effectively metabolized by our oleaginous yeast strain. To that end, we actually obtained a glucose recovery of 95% (w/w) with respect to the dry macroalgae biomass feedstock. The high sugar recovery was essential for qualifying the macroalgae hydrolysis supernatant as a sole fermentation medium without further additives. In contrast to other biomass feedstocks, our enzymatic liquefaction of macroalgae feedstocks did not require any thermo-chemical pre-treatment, which generally is energy (cost) intensive and results in generation fermentation inhibitors, such as furfural. Processing of the hydrolysate resulted in a solid residue fraction containing both alginate and fucoidan polymers, which were successfully applied as an efficient metal biosorbent. By contrast, the supernatant served as the sole fermentation base for cultivation of the oleaginous yeast *C. oleaginosus*. The laboratory process was validated at technical scale of 30 L in a controlled bioreactor setting. Under these conditions, a biomass yield of 44.8 g L⁻¹ yeast biomass containing 37.1% ($w_{lipids} / w_{biomass}$) was achieved. To enhance the economic viability of the process we suggest to use yeast biomass obtained in the process of lipid generation as a performance animal feed additive due to its favourable cell wall sugar composition. Moreover, the integrated production and use of a macroalgae-based biosorbent significantly enhances the ecological footprint of chemical process steps conventionally involved in renewable lipid upgrading to biofuels and oleochemicals. Furthermore, the application of biosorbents can be diversified to the recovery and recycling of precious metals (Loading capacity of 0.679 mmol g⁻¹; with selectivity to Pb = Ce = Cu > Ni), such as lanthanides, from industrial and mining wastewater sources. To our knowledge this is the first account of a bioprocess assembly that demonstrates the production of microbial oil in conjunction with process water remediation options. To facilitate integration of our technology platform in a conventional industrial production setting, we have devised simple, rapid and selective optical control methodologies for monitoring lipid productivity and metal sorption efficiencies with cost-efficient equipment. Specifically, we developed a new, flow cytometry-based method for determining the onset and extent of lipid biogenesis, which is essential to optimize harvest timeframes. Analogously, a spectrophotometric, cerium-based for metal sorption monitoring methodology was developed as a tool to control waste upcycling and remediation within the process chain.

In summary, we devised a zero waste bioprocess where every product outlet (microbial lipid, biosorbent and animal feed additive) is assigned a significant value in a diversified market scenario. A preliminary economic analysis of the reported process chain, indicated that each product is in the range to be cost competitive with current market equivalents. This synaptic nature of these biotechnological processes provides for the economic and ecologic viability of the overall process chain.

Acknowledgements

TB gratefully acknowledges support of the Werner Siemens Foundation for establishing the field of Synthetic Biotechnology at the Technical University of Munich. MM, MH and TB acknowledge financial support by the German Federal Ministry of Education and Research for supporting the “LIPOMAR” [grant number: 031A261] and “Advanced Biomass-Value” [grant number: 03SF0446A] projects.

Information concerning the Advance biomass projects can be obtained: <http://www.ibbnetzwerk-gmbh.com/de/service/pressebereich/pm-06052013-advanced-biomass-value/>. NM and TB also acknowledge financial support for the project “Resource efficient production processes for polyhydroxybutyrate-based biopolymers” of the Bavarian State Ministry for Environment and Consumer Protection [StMUV, grant number TLKO1U-69045]. WJ and TB also acknowledge financial support for the project within the framework of “For Cycle” Project group.

Appendix A. Supplementary material

Supplementary data associated with this article can be found, in the online version, at <http://dx.doi.org/10.1016/j.apenergy.2018.04.089>.

References

- [1] Mekhilef S, Siga S, Saidur R. A review on palm oil biodiesel as a source of renewable fuel. *Renew Sustain Energy Rev* 2011;15:1937–49.
- [2] Basiron Y. Palm oil production through sustainable plantations. *Eur J Lipid Sci Technol* 2007;109:289–95.
- [3] Wicke B, Sikkema R, Dornburg V, Faaij A. Exploring land use changes and the role of palm oil production in Indonesia and Malaysia. *Land Use Policy* 2011;28:193–206.
- [4] Jung KA, Lim S-R, Kim Y, Park JM. Potentials of macroalgae as feedstocks for biorefinery. *Bioresour Technol* 2013;135:182–90.
- [5] Masri MA, Younes S, Haack M, Qoura F, Mehmler N, Brück T. A seagrass based biorefinery for generation of single cell oils targeted at biofuel and oleochemical production. *Energy Technol* 2018.
- [6] Wei N, Quarterman J, Jin Y-S. Marine macroalgae: an untapped resource for producing fuels and chemicals. *Trends Biotechnol* 2013;31:70–7.
- [7] Subhadra B, Edwards M. An integrated renewable energy park approach for algal biofuel production in United States. *Energy Policy* 2010;38:4897–902.
- [8] Gao K, McKinley KR. Use of macroalgae for marine biomass production and CO₂ remediation: a review. *J Appl Phycol* 1994;6:45–60.
- [9] John RP, Anisha G, Nampoothiri KM, Pandey A. Micro and macroalgal biomass: a renewable source for bioethanol. *Bioresour Technol* 2011;102:186–93.
- [10] Yeon J-H, Lee S-E, Choi W-Y, Kang D-H, Lee H-Y, Jung K-H. Repeated-batch operation of surface-aerated fermentor for bioethanol production from the hydrolysate of seaweed *Sargassum sagamianum*. *J Microbiol Biotechnol* 2011;21:323–31.
- [11] Kim N-J, Li H, Jung K, Chang HN, Lee PC. Ethanol production from marine algal hydrolysates using *Escherichia coli* K011. *Bioresour Technol* 2011;102:7466–9.
- [12] Jang J-S, Cho Y, Jeong G-T, Kim S-K. Optimization of saccharification and ethanol production by simultaneous saccharification and fermentation (SSF) from seaweed, *Saccharina japonica*. *Bioprocess Biosyst Eng* 2012;35:11–8.
- [13] Pham TN, Nam WJ, Jeon YJ, Yoon HH. Volatile fatty acids production from marine macroalgae by anaerobic fermentation. *Bioresour Technol* 2012;124:500–3.
- [14] Gupta S, Abu-Ghannam N, Scannell AG. Growth and kinetics of *Lactobacillus plantarum* in the fermentation of edible Irish brown seaweeds. *Food Bioprod Process* 2011;89:346–55.
- [15] Horn S, Aasen I, Østgaard K. Ethanol production from seaweed extract. *J Ind Microbiol Biotechnol* 2000;25:249–54.
- [16] van der Wal H, Sperber BL, Houweling-Tan B, Bakker RR, Brandenburg W, López-Contreras AM. Production of acetone, butanol, and ethanol from biomass of the green seaweed *Ulva lactuca*. *Bioresour Technol* 2013;128:431–7.
- [17] Soleymani M, Rosentrater KA. Techno-economic analysis of biofuel production from macroalgae (seaweed). *Bioengineering*. 2017;4:92.
- [18] Liang Y, Tang T, Siddaramu T, Choudhary R, Umagiliyage AL. Lipid production from sweet sorghum bagasse through yeast fermentation. *Renewable Energy* 2012;40:130–6.
- [19] Yu X, Zheng Y, Dorgan KM, Chen S. Oil production by oleaginous yeasts using the hydrolysate from pretreatment of wheat straw with dilute sulfuric acid. *Bioresour Technol* 2011;102:6134–40.
- [20] McCurdy AT, Higham AJ, Morgan MR, Quinn JC, Seefeldt LC. Two-step process for production of biodiesel blends from oleaginous yeast and microalgae. *Fuel* 2014;137:269–76.
- [21] Görner C, Redai V, Bracharz F, Schrepfer P, Garbe D, Brück T. Genetic engineering and production of modified fatty acids by the non-conventional oleaginous yeast *Trichosporon oleaginosus* ATCC 20509. *Green Chem* 2016;18:2037–46.
- [22] Fitzherbert EB, Struebig MJ, Morel A, Danielsen F, Brühl CA, Donald PF, et al. How will oil palm expansion affect biodiversity? *Trends Ecol Evol* 2008;23:538–45.
- [23] Meo A, Priebe XL, Weuster-Botz D. Lipid production with *Trichosporon oleaginosus* in a membrane bioreactor using microalgae hydrolysate. *J Biotechnol* 2017;241:1–10.
- [24] Volesky B. Biosorbents for metal recovery. *Trends Biotechnol* 1987;5:96–101.
- [25] Yu Q, Matheickal JT, Yin P, Kaewsarn P. Heavy metal uptake capacities of common marine macro algal biomass. *Water Res* 1999;33:1534–7.
- [26] Davis TA, Volesky B, Mucci A. A review of the biochemistry of heavy metal biosorption by brown algae. *Water Res* 2003;37:4311–30.
- [27] He J, Chen JP. A comprehensive review on biosorption of heavy metals by algal biomass: materials, performances, chemistry, and modeling simulation tools. *Bioresour Technol* 2014;160:67–78.

- [28] Fu F, Wang Q. Removal of heavy metal ions from wastewaters: a review. *J Environ Manage* 2011;92:407–18.
- [29] Tchounwou PB, Yedjou CG, Patlolla AK, Sutton DJ. Heavy metal toxicity and the environment. *Molecular, clinical and environmental toxicology*: Springer; 2012. p. 133–64.
- [30] Karmakar G, Ghosh P, Sharma BK. Chemically modifying vegetable oils to prepare green lubricants. *Lubricants* 2017;5:44.
- [31] McLellan BC, Corder GD, Golev A, Ali SH. Sustainability of the rare earths industry. *Procedia Environ Sci* 2014;20:280–7.
- [32] Binnemans K, Jones PT, Blanpain B, van Gerven T, Yang Y, Walton A, et al. Recycling of rare earths: a critical review. *J Cleaner Prod* 2013;51:1–22.
- [33] Jarosiński A, Kowalczyk J, Mazanek C. Development of the Polish wasteless technology of apatite phosphogypsum utilization with recovery of rare earths. *J Alloys Compd* 1993;200:147–50.
- [34] Ochsenkühn-Petropulu M, Lyberopulu T, Ochsenkühn KM, Parissakis G. Recovery of lanthanides and yttrium from red mud by selective leaching. *Anal Chim Acta* 1996;319:249–54.
- [35] Griffiths M. Hille Rv, Harrison S. Selection of direct transesterification as the preferred method for assay of fatty acid content of microalgae. *Lipids* 2010;45:1053–60.
- [36] Chang SK, Zhang Y. Protein analysis. *Food analysis*. Springer; 2017. p. 315–31.
- [37] Bligh EG, Dyer WJ. A rapid method of total lipid extraction and purification. *Can J Biochem Physiol* 1959;37:911–7.
- [38] Lahaye M, Robic A. Structure and functional properties of ulvan, a polysaccharide from green seaweeds. *Biomacromolecules* 2007;8:1765–74.
- [39] Yanagisawa M, Nakamura K, Ariga O, Nakasaki K. Production of high concentrations of bioethanol from seaweeds that contain easily hydrolyzable polysaccharides. *Process Biochem* 2011;46:2111–6.
- [40] XU X, Ji-Young K, Min-Woo L, Jong-Moon P. Continuous fermentative butyric acid and acetic acid production from *Laminaria japonica* using a two-stage fermentation system. *한국생물공학회 학술대회* 2013:275.
- [41] Zhu J, Pan X. Woody biomass pretreatment for cellulosic ethanol production: technology and energy consumption evaluation. *Bioresour Technol* 2010;101:4992–5002.
- [42] Pan JG, Kwak MY, Rhee JS. High density cell culture of *Rhodotorulaglutinis* using oxygen-enriched air. *Biotechnol Lett* 1986;8:715–8.
- [43] Chi Z, Zheng Y, Ma J, Chen S. Oleaginous yeast *Cryptococcus curvatus* culture with dark fermentation hydrogen production effluent as feedstock for microbial lipid production. *Int J Hydrogen Energy* 2011;36:9542–50.
- [44] Yong-Hong L, Bo L, Zong-Bao Z, Feng-Wu B. Optimization of culture conditions for lipid production by *Rhodospiridium toruloides*. *Chin J Biotechnol* 2006;22:650–6.
- [45] Hornsey I, Hide D. The production of antimicrobial compounds by British marine algae I. Antibiotic-producing marine algae. *Br Phycol J* 1974;9:353–61.
- [46] Hornsey I, Hide D. The production of antimicrobial compounds by British marine algae II. Seasonal variation in production of antibiotics. *Brit Phycol J* 1976;11:63–7.
- [47] Wang J, Gao Q, Zhang H, Bao J. Inhibitor degradation and lipid accumulation potentials of oleaginous yeast *Trichosporon cutaneum* using lignocellulose feedstock. *Bioresour Technol* 2016;218:892–901.
- [48] Chen X, Li Z, Zhang X, Hu F, Ryu DD, Bao J. Screening of oleaginous yeast strains tolerant to lignocellulose degradation compounds. *Appl Biochem Biotechnol* 2009;159:591.
- [49] Awad NE. Biologically active steroid from the green alga *Ulva lactuca*. *Phytotherap Res* 2000;14:641–3.
- [50] Xu X, Kim JY, Oh YR, Park JM. Production of biodiesel from carbon sources of macroalgae, *Laminaria japonica*. *Bioresour Technol* 2014;169:455–61.
- [51] Zhu L, Zong M, Wu H. Efficient lipid production with *Trichosporonfermentans* and its use for biodiesel preparation. *Bioresour Technol* 2008;99:7881–5.
- [52] Huang C, Zong M-h, Wu H, Liu Q-p. Microbial oil production from rice straw hydrolysate by *Trichosporon fermentans*. *Bioresour Technol* 2009;100:4535–8.
- [53] Qin L, Liu L, Zeng A-P, Wei D. From low-cost substrates to single cell oils synthesized by oleaginous yeasts. *Bioresour Technol* 2017.
- [54] Salimon J, Salih N, Yousif E. Industrial development and applications of plant oils and their biobased oleochemicals. *Arab J Chem* 2012;5:135–45.
- [55] Fonseca FL, Frases S, Casadevall A, Fischman-Gompertz O, Nimrichter L, Rodrigues ML. Structural and functional properties of the *Trichosporon asahii* glucuronoxylomannan. *Fungal Genet Biol* 2009;46:496–505.
- [56] White L, Newman M, Cromwell G, Lindemann M. Brewers dried yeast as a source of mannan oligosaccharides for weanling pigs. *J Anim Sci* 2002;80:2619–28.
- [57] Robinson JP. Handbook of flow cytometry methods. Wiley-Liss; 1993.
- [58] Da Silva TL, Santos CA, Reis A. Multi-parameter flow cytometry as a tool to monitor heterotrophic microalgal batch fermentations for oil production towards biodiesel. *Biotechnol Bioprocess Eng* 2009;14:330–7.
- [59] Santos C, Ferreira M, Da Silva TL, Gouveia L, Novais J, Reis A. A symbiotic gas exchange between bioreactors enhances microalgal biomass and lipid productivities: taking advantage of complementary nutritional modes. *J Ind Microbiol Biotechnol* 2011;38:909–17.
- [60] Da Silva TL, Feijão D, Reis A. Using multi-parameter flow cytometry to monitor the yeast *Rhodotorula glutinis* CCM1 145 batch growth and oil production towards biodiesel. *Appl Biochem Biotechnol* 2010;162:2166–76.
- [61] Ageitos JM, Vallejo JA, Veiga-Crespo P, Villa TG. Oily yeasts as oleaginous cell factories. *Appl Biochem Biotechnol* 2011;90:1219–27.
- [62] Fourest E, Volesky B. Contribution of sulfonate groups and alginate to heavy metal biosorption by the dry biomass of *Sargassum fluitans*. *Environ Sci Technol* 1995;30:277–82.
- [63] Bulgariu D, Bulgariu L. Equilibrium and kinetics studies of heavy metal ions biosorption on green algae waste biomass. *Bioresour Technol* 2012;103:489–93.
- [64] Heilmann M, Jurkowski W, Buchholz R, Brueck T, Becker AM. Biosorption of neodymium by selected photoautotrophic and heterotrophic species. *J Chem Eng Process Technol* 2015;6:1.
- [65] Christophe G, Kumar V, Nouaille R, Gaudet G, Fontanille P, Pandey A, et al. Recent developments in microbial oils production: a possible alternative to vegetable oils for biodiesel without competition with human food? *Braz Archiv Biol Technol* 2012;55:29–46.
- [66] Koutinas AA, Chatzifragkou A, Kopsahelis N, Papanikolaou S, Kookos IK. Design and techno-economic evaluation of microbial oil production as a renewable resource for biodiesel and oleochemical production. *Fuel* 2014;116:566–77.
- [67] Lorenzen J, Horsch R, Waldow A, Qoura F, Loll B, Brück T. *Rhodococcus erythropolis* oleate hydratase: a new member in the oleate hydratase family tree—biochemical and structural studies. *ChemCatChem* 2018.
- [68] Malla ME, Alvarez MB, Batistoni DA. Evaluation of sorption and desorption characteristics of cadmium, lead and zinc on Amberlite IRC-718 iminodiacetate chelating ion exchanger. *Talanta* 2002;57:277–87.

A waste free, microbial oil centered cyclic bio-refinery approach based on flexible macroalgae biomass

Mahmoud A. Masri^[a], Wojciech Jurkowski^[a], Pariya Shaigani^[a], Martina Haack^[a], Norbert Mehlmer^{*[a]} and Thomas Brück^{*[a]}

[a] M. A. Masri, W. Jurkowski, P. Shaigani, M. Haack, Dr. N. Mehlmer and Prof. Dr. T. Brück
Department of Chemistry -Professorship of Industrial Biocatalysis
Technical University of Munich
E-mail: mahmoud.masri@tum.de; w.jurkowski@tum.de; pariya.shaigani@tum.de; martina.haack@tum.de; norbert.mehlmer@tum.de; andbrueck@tum.de

* Corresponding authors

Supporting information for this article is given via a link at the end of the document

Supplementary Data

Table 1S: Performance of the cerium luminescence measurement close to the limit of determination

Cerium (μM)	Sample 1	Sample 2	Sample 3	Mean	Std. deviation
33,33333	21127,6	19953,4	21512,6	20864,5333	812,20639
16,66667	10650	9845,2	10419,8	10305	414,49975
8,33333	5404,6	5529,6	4892,6	5275,6	337,52481
3,33333	2261,6	2901,6	2729,6	2630,93333	331,21192
0,83333	609,8	645,4	659,4	638,2	25,57186
blank	196,4	201,4	179,2	192,33333	11,64531

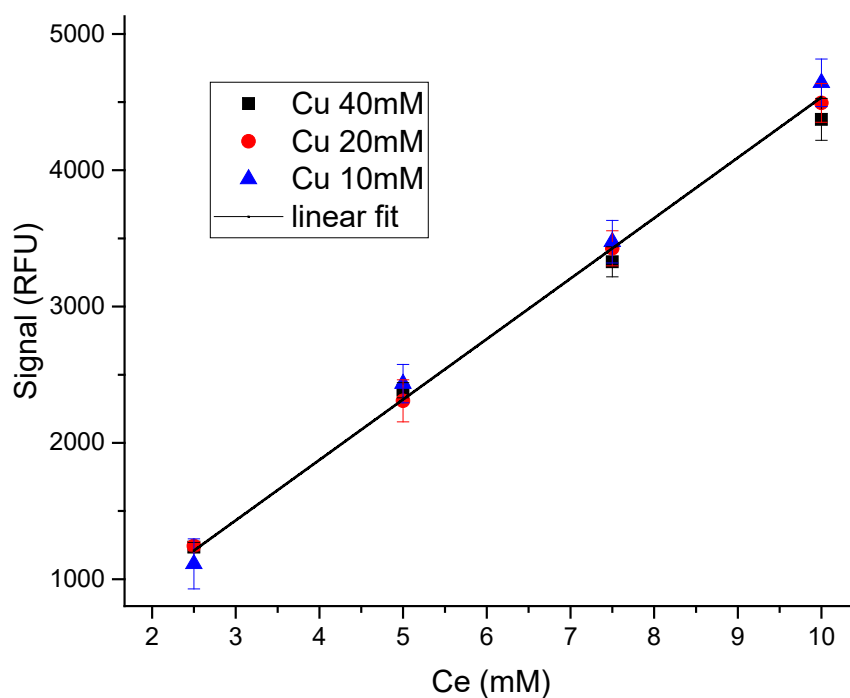


Figure 1S: Performance of the cerium luminescence method under different concentrations of copper in the sample.

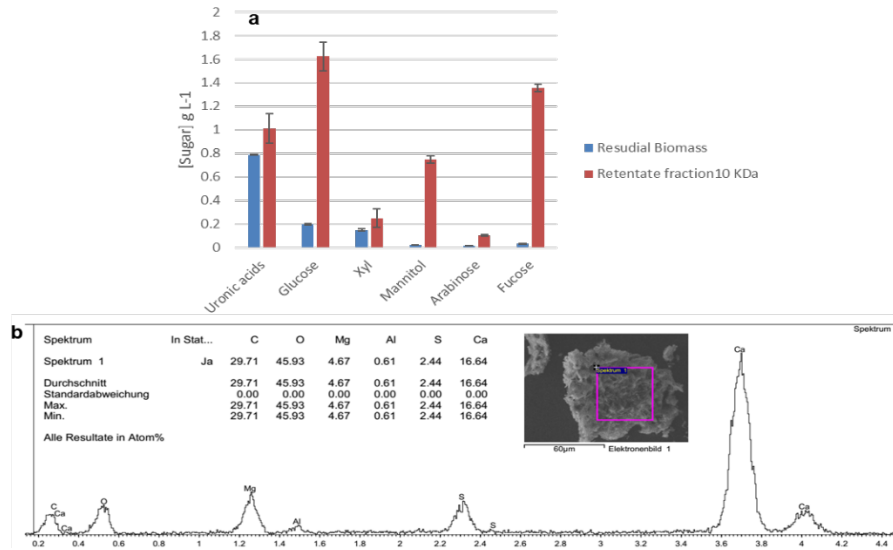


Figure 2S supplementary: **a.** Sugar Analysis of the Residual biomass after enzymatic hydrolysis and Retentate fraction after cross-flow filtration using 10 KDa filter. **B.** the EDX-data of the ash analysis of the Residual biomass.

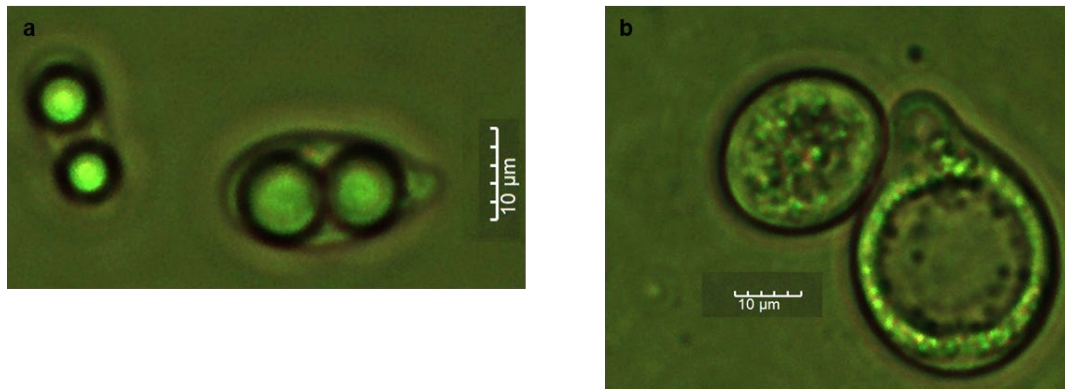


Figure 3S supplementary: Microscope image of *Cutaneotrichosporon oleaginosus* (ATCC 20509) after 120h fermentation **a.** in *L. digitata* hydrolysate **b.** *U. lactuca* hydrolysate.

	C16:0	C18:0	C18:1	C18:2	Other
Fermentative based <i>L. digitata</i> hydrolysate	18.2	14.0	48.7	17.2	1.9

Figure 4S supplementary: The fatty acid profile of *C. oleaginosus* triglycerides after fermentation in brown algae hydrolysate *L. digitata*.

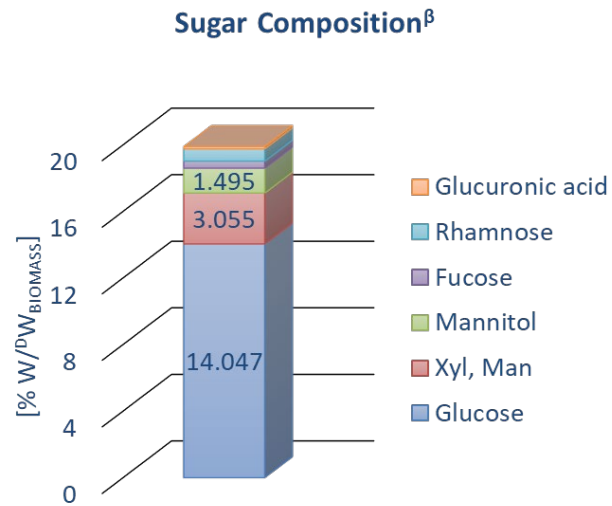


Figure 5S supplementary: Sugar profile of yeast *Cutaneotrichosporon oleaginosus* (ATCC 20509) biomass after lipid extraction.

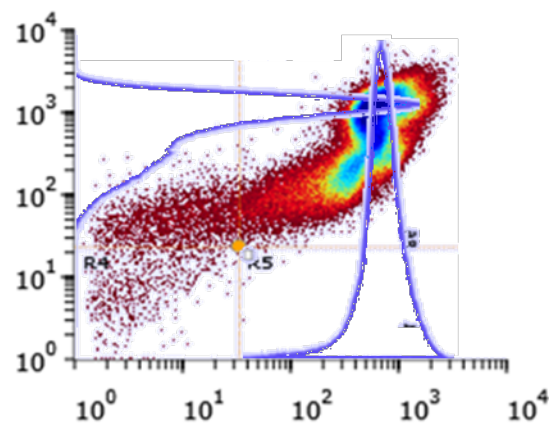


Figure 6S supplementary: The Increase in the cell density plot diagram and in intensity of the Forward scatter [FSC] and side scatter [SSC] at lipid concentration of 75 % (w/w).

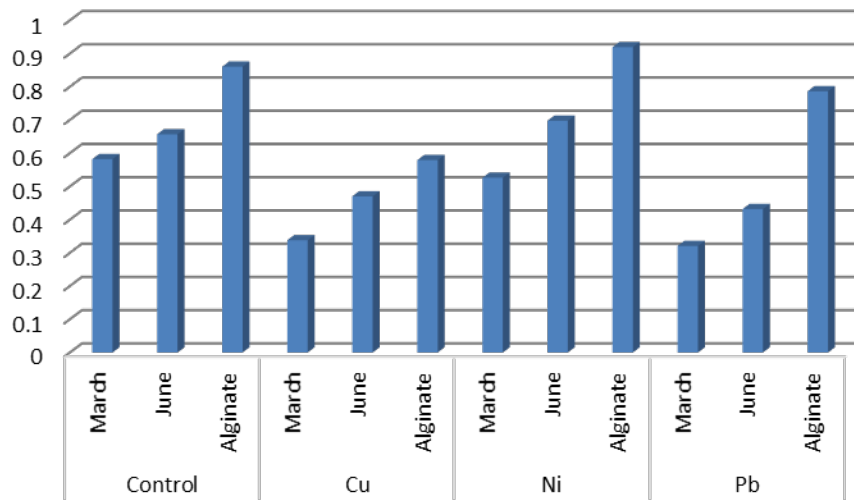
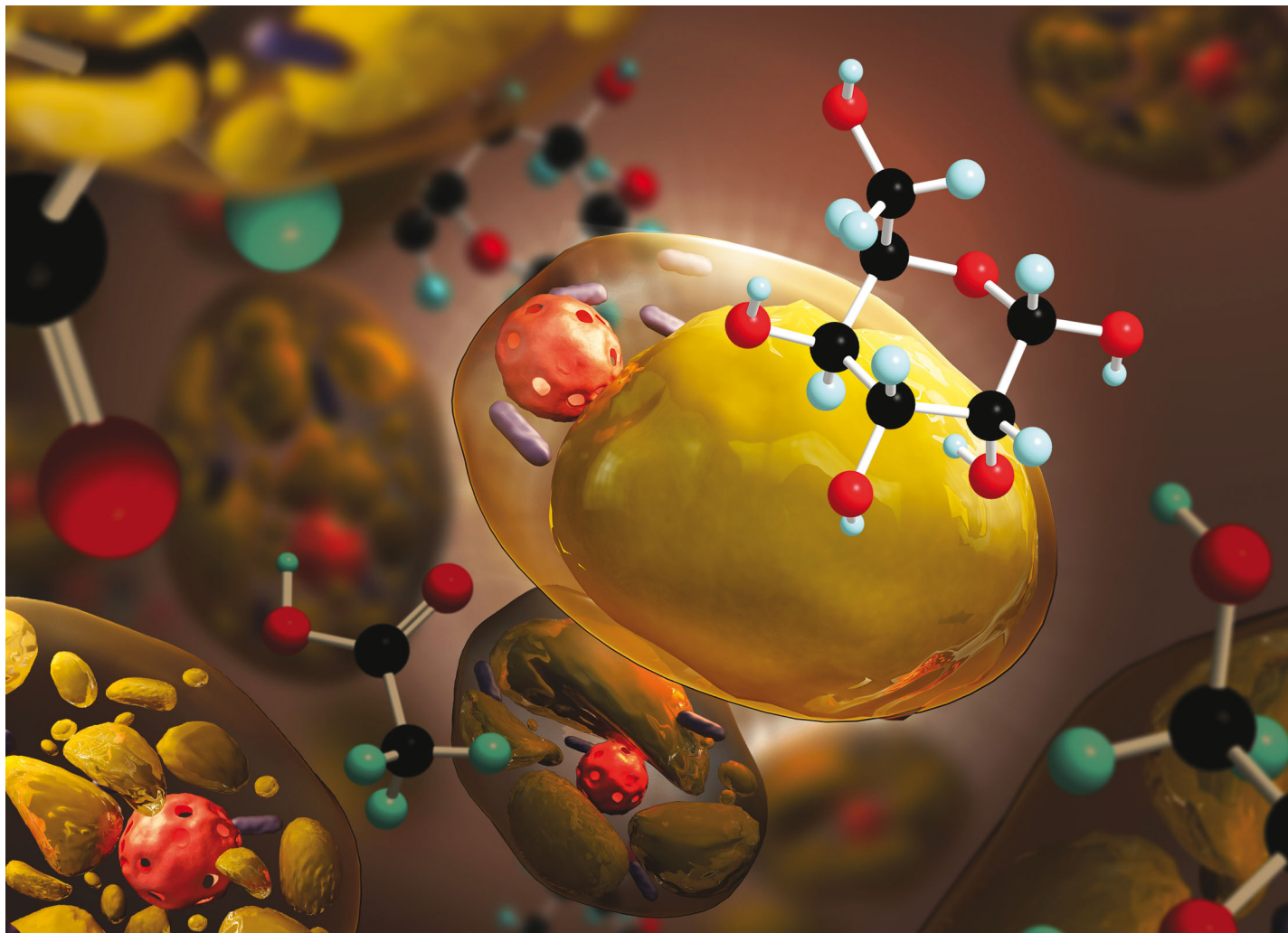


Figure 7S supplementary: Capacity of brown algae samples in comparison to pure sodium alginate.

A sustainable, high-performance process for the economic production of waste-free microbial oils that can replace plant-based equivalents



Showcasing research from Professor Thomas B. Brück's laboratory, Werner Siemens Chair of Synthetic Biotechnology, Department of Chemistry, Technical University of Munich, Bavaria, Germany.

A sustainable, high-performance process for the economic production of waste-free microbial oils that can replace plant-based equivalents

Plant oil-based biofuel production is associated with land use change, thereby releasing a massive amount of CO₂ while impacting biodiversity. To date, biofuel based on oleaginous yeast oil cannot replace plant lipids due to the low productivity of diauxic lipid formation and its dependence on organic solvents for intracellular product recovery. Acetic acid and sugar co-fermentation offers a path to efficient monoauxic lipid production. *In situ* hydrolase application facilitated a one-step and solvent-free lipid recovery method and enabled the recycling of the nutrient-rich aqueous fermentation phase in subsequent fermentation cycles.

As featured in:





See Norbert Mehlmer,
Thomas B. Brück *et al.*,
Energy Environ. Sci., 2019, 12, 2717.

PAPER



Cite this: *Energy Environ. Sci.*,
2019, 12, 2717

A sustainable, high-performance process for the economic production of waste-free microbial oils that can replace plant-based equivalents†

Mahmoud A. Masri,  Daniel Garbe,  Norbert Mehlmer * and
Thomas B. Brück *

Globally, biofuel and oleochemical production based on plant oils negatively affects biodiversity. As an alternative triglyceride source, lipid production from oleaginous yeasts faces numerous challenges in feedstock availability, lipid productivity, downstream processing, and waste treatment, prohibiting the design of a cost-competitive process with regard to plant equivalents. In this study, we present a fully integrated operation for microbial oil production, which consolidates upstream and downstream processing with side-stream recycling. Co-fermentation of sugar and acetic acid was successfully implemented in fed-batch, semi-continuous, and continuous fermentation modes. Process validation was conducted at a 25 L scale with a lipid productivity of $1.2 \text{ g L}^{-1} \text{ h}^{-1}$. *Cutaneotrichosporon oleaginosus* cell debris was used as an inducer in *Trichoderma reesei* fermentation for on-site generation of yeast-specific cell-wall hydrolases. *In situ* hydrolase application allowed for efficient *C. oleaginosus* cell lysis (85% w/w) and simultaneous lipid release. A subsequent centrifugation step yielded 90% (w/w) recovery of intracellular lipids without the need for any organic solvent. The nutrient-rich water phase was applied as an internal sugar source for subsequent yeast fermentation cycles. With this yeast hydrolysate, the lipid productivity was considerably increased to $2.4 \text{ g L}^{-1} \text{ h}^{-1}$. A techno-economic analysis of the current lipid production processes estimated costs at \$1.6 per kg lipid. Moreover, life cycle assessment analysis indicated an emission of 3.56 kg CO₂ equivalents for every 1 kg produced yeast oil. Accordingly, we established an integrated operation for bioconversion of acetic acid and sugar to sustainable lipids at maximum productivity coupled with minimal waste generation and energy consumption.

Received 20th January 2019,
Accepted 19th June 2019

DOI: 10.1039/c9ee00210c

rsc.li/ees

Broader context

Climate change drives the development of alternative low-carbon energy sources such as biofuels. Plant oil based biofuels promise to reduce greenhouse gases. However, the overhasty large scale plant oil production is responsible for releasing massive amounts of CO₂ by deforestation and land use change, which competes with food production and impacts biodiversity. Circumventing these issues, fermentative yeast lipid production is flagged as an alternative feedstock, which can be generated from biogenic waste streams at enhanced areal and space-time productivities. Consequently, it is promoted as an alternative platform for biofuel production. Currently, conventional yeast lipogenesis is economically and ecologically inefficient, since it is a diauxic process that requires organic solvents for lipid recovery. In this study, a highly efficient monoauxic biomass and lipid production process provides for an integrated yeast lipid process chain. Yeast cell-wall residues were used as an inducer for on-site yeast cell-wall specific hydrolase production. *In situ* hydrolase application facilitated a one-step, solvent-free, lipid recovery and enabled the recycling of the nutrient-rich aqueous fermentation phase in subsequent fermentation cycles. The co-conversion of acetic acid and biomass-derived carbohydrates to sustainable lipids results in product costs and CO₂ emissions comparable with plant oils. This improved the overall ecological footprint of yeast oil production.

Introduction

Globally, the production and use of high-energy biofuels (*i.e.*, biodiesel, biokerosene) and renewable oleochemicals (*i.e.*, bio-lubricants, cosmetic/pharmaceutical bases) are associated with a negative eco-impact owing to their dependence on plant oil

Department of Chemistry, Werner Siemens Chair of Synthetic Biotechnology,
Technical University of Munich, Germany. E-mail: norbert.mehlmer@tum.de,
brueck@tum.de

† Electronic supplementary information (ESI) available. See DOI: 10.1039/c9ee00210c

feedstocks.¹ Plant oil production for generation of biofuels and chemicals competes with food production, accelerates land use change in sensitive ecosystems, and thereby negatively affects biodiversity.² Moreover, the generation of biofuels from converted lands (*i.e.*, rainforests) has even greater effects on greenhouse gas emission than the fossil fuels that these biofuels displace.^{2,3} One of the most prominent examples is the clearing of tropical rainforests for palm oil cultivation, which leads to the ultimate displacement and decline of critically endangered species, such as the orangutan.^{4,5} Therefore, to enable global development of biofuels and oleochemicals without negatively affecting the environment, the process of bio-oil production needs to be uncoupled from terrestrial plant feedstocks and land use change.

In January 2017, the European Parliament decided to phase-out palm oil and cap crop-based biofuels by 2021 for all member states. However, this will not be achievable without alternative production routes that can satisfy the increased energy demand and biofuel criteria to yield low-carbon energy resources. In contrast to current biofuel options, future processes must avoid clearing of sensitive ecosystems, such as rainforests, which function as a high-impact and long-term carbon sink. In this regard, microbial oils have long been recognised as the best alternatives to plant based-oil production,^{6,7} and the yeast *Cutaneotrichosporon oleaginosus* (*C. oleaginosus*, ATCC20509) has been flagged as a prime candidate for microbial oil production over other oleaginous microorganisms owing to its rapid growth rates, high cell density cultivation, and catabolism of various biogenic waste streams.⁷

Economically, feedstock availability and cost, triglyceride oil productivity, and the number of process steps to achieve oil recovery are key challenges that block the industrial-scale manufacturing of yeast-based oils. According to reported production processes, microbial oil costs are estimated to be around \$5.5 per kg.⁸ In comparison, soybean and palm oil costs are around \$0.5–0.68 per kg (October 2018).⁹ Therefore, to meet the economic boundary conditions for microbial oil production, the entire process chain and feedstock utilisation has to be reorganised. Drivers in this process include feedstock selection and maximising oil productivity while minimising the number of process steps, including value-added exploitation of by-product streams. Accordingly, the development of an inexpensive and sustainable feedstock is essential for economic process design. In current studies, most resources have been focused on the identification of sustainable feedstocks, including sugar sources obtained from forestry waste and agro-industrial residues, such as crude glycerol,¹⁰ sweet sorghum bagasse,¹¹ and thermally/chemically pretreated sludge,^{12,13} as potential carbohydrate sources. Recent studies have demonstrated that marine feedstocks, including macroalgae,^{14,15} microalgae,¹⁶ and seagrass,¹⁷ have additional advantages over terrestrial biomass feedstocks. Specifically, these feedstocks can be harvested sustainably without affecting agricultural activity, inducing land use change or damaging sensitive marine ecosystems.¹⁸ Moreover, marine biomass feedstocks have a 6–10 fold higher area productivity than terrestrial biomass resources, such as cereal straw.^{19,20}

In addition to complex biomass feedstocks, acetic acid is also used as a sustainable carbon source because it can be generated from ecologically sound starting materials, such as CO, waste gases, and CO₂/H₂,^{21–23} using biotechnological processes (*i.e.*, fermentation of *Clostridium acetium* and *Acetobacterium woodii*).^{21,22,24,25} Moreover, acetic acid has a low market price,²⁴ which favours economically sound production routes.

Recently, some reports have demonstrated that acetic acid can serve as the sole feedstock for *C. oleaginosus* cultivation.^{26–31} However, although application of acetic acid as the sole carbon source results in a considerably high intracellular lipid content (60–73%, $w_{\text{lipid}}/w_{\text{biomass}}$), biomass productivity is inhibited, leading to poor overall oil yields.^{26,28,29} Moreover, multistep,³⁰ continuous,²⁶ and pH-stat^{27,29} fermentations have been tested in order to identify the best implementation of acetic acid as the sole carbon source feedstock. The pH-stat approach shows promising lipid productivity.²⁷ However, constant feeding of costly yeast extract, peptone, vitamins, and other nutrients in all pH-stat trials prohibits the economic development of this process. Thus, further studies are needed to achieve optimal integration of acetic acid in the microbial oil production process.

Typically, oleaginous yeast fermentation is subjected to a diauxic shift from biomass formation to lipid accumulation, which is induced under nutrient limitation. The diauxic shift increases the fermentation time, thereby reducing lipid productivity and adversely increasing operation costs owing to the requirement for excess aeration and cooling.⁸ These factors adversely affect the economic and ecologic feasibility of microbial lipid production. Therefore, the short fermentation time enabled by monoauxic biomass and consecutive lipid formation is essential to improve both economic and ecological process parameters.

In addition, lipid recovery from intracellular compartments and subsequent downstream processing represent additional challenges in the design of an economically relevant microbial oil process. However, conventional lipid extraction procedures require cell wall destruction (*e.g.*, *via* temperature shock, chemical treatment, and high-pressure homogenisation),³² followed by lipid extraction with toxic organic solvents (*i.e.*, chloroform and hexane). The scale up of such mechanically and energy-demanding processes results in additional technical complications and increased cost.^{33,34} Ecologically, application of organic solvent results in accumulation of solvent traces in all process outlets (lipid, water phase, and residual biomass). Thereby, solvent application will reduce the final product quality and yield side product streams as toxic waste.³⁴

Enzymatic hydrolysis may be an alternative strategy for cell wall destruction. In fact, enzymatic hydrolysis should be a holistic cell lysis route that entirely circumvents the need for solvent extraction. However, because of the biochemical complexity of the yeast cell wall, holistic cell lysis requires synergistic effects of multi-enzyme activities. To date, there is no single commercial enzyme system that comprises all the required hydrolase activities. Therefore, on-site hydrolase production is an alternative for tailored hydrolase generation. The filamentous

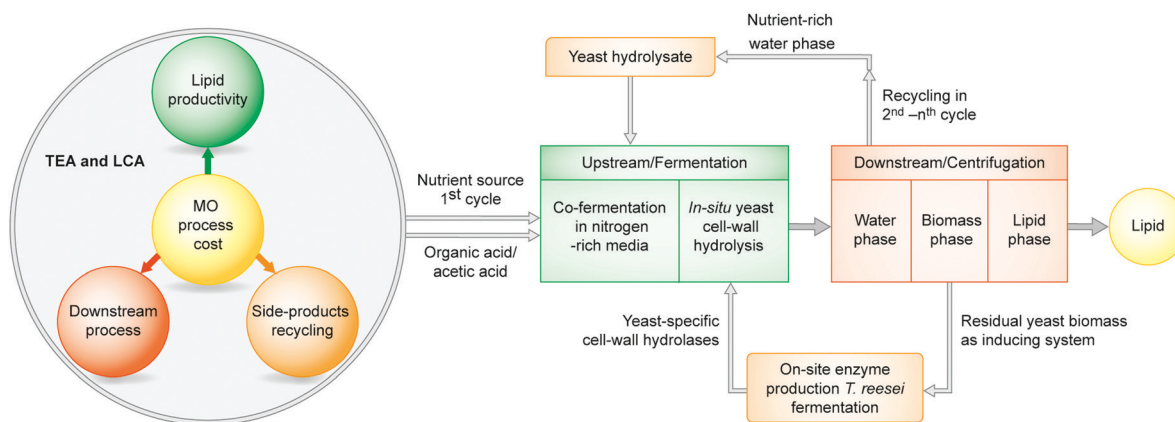


Fig. 1 Overview of workflow of the study (left) and biomass flow for the developed yeast lipid production process (right).

fungus *Trichoderma reesei* (*T. reesei*) is considered one of the most efficient extracellular hydrolase producers and is capable of customized hydrolase production, when fed with appropriate inducer systems. Consequently, *T. reesei* is a potential host for the generation of a dedicated enzyme system for targeted yeast cell lysis.

In this study, we established a new process chain for production of yeast-based lipids, enabling highly efficient monoauxic biomass and lipid production, one-step lipid recovery without solvent extraction to recover lipids, and complete recycling of water and side product streams (Fig. 1). This process permitted operation in a continuous or batch fermentation mode using terrestrial or marine carbon sources as well as acetic acid. Additionally, a comprehensive techno-economic analysis (TEA) and life cycle assessment (LCA) of the new yeast lipid production process was performed. We also evaluated the economic feasibility of the process to minimise feedstock, energy, and water consumption costs. In summary, we developed a newly designed process using non-terrestrial biomass hydrolysates that were not associated with land use change, ecosystem destruction, or biodiversity reduction.

Experimental

Strains and preculture

C. oleaginosus (ATCC 20509) was cultivated in Erlenmeyer flasks containing YPD media broth (10 g L⁻¹ yeast extract, 20 g L⁻¹ peptone, and 20 g L⁻¹ glucose) containing antibiotics (10 mg L⁻¹ ampicillin, 10 mg L⁻¹ kanamycin, and 12 mg L⁻¹ tetracycline). The yeast was incubated in a rotary shaker at 100 rpm and 28 °C for 2 days and was then used as the inoculum.

T. reesei ATCC 56765 (RUT C-30) and ATCC 13631 were activated in LB media (5 g L⁻¹ yeast extract, 10 g L⁻¹ tryptone) and was then used as inoculum for fermentation.

Medium

Different media were applied for each experiment. These media contained major nutrient components (carbon and nitrogen sources) plus base medium. The composition of the base

medium was as follow: 0.05 g L⁻¹ NH₄Cl, 2.4 g L⁻¹ KH₂PO₄, 0.9 g L⁻¹ Na₂HPO₄·12H₂O, 1.5 g L⁻¹ MgSO₄·7H₂O, 0.025 g L⁻¹ FeCl₃·6H₂O, 0.001 g L⁻¹ ZnSO₄·7H₂O, 0.2 g L⁻¹ CaCl₂·2H₂O, 0.024 g L⁻¹ MnSO₄·5H₂O, 0.025 g L⁻¹ CuSO₄·5H₂O, and 0.003 g L⁻¹ Co(NO₃)₂·6H₂O. The composition of the main nutrition was as follows: medium A (C/N ratio 125) was composed of 30.0 g L⁻¹ glucose and 0.5 g L⁻¹ yeast extract; medium B (C/N ratio 125) was composed of 0.5 g L⁻¹ yeast extract and 4.1 g L⁻¹ CH₃COONa; medium C (C/N ratio 130) was composed of 30.0 g L⁻¹ glucose, 0.5 g L⁻¹ yeast extract, and 4.1 g L⁻¹ CH₃COONa; medium D (C/N ratio 34) was composed of 30.0 g L⁻¹ glucose, 0.5 g L⁻¹ yeast extract, and 5.0 g L⁻¹ peptone; medium E was composed of 1.0 g L⁻¹ yeast extract, 1.0 g L⁻¹ peptone, and 4.1 g L⁻¹ CH₃COONa; and medium G (C/N ratio 28) was composed of 60.0 g L⁻¹ glucose, 5.0 g L⁻¹ yeast extract, 5.0 g L⁻¹ peptone, and 4.1 g L⁻¹ CH₃COONa.

Brown algae hydrolysate (C/N ratio 85) was prepared by enzymatic hydrolysis of *Laminaria digitata* without any chemical pretreatment. Detailed information for the enzymatic hydrolysis is presented in our previous publication.¹⁵

For *T. reesei* cultivation, medium F was composed of 10 g L⁻¹ *C. oleaginosus* cell wall, 10 g L⁻¹ yeast extract, 10.0 g L⁻¹ glucose, 1.4 g L⁻¹ (NH₄)₂SO₄, 2 g L⁻¹ KH₂PO₄, 0.4 g L⁻¹ CaCl₂·2H₂O, 0.3 g L⁻¹ MgSO₄·7H₂O, 0.005 g L⁻¹ FeSO₄·7H₂O, 0.004 g L⁻¹ CoCl₂·6H₂O, 0.003 g L⁻¹ MnSO₄·H₂O, and 0.002 g L⁻¹ ZnSO₄·7H₂O. Glucose was obtained from Roth-Germany (Art. No. 6780.2), yeast extract was obtained from PanReac AppliChem-Germany (A1552,1000), peptone from casein was obtained from Roth-Germany (Art. No. 8952.2), and other chemicals were obtained from Merck-Germany.

Bioreactors

For cultivation of *C. oleaginosus*, the following bioreactor systems were used: (1) a DASGIP four parallel bioreactor system (Eppendorf, Germany) with a working volume of 1 L (4 × 1 L); (2) INFORS HT three parallel System (Switzerland) with a working volume of 3 L (3 × 3 L); and (3) Bio-Engineer fermentation system (Bio-Engineer, USA) with a working volume of 50 L. The temperature was set to 28 °C, and the pH of the bioreactor was adjusted to pH 6.5 ± 0.02 with 3 M NaOH or 70–100% (w/w) acetic acid.

Stirring (350–800 rpm), oxygen ratio (21–100%), aeration (8.0–1.5 vvm), and pressure (1.25–1.5 bar) were regulated automatically to maintain dissolved oxygen at a pO_2 of 50% or more. Foam was prevented by the addition of 0.01% (v/v) of an antifoam agent (Antifoam 204; Merck). To evaluate reproducibility, each fermentation was carried out three times. The values are presented as averages, and each point was analysed in triplicate. Error bars represent the standard deviation.

Analysis

Sugar, lipid, and fatty acid profiles; cell counting, and dry biomass analyses. Sugars consumption and release were analysed by high-performance liquid chromatography (HPLC; Agilent 1100 series) with a Rezex ROA-Organic Acid (Aminex HPX 87H) column. Biomass growth was monitored by measuring the optical density at 600 nm, using the gravimetric method (lyophilisation of 5×2 mL washed culture for 2 days [Christ alpha 2-4 LD Plus]), and using cell counting (FACS S3 [Bio-Rad, Germany]). Lipid content was analysed using the Bligh-Dyer method.³⁵ Detailed procedures are described in our previous work.¹⁵ To evaluate reproducibility, all experiments were repeated three times. The values are presented as averages, and error bars represent standard deviations. Fatty acid profiles were measured using GC-FID (Shimadzu, Japan) after methylation. The methylation procedure and analysis set up were reported previously.¹⁵

On-site production of yeast-specific cell wall hydrolases. The fermentation of *T. reesei* ATCC 56765 (RUT C-30) and ATCC 13631 was carried out in the Bio-Engineer fermentation system. Fermentation parameters were set according to a previously established protocol.³⁶ Medium F was applied as the cultivation medium.

As part of medium F, the partially purified cell wall was prepared as follows. Briefly, after lipid extraction, residual *C. oleaginosus* biomass was washed with double distilled water three times, dried by lyophilisation for 2 days, ground, and then used as a hydrolase-inducing system in the *T. reesei* fermentation.

After fermentation, *T. reesei* biomass was removed by centrifugation. The resulting water phase (50 L supernatant) contained all secreted hydrolase enzymes, which were subsequently purified and concentrated by cross-flow filtration (10 kDa polyether-sulfone filter; Pall). The final volume of the resulting hydrolase enzyme system was 1 L.

Hydrolase activity assays. Multiple hydrolase activities were detected in the on-site generated enzyme system. For yeast cell wall hydrolysis, activities of cellulase, xyloglucanase, β -glucosidase, mannanase, xylanase, and laminarinase were evaluated. Therefore, 50.0 mg cellulose, xyloglucan, cellobiose, mannan, xylan, and laminarin was incubated with 1 mL buffer (Na acetate, 50 mM, pH 5.0) and 0.35% (w/w_{biomass}) enzyme solution. To test the enzyme activity of *C. oleaginosus* biomass, 50.0 mg of partially purified cell wall was incubated with 1 mL buffer (Na acetate, 50 mM, pH 5.0) and 0.35% (w/w_{biomass}) enzyme solution. All tests were incubated for 28 h at 50 °C. Gravimetric/sugar analyses (HPLC) were used after hydrolysis.

To evaluate the performance of the on-site generated system, a tailored hydrolase system with regard to commercial equivalents, we conducted comparative experiments. The evaluated commercial enzyme systems were as follows: mix 1 (mannanase [Clariant, Switzerland], Cellic Ctec2 [Novozymes, Denmark], Cellic Htec [Novozymes], and β -glucosidase [Novozymes]); mix 2 (Liquebeet [Clariant], CLA [Clariant], mannanase [Clariant], 1,3- β -glucanase [Megazyme, France], and β -glucosidase [Novozymes]). To ensure reproducibility, all experiments were conducted in triplicate. The reported values are presented as averages, and error bars represent standard deviations.

Techno-economic analysis. Techno-economic analysis (TEA) was carried out to estimate the total capital investment and operating cost for process flowsheets that could be used for the production of lipids from oily yeast.

As there is a lack of major databases (such as NREL) for process design related to oleaginous yeasts oil production, process and economic data were collected from current results and those reported in the available literature,^{8,37–39} as well as integrated mathematical functions in SuperPro Designer version 10 (Intelligen, Inc., Scotch Plains, NJ, USA).^{40,41}

The *in silico* process simulation created a production plant with an annual lipid production capacity of 23 000 metric tonnes. The required feedstock (*i.e.*, acetic acid, glucose, and amino acids) and chemicals were estimated based on current media compositions and the results of the current work. The individual yeast biomass, lipid formation, and enzymatic hydrolysis are represented by respective equations in the ESI.† The built-in material and energy balance data in SPD were applied to determine the required equipment sizing and respective purchasing prices.

Therefore, the simulated plant consisted of multiple unit operations, encompassing feed handling, fermentation, hydrolysis, product recovery, and side-product recycling. Hence, 11 fermenters (10 in use, one as standby, 250 m³ each), four stirred tank reactors for *C. oleaginosus* lysis and lipid mobilization (three in use, one as standby, 250 m³ each), five bending/storage/receiving tanks (250 m³ each), three decanter centrifuges (two in use, one as standby, 159 920 L h⁻¹ each), a centrifugal compressor, an air filter, and an ultrafiltration unit were modelled in SPD (see the simplified process flow diagram in Fig. S8, ESI†). The standby units were included to avoid maintenance-based downtime.

Major process parameters and assumptions applied to develop the process model and determine the required materials, energy, and costs are presented in Table S2 (ESI†).

As lipid productivity had the highest impact on cost with respect to all other process parameters, the baseline scenario was established based on harvesting 4 days after initiation of the fermentation process. Thus, baseline lipid productivity was approximately 1.4 g L⁻¹ h⁻¹ (biomass: 200 g L⁻¹, lipids: 85% [w_{lipid}/^dw_{biomass}], after 120 h). However, the optimal scenario was consistent with the best productivity reported in this study, which was 2.4 g L⁻¹ h⁻¹ (biomass: 147 g L⁻¹, lipids: 73% [w_{lipid}/^dw_{biomass}], after 42 h). These productivity values represented the average value of six biological replications with \pm 5%

relative standard deviation (Fig. S13, ESI†). Fig. S9–S11 (ESI†) show data for the sensitivity analysis during lipid productivity.

An internal SPD mathematical function adjusted the equipment purchase cost (PC) based on the required process equipment sizing with respect to the analysis year (2018).⁴² Relevant installation cost factors of 1.6 and 1.8, derived from the initial PC, were extracted from a very detailed biomass conversion focused TEA study.^{41,43} Process piping, warehouse and site development were estimated as 4.5, 4.4 and 9.0% of the inside-battery-limit (ISBL) equipment costs respectively.⁴³ The indirect plant costs, including engineering and construction, were estimated as 20% and 10% of total direct cost (TDC), respectively, where TDC is defined as PC plus installation cost plus process piping.⁴³ A capital interest factor of 6% was added to the total capital investment. The annual operating cost was estimated by the facility-dependent cost (including maintenance) as 3% of TDC.⁴³ The operator cost was adjusted to German full-cost tariff TV-L 11, 13, and 14.⁴⁴ Raw material costs were estimated based on the available whole-sale market price. The cooperate insurance was calculated as 0.7% of the total capital investment (TCI).⁴³ A detailed cost analysis is presented in Tables S3–S11 (ESI†).

Life-cycle for global warming potential (GWP). The life cycle and environmental analysis (LCA) for the entire process chain described in this study was investigated in order to identify environmental process hotspots that could indicate whether the yeast products were a viable alternative to conventional plant oils. An attributional cradle-to-gate assessment of a fully integrated, commercial-scale yeast lipid production unit based on the data presented in the TEA section was performed. Allocation was not applied. All side product streams were entirely recycled within a process loop. The underlying models were based on experimental data generated within the project (lab-scale) and fed into process simulation models for the initial TEA analysis; all other required datasets were complemented by literature data (*e.g.*, transport). The environmental data are based on publicly available LCA databases, such as US LCI⁴⁵ and the BioEnergieDat⁴⁶ database. The mass balance for the functional unit of 1 kg oil is illustrated in Fig. S15 (ESI†). This Sankey diagram of the complete process chain highlights two aspects: the large share of acetic acid as a feedstock and the importance of medium recycling for process efficiency. *In papyro*, the model reflected a simulated business case in North Germany near the North Sea coast, designed with minimal land requirements in order to avoid competition with food production. The model also included all processes from sourcing initial feedstocks, such as acetic acid and macroalgae carbohydrates, followed by processing steps that encompasses yeast fermentation, side-stream recycling, and subsequent downstream processing for lipid production. The algae *L. digitata* could be collected by tractor and subsequently hydrolysed. Transport of feedstocks was included in the analysis. However, like numerous other LCA studies,^{47,48} infrastructure, such as fermenters and centrifuges, was not considered. Moreover, chemicals, such as sodium hydroxide, calcium chloride, magnesium sulfate, and other inorganic chemical components required for growth medium and process cleaning activities, were excluded from the LCA

matrix because they were used in minor amounts that did not affect the overall material flow. The full system boundary is depicted in Fig. S14c (ESI†). The impact analysis, as defined in the process flow diagram (Fig. S14c, ESI†), was calculated based on the CML method (Faculty of Science in Leiden University method [Centrum voor Milieuwetenschappen, V4.4, 2015]); however, because of its relevance, this publication concentrates on the global warming potential. The life cycle inventory is documented in the ESI† (Tables S12–S21).

Results and discussion

Maximizing lipid productivity

To identify the best operation mode, various fermentation setups (only acetic acid, only glucose, and co-fermentation of acetic acid and glucose) with nitrogen-limited and -rich media were investigated. For single-substrate fermentation, glucose fermentation (medium A; Fig. 2a) showed higher biomass productivity than acetic acid alone (medium B; Fig. 2b). However, acetic acid fermentation yielded slightly higher lipid productivity (Fig. 2f and j) than glucose fermentation (Fig. 2e and i), measuring $0.13 \text{ g L}^{-1} \text{ h}^{-1}$ (biomass: 22 g L^{-1} , lipids: $72\% [w_{\text{lipid}}/d w_{\text{biomass}}]$) and $0.09 \text{ g L}^{-1} \text{ h}^{-1}$ (biomass: 34 g L^{-1} , lipids: $45\% [w_{\text{lipid}}/d w_{\text{biomass}}]$), respectively.

In comparison, co-fermentation of glucose and acetic acid in nitrogen-limited medium (medium C; Fig. 2c) yielded a biomass of 20 g L^{-1} with a lipid content of 20% ($w_{\text{lipid}}/d w_{\text{biomass}}$) in the first 24 h (Fig. 2g and k). In contrast, at the same time point, individual glucose and acetic acid fermentation biomasses reached only 10 g L^{-1} with a lipid content of 12% ($w_{\text{lipid}}/d w_{\text{biomass}}$) and 5 g L^{-1} with a lipid content of 30% ($w_{\text{lipid}}/d w_{\text{biomass}}$), respectively. This corresponded to a lipid productivity of $0.2 \text{ g L}^{-1} \text{ h}^{-1}$ from day 1 compared with $0.075 \text{ g L}^{-1} \text{ h}^{-1}$ with respect to individual glucose and acetic acid batch fermentation.

Under nitrogen-limited conditions, lipid production decreased to $0.18 \text{ g L}^{-1} \text{ h}^{-1}$ (biomass: 43 g L^{-1} , lipids: $73.5\% [w_{\text{lipid}}/d w_{\text{biomass}}]$) by day 5 of fermentation. The calculated carbon:carbon efficiency was 0.22 g g^{-1} lipid per total carbon. This decrease could be attributed to the limited nitrogen resources.

Interestingly, the fermentation based on nitrogen-rich medium (medium D) enhanced lipid productivity, reaching $0.67 \text{ g L}^{-1} \text{ h}^{-1}$ by day 1 (Fig. 2d, h, and l). Notably, nitrogen-rich medium-based co-fermentation resulted in simultaneous formation of both biomass and intracellular lipids immediately after the start of fermentation. Under these conditions, lipid contents in excess of 70% ($w_{\text{lipid}}/d w_{\text{biomass}}$) were obtained by day 2 of fermentation. Thereafter, the lipid yield increased further, reaching 85% ($w_{\text{lipid}}/d w_{\text{biomass}}$) after 120 h. This was the highest intracellular lipid yield ever observed with oleaginous yeasts. Under these experimental conditions, the biomass yield also continued to increase linearly without levelling out into a plateau phase (Fig. 2d). The applied acetic acid and sugar co-fermentation protocol improved lipid productivity up to $0.53 \text{ g L}^{-1} \text{ h}^{-1}$ (biomass: 84 g L^{-1} , lipids: $84.9\% [w_{\text{lipid}}/d w_{\text{biomass}}]$). However, the carbon:carbon efficiency

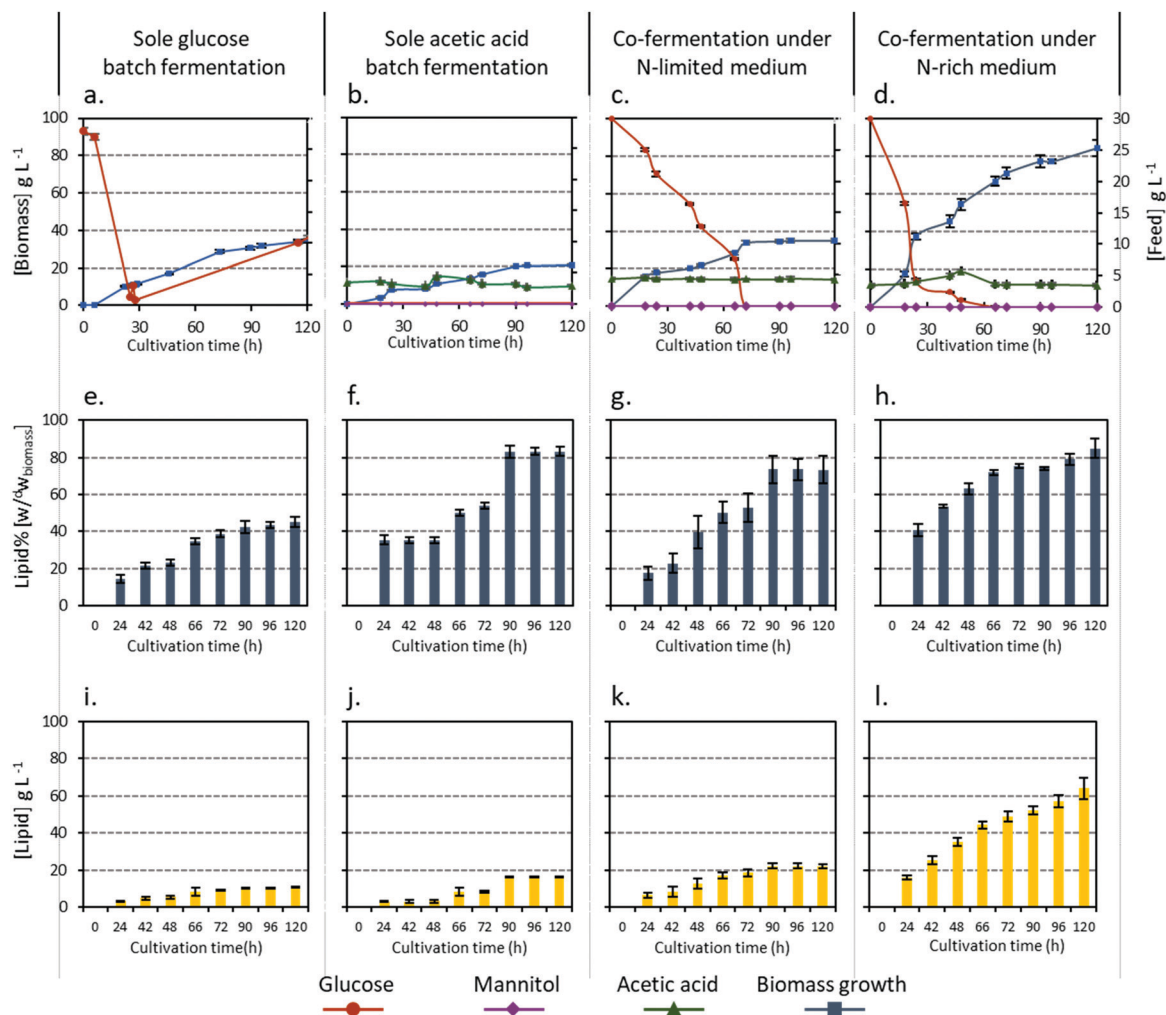


Fig. 2 (a, e and i) Growth rates, substrate consumption, lipid accumulation, and lipid titres with glucose as the only feedstock. (b, f and j) Growth rates, substrate consumption, lipid accumulation, and lipid titres with acetic acid as the only feedstock. (c, g and k) Growth rates, substrate consumption, lipid accumulation, and lipid titres with co-fermentation of glucose and acetic acid as the feedstock using nitrogen-limited medium. (d, h and l) Growth rates, substrate consumption, lipid accumulation, and lipid titres with co-fermentation of glucose and acetic acid as the feedstock using nitrogen-rich medium.

was 0.24 g g^{-1} lipid per total carbon. Consistent with these findings, fluorescence microscopy imaging indicated a remarkable increase in cell volume and lipid content (Fig. S1, ESI[†]).

In previous runs, synthetic medium with pure glucose was applied. However, to avoid the effects of land use change on our co-fermentation, the marine brown algae biomass *L. digitata* served as a sugar source. A previously reported *L. digitata* hydrolysate¹⁵ was used in co-fermentation with acetic acid. The co-fermentation of *L. digitata* hydrolysate with acetic acid resulted in concurrent biomass and lipid formation without nutrient limitation. In addition, the biomass yield surpassed the intracellular lipid formation, and the total lipid productivity increased to $0.59 \text{ g L}^{-1} \text{ h}^{-1}$ (biomass: 114 g L^{-1} , lipids: $64\% [w_{\text{lipid}}/w_{\text{biomass}}]$) owing to the higher biomass yield. In this experimental setup, the carbon efficiency was 0.24 g g^{-1} lipid per total carbon (Fig. 3a, d and g).

Different operation modes were tested to verify the most economic approach, and semi-continuous and continuous

operation modes were tested with extended run times. First, a semi-continuous operation mode with two harvesting points was run for about 12 days. Two partial harvests were conducted at 162 and 234 h, where 40–50% (v/v) of the culture was removed from the bioreactor and replaced with fresh medium E. The initial co-fermentation with nitrogen-rich medium (medium D) and acetic acid over an extended time period is depicted in Fig. 3b, e and j. As observed previously, biomass and lipid formation yielded a lipid productivity of $0.57 \text{ g L}^{-1} \text{ h}^{-1}$ (biomass: 106 g L^{-1} , lipids: $87\% [w_{\text{lipid}}/w_{\text{biomass}}]$) after 162 h. At this time, the first harvesting point had taken place by harvesting 40% (v/v) of the culture, resulting in decreased biomass (69 g L^{-1}).

In the next 42 h of operation, the biomass concentration increased rapidly to reach 235 g L^{-1} . Moreover, the lipid content could be maintained above 80% ($w_{\text{lipid}}/w_{\text{biomass}}$), with a lipid productivity of $0.90 \text{ g L}^{-1} \text{ h}^{-1}$. This was the highest lipid productivity observed at this point of process optimisation.

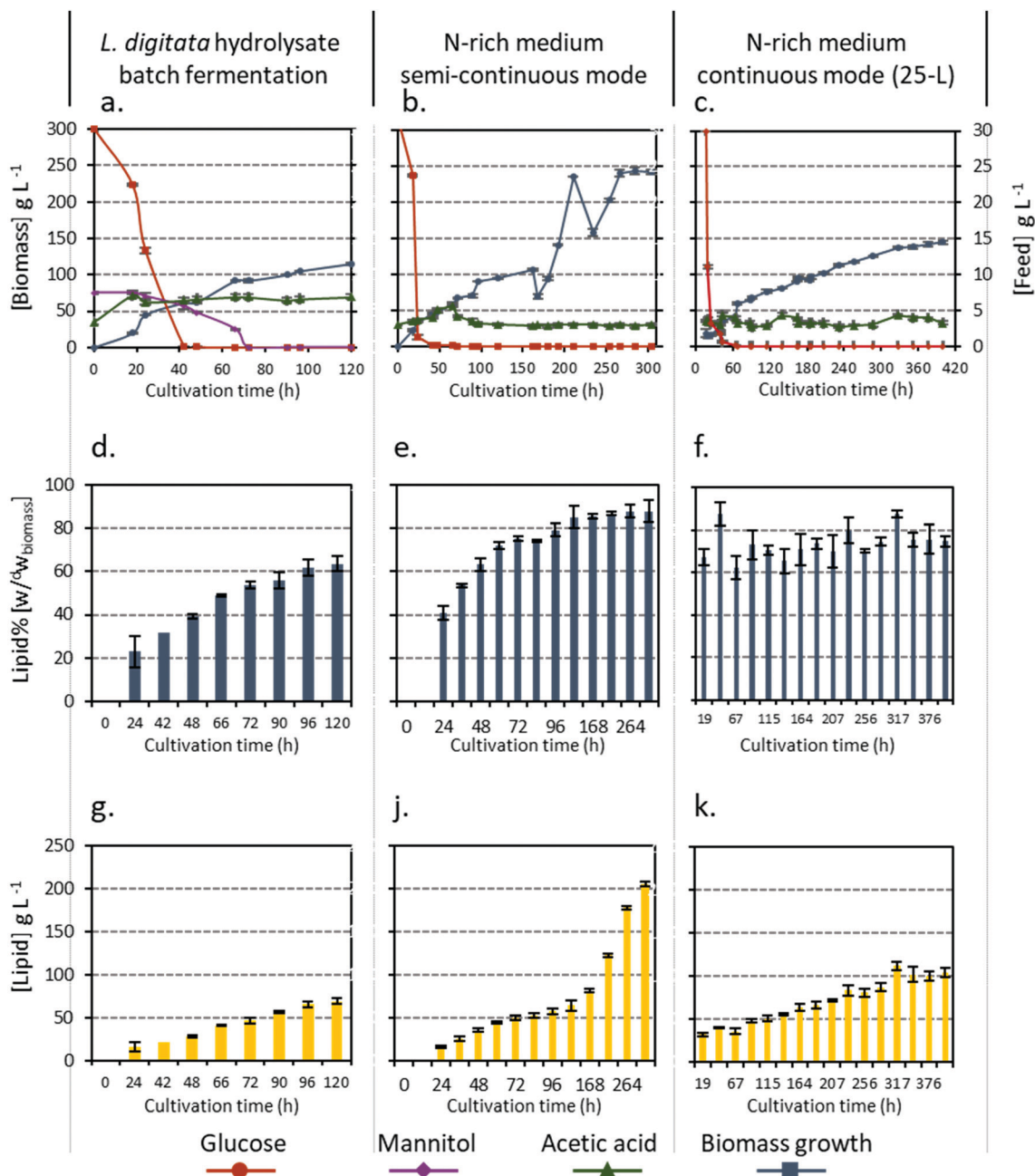


Fig. 3 (a,d and g) Growth rates, substrate consumption, lipid accumulation, and lipid titres with *Laminaria digitata* hydrolysate as the only feedstock. (b, e and j) Growth rates, substrate consumption, lipid accumulation, and lipid titres with co-fermentation of glucose and acetic acid as the feedstock using nitrogen-rich medium with semi-continuous mode. (c, f and k) Growth rates, substrate consumption, lipid accumulation, and lipid titres with co-fermentation of glucose and acetic acid as the feedstock using nitrogen-rich medium with continuous mode (25 L).

At 234 h, the second harvesting step was performed, wherein 50% (v/v) of the culture volume was removed (Fig. 3b). Hence, the biomass concentration was decreased to 158 g L⁻¹. Interestingly, the biomass concentration was returned to 240 g L⁻¹ with a lipid content of 87.5% ($w_{\text{lipid}}/d w_{\text{biomass}}$) within the next 32 h of fermentation.

At the end of the operation, the total lipid productivity was 0.8 g L⁻¹ h⁻¹ (biomass: 240 g L⁻¹; lipids: 87.6% [$w_{\text{lipid}}/d w_{\text{biomass}}$]). However, the carbon efficiency with respect to lipid formation was 0.39 g g⁻¹. This productivity figure did not consider the harvested

culture amount, which exceeded 80% (v/v) of the original culture volume. The comprehensive yeast biomass analysis is shown in Table S1 (ESI[†]). The extremely high cell density and lipid content could be visually observed though the extremely high viscosity and hydrophobicity of the cells when exposed to water (see the video in the ESI[†]).

To validate the presented data at technically relevant scales, co-fermentation in nitrogen-rich medium was conducted at a scale of 25 L. The fermentation was operated in continuous mode using 50% (w/w) acetic acid as the continuous dilution.

Because the yeast initiated significant acetic acid metabolism about 48 h after the start of the experimental run, there was increasing dilution of the reactor volume under these conditions. Notably, because acetic acid metabolism increased during the experimental period, the dilution factor also increased.

Within the first 24 h, the acetic acid feed was 2 kg per day and thereafter increased exponentially to 6 kg at 96 h. At this feeding rate, the culture volume increase by 4.5 L over 96 h (18% [v/v] volume increase), corresponding to a dilution of $7.5 \text{ mL L}^{-1} \text{ h}^{-1}$. This volume increase was compensated by a daily harvest of an equivalent culture volume (4.5 L day^{-1}). After 96 h, a constant optical density and cell count (by flow cytometry) were reached, and this result was attributed to a balance between the growth rate and the applied dilution factor of the reaction (Fig. S2, ESI†). Although the cell count was constant, a continuous increase in biomass formation was observed and could be attributed to a constant rise in intracellular lipids (Fig. 3c, f and k). Therefore, the increase in biomass could be explained by the expansion of cell volume, which was correlated with a volumetric expansion of intracellular lipid vesicles, as detected by flow cytometry (Fig. S3, ESI†). Fatty acid profiles were measured over the fermentation time. Fig. S4 (ESI†) displays the decrease of $C_{16:0}$ and the increase of $C_{18:0}$ over the fermentation time.

Based on the current data for production in a 25 L volume, feeding with 50% ($w_{\text{lipid}}/d_{\text{w}_{\text{biomass}}}$) acetic acid permitted 20% (v/v) harvesting of the fermentation volume on a daily basis or continuous harvesting without any effect on culture density. However, scaling up this process to a 10 000 L fermenter would result in a daily harvest volume of 1800 L, including 108 kg oil. This amount could then be continuously transferred to downstream processes.

From data found in the literature, *C. oleaginosus* fermentation with either glucose or acetic acid under conditions of limited or excess nitrogen has been well documented.^{27,28,31} Generally, with sugar-based fermentation, lipid biogenesis can only be induced when stress conditions, such as nitrogen limitation, are applied. In contrast, fermentation in the presence of high sugar and nitrogen concentrations results in high yeast biomass yields with low intracellular lipid contents (~20–30% w/w). Therefore, the relative carbon:nitrogen concentration has a major impact on lipid productivity. Conversely, when acetic acid is the sole carbon source in the fermentation, lipogenesis is upregulated, but biomass formation is limited due to toxic effects.^{26,28,29,49}

Conventional lipid production with oleaginous organisms is a two-stage process, in which the first step results in biomass formation under non-limiting conditions (exponential growth phase) and the second lipid induction step (nutrient limitation phase) affords high intracellular lipid accumulation at stagnant cell counts. The presented data demonstrated, for the first time, that co-fermentation of sugars and acetic could result in simultaneous biomass and lipid formation without the need for metabolic stressors, such as nitrogen limitation. This current fermentation strategy achieved biomass and lipid production rates (biomass: 240 g L^{-1} , lipids: 87% [w/w]) exceeding those in previously published data.

Acetic acid is thought to be able to be assimilated from the medium and converted directly into acetyl-CoA, a general platform metabolite associated with cell growth, lipid biosynthesis, and energy metabolism.^{50,51} This transformation is catalysed by acetate-CoA ligase, which has previously been reported in a transcriptomic analysis of *C. oleaginosus*.⁵² Therefore, acetate-CoA ligase may facilitate the high lipid content by affecting the lipid biosynthesis pathway, independent of the relative C:N ratio, as reported for sugar-based fermentation. Indeed, acetate-CoA is a central tricarboxylic acid intermediate associated with cellular homeostasis and growth.^{53,54} However, our experiments using acetic acid as the sole carbon source indicated that acetate was preferentially channelled to fatty acid biosynthesis and did not ensure cell propagation. Thus, it is essential to clarify whether biomass production can be induced in parallel with lipid biosynthesis. Concurrent formation of biomass and lipids is a key factor affecting the economic feasibility of the process. Accordingly, co-fermentation of sugars and acetic acid appeared to be an efficient procedure for initiating rapid biomass propagation and lipid accumulation.

Biofuel and oleochemical production from converted land creates an inherent carbon debt by releasing 17–420 times more CO_2 than the annual greenhouse gas reductions that biofuels could provide.² For example, biodiesel from oil palm planted on converted peatland rainforest requires approximately 423 years to repay the created carbon debt. In contrast, biofuels and oleochemicals made from waste biomass (such as forestry waste) or abandoned agricultural lands incur little or no carbon debt. Such waste biomass or use of abandoned agricultural lands will create a high pressure on the food industry, resulting in price increases due to land limitations.

Second-generation feedstocks based on lignocellulosic waste biomass, such as paper mill sludge,⁵⁵ corncob residues,⁵⁶ sugarcane bagasse,⁵⁷ and forestry waste (e.g., Douglas fir residues),^{58,59} are considered an inexpensive substrate for microbial lipid production. However, using lignocellulosic biomass in second-generation bioprocesses requires harsh chemical pre-treatments (such as alkaline or acid hydrolysis), which result in byproducts (i.e., furfural, HMF, formic acid, etc.) that act as fermentation inhibitors.^{60,61} The pretreatment and subsequent detoxification steps required to remove fermentation inhibitors and enable the use of lignocellulosic hydrolysates increase both the energy consumption and costs of these processes. However, even with these process prerequisites, the best lipid titres reported for generation of yeast oil based on lignocellulosic hydrolysates did not exceed 13.4 g L^{-1} .^{55–59}

Based on this economic consideration, we decided to use an enzymatic hydrolysate from the brown algae *L. digitata*, which we previously demonstrated to be an excellent fermentation base for *C. oleaginosus*.¹⁵

With the current fermentation system, lipid productivity exceeded any previously reported productivities to date for various oleaginous yeasts and cultivation conditions. Indeed, the lipid productivity of *Lipomyces starkeyi* in a co-fermentation of 90 g L^{-1} cellobiose and xylose was $0.12 \text{ g L}^{-1} \text{ h}^{-1}$ (biomass: 31.5 g L^{-1} , lipids: 55% [$w_{\text{lipid}}/d_{\text{w}_{\text{biomass}}}$]).⁶² Using corn stover

hydrolysate as the medium, a lipid productivity of $0.23 \text{ g L}^{-1} \text{ h}^{-1}$ (biomass: 48 g L^{-1} , lipids: $34\% [w_{\text{lipid}}/d_{\text{wbiomass}}]$) was reported with *Rhodotorula graminis*.⁶³ Similarly, *Rhodospiridium toruloides* Y4 cultivated in a 15 L stirred-tank fermenter on glucose afforded a lipid productivity of $0.54 \text{ g L}^{-1} \text{ h}^{-1}$ (biomass: 106.5 g L^{-1} , lipids: $67.5\% [w_{\text{lipid}}/d_{\text{wbiomass}}]$).⁶⁴

With respect to the reported performance of *C. oleaginosus*, pH-stat fermentation based on acetic acid yielded a productivity of $0.66 \text{ g L}^{-1} \text{ h}^{-1}$ (biomass: 168 g L^{-1} , lipids: $75\% [w_{\text{lipid}}/d_{\text{wbiomass}}]$).²⁷ Moreover, a genetically optimized strain of *Yarrowia lipolytica* NS432 showed a productivity of $0.73 \text{ g L}^{-1} \text{ h}^{-1}$ (biomass: 110 g L^{-1} , lipids: $77\% [w_{\text{lipid}}/d_{\text{wbiomass}}]$) in fed-batch glucose fermentation.⁶⁵ However, the best yield reported in the literature was obtained in an oxygen-rich batch culture of *Rhodotorula glutinis*, with a productivity of $0.87 \text{ g L}^{-1} \text{ h}^{-1}$ (biomass: 185 g L^{-1} , lipids: $40\% [w_{\text{lipid}}/d_{\text{wbiomass}}]$).⁶⁶ In comparison, the current productivity ($1.2 \text{ g L}^{-1} \text{ h}^{-1}$) represented a 138% improvement in lipid formation with regard to the best lipid productivity reported for *Rhodotorula glutinis*. Moreover, for *Rhodotorula glutinis*, this oleaginous yeast generates abundant triglycerides and significant amounts of β -carotene (terpene-based lipids), which may have affected the overall lipid yield in this report. Based on our current data and additional literature, various parameters, including acetic acid concentrations, general medium composition, pH, fermentation time, aeration, and the fermentation system, can modulate lipid productivity.

Downstream processing and lipid recovery

To generate on-site yeast-specific cell wall hydrolases, two mutant strains of *T. reesei*, ATCC 56765 and ATCC 13631, were individually cultivated in a 50 L fermenter using glucose as the initial carbon source. The fermentation was operated as previously described.³⁶ By day 2 of the fermentation, the glucose concentration in the medium was almost depleted. Thereafter, the partially purified *C. oleaginosus* biomass was added to the fermentation medium at a concentration of 10 g L^{-1} (medium F). Visual observation and subsequent sugar analysis were applied to measure the decrease of intact *C. oleaginosus* cells over time (data not shown). The data indicated that *T. reesei* could hydrolyse the *C. oleaginosus* cells and utilise them as a carbon source. By day 3 of the cultivation, the *C. oleaginosus* cell debris was completely decomposed. The fermentation continued for another day to stress the fungi and induce maximum hydrolase enzyme secretion. Centrifugation and medium filtration with a 10 kDa crossflow filtration and buffer exchange were subsequently applied to concentrate, enrich, and purify the tailored hydrolase system. The final enzyme solution was approximately 1 L, with a protein concentration of $32\text{--}35 \text{ g L}^{-1}$ for the enzyme solutions of ATCC 56765 and ATCC 13631, respectively.

Four verification steps were carried out to test the efficiency of the generated hydrolase system. The verification steps included incubation with pure polysaccharides, incubation with the purified yeast biomass and evaluation using a single real culture as well as scaling to 25 L culture to verify the enzyme activity.

After incubation of the enzyme solution ($0.35\% [w_{\text{enzyme}}/d_{\text{substrate}}]$) with pure polymeric sugar substrates, cellulase,

xyloglucanase, β -glucosidase, mannanase, xylanase, and laminarinase enzyme activities were detected in both preparations (data not shown). Subsequently, the resulting enzyme systems were tested on the purified cell wall preparations of *C. oleaginosus*. Fig. S5a and b (ESI[†]) show the decreases in residual biomass weight over the incubation time, where less than 16% and 20% (w/w) biomass remained after 28 h of incubation with the enzyme solutions from ATCC13631 and ATCC56765, respectively.

Next, enzyme solutions were tested using a fresh *C. oleaginosus* culture. For comparison, two mixtures of the commercial enzyme systems were prepared. These two mixtures, termed Mix 1 and 2, comprised identical enzyme activities as our *T. reesei*-derived enzyme system. The final protein concentration in both mixtures was $14.2\text{--}14.5\% (w_{\text{protein}}/v_{\text{solution}})$. Individually, 100 μL of each of the four enzyme systems was incubated with 1.0 g biomass in 5.0 mL acetate buffer (50 mM, pH 5.0) for 18 h. Using the same volume of the enzyme preparation provided different enzyme/biomass ratios (w/w); the enzyme:biomass ratios were approximately $1.4\% (w_{\text{enzyme}}/d_{\text{wbiomass}})$ in the commercial mixtures and approximately $0.35\% (w_{\text{enzyme}}/d_{\text{wbiomass}})$ for the *T. reesei*-generated enzyme system. For the commercial mixtures, 40–48% (w/w) biomass was solubilized compared with 57–63% (w/w) with the *T. reesei*-derived enzyme preparation (Fig. S5c, ESI[†]). However, approximately 40% (w/w) of the generated lipids was released in all preparations (Fig. S5d, ESI[†]).

After these laboratory-based experiments, we validated our enzyme-based *C. oleaginosus* lysis procedure at a 25 L scale fermentation. The initial fermentation was carried out as described previously. Yeast growth was terminated by stopping aeration. At this point, neither biomass harvest nor any treatment was carried out. Instead, the temperature of the fermenter was increased to $45 \text{ }^\circ\text{C}$, the pH was adjusted to 4.5, and the stirring speed was increased to 800 rpm. At this point, the hydrolase system was directly added to the fermenter. Cell lysis was initiated by adding $0.4\% (w_{\text{enzyme}}/d_{\text{wbiomass}})$ of each *T. reesei* enzyme preparation (total concentration: $0.8\% [w_{\text{enzyme}}/d_{\text{wbiomass}}]$). After 20 h of treatment, the reaction conditions were modified; the pH was adjusted to 7.0, and the temperature was changed to $37 \text{ }^\circ\text{C}$. Next, $0.5\% (w_{\text{enzyme}}/d_{\text{wbiomass}})$ of the commercial protease preparation (Lavery, BASF) was added to break down cellular proteins and induce demulsification to assist with lipid release.

The time-dependent cell lysis and lipid release procedures were analysed by flow cytometry for cell counting and HPLC for assessment of sugar release. Fig. 4a shows the cell density plot as one population located in the intact cell area (R3). During hydrolysis, the cell density in area R3 decreased, and a new population in the smaller area (R4) was generated. This new population represented the cell debris. Cell counting (Fig. 4c) confirmed that the cell number dropped from $983 \times 10^6 \text{ cells mL}^{-1}$ before the enzymatic hydrolysis to $139 \times 10^6 \text{ cells mL}^{-1}$. Sugar analysis (Fig. 4b) showed that the sugar content increased with hydrolysis. Furthermore, fluorescence microscopy confirmed these findings and allowed visualisation of the lysis process (Fig. 5a).

Thereafter, biomass was subjected to centrifugation, in which the upper layer fraction contained the released lipid in a surprisingly pure form. Fig. 5b–d shows the released lipids

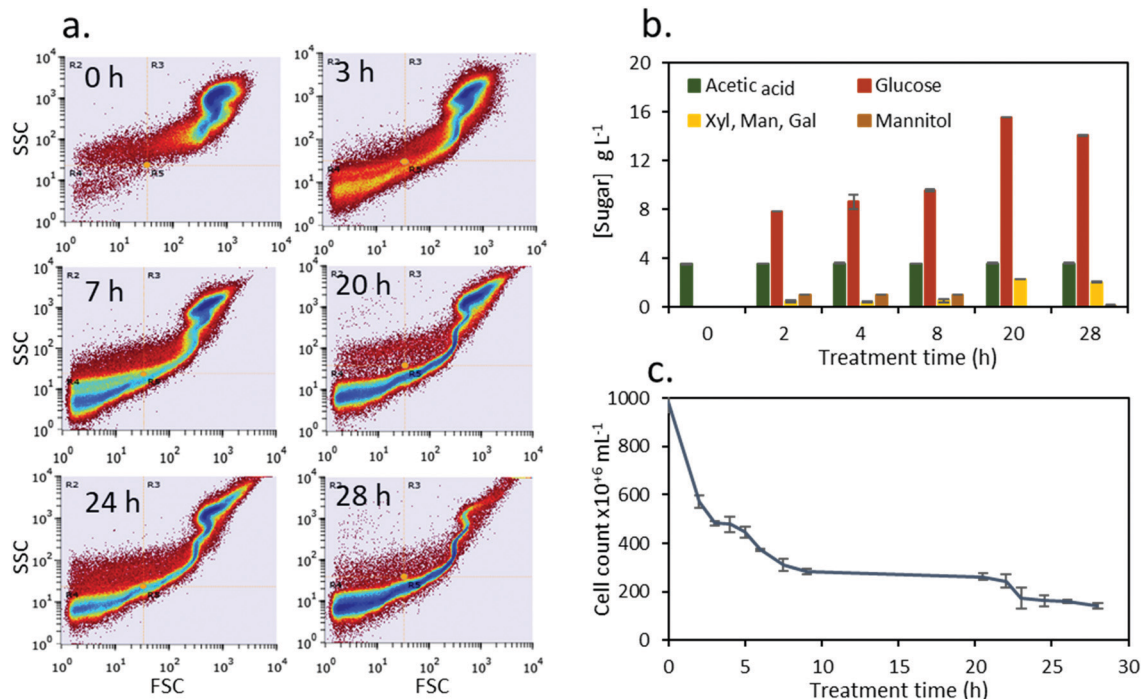


Fig. 4 Evaluation of the produced enzymes from *Trichoderma reesei* ATCC 13631 and RUT C-30 (ATCC 56765) at a scale of 25 L. (a) Cell density plot diagrams of *C. oleaginosus* over the enzymatic hydrolysis time. The cell density plot shows the intensity of the forward scatter (FSC; on the x-axis) and side scatter (SSC; on the y-axis). (b) Increase in sugar concentration over the enzymatic hydrolysis time. (c) Decreased cell counts of *C. oleaginosus* over the enzymatic hydrolysis time.

after the enzymatic treatment before and after centrifugation. The data demonstrated that 85% (w/w) of the *C. oleaginosus* yeast cells were hydrolysed and that approximately 90% (w/w) of total intracellular lipids was successfully released.

The downstream process, *i.e.*, lipid extraction, has a significant effect on economic and ecological process efficiency and on product quality with regard to certifiable market sectors, including the food industry.^{34,67} Lipid production is conventionally processed

using five steps: (1) density-based biomass concentration (*e.g.*, disk-separator³²), (2) cell destruction (*e.g.*, high-pressure homogenisation³²), (3) solvent extraction (*e.g.*, hexane or chloroform), (4) solvent separation, and (5) solvent recovery (*e.g.*, a solid/liquid-type separator followed by a single-effect evaporator^{68,69}). In addition to the high cost, many technical obstacles prevent the industrial application of these processes for the commercial generation of microbial oils. First, the high lipid content (more

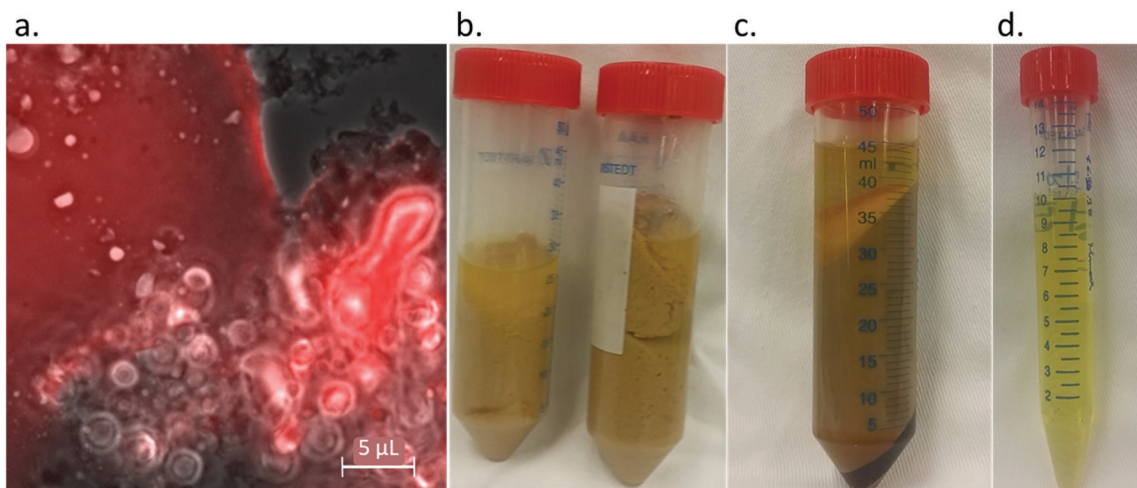


Fig. 5 Lipid extraction after enzymatic hydrolysis. (a) Fluorescence microscope image of yeast cells after 10 h of enzymatic hydrolysis. The lipids were stained with Nile Red (red). (b) Cultures after the enzymatic hydrolysis. The culture was left overnight on the working bench. (c) The culture after centrifugation (at 9000 × *g* for 20 min). (d) Floating lipids after pouring out without any further purification.

that 50% [$w_{\text{lipid}}/d_{\text{w}_{\text{biomass}}}$] of cells prevented efficient separation as cells with high lipid contents would remain suspended in the supernatant or floating as a layer on the top after high g-force centrifugation (approximately $50\,000 \times g$; Fig. S6, ESI[†]), making the harvesting step inefficient. In the subsequent step, the rigidity of the yeast cells caused the high-pressure homogenisation to be insufficient. Fig. S7 (ESI[†]) shows an electron scatter for yeast cells after three cycles of high-pressure homogenisation (2400 bar). Finally, homogenised cells were extracted using an organic solvent. However, lipids extracted with organic solvents are difficult to certify for high-value food and feed applications. In addition to their effects on product quality, organic solvents will accumulate in process water and cell residue streams, causing significant environmental issues.

In recent reports, partial enzymatic-assisted lipid extraction was applied to enhance the lysis of oleaginous yeast cells.^{32,70–73} However, this process requires various pre-treatments prior to enzymatic cell lysis (*i.e.*, ultrasonic irradiation or heating at 95 °C). Despite this, harsh treatments with organic solvents, such as ethyl acetate³² and hexane,⁷⁰ are required for triglyceride recovery.^{70–73}

Thus, it is essential to generate an enzyme system for holistic cell lysis that contains all essential enzyme activities to afford specific, quantitative lysis of *C. oleaginosus* cell walls. The filamentous fungus *T. reesei* is considered one of the most efficient extracellular hydrolase producers and harbours various enzymes with important activities, including cellulase, 1,3- β -glucosidase, β -D-1,3-glucanase, *exo*-1,3-beta-glucanase, *exo*-1,3-beta-glucosidase, *exo*-1,4- β -D-xylosidase, β -xylosidase *endo*-1,4- β -mannanase, chitinases, and cell wall lytic enzymes.^{36,74,75} This unique induction system was applied in the enzyme production step to promote the production of required enzyme activities, and the induction was evaluated using several verification steps. However, the in-house generated enzyme system featured increased activity and specificity compared with commercial equivalents, even when a lower total protein (enzyme) concentration was applied for hydrolysis. Moreover, our on-site enzyme production will eliminate the necessity for external sourcing and transport of commercial enzyme systems, thereby improving cost and the carbon emission footprint of the process chain.

The new, *in situ* enzymatic treatment process developed in this study enabled quantitative cell lysis and lipid recovery/purification without the need for biomass pretreatment (such as harvesting, drying, and high-pressure homogenization) or application of an organic solvent to assist the lipid recovery step. Additionally, the carbohydrate and protein hydrolysis products (monomeric sugars and amino acids) could potentially be reused in subsequent fermentations because they were not contaminated with solvent traces.

Recycling biomass and hydrolysate fractions

Initially, 500 mL medium G was used in the first *C. oleaginosus* cultivation cycle. Fig. 6 shows the initial *C. oleaginosus* growth rate during the fermentation time. With these experimental conditions, lipid productivity was $1.23 \text{ g L}^{-1} \text{ h}^{-1}$ (biomass: 72 g L^{-1} , lipids: 77% [$w_{\text{lipid}}/d_{\text{w}_{\text{biomass}}}$]) after 45 h. At the end of the fermentation (at 138 h), lipid productivity was $0.71 \text{ g L}^{-1} \text{ h}^{-1}$ (biomass: 115.6 g L^{-1} , lipids: 85% [$w_{\text{lipid}}/d_{\text{w}_{\text{biomass}}}$]).

C. oleaginosus biomass lysis and lipid release were mediated by subsequent glucohydrolase and protease treatments, as described previously. The resulting liquid hydrolysate, which contained sugars, amino acids, and micronutrients, was filtered using a 10 kDa cross-filter for sterilisation and to remove the remaining enzyme residues. Thereafter, the hydrolysate was adjusted to 60 g L^{-1} glucose and used as the fermentation medium in an additional cultivation cycle.

Interestingly, with this hydrolysate containing fermentation medium, the biomass productivity was considerably increased to 147 g L^{-1} after 45 h. Concurrently, the lipid productivity was found to be $2.4 \text{ g L}^{-1} \text{ h}^{-1}$ (biomass: 147 g L^{-1} , lipids: 73% [$w_{\text{lipid}}/d_{\text{w}_{\text{biomass}}}$]). These results could be exactly reproduced in the subsequent third cultivation run (Fig. 6). The biomass and lipid productivities as well as respective total yields, were superior to any previous results. Consequently, these values significantly exceeded the highest values for biomass and lipid productivities reported in the literature by 1.5- and 2.9-fold, respectively⁶⁴ (Table 1). Moreover, current data indicated that superior biomass and lipid productivities were obtained within the first 45 h of the experiment. Therefore, we suggest that for cost efficiency and improved mass production, fermentation

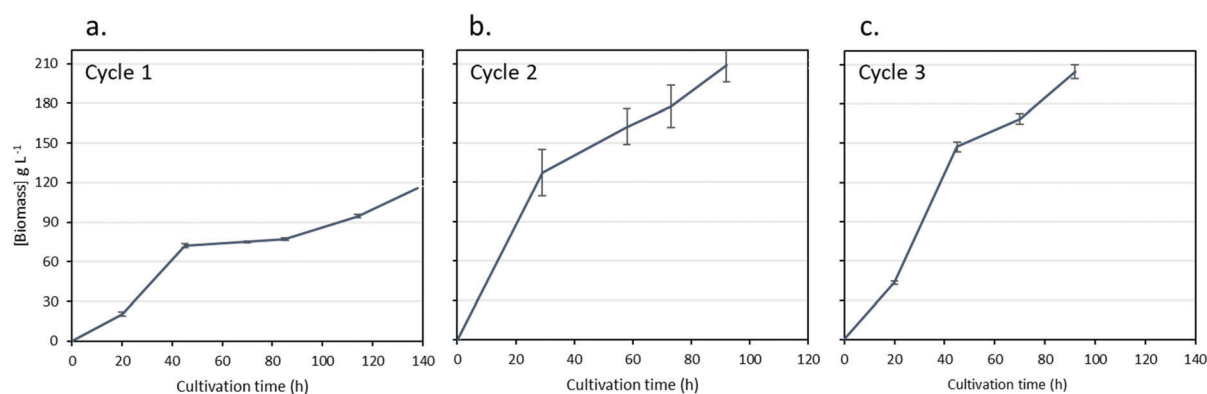


Fig. 6 Biomass growth (*via* the gravimetric method) over acetic acid and glucose co-fermentation time. In cycle 1, nitrogen-rich medium was used; in cycles 2 and 3, medium was the generated yeast cell hydrolysate from the previous cultivation run.

Table 1 Overall summary of lipid productivity obtained in this work in comparison with the best records for different oleaginous yeasts

Operation mode	Fermentation based	Medium	Oleaginous yeasts	Lipid productivity ($\text{g L}^{-1} \text{h}^{-1}$)	Biomass concentration (g L^{-1})	Lipid content $\frac{w_{\text{lipid}}}{w_{\text{biomass}}}$	Ref.
Batch-fermentation	Glucose	N-limited medium (A)	<i>C. oleaginosus</i>	0.09	34	45	Current work
Batch-fermentation	Acetic acid	N-rich medium (B)	<i>C. oleaginosus</i>	0.13	22	72	Current work
Batch-fermentation	Co-fermentation	N-limited medium (C)	<i>C. oleaginosus</i>	0.18	43	73.5	Current work
Batch-fermentation	Co-fermentation	N-rich medium (D)	<i>C. oleaginosus</i>	0.53	84	85	Current work
Batch-fermentation	Co-fermentation	<i>Laminaria digitata</i> hydrolysate	<i>C. oleaginosus</i>	0.59	114	64	Current work
Semi-continuous	Co-fermentation	N-rich medium (D)	<i>C. oleaginosus</i>	0.9	235	85	Current work
Continuous	Co-fermentation	N-rich medium (D)	<i>C. oleaginosus</i>	1.2	240	84	Current work
Batch-fermentation	Co-fermentation	<i>C. oleaginosus</i> hydrolysate	<i>C. oleaginosus</i>	2.4	147	73	Current work
Batch-fermentation	Co-fermentation with cellobiose and xylose	N-limited	<i>L. starkeyi</i>	0.12	31.5	55	41
Batch-fermentation	Glucose	Corn stover hydrolysate	<i>R. graminis</i>	0.23	48	34	42
Batch-fermentation	Glucose	N-limited	<i>R. toruloides</i> Y4	0.54	106.5	67.5	43
pH-Stat fermentation	Acetic acid	N-rich	<i>C. oleaginosus</i>	0.66	168	75	18
Fed-batch fermentation	Glucose	N-limited	<i>Y. lipolytica</i> NS432	0.73	110	77	44
Oxygen-rich batch fermentation	Glucose	N-limited	<i>R. glutinis</i>	0.87	185	40	45

times as short as 45–72 h may be sufficient to obtain maximum yields.

Techno-economic analysis

To evaluate the economic advantages of the presented process and to determine the best operational set-up, a TEA was conducted.

The capital investment charged to this project was estimated to be \$133.4 M for commercial-scale realisation. This cost included equipment installation, engineering, construction, start-up costs, and working capital with a 6% interest factor for 20-year capital depreciation. Based on the baseline scenario, an annual operation cost of \$15.5 M was estimated (Fig. 7c). The raw material cost, based on the wholesale market price, was estimated at \$15.3 M (Fig. 7b). The total annual costs were subsequently estimated at \$37.49 M (Fig. 7a). Based on these figures, the baseline scenario for microbial lipid cost was estimated at \$1.6 per kg (Tables S3–S11, ESI[†]).

Fig. S9–S11 (ESI[†]) represent a sensitivity analysis for the lipid costs based on the most influential process input parameters. Based on this analysis, lipid productivity, acetic acid cost, electric tariffs, and consumption had the highest impact on lipid cost.

More specifically, the lipid productivity in turn correlated very well with the biomass harvesting time and data reproducibility. Within the six represented biological replica (Fig. S13, ESI[†]), the lipid productivity could vary between 1.33 and 1.47 $\text{g L}^{-1} \text{h}^{-1}$ (with a relative standard deviation of $\pm 5\%$), which corresponded to a lipid cost variation between \$1.67 and \$1.53 per kg. Interestingly, the fermentation time had the highest influence on the lipid cost; harvesting times of 24, 48, 72, and 120 h after fermentation initiation corresponded to lipid productivities of 1.13, 1.93, 2.4, and 1.4 $\text{g L}^{-1} \text{h}^{-1}$, respectively, which translated to lipid costs of \$2.0, \$0.96, \$1.1 and \$1.6 per kg, respectively (Fig. S11, ESI[†]).

The raw materials cost was driven by the cost of acetic acid, which accounted for 85% of the total raw materials cost. Accordingly, because acetic acid was the main cost driver in the process chain, the lipid cost varied between \$1.06 and \$1.97 per kg when the acetic acid cost varied from \$0.1 to \$0.3 per kg.

Aeration (centrifugal compressor) consumed about 70% of the total electricity required for the entire plant operation (Fig. S12, ESI[†]). Therefore, the plant electricity consumption was controlled mainly by compressor efficiency (with 70% in the baseline scenario) and aeration required (at 0.8 vvm in the baseline scenario). Please see Fig. S10 and S11 (ESI[†]) for sensitivity cost analysis of compressor efficiency, and aeration. Hence, a fermentation carried out at 1.25–1.5 bar is preferable to maintain the aeration at lower vvm values. Notably, the electricity costs vary with local conditions and pricing regimens. In that regard, Germany has one of the highest electric tariffs in the EU. In contrast, other EU countries, such as Sweden, have significantly lower electric tariffs (\$0.053 kW h). Consequently, the lipid cost can be varied from \$1.42 to \$1.6 per kg when alternative electric tariff scenarios are assumed (Fig. S10 and S11, ESI[†]).

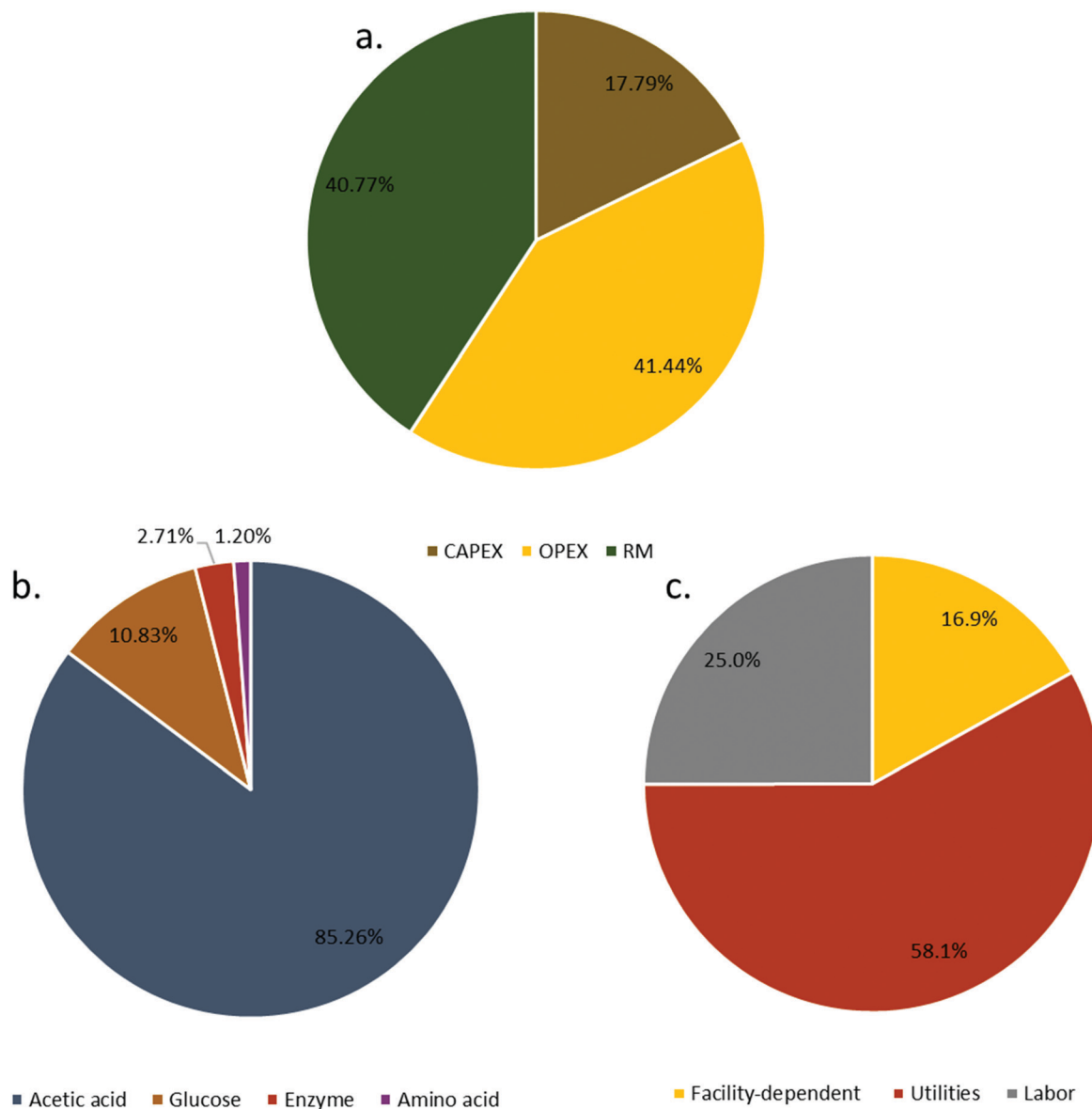


Fig. 7 Comprehensive techno-economic cost analysis. (a) The contribution of capital cost (CAPEX), operation cost (OPEX), and raw material (RM) cost to the overall MO lipid cost. (b) The contribution of major chemicals to the total raw material cost. (c) The contribution of operation cost sectors to the total operation cost.

A literature glucose-based TEA of yeast oil production previously proposed \$5.5 per kg as the estimated yeast lipid cost.⁸ The designed production plant had 12 fermenters (250 m³ each), with a total capacity of 10 000 megatons year⁻¹. However, plant construction as part of the capital cost and maintenance as part of the operational cost were not considered in this report. Moreover, labour and electricity costs were estimated to be \$25 000 year⁻¹ worker⁻¹ and \$0.06 kW h, respectively; these costs have doubled since 2014.

The price of conventional palm oil is still quite low (\$0.50 per kg).⁹ However, eco-certified products, implying the use of organic-certified oils in the matrix, are significantly more expensive (\$2.1 per kg).⁷⁶ Thus, the cost of the yeast-based oil is similar to or less than that of eco-certified palm oil.

LCA for global warming potential GWP

Although we conducted a comprehensive LCA (see Table S22, ESI[†]) of the presented process chain for yeast oil production, we were particularly interested in the GWP of the process compared with that of plant oil production. This focus was implemented in the context of LCA analysis, in which GWP is the largest factor affecting production of plant oil *versus* yeast oil.

The LCA indicated an overall global warming potential of 3.56 kg CO₂ equivalents to be emitted for every 1 kg yeast oil produced. Yeast fermentation and electricity production contributed 30% and 25% of the total CO₂ emission, respectively (Fig. 8).

According to our defined model, procurement of the acetic acid generated 45% of the total CO₂ emission. More specifically, in this acetic acid procurement chain, initial methanol production

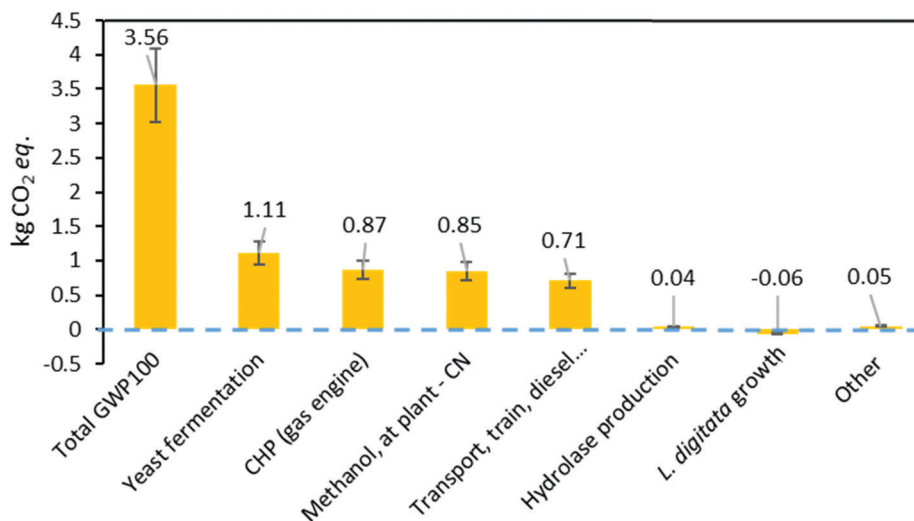


Fig. 8 GHG emission from yeast lipid production during the production steps, starting from raw material procurement to the final product.

from natural gas and acetic acid transport from China to Germany *via* diesel-powered train (approximately 12 500 km) were the main elements responsible for significant CO₂ emission. Therefore, obtaining the acetic acid in our defined process model would have the most negative impact on the environment. Although our defined model represented the conventional route for procurement of acetic acid, alternative methods for procuring this feedstock using existing bio-based acetic acid production processes would significantly improve the environmental impact of the presented process chain.^{21–23} In this context, acetate production using both carbon dioxide and hydrogen (generated by water electrolysis with sustainable energy) as fermentation substrates could significantly enhance the climate potential in the LCA.^{21–23} This particular scenario would reduce the reported 45% CO₂ emission contribution and offer an indirect recycling method for the generated CO₂ during fermentation and electricity production. Alternatively, oxidation of bio-ethanol to yield acetic acid may be used and has already been established at an industrial scale in Sweden.⁷⁷ This scenario could considerably reduce the climate impact because it is based on bio-ethanol, which is generated by fermentative conversion of forestry waste streams. Alternatively, the use of an acetic acid supplier in Europe would significantly reduce the distance required for acetic acid transportation. However, in the current model, petrochemical acetic acid was used as a main feedstock for the yeast because of economic reasons and a lack of commercial-scale LCA data. In order to obtain fully renewable oils, future work will focus on the use of bio-based acetic acid.

A literature-based LCA of five plant-based oil production processes indicated that generation of 1 kg palm oil, soybean oil, rapeseed oil, sunflower oil, and peanut oil will generate 4.2, 4.5, 2.9, 3.5, and 7.5 kg CO₂ equivalents, respectively.⁴⁸ These results were similar to those obtained for current yeast oil production processes. Moreover, the CO₂ emissions for yeast oil production were lower than those reported for the conventional palm oil production process. While palm oil is the most

industrially relevant plant oil, current yeast oil processes may represent a favourable alternative. Indeed, the presented yeast oil production process has several inherent advantages over plant-based oils; in particular, it does not induce land use change or negatively impact agricultural activity. Consequently, it does not compete with food production. Since fermentation can be carried out in conventional stirred tank fermenters, it also has no negative impact on biodiversity.

In addition to these LCA results, the new process is completely free of organic solvents, whereas conventional yeast lipid production and some plant oil processing requires toxic solvent extraction.⁷⁸ A previous TEA of conventional yeast oil production estimated an annual hexane need of about 444 tons year⁻¹.⁸ By accepting the assumption that 98% of that hexane can be recovered, a mean fugitive hexane emission of 2% during the storage, handling, distillation, and purification would result in emission of 8.9 tons year⁻¹ hexane.

Conclusions

The production of plant-based oil-derived biofuels and sustainable oleochemicals negatively affects biodiversity. This competition results in increased food prices and accelerates changes in land use. The scenario intensifies, when the food demand of a globally increasing population is taken into account, further damaging sensitive ecosystems. Accordingly, it is important to identify sustainable triglyceride production routes independent of terrestrial plant biomass. Yeasts have advantages over other single-cell lipid producers, such as microalgae or bacteria, because yeasts can grow rapidly to a relatively high cell density, facilitating their applications in single-cell lipid production. However, the carbon source, productivity, downstream processing, and waste treatment may cause yeast oil production to be costly, creating a great price gap compared with plant-based lipids.

In this study, we established an integrated operation for bioconversion of acetic acid and sugar to sustainable lipids at maximum productivity with minimal waste generation and energy consumption; the cost gap compared with plant-based lipids was considerably reduced.

Microalgae are also promising lipid producers, and the process loop may be closed by direct fixation of the fermentative CO₂ during biomass and lipid formation. Additionally, yeast can utilise the O₂ and sugars generated from microalgae biomass, and fermentative production of acetic acid, whether from bioethanol (based on microalgae biomass as feedstock) or CO₂ and H₂, can improve the cycle sustainability. Application of such potential future-state integrated autotrophic processes may help satisfy global demand for triglycerides while maintaining environmental ecosystems. We are currently performing studies to enhance and diversify the productivity and applicability of the technology platform with respect to bio-based feedstocks and the generation of tailored lipid products for the food and pharmaceuticals markets. The latter will be achieved by combining both process- and genetic engineering-related aspects associated with the microbial production host.⁷⁹

The approach established in this report links previous efforts to a forward-thinking optimised approach. Thus, we believe there are still many possible parameters to be optimised and metabolic modifications that can be implemented to further improve productivity. Moreover, proteomic and metabolomic analyses could further guide process development.

Conflicts of interest

There are no conflicts of interest to report.

Acknowledgements

MM, DG, NM, and TB gratefully acknowledge the support of the Werner Siemens Foundation for establishing the Department of Synthetic Biotechnology at the Technical University of Munich. MM and TB gratefully acknowledge financial support from the German Federal Ministry of Education and Research for the “LIPOMAR” (grant number: 031A261) and “CO₂ Lubricants” (grant number: 033RC012B) projects. DG and TB would like to acknowledge the financial support of the ChiBio project (grant number: 289284) by the EU. We would like to gratefully acknowledge the expert opinion and consultation of Prof. Dr Uwe Arnold, managing director of AHP Group GmbH that allowed for significant improvements in our techno-economic analysis layout. Moreover, we gratefully acknowledge the expertise and assistance of Mrs Elke Breitmayer (MSc) in improving our LCA assessment of the presented yeast oil production process.

References

- 1 US Energy Information Administration, Monthly Energy Review July 2017, U.S. Department of Energy, USA, 2017.
- 2 J. Fargione, J. Hill, D. Tilman, S. Polasky and P. J. S. Hawthorne, *Science*, 2008, **319**, 1235–1238.
- 3 T. Searchinger, R. Heimlich, R. A. Houghton, F. Dong, A. Elobeid, J. Fabiosa, S. Tokgoz, D. Hayes and T.-H. J. S. Yu, *Science*, 2008, **319**, 1238–1240.
- 4 E. B. Fitzherbert, M. J. Struebig, A. Morel, F. Danielsen, C. A. Brühl, P. F. Donald and B. Phalan, *Trends Ecol. Evol.*, 2008, **23**, 538–545.
- 5 B. Wicke, R. Sikkema, V. Dornburg and A. Faaij, *Land Use Policy*, 2011, **28**, 193–206.
- 6 A. T. McCurdy, A. J. Higham, M. R. Morgan, J. C. Quinn and L. C. Seefeldt, *Fuel*, 2014, **137**, 269–276.
- 7 S. Pinzi, D. Leiva, I. López-García, M. D. Redel-Macías and M. P. Dorado, *Biofuels, Bioprod. Biorefin.*, 2014, **8**, 126–143.
- 8 A. A. Koutinas, A. Chatzifragkou, N. Kopsahelis, S. Papanikolaou and I. K. Kookos, *Fuel*, 2014, **116**, 566–577.
- 9 Q. Gao, D. D. Binns, L. N. Kinch, N. V. Grishin, N. Ortiz, X. Chen and J. M. Goodman, *J. Cell Biol.*, 2017, **216**, 3199–3217.
- 10 P. Meesters, G. Huijberts and G. Eggink, *Appl. Microbiol. Biotechnol.*, 1996, **45**, 575–579.
- 11 Y. Liang, T. Tang, T. Siddaramu, R. Choudhary and A. L. Umagiliyage, *Renewable Energy*, 2012, **40**, 130–136.
- 12 Y. Hwan Seo, I. Gyu Lee and J. In Han, *Bioresour. Technol.*, 2013, **135**, 304–308.
- 13 X. Zhang, S. Yan, R. D. Tyagi, R. Y. Surampalli and J. R. Valéro, *Fuel*, 2014, **134**, 274–282.
- 14 X. Xu, J. Y. Kim, Y. R. Oh and J. M. Park, *Bioresour. Technol.*, 2014, **169**, 455–461.
- 15 M. A. Masri, W. Jurkowski, P. Shaigani, M. Haack, N. Mehlmer and T. Brück, *Appl. Energy*, 2018, **224**, 1–12.
- 16 A. Meo, X. L. Priebe and D. Weuster-Botz, *J. Biotechnol.*, 2017, **241**, 1–10.
- 17 M. A. Masri, S. Younes, M. Haack, F. Qoura, N. Mehlmer and T. Brück, *Energy Technol.*, 2018, **6**, 1026–1038.
- 18 L. Lardon, A. Helias, B. Sialve, J.-P. Steyer and O. Bernard, *Environ. Sci. Technol.*, 2009, **43**, 6475–6481.
- 19 K. A. Jung, S.-R. Lim, Y. Kim and J. M. Park, *Bioresour. Technol.*, 2013, **135**, 182–190.
- 20 K. Gao and K. R. McKinley, *J. Appl. Phycol.*, 1994, **6**, 45–60.
- 21 J. H. Sim, A. H. Kamaruddin, W. S. Long and G. Najafpour, *Enzyme Microb. Technol.*, 2007, **40**, 1234–1243.
- 22 J. L. Gaddy, *US Pat.*, US5593886A, 1997.
- 23 M. Straub, M. Demler, D. Weuster-Botz and P. Dürre, *J. Biotechnol.*, 2014, **178**, 67–72.
- 24 P. Pal and J. Nayak, *Sep. Purif. Rev.*, 2017, **46**, 44–61.
- 25 E. V. LaBelle and H. D. May, *Front. Microbiol.*, 2017, **8**, 756.
- 26 Z. Gong, H. Shen, W. Zhou, Y. Wang, X. Yang and Z. K. Zhao, *Biotechnol. Biofuels*, 2015, **8**, 189.
- 27 Z. Chi, Y. Zheng, J. Ma and S. Chen, *Int. J. Hydrogen Energy*, 2011, **36**, 9542–9550.
- 28 X. Xu, J. Y. Kim, H. U. Cho, H. R. Park and J. M. Park, *Chem. Eng. J.*, 2015, **264**, 735–743.
- 29 V. Béliçon, L. Poughon, G. Christophe, A. Lebert, C. Larroche and P. Fontanille, *Bioresour. Technol.*, 2015, **192**, 582–591.
- 30 P. Fontanille, V. Kumar, G. Christophe, R. Nouaille and C. Larroche, *Bioresour. Technol.*, 2012, **114**, 443–449.

- 31 Z. Gong, W. Zhou, H. Shen, Z. Yang, G. Wang, Z. Zuo, Y. Hou and Z. K. Zhao, *Bioresour. Technol.*, 2016, **207**, 102–108.
- 32 Z. Li, L. Zhang, X. Shen, B. Lai and S. Sun, *Weishengwuxue Tongbao*, 2000, **28**, 72–75.
- 33 A. L. Colombo, A. C. B. Padovan and G. M. Chaves, *Clin. Microbiol. Rev.*, 2011, **24**, 682–700.
- 34 J. M. Ageitos, J. A. Vallejo, P. Veiga-Crespo and T. G. Villa, *Appl. Microbiol. Biotechnol.*, 2011, **90**, 1219–1227.
- 35 E. G. Bligh and W. J. Dyer, *Can. J. Biochem. Physiol.*, 1959, **37**, 911–917.
- 36 A. Ahamed and P. Vermette, *Biochem. Eng. J.*, 2008, **40**, 399–407.
- 37 N. R. Baral, O. Kavvada, D. Mendez-Perez, A. Mukhopadhyay, T. S. Lee, B. A. Simmons and C. D. Scown, *Energy Environ. Sci.*, 2019, **12**, 807–824.
- 38 F. Xu, J. Sun, N. Konda, J. Shi, T. Dutta, C. D. Scown, B. A. Simmons and S. Singh, *Energy Environ. Sci.*, 2016, **9**, 1042.
- 39 J. Sun, N. M. Konda, J. Shi, R. Parthasarathi, T. Dutta, F. Xu, C. D. Scown, B. A. Simmons and S. Singh, *Energy Environ. Sci.*, 2016, **9**, 2822–2834.
- 40 D. P. Petrides, *Comput. Chem. Eng.*, 1994, **18**, S621–S625.
- 41 D. Petrides, *Bioseparations Science and Engineering*, 2000.
- 42 SuperPro Designer, User's Guide V10, http://www.intelligen.com/downloads/SuperPro_ManualForPrinting_v10.pdf, accessed 2019.
- 43 D. Humbird, R. Davis, L. Tao, C. Kinchin, D. Hsu, A. Aden, P. Schoen, J. Lukas, B. Olthof and M. Worley, *Process design and economics for biochemical conversion of lignocellulosic biomass to ethanol: dilute-acid pretreatment and enzymatic hydrolysis of corn stover*, National Renewable Energy Lab. (NREL), Golden, CO (United States), 2011.
- 44 F. government, public service information, <https://oeffentlicherdienst.info/tv-l/west/>.
- 45 National Renewable Energy Laboratory (NREL), U.S. Life Cycle Inventory Database, <https://www.nrel.gov/lci/>.
- 46 L. Schebek, The open source data platform for bio-energy in Germany, <http://www.bioenergiesdat.de/>, accessed 2018.
- 47 C. Liptow, A.-M. Tillman, M. Janssen, O. Wallberg and G. A. Taylor, *Int. J. Life Cycle Assess.*, 2013, **18**, 1071–1081.
- 48 J. H. Schmidt, *J. Cleaner Prod.*, 2015, **87**, 130–138.
- 49 S. Giannattasio, N. Guaragnella, M. Ždravlečić and E. Marra, *Front. Microbiol.*, 2013, **4**, 33.
- 50 S. Papanikolaou and G. Aggelis, *Eur. J. Lipid Sci. Technol.*, 2011, **113**, 1031–1051.
- 51 Z. Ruan, W. Hollinshead, C. Isaguirre, Y. J. Tang, W. Liao and Y. Liu, *Bioresour. Technol.*, 2015, **183**, 18–24.
- 52 R. Kourist, F. Bracharz, J. Lorenzen, O. N. Kracht, M. Chovatia, C. Daum, S. Deshpande, A. Lipzen, M. Nolan and R. A. Ohm, *mBio*, 2015, **6**, e00918.
- 53 L. Liu, H. Redden and H. S. Alper, *Curr. Opin. Biotechnol.*, 2013, **24**, 1023–1030.
- 54 Z. Zhu, S. Zhang, H. Liu, H. Shen, X. Lin, F. Yang, Y. J. Zhou, G. Jin, M. Ye and H. Zou, *Nat. Commun.*, 2012, **3**, 1112.
- 55 F. Deeba, V. Pruthi and Y. S. Negi, *Bioresour. Technol.*, 2016, **213**, 96–102.
- 56 Q. Gao, Z. Cui, J. Zhang and J. Bao, *Bioresour. Technol.*, 2014, **152**, 552–556.
- 57 M. Xavier, A. Coradini, A. Deckmann and T. Franco, *Biochem. Eng. J.*, 2017, **118**, 11–19.
- 58 B. S. Dien, J. Zhu, P. J. Slininger, C. P. Kurtzman, B. R. Moser, P. J. O'Bryan, R. Gleisner and M. A. Cotta, *RSC Adv.*, 2016, **6**, 20695–20705.
- 59 S. Harde, Z. Wang, M. Horne, J. Zhu and X. Pan, *Fuel*, 2016, **175**, 64–74.
- 60 E. Palmqvist and B. Hahn-Hägerdal, *Bioresour. Technol.*, 2000, **74**, 17–24.
- 61 E. Palmqvist and B. Hahn-Hägerdal, *Bioresour. Technol.*, 2000, **74**, 25–33.
- 62 Z. Gong, Q. Wang, H. Shen, C. Hu, G. Jin and Z. K. Zhao, *Bioresour. Technol.*, 2012, **117**, 20–24.
- 63 S. Galafassi, D. Cucchetti, F. Pizza, G. Franzosi, D. Bianchi and C. Compagno, *Bioresour. Technol.*, 2012, **111**, 398–403.
- 64 Y. Li, Z. K. Zhao and F. Bai, *Enzyme Microb. Technol.*, 2007, **41**, 312–317.
- 65 J. Friedlander, V. Tsakraklides, A. Kamineneni, E. H. Greenhagen, A. L. Consiglio, K. MacEwen, D. V. Crabtree, J. Afshar, R. L. Nugent and M. A. Hamilton, *Biotechnol. Biofuels*, 2016, **9**, 77.
- 66 J. G. Pan, M. Y. Kwak and J. S. Rhee, *Biotechnol. Lett.*, 1986, **8**, 715–718.
- 67 K. V. Probst, L. R. Schulte, T. P. Durrett, M. E. Rezac and P. V. Vadlani, *Crit. Rev. Biotechnol.*, 2016, **36**, 942–955.
- 68 E. M. Grima, E.-H. Belarbi, F. A. Fernández, A. R. Medina and Y. Chisti, *Biotechnol. Adv.*, 2003, **20**, 491–515.
- 69 A. L. Stephenson, E. Kazamia, J. S. Dennis, C. J. Howe, S. A. Scott and A. G. Smith, *Energy Fuels*, 2010, **24**, 4062–4077.
- 70 J.-Y. You, C. Peng, X. Liu, X.-J. Ji, J. Lu, Q. Tong, P. Wei, L. Cong, Z. Li and H. Huang, *Bioresour. Technol.*, 2011, **102**, 6088–6094.
- 71 K. Liang, Q. Zhang and W. Cong, *J. Agric. Food Chem.*, 2012, **60**, 11771–11776.
- 72 C.-C. Fu, T.-C. Hung, J.-Y. Chen, C.-H. Su and W.-T. Wu, *Bioresour. Technol.*, 2010, **101**, 8750–8754.
- 73 G. Jin, F. Yang, C. Hu, H. Shen and Z. K. Zhao, *Bioresour. Technol.*, 2012, **111**, 378–382.
- 74 I. Herpoël-Gimbert, A. Margeot, A. Dolla, G. Jan, D. Mollé, S. Lignon, H. Mathis, J.-C. Sigoillot, F. Monot and M. Asther, *Biotechnol. Biofuels*, 2008, **1**, 18.
- 75 V. G. Gupta, M. Schmoll, A. Herrera-Estrella, R. Upadhyay, I. Druzhinina and M. Tuohy, *Biotechnol. Biol. Trichoderma*, Newnes, 2014.
- 76 Whole sell Alibaba, https://www.alibaba.com/product-detail/Best-Quality-cheap-organic-refined-Crude_60360488487.html?spm=a2700.7724838.2017115.32.19e47183hns6af&s=p.
- 77 SEKAB, a chemical & cleantech company, <http://www.sekab.com/>.
- 78 S. Bemesson, Life cycle assessment of rapeseed oil, rape methyl ester and ethanol as fuels – a comparison between large- and smallscale production, 2004, <https://www.osti.gov/etdeweb/servlets/purl/20567425>.
- 79 C. Görner, V. Redai, F. Bracharz, P. Schrepfer, D. Garbe and T. Brück, *Green Chem.*, 2016, **18**, 2037–2046.

 BIOFUELS

Palms make way for oleaginous yeast



The short fermentation time ... and solvent-free lipid recovery improve economic and ecological process parameters



Palm oil is useful because its low unsaturation confers oxidative stability desirable in kitchens and energy density desirable in fuels. The economic cost of palm oil is low, but the same cannot be said for its environmental cost, which includes habitat destruction and a net release of greenhouse gases. Triglycerides comparable to palm oil can be found in yeast grown on sugars produced from waste biomass and acetic acid from bacterial fermentation of CO/H₂ or CO₂/H₂ mixtures. Although sustainable, these feedstocks can be expensive, and yeast oils form in low abundance and must be extracted with an organic solvent. In view of this, Mahmoud Masri, Daniel Garbe, Norbert Mehlmer and Thomas Brück describe in *Energy & Environmental Science* a sustainable and economical process in which yeast cells, cultured in a nitrogen-rich medium, are enzymatically digested to liberate high yields of biodiesel-ready oils.

When yeast has plenty of C, N, P and S, it readily produces nucleic acids, proteins and polysaccharides, the latter two constituting a large fraction of the biomass of what is a

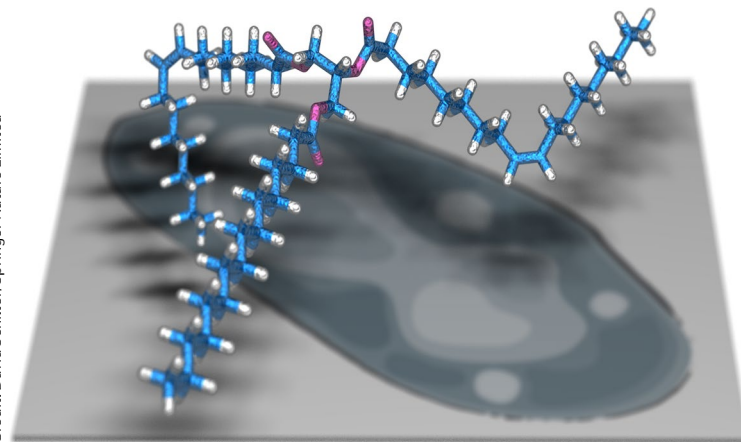
rapidly growing culture. When the heteroatoms are in short supply, yeast instead expresses fatty acid synthases to store C, via acetyl coenzyme A, as triglycerides that can be converted into other biomass when heteroatoms are available. To produce biomass quickly but not at the expense of triglycerides, Brück's team studied *Cutaneotrichosporon oleaginosus*, an oleaginous yeast that can comprise 80–90% triglyceride by dry weight (for reference, baker's yeast is <10% triglyceride). Culturing *C. oleaginosus* with different concentrations of sugars, acetic acid and yeast extract (a source of nitrogen) gave different profiles of total biomass and lipid mass fraction over time. Although some conditions result in diauxic yeast growth (phases of low and high triglyceride production), using glucose and acetic acid with nitrogen in abundance results in high monoauxic growth, a desirable regime in which lipid and biomass production are decoupled. This high-yielding fermentation in aerated, stirred tanks has a smaller spatial footprint than a palm plantation and is not subject to seasonal variability.

A fraction of the *C. oleaginosus* culture was periodically harvested and the cell walls (comprising chitin, glucans and proteins) digested using extracellular hydrolases expressed in *Trichoderma reesei*, grown in a separate vessel. The *C. oleaginosus* lysate comprises a biomass phase used to feed *T. reesei* and an aqueous phase that is recycled to sustain the remaining *C. oleaginosus*, which can be further supported with a brown-algae-derived feed instead of glucose. A third gravimetrically separable oil phase (a mixture similar to palm oil), rich in triglycerides of oleic (C₁₈, monounsaturated) and palmitic acid (C₁₆, saturated), is produced that can be hydrolysed to produce fatty acids for biodiesel use. “The short fermentation time (enabled by simultaneous lipid and biomass production) and solvent-free lipid recovery improve economic and ecological process parameters,” notes Masri. Techno-economic analyses predict that the yeast oil (US\$1.6 kg⁻¹) would be cheaper than eco-certified palm oil (US\$2.1 kg⁻¹) and result in lower CO₂ emissions.

It is remarkable how monoauxic growth with continually high triglyceride production can occur even in media with high N:C ratios. Brück and colleagues note that, regardless of the N:C ratio, *C. oleaginosus* expresses acetate coenzyme A ligase to directly convert acetic acid into acetyl coenzyme A. This enables fast and selective triglyceride production because fatty acid synthases from *C. oleaginosus* are particularly active. “We are working on a full proteomic and genomic analysis to identify these enzymes,” concludes Masri. A deeper understanding of the cellular systems biology would help improve an already promising system.

David Schilter

Credit: David Schilter/Springer Nature Limited



ORIGINAL ARTICLE Masri, M. A. et al.

A sustainable, high-performance process for the economic production of waste-free microbial oils that can replace plant-based equivalents. *Energy Environ. Sci.* <https://doi.org/10.1039/C9EE00210C> (2019)

A sustainable, high-performance process for the economic production of waste-free microbial oils that can replace plant-based equivalents

Mahmoud A. Masri^a, Daniel Garbe^a, Norbert Mehlmer^{*a}, and Thomas Brück^{*a}

^aDepartment of Chemistry, Werner Siemens Chair of Synthetic Biotechnology, Technical University of Munich

*Corresponding authors (norbert.mehlmer@tum.de; brueck@tum.de)

Supplementary Data

1.1. Maximizing lipid productivity

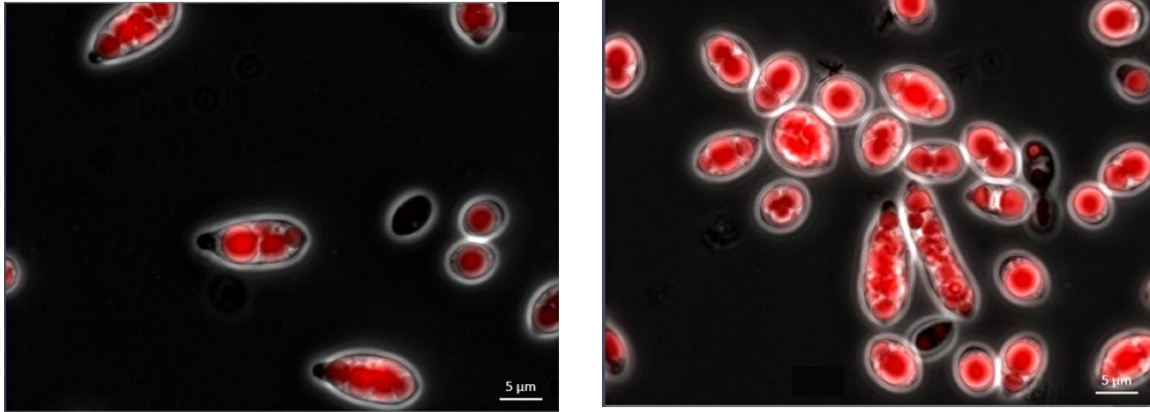


Figure S1: fluorescence microscope imaging shows a remarkable increase in the cell volume and lipid content for: Glucose-based fermentation in minimal nitrogen media (on the left) and co-fermentation in rich nitrogen media (on the right).

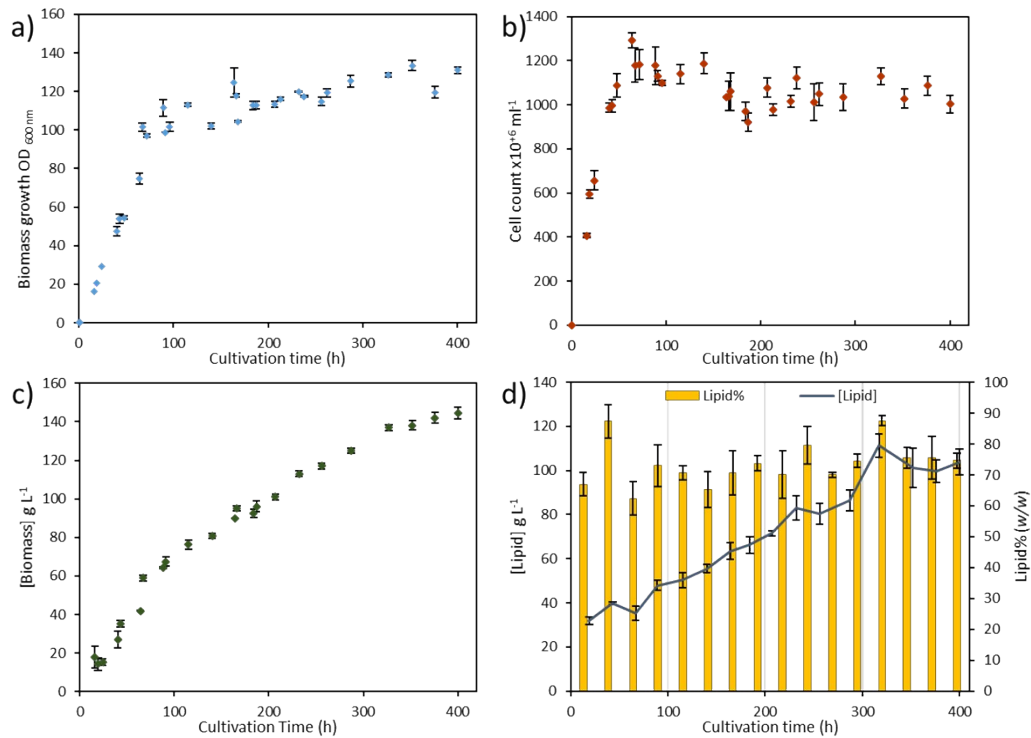


Figure S2: Growth rates and lipid accumulation during acetic acid and glucose co-fermentation in nitrogen-rich medium applying continuous fermentation mode. (a) Growth rates determined via the optical density. (b) Growth rates determined via the cell count. (c) Growth rates determined via the gravimetric method. (d) Lipid accumulation and productivity determined via the gravimetric method.

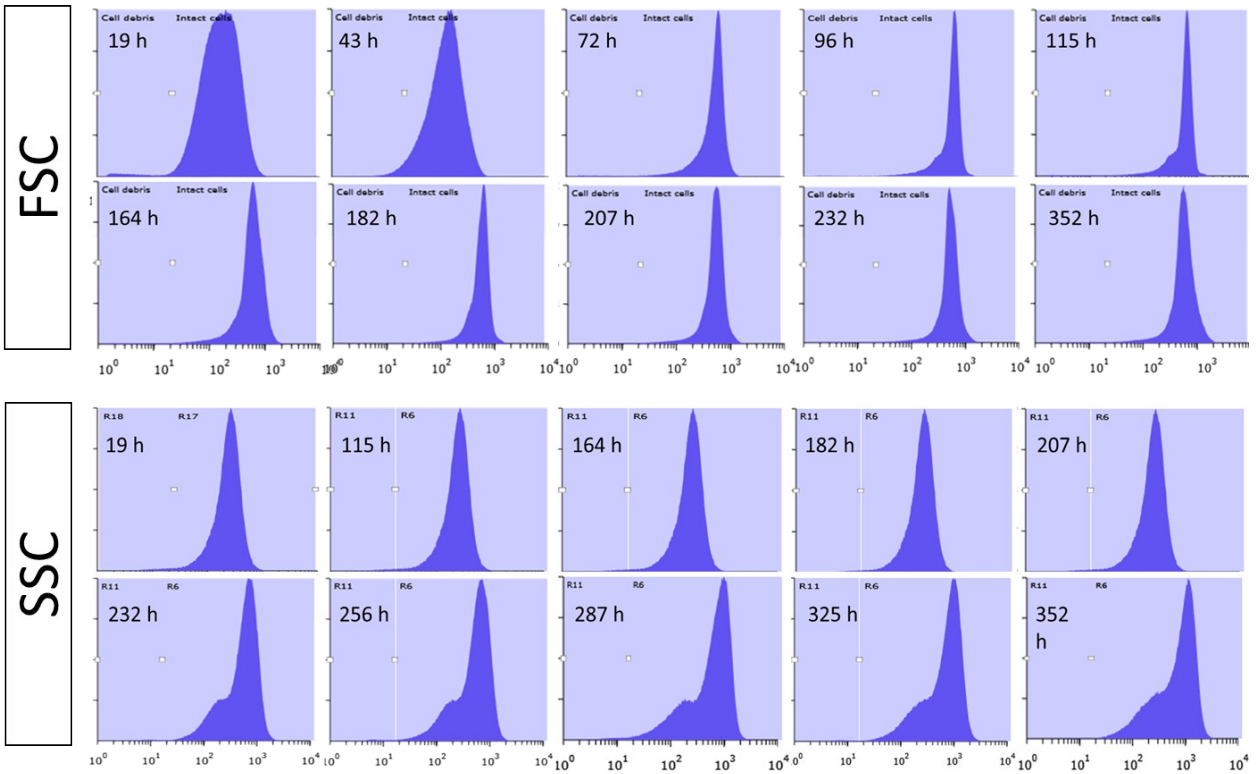


Figure S3: The increase in intensity of the forward scatter [FSC] (on x axis) and side scatter [SSC] (on y axis) over the acetic acid and glucose co-fermentation time in rich nitrogen media. The fermentation was carried out at: 25-liters, temp.: 28°C, pH 6.5 and $pO_2 \geq 50\%$.

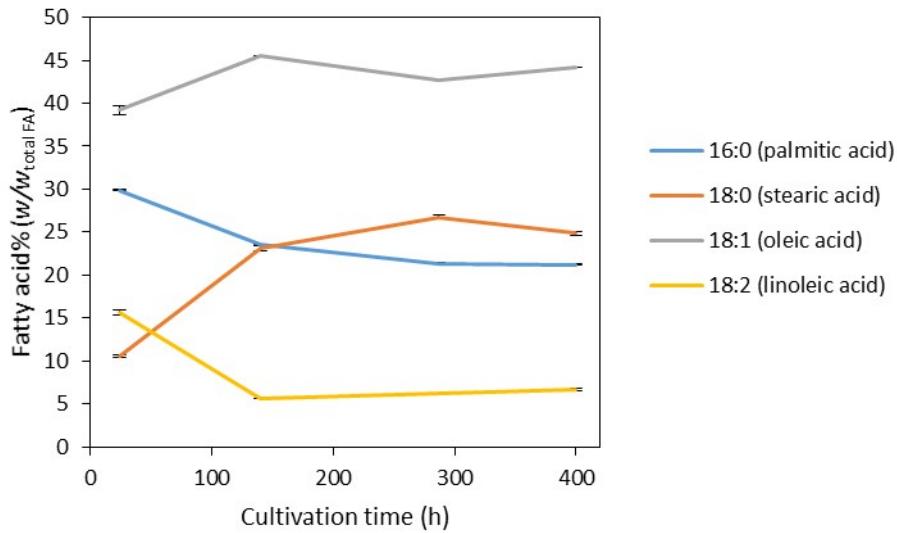


Figure S4: The changes in fatty acid profile over the acetic acid and glucose co-fermentation time in rich nitrogen media. The fermentation was carried out at: 25-liters, temp.: 28°C, pH 6.5 and $pO_2 \geq 50\%$.

Table S1: Yeast biomass analysis at the end of the semi-continuous run

	%(w/w)	Method
Sugar	8.3	Chemical hydrolysis with H ₂ SO ₄ at 1% and 3%
Lipid	87.6	3 times extraction with Folch solution (chloroform : methanol, in a 2:1 (vol/vol) ratio)
protein	3.5	Kjeldahl method, Kjeldahl factor 6.25
Ash	0.6	Incineration at 1200°C, 3h

1.2. Downstream processing and lipid recovery

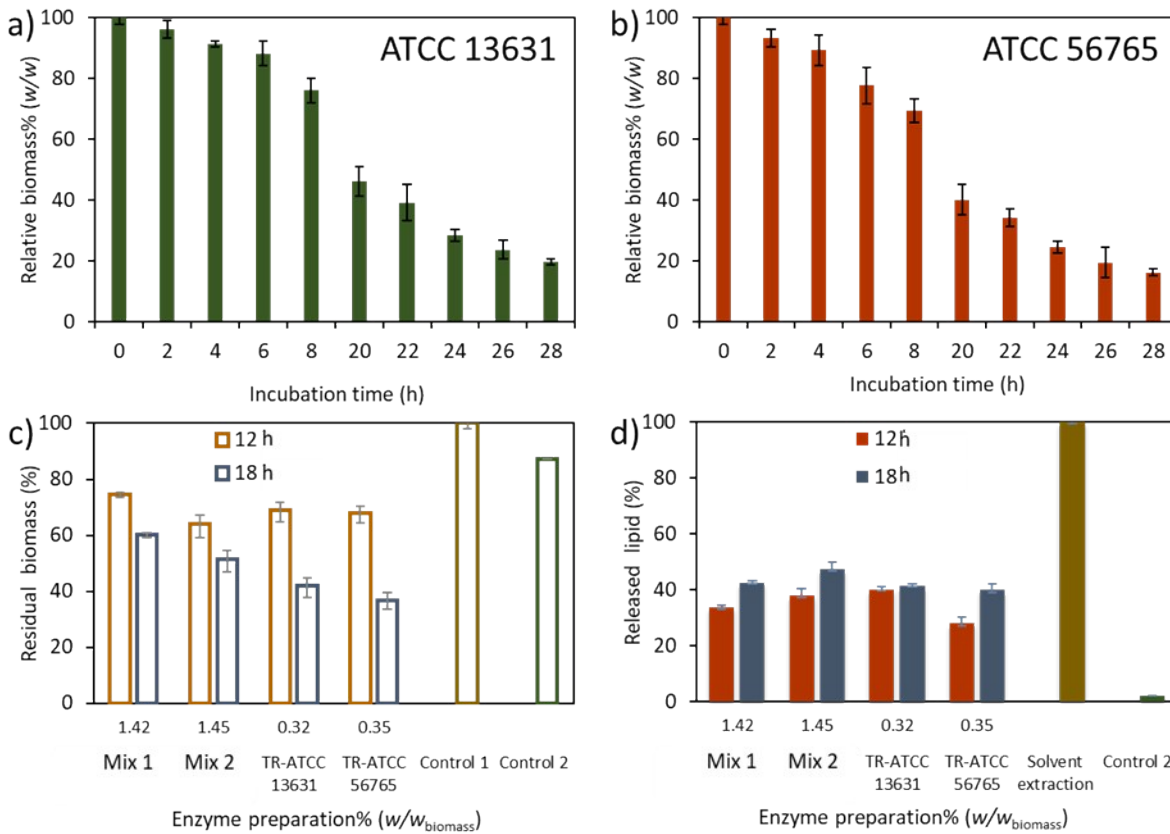


Figure S5: Evaluation of produced enzymes from *T. reesei* ATCC 13631 and RUT C-30 (ATCC 56765) on purified *C. oleaginosus*-processed biomass (a b) and fresh culture (c d). (a) Relative decrease in the *C. oleaginosus* biomass weight over the enzymatic hydrolysis time using *T. reesei* (ATCC 13631). (b) Relative decrease in the biomass weight over the enzymatic hydrolysis time using *T. reesei* RUT C-30 (ATCC 56765). (c) Relative residual biomass weight after 12 and 18 h of incubation with the following enzyme systems: mixes 1 and 2 (commercial mixtures), *T. reesei* ATCC 13631, and *T. reesei* RUT C-30 (ATCC 56765). (d) Relative released lipid weight after 12 and 18 h of incubation with the following enzyme systems: mixes 1 and 2 (commercial mixtures), *T. reesei* ATCC 13631, and *T. reesei* RUT C-30 (ATCC 56765). Controls: Control1(negative control): the biomass amount before treatment. Control2(positive control): Samples are incubated at same pH, tempreture and time but without adding enzyme. Solvent extreacton: amout of lipid which obtained after 3 times extraction with Folch solution (chloroform : methanol, in a 2:1 (vol/vol) ratio.

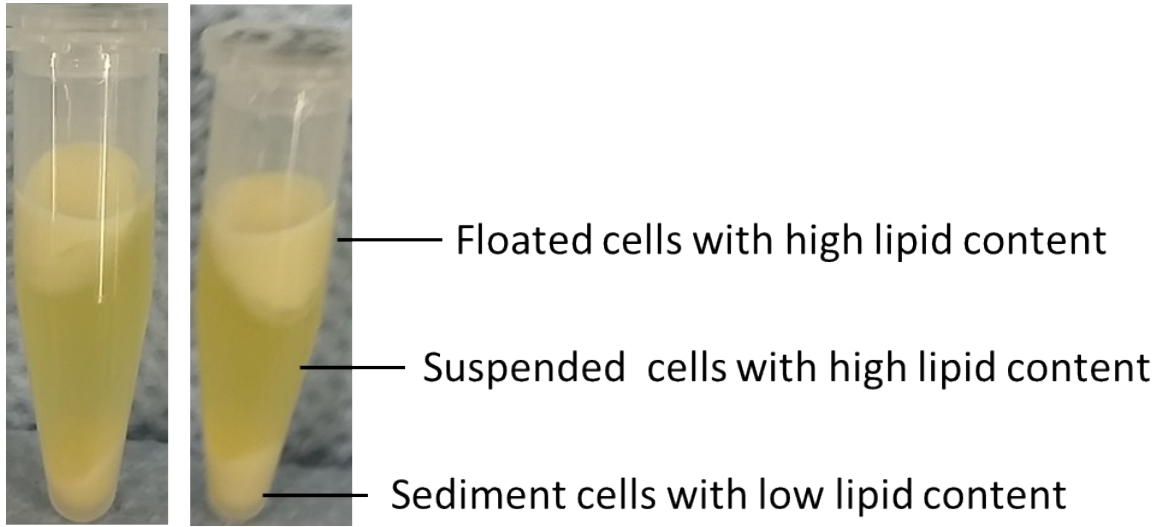


Figure S6: Yeast culture with high lipid content (75% w/w) after centrifugation at 15,000g for 30 min.

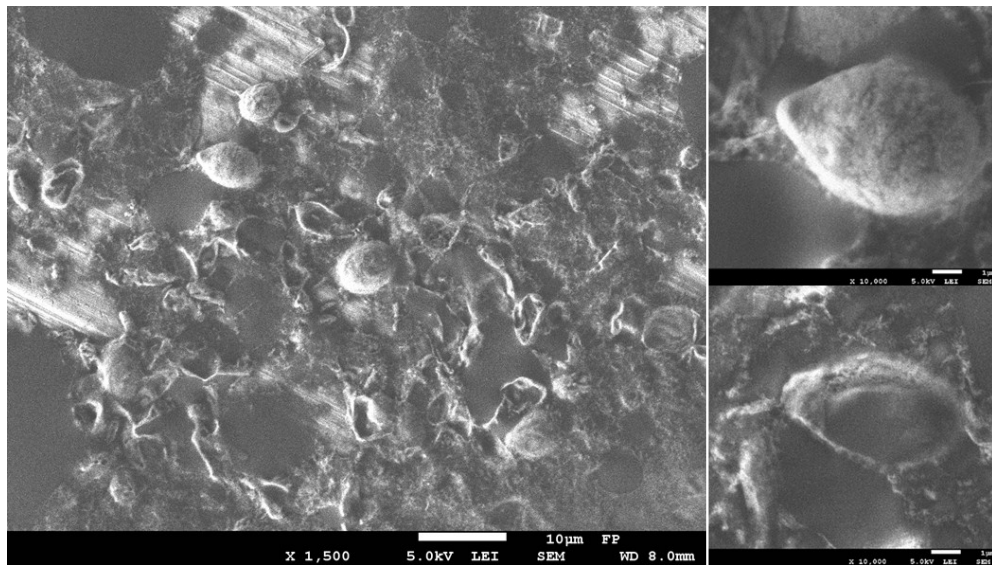


Figure S7: Electron microscope image for *C. oleaginosus* cells after treatment with high pressure homogenizer for 3 times at 2400 bar.

1.4. TEA

The TEA was carried out to estimate the total capital investment and operating cost for process flowsheets that could be used for the production of lipids from oleaginous yeast.

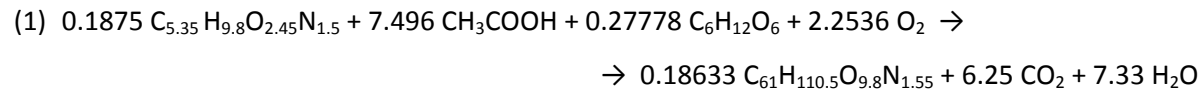
Due to the lack of major databases (such as NREL) in process design related to the oil production from oleaginous yeasts, process and economic data were collected from data generated in this study. Additionally, parameters extracted from available literature sources^{1-3, 4} and integrated mathematical function in SuperPro Designer version 10 - Intelligen, Inc. (SPD) were applied.

The Techno-Economic Analysis (TEA) was carried out for the estimation of the total capital investment and operating cost for process flowsheets that can be used for the production of yeast lipids. The industrial plant is required to operate 24 h daily, 7 days per week, which amounts to 8300 h y⁻¹. A standby fermenter and centrifuge are used to avoid maintenance-based operation downtime. With these prerequisites, the production capacity is of 23,000 t y⁻¹. The mass and energy balances as well as equipment sizing were determined using Excel spreadsheets and validated by SuperPro Designer V10 (Intelligen, Inc.). Installation factors, additional direct and indirect capital costs were estimated as percentage based on a Previous NREL publication about bioethanol production.⁵

Raw materials amounts were estimated based on the final lipid yield. A built-in mathematical function in SPD adjusts the equipment purchase price based on the required size of process equipment and the analysis year (2018). All the capital and operating data extracted from SPD are used to determine the minimum selling price.

A simplified process flow diagram (fig. S8) was generated based on the data presented in the paragraphs (2.1, 2.2 and 2.3). Thus, the co-fermentation in rich nitrogen media was carried out in consuming base feeding mode. The applied lipid productivity was of 1.4 g L⁻¹ h⁻¹ [biomass: 200 g L⁻¹ with lipid content of 83% (w/w), after 120 h]. The applied lipid productivity considers a baseline productivity value that was determined in the current study current for generation of a conservative TEA scenario.

As co-fermentation enables concurrent biomass growth and the lipid accumulation the mass balances were calculated by a single stoichiometric equation during the fermentation. The stoichiometric coefficients were appropriately calculated based on applied media and feed composition as well as the recorded biomass and lipid yields respectively. Lipid-biomass (biomass including the lipid, C₆₁H_{110.5}O_{9.8}N_{1.55}) was formulated based on the element analysis of C, H, N, and O. Amino acids formula C_{5.35}H_{9.8}O_{2.45}N_{1.5} is the average molecular of amino acid and it taken from Koutinas *et al*¹:



By enzymatic hydrolysis, lipid-biomass is converted to glucose, amino acid, released lipid ($C_{57} H_{104} O_6$), and non-lipid biomass ($C_4 H_{6.5} O_{1.9} N_{0.7}$). Glycerol trioleate ($C_{57} H_{104} O_6$) has been used representatively for the lipid formula since the $C_{18:1}$ fatty acid comprises 53% (*w/w*) of total fatty acid profile (Based on FAMES analysis). The non lipid-biomass formula ($C_4H_{6.5}O_{1.9}N_{0.7}$) was extracted from Babel and Muller.⁶

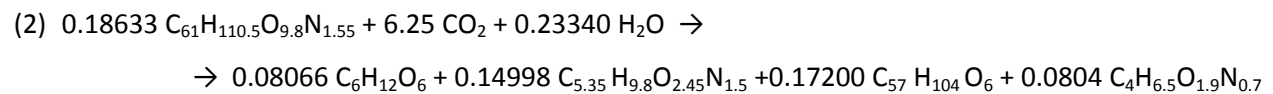


Figure S8 shows the process flow diagram for the yeast lipid production. Water, glucose and nitrogen sources (such as peptone and yeast extracts) are fed to the bioreactor (FR-101) (estimated process duration:6 h). Acetic acid is used as a feed during the fermentation time. *In-situ* sterilization is performed for 20 min at 121°C. After cooling, the fermentation starts by adding the inoculum at OD:0.1. The fermentation is controlled at 28°C, pH 6.5 (process duration:120h). The whole culture is transferred out to the enzymatic hydrolysis reactor (R-101). Transferring out, and transferring in are connected processes, running in parallel (estimated process duration:8 h). The enzymatic hydrolysis starts by adding the enzyme (process duration:20h). The final centrifugation (CD-101) will start in parallel to transferring the culture out from R-101 (estimated process duration:8 h). After centrifugation, 3 phases are generated. The upper phase contains pure lipid. The middle phase contains residual biomass. The lower phase contains the hydrolysate which is transferred (in parallel to centrifugation) into a cross-flow filtration unit (UF-101). The filtration results in a retentate fraction estimated to be 10% (*v/v*), the remaining filtrate will be about 90% (*v/v*). The filtrate will be mixed with additional amount of sugar and nutrition (in MX-103) and used for subsequent fermentation processes. Major operating and process parameters used to develop the process model and determine the required material are listed in the **Table2**.

Table S2: Major operating and process parameters used to develop the process model and determine the required material

Process parameters	Unite	Baseline	Optimal	Process parameters	Unite	Baseline	Optimal
Feed stock				Enzymatic hydrolysis			
Acetic acid	\$ per kg	0.2	0.1	hydrolysis time	h	24	20
Sugar	\$ per kg	0.3	0.2	Lipid release	% w/w	86	86
Peptone/ yeast extract	\$ per kg	0.3	0.2	non-lipid biomass conversion to nutrition*	% w/w	80	95
				Enzyme load*	% (w/w _{biomass})	1.4	-
				Enzyme price ⁵	\$ per kg	4	2
Centrifugal gas compressor							
volumetric throughput ^{7, 8}	m ³ min ⁻¹	380	-	Power consumption	kw m ⁻³	0.05	-
Pressure change ⁴	bar	5	-	hydrolysis temperature*	°C	45/37	50/37
				Steam flow rate	kg h ⁻¹	1300	-
Power consumption ^{9, 10}	kw	6348	-	Heat transfer efficiency	%	98	100
Efficiency	%	70	90	Power dissipation to heat	%	100	-
Fermentation				Centrifugation			
RM loading time ¹	h	8	6	volumetric throughput	m ³ h ⁻¹	160	-
Sterilization ¹	h	1.5	1.5	Lipid separation efficiency ^{7, 8}	% w/w	90	95
Lipid Productivity*	g L ⁻¹ h ⁻¹	1.4	2.4	water contain in the non-lipid biomass ⁷	% w/w	50	-
Fermentation time*	h	120	72	Centrifugation time	h	contentious	
Biomass content*	g L ⁻¹	200	190	Power consumption ⁹	kw m ⁻²	0.2	-
Lipid content*	% (w/w)	83	85	Sedimentation efficiency ^{7, 8}	%	30	50
transfer out to reactor ¹	h	8	6	Filtration			
Power consumption ^{9, 10}	kw m ⁻³	3	-	Rejection co-efficient for protein ^{7, 8}	% w/w	95	-
Aeration rate ^{1, 11}	vvm	0.8	0.5	Filtration time	h	10	8
Power dissipation to heat ¹²	%	50	-	Recovery (filtrate/feed) ^{***}	% w/w	90	95
Pressure inside fermenter**	bar	1.25 - 1.5		Power consumption	kw	156	-
Yeast Hydrolysate				Power dissipation to heat ¹²	%	10	-
Sugar content*	g L ⁻¹	18	24	Filtrate flux	L m ⁻² h	32	
Nitrogen content*	g L ⁻¹	8	15				

*Based on the current process parameters and current results. ** Based on the fermentation parameters at 25-L to red.

***Based on the recycling experiments.

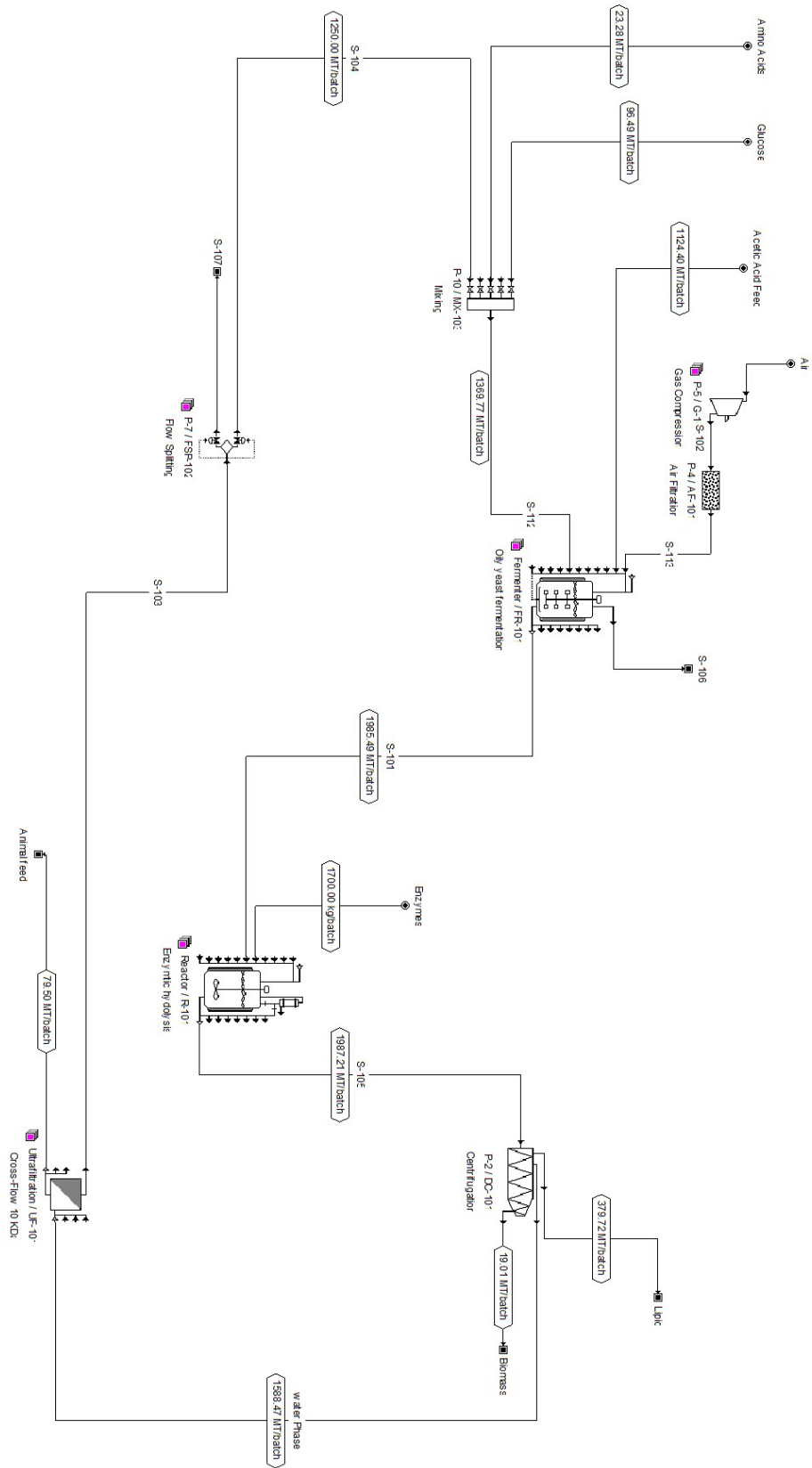


Figure S8: The simplified process flow diagram for the lipid production from yeast.

Table S3: Capital cost-list of equipment specification and PC cost according to market analysis in 2018-SuperPro designer V10.

#	Item	Unite Purchased Cost(PC)	Quantity			Total Purchased Cost (PC)	Installation factor*	Installed cost	Ref.
			In process	Standby	Total				
1	Fermenter, Vessel Volume = 250.00 m3	2,333,000	10	1	11	25,663,000	1.60	41,060,800	SuperPro Designer (V10) Built-in cost model (Year analysis 2018)
2	Stirred Reactor Vessel Volume = 248.76 m3	1,773,000	3	1	4	7,092,000	1.60	11,347,200	SuperPro Designer (V10) Built-in cost model (Year analysis 2018)
3	Bending Tank, Vessel Volume = 150.00 m3	178,000	2	-	2	356,000	1.60	569,600	SuperPro Designer (V10) Built-in cost model (Year analysis 2018)
4	Storage/ Receiving Tank, Vessel Volume = 250.00 m3	78,000	3	-	3	234,000	1.70	397,800	SuperPro Designer (V10) Built-in cost model (Year analysis 2018)
5	Decanter Centrifuge, Throughput = 159919.85 L/h	243,000	1	1	2	486,000	1.60	777,600	SuperPro Designer (V10) Built-in cost model (Year analysis 2018)
7	Centrifugal Compressor Compressor Power = 2115.79 kW	2,212,000	3	-	3	6,636,000	1.60	10,617,600	SuperPro Designer (V10) Built-in cost model (Year analysis 2018)
8	Ultrafilter Membrane Area = 77.69 m2, shell & tube, stainless steel	124,000	27	-	27	3,348,000	1.8	6,026,400	SuperPro Designer (V10) Built-in cost model (Year analysis 2018)
9	Air Filter Rated Throughput = 12112043.16 L/h, shell & tube, stainless steel	43,000	1	1	2	86,000	1.80	154,800	SuperPro Designer (V10) Built-in cost model (Year analysis 2018)
	Total cost					43,901,000		70,951,800	
	Interest							4,257,108	Estimated as: 6% of the PC
	Total Installed Costs							75,208,908	

*The installation Factor is obtained from Provoius NREL publication about bioethanol production.⁵

Table S4: Capital cost-list of additional direct capital cost.

Additional direct capital cost	#	Item	Description	Installed Cost	Factor	Cost	Ref.
	1	Warehouse ,	On-site storage of equipment and supplies.	70,951,800	0.04	2,838,072	Estimated as: 4.0%% of the ISBL
	2	Site development	Includes fencing, curbing, parking lot, roads, well drainage, rail system, soil borings, and general paving. This factor allows for minimum site development assuming a clear site with no unusual problems such as right-of-way, difficult land clearing, or unusual environmental problems.	70,951,800	0.090	6,385,662	Estimated as: 9%% of the ISBL
	3	Additional piping	To connect ISBL equipment to storage and utilities outside the battery limits	70,951,800	0.045	3,192,831	Estimated as: 4.5%% of the ISBL
		Total				12,416,565	
	Total Direct Costs (TDC)				83,368,365		

Table 5: Capital cost-list of additional indirect capital cost.

Indirect capital cost	#	Item	Description	Total Direct Costs	Factor	Cost	Ref.
	1	Prorateable costs	This includes fringe benefits, burdens, and insurance of the construction contractor.	83,368,365	0.10	8,336,837	Estimated as: 10% of total direct cost (TDC)
	2	Field expenses	Consumables, small tool and equipment rental, field services, temporary construction facilities, and field construction supervision.	83,368,365	0.10	8,336,837	Estimated as: 10% of total direct cost (TDC)
	3	Home office and construction	Engineering plus incidentals, purchasing, and construction	83,368,365	0.20	16,673,673	Estimated as: 20% of total direct cost (TDC)
	4	Project contingency	Extra cash on hand for unforeseen issues during construction.	83,368,365	0.10	8,336,837	Estimated as: 10% of total direct cost (TDC)
	5	Other costs	Start-up and commissioning costs. Land, rights-of-way, permits, surveys, and fees. Piling, soil compaction/dewatering, unusual foundations. Sales, use, and other taxes. Freight, insurance in transit, and import duties on equipment, piping, steel, instrumentation, etc. Overtime pay during construction. Field insurance. Project team. Transportation equipment, bulk shipping containers, plant vehicles, etc.	8,336,837	0.10	8,336,837	Estimated as: 10% of total direct cost (TDC)
		Total Indirect Costs				50,021,019	
	Total Capital Investment (TCI)		Total Direct Costs (TDC) + Indirect costs				133,389,384

Table S6: Operation cost-list of labor cost according to German TV-L tariff.

LABOR COST	#	Item	Annual cost per person	Amount	Cost	Ref.
	1	Operator (Full Cost) E10	83,305	30	2,499,150	Official service, full-cost list based on TV-L E10
	2	QC Analyst (Full Cost) E13	114,599	9	1,031,391	Official service, full-cost list based on TV-L E13
	3	Management/ Administration (Full Cost) E14	119,415	3	358,245	Official service, full-cost list based on TV-L E14
		Total			3,888,786	

Table S7: Operation cost-list of Facility-dependent cost.

FACILITY-DEPENDENT COST	#	Item	Annual cost	Factor	Cost	Ref.
	1	Maintenance	83,368,365	0.03	2,128,554	Estimated as 3% of total direct fixed capital.
	2	Property insurance	133,389,384	0.007	496,663	Estimated as 0.7% of total capital investment (TCI).
		Facility-dependent Total			2,625,217	
	Total fixed operating costs	Labor cost + facility-dependent		6,514,003		

Table S8: Operation cost-list of Utility cost, Ref.: SuperPro designer V10

UTILITIES COST (Germany 2018 prices in \$)	#	Item	Unite cost	Quantity	Ref. Units	Total	Cost	Ref.
	1	Std Power	0.1	81,588,099	kW-h/year	81,588,099	8,158,809.90	The consumption amount based on SuperPro Designer (V10). The cost of kW-h is based on German price of Std power
	2	Steam	5.0	101,320	MT/year	101,320	506,600	
	3	Cooling water	0.05	11,356,146	MT/year	11,356,146	567,807	SuperPro Designer (V10)
	4	Chilled water	0.40	5,693,853	MT/year	5,693,853	2,277,541	
	5	Saving (Exist in the process due to heat recovery)	1.00	1,573,600	-	1,573,600	1,573,600	uperPro Designer (V10)
	6	Saving (Steam Recycling)	5.00	99,588	MT/year	99,588	497,940	uperPro Designer (V10)
	7	Saving (Cooling water Recycling)	0.05	8,327,840	MT/year	8,327,840	416,392	SuperPro Designer (V10)
	Total					9,022,826		

Table S9: RM cost according to market analysis in 2018.

RAW MATERIALS	#	Item	Unit cost	Quantity	Cost	Ref.
	1	Acetic acid	0.2	68,588,400	13,031,796	Whole sell market "Alibaba website"
	2	Glucose	0.3	5,517,770	1,655,331	Whole sell market "Alibaba website"
	3	Enzyme	4	103,700	414,800	Novozymes company.
	4	Amino acid	0.2	915,398	183,080	Source like yeast extract or peptone. Whole sell market "Alibaba website"
		Total			15,285,007	

Table S10: Revenues- the annual productivity of lipid, biomass and animal feed based on designee process.

REVENUES	#	Item	Unit cost	Quantity	Total Cost	
	1	Lipid	1.60	23,163,170	37,061,072	Estimated
	2	Biomass	0.35	1,159,905	405,967	Market cost
	3	Animal Feed (concentrated protein after cross-flow)	0.35	439,787	153,925	Market cost
		Total			37,620,964	

Table S11: The cost summary of Capital cost (CAPX), Operation cost (OPEX) and Raw Martials cost (RM) against the revenues.

SUMMARY	#	Items	Description	Cost
	1	CAPEX	Total / 20 years depreciation	6,669,469.20
	2	OPEX	Including: Lab, maintenance and utility	15,536,828.78
	3	RM	All chemicals are included	15,285,006.60
			Total cost	37,491,305
			Revenues	37,620,964

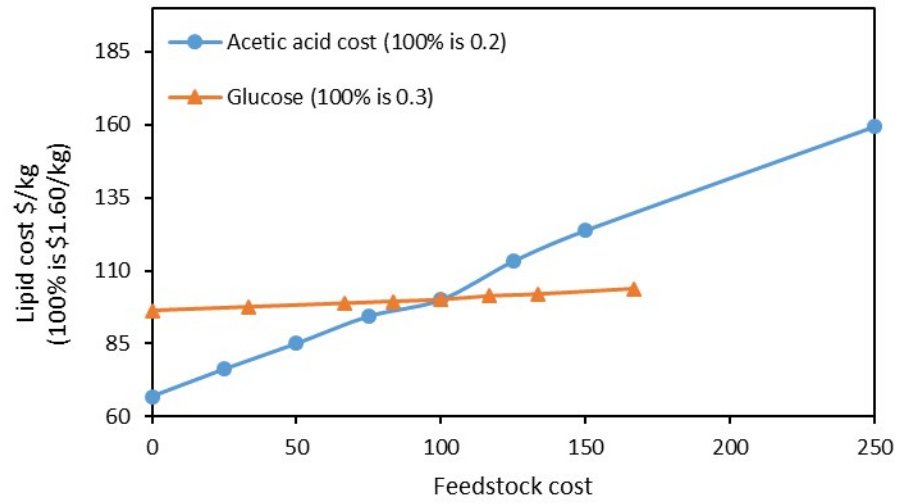


Figure S9: Lipid cost sensitivity to acetic acid and glucose cost.

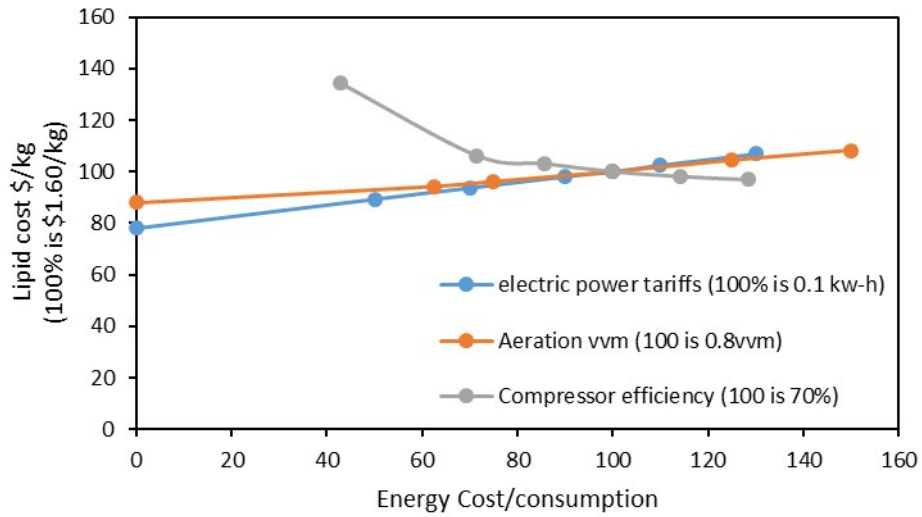


Figure 10: Lipid cost sensitivity to aerations need, electric power tariffs and compressor efficiency.

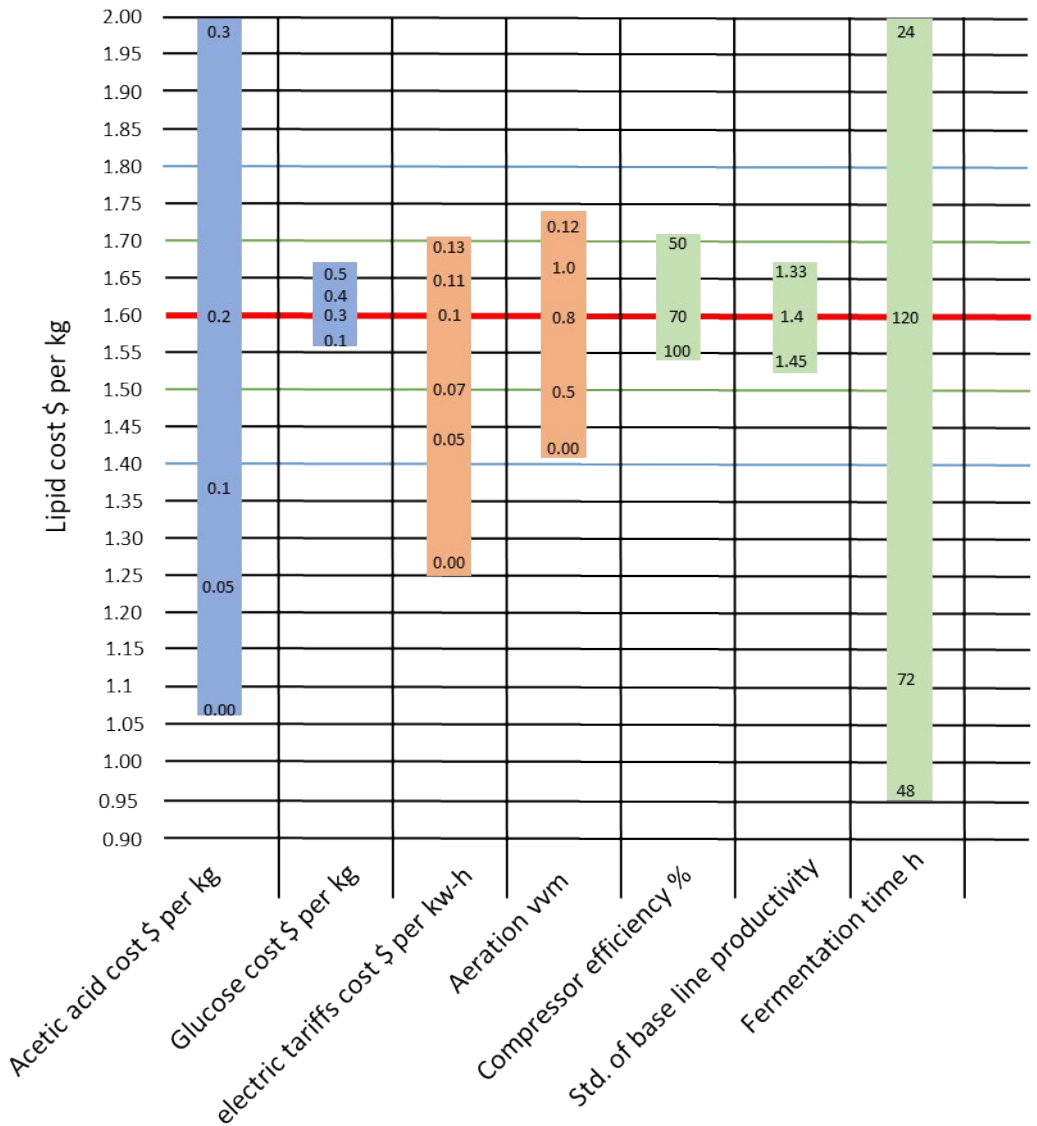


Figure S11: Lipid cost sensitivity to the main process input parameters.

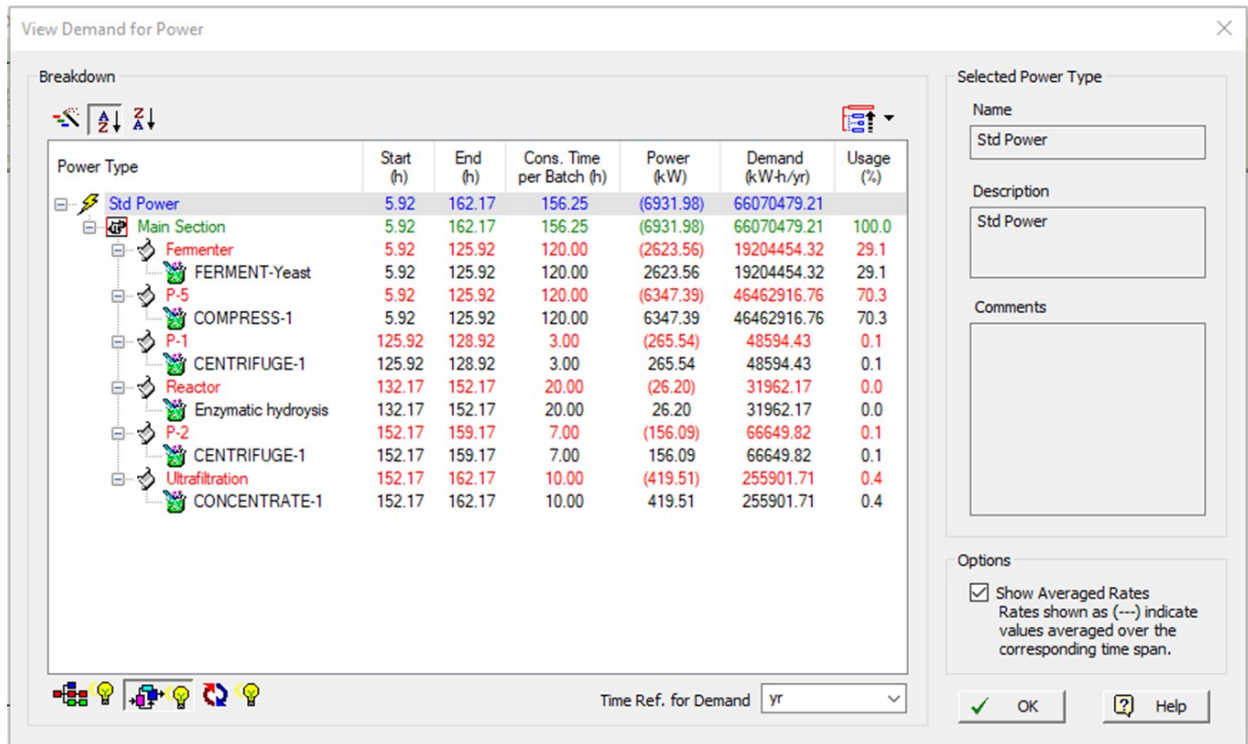


Figure S12: Eclectic power usage in the plant

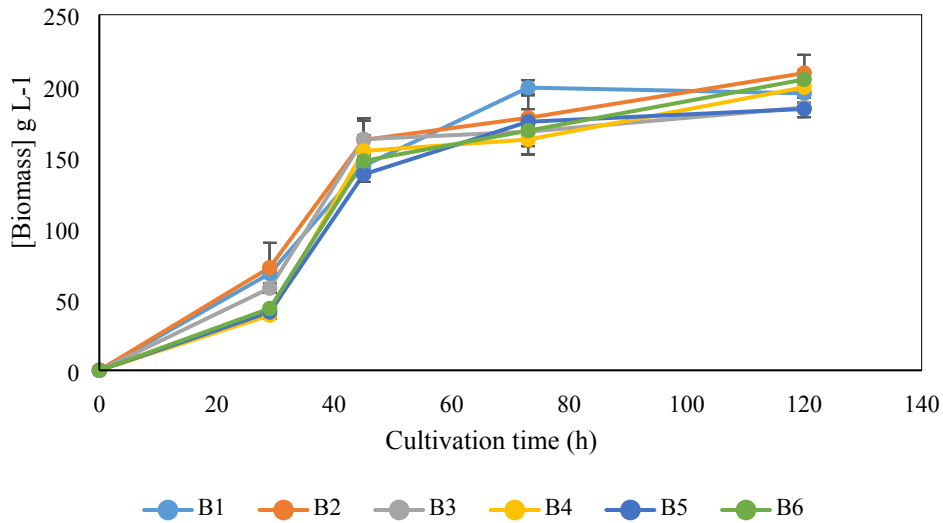


Figure S13: Six biological replication to validate the reproducibility of achieved lipid productivity.

1.5 LCA

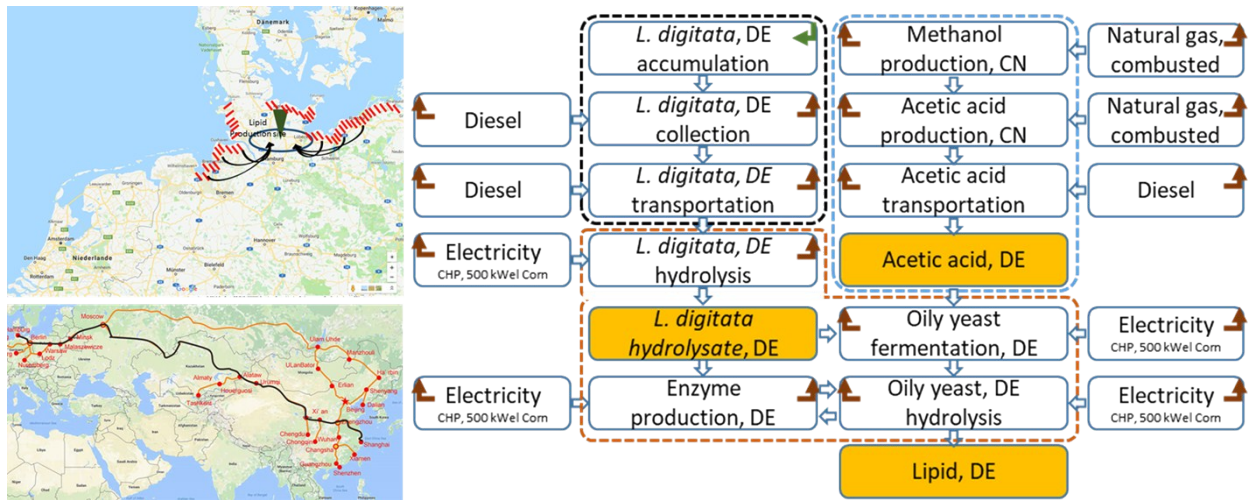


Figure S14: (a) Map showing the proposed location for the production plant. The brown algae collection area is shadowed in red. (b) Map showing the train route for acetic acid transportation from China. (c) The production system used in this study.

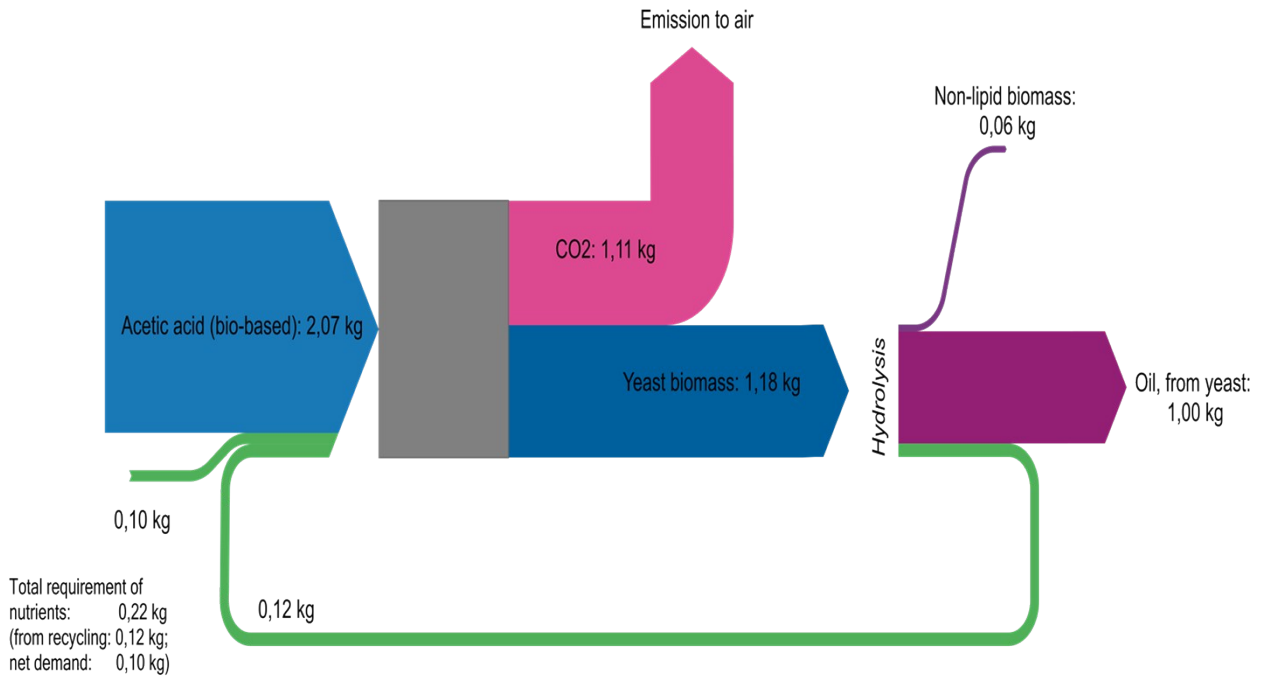


Figure S15: The Sankey diagram of the mass balance for the functional unit 1 kg Oil.

Table S12: Inventory of yeast fermentation according to the chosen productivity and current process design (This work).

Input				
	Flow	Amount	Unit	Description
	<i>Acetic acid, at fermentation plant,</i>	2.96	kg	According to the SuperPro Designer, based on amount of acetic acid consumed during the fermentation
	<i>Calcium chloride, CaCl₂, at regional storage</i>	5.48E-06	kg	Medium formula
	<i>Yeast hydrolysate</i>	4.16	kg	According the current process design
	<i>Digitata hydrolysate</i>	8.2E-05	m ³	According to the SuperPro Designer, based on amount of sugar consumed during the fermentation
	<i>Magnesium sulphate, at plant</i>	1.64E-05	kg	Medium formula
	<i>Electricity, biogas CHP, at plant</i>	1.547	kWh	According to the SuperPro Designer, the total Electricity consuming by Air compressor, Air filtration, fermenter 250m ³ , and centrifuge is 813496 m ³ , the no. of batches per year 63, mass of biomass per batch 50000 kg
	<i>Water, process and cooling, surface</i>	0.258	m ³	According to the SuperPro Designer, the total cooling water consuming by Air compressor, Air filtration, fermenter 250m ³ , and centrifuge is 813496 m ³ , the no. of batches per year 63, mass of biomass per batch 50000 kg
Output				
	Flow	Amount	Unit	Description
	<i>Acetic acid/ emission to air</i>	1.14E-10	kg	According to the SuperPro Designer,
	<i>Carbon dioxide/emission to air</i>	1.11	kg	According to the SuperPro Designer,
	<i>Oily-yeast biomass (200 g/L) culture</i>	5	kg	Based on the biomass productivity 1.7 g L ⁻¹ h ⁻¹ [biomass: 200 g L ⁻¹ with lipid content of 85% ($w_{lipid}/d_w_{biomass}$), after 120 h]

Table S13: Inventory of the enzymatic hydrolysis of the yeast culture after the fermentation (This work).

Input			
<i>Flow</i>	Amount	Unit	Description
<i>Cell hydrolase</i>	0.027	kg	Based on the enzyme dose hydrolase: 0.8% (w/dw_{biomass}) & Protease: 0.5% (w/dw) Enzyme/ biomass
<i>Oily-yeast biomass (200 g/L) culture</i>	5	kg	Resulted from fermentation
<i>Electricity, biogas CHP, at plant</i>	1.13	kWh	According to the SuperPro Designer, the total Electricity consuming by 5 times reactor 250m ³ , and steam generator for (20 h at 50°C & (8 h at 37°C), then centrifuge is 813496 m ³ , the no. of batches per year 63, mass of biomass per batch 50000 kg
Output			
<i>Flow</i>	Amount	Unit	Description
<i>C. oleaginosus hydrolysate</i>	4.16	kg	According the current process design
<i>Non-lipid biomass</i>	0.04	kg	Based on the enzyme hydrolysis yield: 80% (w/w)
<i>Oil, from oily yeast, TAG</i>	1	kg	Based on the lipid productivity 1.4 g L ⁻¹ h ⁻¹ [biomass: 200 g L ⁻¹ with lipid content of 85% ($w_{\text{lipid}}/dw_{\text{biomass}}$), after 120 h]

Table S14: Inventory of the enzymatic hydrolysis of *L. Digitata* (This work).

Input			
Flow	Amount	Unit	Description
Acetic acid, at Fermentation plant,	4	kg	Used As buffer solution (50mM)
Cell hydrolase	1.05	kg	Based on the enzyme dose hydrolase: 1.3 % (w/dw). (Masri et al, 2018)
<i>L. digitata</i> , at plant, truck	70	kg	form The previous inventory (Table xx)
Sodium hydroxide	2	kg	Used As buffer solution (50mM)
Electricity, biogas CHP, at plant	1.325	kWh	According to the SuperPro Designer, the total Electricity consuming by 5 times reactor 250m3, and steam generator for 72h, 50°C.
Water, unspecified natural origin/m ³	0.9	m ³	According to the SuperPro Designer, the total water consuming steam generator for 72h, 50°C.
Output			
Flow	Amount	Unit	Description
<i>L. digitata</i> Hydrolysate	1	m ³	Based on results presented in (Masri et al, 2018)
Residual <i>L. digitata</i> biomass	21.05	kg	Based on results presented in (Masri et al, 2018)

Table S15: Inventory of hydrolase production from *T. reesei* (This work).

Input			
Flow	Amount	Unit	Description
<i>L. digitata</i> Hydrolysate	0.02	m ³	Based on the media composition according to(Aftab et al 2008)
Non-Lipid Biomass	10	kg	Based on the media composition 10g L-1
Strom, Biogas BHKW, ab Anlage	1.12	kWh	According to the SuperPro Designer, the total Electricity consuming by fermenter 250m3, and steam generator for 120h, 28°C.
Output			
Flow	Amount	Unit	Description
Carbon dioxide	1.40	kg	According to the SuperPro Designer, estimated CO2 released.
Enzyme, Mixed activities, <i>T. reesei</i>	1	kg	Based on the results presented in the work

Table S16: Inventory of *L. digitata* growth (This work).

Input			
--------------	--	--	--

Flow		Amount	Unit	Description
<i>Carbon dioxide/ absorption from air</i>		1.47	kg	A theoretical calculation based on the C content in the produced biomass
<i>Nitrate/ absorption from soil</i>		0.031	kg	A theoretical calculation based on the N content in the produced biomass
Output				
Flow		Amount	Unit	
<i>L.digitata</i>		1	kg	

Table S17: Inventory of truck (>32 ton) operation (BioEnergieDat Database).

Input				
Flow		Amount	Unit	Description
<i>Diesel, low-Sulphur, at regional storage</i>		0.042	kg	
Output				
Flow		Amount	Unit	
<i>Operation Truck >32t, EURO3_ei/Tremod</i>		1	t*km	
<i>Acetaldehyde /emission to air</i>		1.32E-05	kg	
<i>Ammonia /emission to air</i>		0.15	kg	
<i>Benzene /emission to air</i>		1.28E-06	kg	
<i>Cadmium /emission to air</i>		6.05E-06	kg	
<i>Cadmium /emission to soil</i>		3.61E-06	kg	
<i>Cadmium, ion /emission to water</i>		3.61E-06	kg	
<i>Carbon dioxide /emission to air</i>		0.14	kg	
<i>Carbon monoxide /emission to air</i>		0.0003	kg	
<i>Chromium /emission to air</i>		0.000064	kg	
<i>Chromium /emission to soil</i>		1.71E-05	kg	
<i>Chromium VI /emission to air</i>		5.12E-09	kg	
<i>Chromium, ion /emission to water</i>		1.71E-05	kg	
<i>Copper /emission to soil</i>		0.0002	kg	
<i>Copper /emission to air</i>		0.004	kg	
<i>Copper, ion /emission to water</i>		0.0002	kg	
<i>Dinitrogen monoxide /emission to air</i>		0.22	kg	
<i>Ethane, 1,1,1,2-tetrafluoro-, HFC-134a /emission to air</i>		3.92E-07	kg	

<i>Formaldehyde /emission to air</i>	2.43E-05	kg
<i>Heat, waste /emission to air</i>	2326.92	MJ
<i>Hydrocarbons, halogenated, unspecified /emission to air</i>	6.75E-05	kg
<i>Lead /emission to soil</i>	0.0002	kg
<i>Lead /emission to water</i>	0.0002	kg
<i>Lead /emission to air</i>	0.0002	kg
<i>Mercury /emission to air</i>	1.03E-08	kg
<i>Methane, fossil /emission to air</i>	1.62E-06	kg
<i>Nickel/emission to air</i>	6.39E-05	kg
<i>Nickel /emission to soil</i>	4.66E-05	kg
<i>Nickel, ion /emission to water</i>	4.66E-05	kg
<i>Nitrogen oxides /emission to air</i>	0.001	kg
<i>NMVOC, non-methane volatile organic compounds, unspecified origin /emission to air</i>	6.59E-05	kg
<i>PAH, polycyclic aromatic hydrocarbons /emission to air</i>	1.71E-10	kg
<i>Particulates, < 10 um /emission to air</i>	9.45E-07	kg
<i>Particulates, < 2.5 um /emission to air</i>	2.97E-05	kg
<i>Particulates, > 2.5 um, and < 10um /emission to air</i>	8.58E-07	kg
<i>Selenium /emission to air</i>	5.12E-07	kg
<i>Sulfur dioxide /emission to air</i>	7.06E-07	kg
<i>Toluene /emission to air</i>	5.40E-07	kg
<i>Xylene /emission to air</i>	5.40E-07	kg
<i>Zinc /emission to air</i>	0.002	kg
<i>Zinc /emission to soil</i>	0.01	kg
<i>Zinc, ion /emission to water</i>	0.01	kg

Table 18: Inventory of tractor operation (BioEnergieDat Database).

Input		Amount	Unit	Description
Flow	<i>Diesel, low-Sulphur, at regional storage</i>	1	kg	
Output				

Flow	Amount	Unit
<i>Operation Tractor</i>	1	kg
<i>Carbon dioxide /emission to air</i>	3.12	kg
<i>Carbon monoxide /emission to air</i>	0.003	kg
<i>Dinitrogen monoxide /emission to air</i>	0.22	kg
<i>Methane, fossil /emission to air</i>	0.000128	kg
<i>Sulfur dioxide /emission to air</i>	0.001	kg
<i>Nitrogen dioxide</i>	0.0001	kg
<i>Nitrogen oxides</i>	0.04	kg

Table S19: Inventory of acetic acid production and transportation from China (US LCI database).

Input			
Flow	Amount	Unit	Description
<i>CUTOFF Disposal, solid waste, unspecified, to sanitary landfill</i>	0.001	kg	
<i>Electricity, at cogent, for natural gas turbine</i>	0.002	kWh	
<i>Electricity, at grid, US, 2000</i>	0.02	kWh	
<i>Methanol, at plant</i>	0.54	kg	
<i>Natural gas, combusted in industrial boiler</i>	0.22	m3	
<i>Natural gas, processed, at plant</i>	0.44	m3	
<i>Transport, barge, diesel powered</i>	0.01	t*km	
<i>Transport, barge, residual fuel oil powered</i>	0.03	t*km	
<i>Transport, combination truck, diesel powered</i>	0.005	t*km	
<i>Transport, pipeline, natural gas</i>	0.49246	t*km	
<i>Transport, pipeline, unspecified petroleum products</i>	0.000867	t*km	
<i>Transport, train, diesel powered</i>	0.004925	t*km	
<i>Transport, train, diesel powered</i>	12.5	t*km	Based on the suggested train way from China to Hamburg (about 12,000 km)
Output			
Flow	Amount	Unit	
<i>Acetic acid, at plant in Hamburg</i>	1	kg	
<i>Acids, unspecified /emission to water</i>	0.00096	kg	

<i>Ammonia/emission to air</i>	0.00057	kg
<i>Ammonia /emission to water</i>	0.000052	kg
<i>Carbon dioxide /emission to air</i>	0.00176	kg
<i>Carbon monoxide /emission to air</i>	0.00397	kg
<i>Methanol /emission to air</i>	0.00004	kg
<i>Recovered energy, at acetic acid production</i>	0.18841	MJ
<i>TOC, Total Organic Carbon /emission to air</i>	0.00217	kg

Table 20: Inventory of methanol production in China (US LCI database).

Input				
	Flow	Amount	Unit	Description
	<i>CUTOFF Disposal, solid waste, unspecified, to sanitary landfill</i>	0.0005	kg	
	<i>Electricity, at grid, US, 2008</i>	0.0081	kWh	
	<i>Natural gas, combusted in industrial boiler</i>	0.13	m3	
	<i>Natural gas, processed, for olefins production, at plant</i>	0.62	kg	
	<i>Oxygen, in air</i>	0.38	kg	
	<i>Transport, combination truck, diesel powered</i>	0.01	t*km	
	<i>Transport, pipeline, natural gas</i>	0.998	t*km	
	<i>Transport, train, diesel powered</i>	0.00997	t*km	
	<i>Water, process, unspecified natural origin/m3</i>	0.00054	m3	
Output				
	Flow	Amount	Unit	
	<i>BOD5, Biological Oxygen Demand /emission to water</i>	0.000058	kg	
	<i>Carbon dioxide /emission to air</i>	0.53	kg	
	<i>Methanol, at plant</i>	1	kg	
	<i>NMVOC, non-methane volatile organic compounds, unspecified /emission to air</i>	0.005	kg	
	<i>Suspended solids, unspecified /emission to water</i>	0.000088	kg	

Table 21: Inventory of natural gas combusted in industrial equipment (US LCI database).

Input				
	Flow	Amount	Unit	Description
	<i>Natural gas, processed, at plant</i>	1	m3	
	<i>Transport, combination truck, average fuel mix</i>	0.20	t*km	
	<i>Transport, pipeline, natural gas</i>	1.19	t*km	
	<i>Transport, train, diesel powered</i>	0.01	t*km	
Output				
	Flow	Amount	Unit	Description
	<i>Acetaldehyde /emission to air</i>	6.54E-07	kg	
	<i>Acrolein /emission to air</i>	1.05E-07	kg	
	<i>Benzene /emission to air</i>	1.96E-07	kg	
	<i>Benzene, ethyl- /emission to air</i>	5.23E-07	kg	
	<i>Butadiene /emission to air</i>	7.03E-09	kg	
	<i>Carbon dioxide, fossil /emission to air</i>	1.96	kg	
	<i>Carbon monoxide, fossil /emission to air</i>	0.00024	kg	
	<i>Formaldehyde /emission to air</i>	0.000012	kg	
	<i>Methane, fossil /emission to air</i>	0.00014	kg	
	<i>Naphthalene /emission to air</i>	2.124E-08	kg	
	<i>Natural gas, combusted in industrial equipment</i>	1	m3	
	<i>Nitrogen oxides /emission to air</i>	0.0017	kg	
	<i>PAH, polycyclic aromatic hydrocarbons /emission to air</i>	3.5945E-08	kg	
	<i>Particulates, > 2.5 um, and < 10um /emission to air</i>	0.00011	kg	
	<i>Propylene oxide /emission to air</i>	4.7383E-07	kg	
	<i>Sulfur oxides /emission to air</i>	0.00001	kg	
	<i>Toluene /emission to air</i>	0.000002	kg	
	<i>VOC, volatile organic compounds /emission to air</i>	0.00003	kg	
	<i>Xylene /emission to air</i>	1.0457E-06	kg	

Table 22: Life cycle assessment and impact analysis for 1 kg yeast lipid production.

	Name	Inventory result	Unit	Impact factor	Impact result	Impact co-factor
1	Eutrophication - generic				0.00339	kg PO4⁻⁻⁻ eq.
1.1	Transport, train, diesel powered - DE				0.00241	kg PO4⁻⁻⁻ eq.
	Nitrogen oxides	0.018	kg	0.13	0.0024	kg PO4 ⁻⁻⁻ eq.
1.2	Acetic acid, at plant - CN				0.00065	kg PO4⁻⁻⁻ eq.
	Ammonia	0.002	kg	0.35	0.00059	kg PO4 ⁻⁻⁻ eq.
	Ammonia	0.0001	kg	0.35	5.39E-05	kg PO4 ⁻⁻⁻ eq.
1.3	Natural gas, combusted in industrial boiler - RNA				0.00019	kg PO4⁻⁻⁻ eq.
	Nitrogen oxides	0.001	kg	0.13	0.00018	kg PO4 ⁻⁻⁻ eq.
	Dinitrogen monoxide	3.13E-05	kg	0.27	8.46E-06	kg PO4 ⁻⁻⁻ eq.
1.4	L.digitata Growth				0.00013	kg PO4⁻⁻⁻ eq.
	Nitrate	0.001	kg	0.1	0.00013	kg PO4 ⁻⁻⁻ eq.
2	Photochemical oxidation - high Nox				0.00043	kg ethylene eq.
2.1	Acetic acid, at plant - CN				0.00033	kg ethylene eq.
	Carbon monoxide	0.01	kg	0.027	0.00032	kg ethylene eq.
	Methanol	0.00012	kg	0.14	1.66E-05	kg ethylene eq.
2.2	Transport, train, diesel powered - DE				4.93E-05	kg ethylene eq.
	Carbon monoxide	0.002	kg	0.027	4.91E-05	kg ethylene eq.
2.3	CHP (gas engine) 500 kWel Mais (90), cattle manure (10), DE				4.52E-05	kg ethylene eq.
	Methane, biogenic	0.007	kg	0.006	4.52E-05	kg ethylene eq.
3	Terrestrial ecotoxicity - TETP inf				0.00026	kg 1,4-dichlorobenzene eq.
3.1	Natural gas, combusted in industrial boiler - RNA				0.00017	kg 1,4-dichlorobenzene eq.
	Mercury	3.62E-09	kg	2.83E+04	0.0001	kg 1,4-dichlorobenzene eq.
	Chromium	1.95E-08	kg	3031.11	5.91E-05	kg 1,4-dichlorobenzene eq.
	Nickel	2.93E-08	kg	116.04	3.40E-06	kg 1,4-dichlorobenzene eq.
3.2	Operation truck >32t, EURO3				9.42E-05	kg 1,4-dichlorobenzene eq.
	Zinc	1.52E-06	kg	24.59	3.74E-05	kg 1,4-dichlorobenzene eq.
	Chromium	9.70E-09	kg	3031.12	2.94E-05	kg 1,4-dichlorobenzene eq.
	Chromium	2.56E-09	kg	6302.86	1.61E-05	kg 1,4-dichlorobenzene eq.
	Copper	5.50E-07	kg	6.99	3.85E-06	kg 1,4-dichlorobenzene eq.
	Zinc	2.32E-07	kg	11.96	2.78E-06	kg 1,4-dichlorobenzene eq.

	Nickel	6.96E-09	kg	238.55	1.66E-06	kg 1,4-dichlorobenzene eq.
	Nickel	9.55E-09	kg	116.04	1.11E-06	kg 1,4-dichlorobenzene eq.
4	Climate change - GWP100				3.56179	kg CO2 eq.
4.1	Yeast Biomass production, Fermentation - DE				1.10924	kg CO2 eq.
	Carbon dioxide	1.10	kg	1	1.10924	kg CO2 eq.
4.2	CHP (gas engine) 500 kWel Mais (90), cattle manure (10), DE				0.87251	kg CO2 eq.
	Carbon dioxide	0.68	kg	1	0.68407	kg CO2 eq.
	Methane, biogenic	0.007	kg	25	0.18843	kg CO2 eq.
4.3	Methanol, at plant - CN				0.8466	kg CO2 eq.
	Carbon dioxide	0.84	kg	1	0.8466	kg CO2 eq.
4.4	Transport, train, diesel powered - DE				0.71149	kg CO2 eq.
	Carbon dioxide	0.70	kg	1	0.70195	kg CO2 eq.
4.5	Enzyme, Mixed activities, T. reesei				0.03711	kg CO2 eq.
	Carbon dioxide	0.04	kg	1	0.03711	kg CO2 eq.
4.6	L.digitata_Growth				-0.06262	kg CO2 eq.
	Carbon dioxide	-0.06	kg	1	-0.06262	kg CO2 eq.
5	Acidification potential - average Europe				0.01267	kg SO2 eq.
5.1	Transport, train, diesel powered - DE				0.00923	kg SO2 eq.
	Nitrogen oxides	0.02	kg	0.5	0.00923	kg SO2 eq.
5.2	Acetic acid, at plant - CN				0.0027	kg SO2 eq.
	Ammonia	0.00169	kg	1.6	0.0027	kg SO2 eq.
5.3	Natural gas, combusted in industrial boiler - RNA				0.0007	kg SO2 eq.
	Nitrogen oxides	0.001	kg	0.5	0.0007	kg SO2 eq.
6	Depletion of abiotic resources - fossil fuels				0	MJ
7	Depletion of abiotic resources - elements, ultimate reserves				0	kg antimony eq.
8	Human toxicity - HTP inf				0.03056	kg 1,4-dichlorobenzene eq.
8.1	Transport, train, diesel powered - DE				0.02254	kg 1,4-dichlorobenzene eq.
	Nitrogen oxides	0.02	kg	1.2	0.02216	kg 1,4-dichlorobenzene eq.
	Particulates, < 10 um	0.0005	kg	0.82	0.00038	kg 1,4-dichlorobenzene eq.
8.2	Natural gas, combusted in industrial boiler - RNA				0.00496	kg 1,4-dichlorobenzene eq.
	Cadmium	1.53E-08	kg	1.45E+05	0.00222	kg 1,4-

						dichlorobenzene eq.
	Nitrogen oxides	0.00139	kg	1.2	0.00167	kg 1,4-dichlorobenzene eq.
	Nickel	2.93E-08	kg	3.50E+04	0.00103	kg 1,4-dichlorobenzene eq.
8.3	Operation truck >32t, EURO3				0.00289	kg 1,4-dichlorobenzene eq.
	Copper	5.50E-07	kg	4295.03	0.00236	kg 1,4-dichlorobenzene eq.
	Nickel	9.55E-09	kg	3.50E+04	0.00033	kg 1,4-dichlorobenzene eq.
	Cadmium	9.03E-10	kg	1.45E+05	0.00013	kg 1,4-dichlorobenzene eq.
9	Ozone layer depletion - ODP steady state				0	kg CFC-11 eq.
10	Marine aquatic ecotoxicity - MAETP inf				0.74621	kg 1,4-dichlorobenzene eq.
10.1	Operation truck >32t, EURO3				0.61477	kg 1,4-dichlorobenzene eq.
	Copper	5.50E-07	kg	8.93E+05	0.49159	kg 1,4-dichlorobenzene eq.
	Nickel	9.55E-09	kg	3.76E+06	0.03587	kg 1,4-dichlorobenzene eq.
	Zinc, ion	1.52E-06	kg	1.38E+04	0.02108	kg 1,4-dichlorobenzene eq.
	Nickel, ion	6.96E-09	kg	2.25E+06	0.01566	kg 1,4-dichlorobenzene eq.
	Zinc	2.32E-07	kg	6.73E+04	0.01561	kg 1,4-dichlorobenzene eq.
	Zinc	1.52E-06	kg	7208.56	0.01098	kg 1,4-dichlorobenzene eq.
	Copper, ion	3.61E-08	kg	2.33E+05	0.0084	kg 1,4-dichlorobenzene eq.
	Nickel	6.96E-09	kg	1.17E+06	0.00818	kg 1,4-dichlorobenzene eq.
10.2	Natural gas, combusted in industrial boiler - RNA				0.13144	kg 1,4-dichlorobenzene eq.
	Nickel	2.93E-08	kg	3.76E+06	0.10999	kg 1,4-dichlorobenzene eq.
	Cadmium	1.53E-08	kg	1.11E+06	0.01695	kg 1,4-dichlorobenzene eq.
	Mercury	3.62E-09	kg	1.20E+06	0.00435	kg 1,4-dichlorobenzene eq.
11	Freshwater aquatic ecotoxicity - FAETP inf				0.00047	kg 1,4-dichlorobenzene eq.
11.1	Operation truck >32t, EURO3				0.00044	kg 1,4-dichlorobenzene eq.
	Zinc, ion	1.52E-06	kg	91.71	0.00014	kg 1,4-dichlorobenzene eq.
	Copper	5.50E-07	kg	221.65	0.00012	kg 1,4-dichlorobenzene eq.
	Zinc	1.52E-06	kg	47.745	7.27E-05	kg 1,4-dichlorobenzene eq.
	Copper, ion	3.61E-08	kg	1157.30	4.18E-05	kg 1,4-dichlorobenzene eq.

	Nickel, ion	6.96E-09	kg	3237.61	2.25E-05	kg 1,4-dichlorobenzene eq.
	Copper	3.61E-08	kg	594.65	2.15E-05	kg 1,4-dichlorobenzene eq.
	Nickel	6.96E-09	kg	1690.25	1.18E-05	kg 1,4-dichlorobenzene eq.
	Nickel	9.55E-09	kg	629.47	6.01E-06	kg 1,4-dichlorobenzene eq.
11.2	Natural gas, combusted in industrial boiler - RNA				2.41E-05	kg 1,4-dichlorobenzene eq.
	Nickel	2.93E-08	kg	629.47	1.84E-05	kg 1,4-dichlorobenzene eq.
	Cadmium	1.53E-08	kg	289.43	4.44E-06	kg 1,4-dichlorobenzene eq.
	Mercury	3.62E-09	kg	316.78	1.15E-06	kg 1,4-dichlorobenzene eq.

Referances

1. A. A. Koutinas, A. Chatzifragkou, N. Kopsahelis, S. Papanikolaou and I. K. Kookos, *Fuel*, 2014, **116**, 566-577.
2. N. R. Baral, O. Kavvada, D. Mendez-Perez, A. Mukhopadhyay, T. S. Lee, B. A. Simmons and C. D. Scown, *Energy & Environmental Science*, 2019, **12**, 807-824.
3. F. Xu, J. Sun, N. Konda, J. Shi, T. Dutta, C. D. Scown, B. A. Simmons and S. Singh, 2015.
4. J. Sun, N. M. Konda, J. Shi, R. Parthasarathi, T. Dutta, F. Xu, C. D. Scown, B. A. Simmons and S. Singh, *Energy & Environmental Science*, 2016, **9**, 2822-2834.
5. D. Humbird, R. Davis, L. Tao, C. Kinchin, D. Hsu, A. Aden, P. Schoen, J. Lukas, B. Olthof and M. Worley, *Process design and economics for biochemical conversion of lignocellulosic biomass to ethanol: dilute-acid pretreatment and enzymatic hydrolysis of corn stover*, National Renewable Energy Lab.(NREL), Golden, CO (United States), 2011.
6. W. Babel and R. H. Müller, *Applied microbiology and biotechnology*, 1985, **22**, 201-207.
7. D. P. Petrides, *Computers & chemical engineering*, 1994, **18**, S621-S625.
8. D. Petrides, *Bioseparations science and engineering*, 2000.
9. S. Y. Lee, J. Nielsen and G. Stephanopoulos, *Industrial Biotechnology: Products and Processes*, John Wiley & Sons, 2016.
10. H.-P. Meyer, W. Minas and D. Schmidhalter, *Industrial Biotechnology: Products and Processes*, 2016, 3-53.
11. A. Meo, X. L. Priebe and D. Weuster-Botz, *Journal of biotechnology*, 2017, **241**, 1-10.
12. J. Hannon, A. Bakker, L. Lynd and C. Wyman, 2007.

*Chemisorption of CO₂ by chitosan oligosaccharide/DMSO:
organic carbamato–carbonato bond formation*

Green Chemistry

Cutting-edge research for a greener sustainable future

rsc.li/greenchem



CO₂

CO₂

CO₂



Bio

ISSN 1463-9262



ROYAL SOCIETY
OF CHEMISTRY

PAPER

Abdussalam K. Qaroush, Ala'a F. Eftaiha *et al.*
Chemisorption of CO₂ by chitosan oligosaccharide/DMSO:
organic carbamate–carbonato bond formation



Cite this: *Green Chem.*, 2017, **19**, 4305

Chemisorption of CO₂ by chitosan oligosaccharide/DMSO: organic carbamato–carbonato bond formation†

Abdussalam K. Qaroush,^a Khaleel I. Assaf,^b Sanaa K. Bardaweel,^c Ala'a Al-Khateeb,^d Fatima Alsoubani,^d Esraa Al-Ramahi,^d Mahmoud Masri,^e Thomas Brück,^e Carsten Troll,^f Bernhard Rieger^f and Ala'a F. Eftaiha^{*d}

A newly formed bond of organic carbamato–carbonato emerged upon bubbling CO₂ in a low molecular weight chitosan hydrochloride oligosaccharide CS-HCl/DMSO binary mixture. The aforementioned bond was detected and confirmed using attenuated total reflectance-Fourier transform Infrared (ATR-FTIR) spectroscopy, with two prominent peaks at 1551 cm⁻¹ and 1709 cm⁻¹ corresponding to ionic organic alkylcarbonate (RCO₃⁻) and carbamate (RNH–CO₂⁻ NH₃⁺–R), respectively. ¹H-, ¹³C-, and ¹H–¹⁵N heteronuclear single quantum coherence (HSQC) NMR experiments were also employed. According to ¹³C NMR, two newly emerged peaks at 157.4 ppm and 161.5 ppm attributed for the carbonyl carbon within the sequestered species RCO₃⁻ and RNH–CO₂⁻ NH₃⁺–R, respectively. Upon CO₂ bubbling, cross peaks obtained from ¹H–¹⁵N HSQC at 84.7 and 6.8 ppm correlated to the ammonium counterpart chemical shift bound to the proton resonances. Volumetric uptake of CO₂ was measured using an ATR-FTIR autoclave equipped with a silicon probe. The equilibrium sorption capacity was 0.6 and 0.2 bars through the formation of RCO₃⁻ and RNH–CO₂⁻ NH₃⁺–R, respectively. Moreover, physisorption by the dried DMSO contributed to additional 0.4 bars. Density functional theory (DFT) calculations supported the occurrence of the suggested dual mechanisms and confirmed the formation of carbonate at **C-6** of the glucosamine co-monomer. Moreover, CS-HCl/DMSO showed a slight impact on cell proliferation after 48 hours; this was a clear evidence of its non-toxicity. The biodegradation test revealed that a degradation of about 80% of CS-HCl/DMSO was achieved after 33 days; these results indicated that this method is suitable for green industry. CS-HCl/DMSO showed modest activities against *Staphylococcus aureus* and *Escherichia coli*. In addition, CS-HCl/DMSO demonstrated a significant antifungal activity against *Aspergillus flavus* in comparison with Fluconazole.

Received 19th June 2017,
Accepted 15th August 2017
DOI: 10.1039/c7gc01830d
rs.li/greenchem

^aDepartment of Chemistry, Faculty of Science, The University of Jordan, Amman 11942, Jordan. E-mail: a.qaroush@ju.edu.jo

^bDepartment of Life Sciences and Chemistry, Jacobs University Bremen, Campus Ring 1, 28759 Bremen, Germany

^cDepartment of Pharmaceutical Sciences, Faculty of Pharmacy, The University of Jordan, Amman 11942, Jordan

^dDepartment of Chemistry, the Hashemite University, P.O. Box 150459, Zarqa 13115, Jordan. E-mail: alaa.eftaiha@hu.edu.jo

^eProfessorship of Industrial Biocatalysis, Department of Chemistry, Technische Universität München, Lichtenbergstraße 4, 85748 Garching, Germany

^fWACKER-Lehrstuhl für Makromolekulare Chemie, Technische Universität München, Lichtenbergstraße 4, 85747 Garching bei München, Germany

†Electronic supplementary information (ESI) available. See DOI: 10.1039/c7gc01830d

1. Introduction

One of the efficient approaches for climate change mitigation is carbon capture and sequestration (CCS). It is considered as an important technology to minimize CO₂ emission from flue gas in order to adhere to emission regulations imposed by several governmental agencies in leading industrial countries, viz., China, USA, and countries in the EU. To overcome problems associated with the mature technology of monoethanolamine (MEA) wet scrubbing agent, 'Green sorbents for carbon dioxide (CO₂) capturing' is a new addition in sustainable chemistry that was introduced very recently by our research group,^{1–3} although others have also reported significant contributions.^{4–10}

These reports are focused on the synthesis/use of eco-friendly materials, viz., cellulose^{11,12} and chitin^{4–7} bio-feedstocks, metal organic frameworks (MOFs)^{8–10} and synthetic

oligomers.¹ Moreover, developing less hazardous materials in terms of energy efficiency through the use of benign solvents for sustainable purposes is a highly demanding task.¹³

Polymers have attracted great interest as CO₂ sorbents due to their mechanical and thermal stability, ease of modification and casting into membranes,¹⁴ and their use in engineering porous/non-porous solids,¹⁵ liquids, and solution forms.¹⁶ Solid polymeric sorbents require a sorption temperature as low as 0 °C due to physical adsorption of CO₂ unless impregnated with pendant groups.¹⁷ The latter point is of major concern due to the leaching of the functionalized material(s). Such unsolved obstacles will persist unless chemisorption with both built-in functional group(s) and fast sorption kinetics are brought into the solution without any crosslinking, decomposition, or evaporative losses that are characteristic of solvents.¹⁸

Apart from synthetic polymers, bio-feedstocks such as chitin (the second most naturally-occurring polymer after cellulose) and its derivatives (primarily chitosan) are strong candidates that might serve as green sorbents (chemical structure is shown in Scheme 1).^{2–6} From an economical point of view, the production of 100 billion tons per annum¹⁹ of chitin was estimated to have a revenue of 63 billion US dollars in 2015²⁰ in the global market. For example, chitosan is used in wastewater treatment and plasters in the Mt and kt scale per year, respectively. The growing market of chitosan industry will pave the way towards worldwide awareness into a prosperous bio-economy that forms a strong pillar for a more sustainable future.

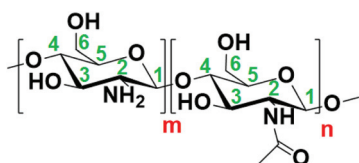
One inherent limitation associated with the use of these motifs is the lack of solubility that hinders their processability. The use of solvent mixtures,²¹ ionic liquids (ILs)²² or even using oligomers^{2,3} might serve as a proper choice to understand the chemistry of macromolecules in solution. The use of ILs is problematic, as shown by Tom Welton.²³ Their high viscosity, high cost, extreme care needed during purification and potential environmental hazards to aquatic and terrestrial ecosystems²⁴ are considered as major disadvantages. In this context, oligomeric sorbents provide a useful platform to act as an attractive tool that combines the parent properties with enhanced processability features by maintaining the unexploited supramolecular interactions that are better resolved.

The chemistry of CO₂ capturing takes place throughout by chemisorption and/or physisorption. The former is attained *via* two well-known approaches: carbonates (whether inorganic

or organic) and carbamates (RNH–CO₂[–] NH₃⁺–R), which follow the 1 : 1 and 1 : 2 mechanisms, respectively. The latter has a significant drawback due to the use of sacrificial bases together with its instability in aqueous solutions when forming bicarbonate (HCO₃[–])/carbonate (CO₃^{2–}) depending on the pH of the respective solution.²⁵ In addition, inorganic carbonates require high temperature for regeneration in the post-combustion capture, *viz.* 100–150 °C, which leads to additional energy expenditure for the industrial sector. Therefore, organic ionic alkylcarbonates (RCO₃[–]) are considered to be a promising approach in terms of regeneration temperature, stability in aqueous media, and reducing additional expenditure associated with highly expensive additives.^{26,27}

In this respect, following the concept of switchable solvents proposed by the Jessop group,^{14,15} several literature reports demonstrated that the usage of superbases is necessary to activate the alcohols, which results in the formation of ionic organic carbonate species upon CO₂ bubbling.^{28–31} Similarly, Sir J. Stoddart^{8,32–34} and co-workers reported that hydroxyl groups located at the rim of γ -cyclodextrin-rubidium based MOFs are capable of reacting with CO₂ reversibly to form a metal-stabilized RCO₃[–]. The chemisorption of CO₂ was confirmed by high-resolution solid-state ¹³C nuclear magnetic resonance (¹³C NMR) that indicated the emergence of a peak at 158 ppm upon CO₂ bubbling. Jessop's breakthrough combined with Stoddart's piece of artistic work led to the solubilization of naturally occurring polymers.²⁸ In 2016, a combination of polymer scission^{2,3} and acetate effect³⁵ resulted in task-specific oligomers for CO₂ capturing. Our research group reported the formation of RCO₃[–] through "supramolecular chemisorption" by reacting chitin-acetate oligomers dissolved in dimethyl sulfoxide (DMSO) at ambient CO₂ conditions without the use of further additives,^{2,3} such as activators or stabilizers (superbases²⁶ and metals,⁸ respectively). In terms of sustainability and greenness, the use of DMSO coincides with the guidelines set by the father of green chemistry Paul Anastas.¹³ DMSO is not only considered as a non-volatile organic compound due to its high boiling point,³⁶ but also a natural product that exists in beverages, fruits and vegetables at the micromolar level.^{37–39} Furthermore, DMSO is also used as a penetration enhancer in topical pharmaceutical formulations.⁴⁰ Together with its use as a polar aprotic solvent with extra merits such as ease of purification and low costs of production compared to ILs, DMSO is a potential greener candidate compared to polar aprotic solvents such as *N*-methyl-2-pyrrolidone (NMP), *N,N*-dimethylformamide (DMF), and *N,N*-dimethylacetamide (DMAc) as reviewed by J. H. Clark.⁴¹

Biodegradability is one of the key characteristic features in the field of green chemistry. To fulfill this need, the International Organization for Standardization (ISO) has issued nine standards⁴² for biodegradation testing in aqueous, compost, disintegration, soil or anaerobic based media.⁴³ ISO 14855-2:2007/Cor.:2009 or BS EN ISO/DIS 14855-2:2009, have been widely reported for many polymers like poly(lactic acid)^{43,44} and poly(butylene succinate).⁴⁵ Based on this method, the degradation was conducted within closed bio-



Scheme 1 Chemical structure of chitin ($n > m$) and its deacetylated form, chitosan ($m > n$). The numbers designate the carbon atoms across the constitutional repeating units.

reactors using a controlled composite to simulate an accelerated environmental decomposition. The reaction vessels were aerated with CO₂-free air. The degree of biodegradation is a percentage of the evolved CO₂ (captured with an alkaline trap) to the theoretical evolved CO₂.

Herein, a sustainable oligochitosan hydrochloride (CS-HCl) dissolved in DMSO (CS-HCl/DMSO) as a green sorbent for CO₂ capturing is exploited. A qualitative and quantitative determination of CO₂-chemisorbed species is determined through the formation of novel organic carbonato-carbamato motifs following the 1:1 and 1:2 mechanisms, respectively. The titled species are well characterized and analyzed *via* ¹H-, ¹³C-, and ¹⁵N-NMR spectroscopy, *ex situ* and *in situ* attenuated total reflectance-Fourier transform infrared (ATR-FTIR) spectroscopy, as well as density functional theory (DFT). This approach gives a straightforward approach towards the use of sustainable green sorbents for CO₂ capturing adapting a *benign-by-design* approach. To further explore the impact of using DMSO on the greenness/toxicity of the applied binary system, ISO/DIS 14855-2:2007 is chosen to evaluate the compatibility of the described CO₂ capturing system using the concept of green chemistry. In addition, the anti-bacterial, as well as anti-fungal activities are further tested for the CS-HCl/DMSO green sorbent.

2. Results and discussion

The main objective of this study was to show the possibility of obtaining a double sequestered species of CO₂ using a commercially available, sustainable, and renewable material, namely chitosan hydrochloride (CS-HCl) oligosaccharide. As reported elsewhere, CO₂ capture is achieved either by carbonate (organic and inorganic) or carbamate (RNH-CO₂⁻ NH₃⁺-R) formation. RCO₃⁻ is thermodynamically more stable than RNH-CO₂⁻ NH₃⁺-R,³ which is less energy demanding to regenerate compared to inorganic carbonates;²⁵ hence, we anticipate that organic carbonato-carbamato sorbents will show a prominent collaborative performance. In order to enhance the likelihood of RNH-CO₂⁻ NH₃⁺-R formation throughout the bio-renewables we used earlier, *viz.* chitin oligosaccharide,^{2,3} we focused our attention towards oligochitosan that can be produced from chitin by hydrolysis to increase the number of amine groups per sorbent. Herein, the degree of deacetylation (DDA) of the used chitosan oligomer was *ca.* 95% as verified by both proton nuclear magnetic resonance (¹H NMR) spectra and elemental analysis (EA) (see ESI, Fig. S1 and Table S1†).

2.1. Spectroscopic investigations

The absorption spectra of CS-HCl/NaOH pellet/DMSO before and after bubbling CO₂ measured by attenuated total reflectance-Fourier transform infrared (ATR-FTIR) spectroscopy (A) and the absorption profiles of CO₂ by neat DMSO (B), CS-HCl/DMSO (C), DMSO/NaOH pellet (D), and CS-HCl/NaOH pellet/DMSO (E) obtained using an *in situ* ATR-FTIR autoclave (4.0 bars, 25 °C, 10 mL dry DMSO) are shown in Fig. 1. In these

experiments, the water content of DMSO utilized was 6.1 ppm as measured using a Karl-Fischer titrator.

CS-HCl/DMSO solution absorbed 0.6 bar CO₂ through the formation of organic carbonate *via* supramolecular chemisorption^{2,3} (1551 cm⁻¹, Fig. 1A). In this context, the pH of CS-HCl aqueous solution was *ca.* 5.6, which implies that the material is fully protonated; therefore, NaOH was added to deprotonate the ammonium group in order to be prone to the nucleophilic attack of CO₂. The absorption profile of neat DMSO indicated that the absorption capacity was 0.4 bar. NaOH pellets were used due to its ease of filtration, which did not interfere with the overall effect on sorption capacity because of the elimination of water needed to make the side reaction to form sodium bicarbonate. CS-HCl/NaOH/DMSO solution absorbed 0.8 bar of CO₂ through the formation of organic carbonate together with an extra contribution of the RNH-CO₂⁻ NH₃⁺-R ion (1709 cm⁻¹, Fig. 1A) (0.2 bar of CO₂ absorbed as RNH-CO₂⁻ NH₃⁺-R upon correcting the DMSO and CS-HCl values from the overall drop in pressure). The sorption capacity of 10% w/v solution through chemisorption was 1.60 mmol CO₂ per g of sorbent. Taking into account an additional 0.81 mmol CO₂ due to physisorption, the total CO₂ absorbed was 2.41 mmol. In comparison with the sorption capacity of MEA aqueous solution (30% in water) reported in the literature, it absorbed 1.59 mmol CO₂ per g of sorbent,⁴⁶ which makes our material a potential candidate to compete with other commercially available compounds in the market.

As inferred from the sorption profiles, two presumed mechanisms (chemisorption and physisorption, *vide supra*) were involved during the capturing process. The chemisorption takes place through two independent pathways. The first one is the formation of RCO₃⁻ through supramolecular chemisorption *via* a 1:1 reaction mechanism, where DMSO activates the primary hydroxyl group of the amino pyranose ring towards nucleophilic attack.^{2,3} The organic carbonate adduct is stabilized through non-bonding interactions along the oligomer backbone. The second pathway results in the formation of RNH-CO₂⁻ NH₃⁺-R following a 1:2 reaction mechanism, through the nucleophilic attack of CO₂ by the amine's nitrogen.⁴⁷ The latter does not proceed unless sodium hydroxide is used to activate the glucopyranose amine groups towards nucleophilic attack through deprotonation. It is noteworthy that the faster kinetics of carbamate formation compared to organic carbonate is explained by the higher nucleophilicity of nitrogen compared to oxygen. Chemisorption was the principal competitor to the physisorption process (blue trace, Fig. 1) as demonstrated in both C and E where the kinetic profiles showed a slower sorption for the latter. Scheme 2 summarizes the two suggested chemisorption mechanisms of CO₂ capture by CS-HCl dissolved in DMSO; path A and B represent the formation of the RCO₃⁻ and RNH-CO₂⁻ NH₃⁺-R *via* the 1:1 and 1:2 mechanisms, respectively.

Nuclear magnetic resonance (NMR) was used to confirm the formation of carbonato-carbamato sequestered species in the CS-HCl/NaOH/DMSO solution. ¹³C NMR (Fig. 2A) showed

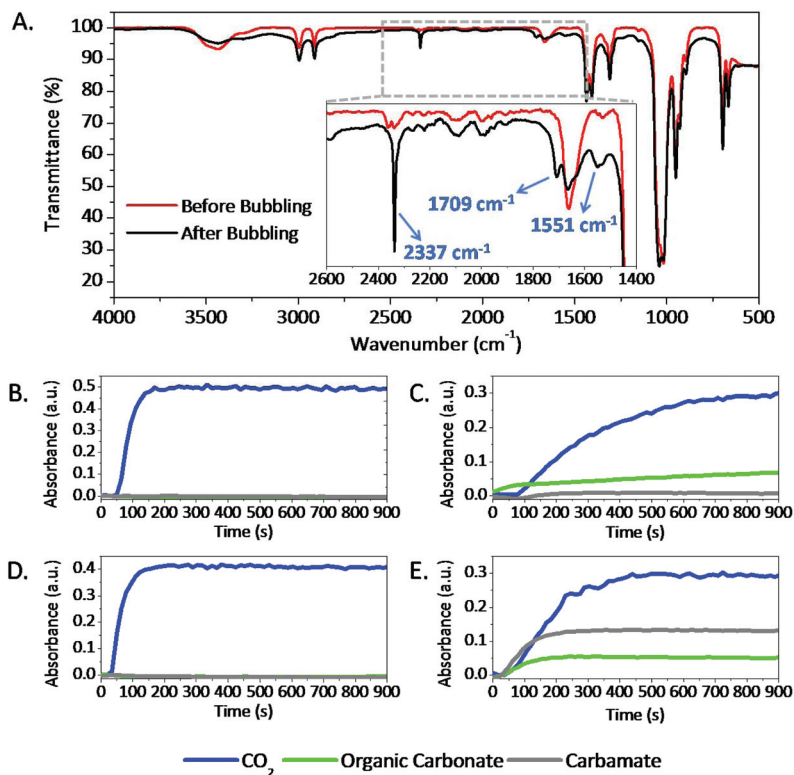
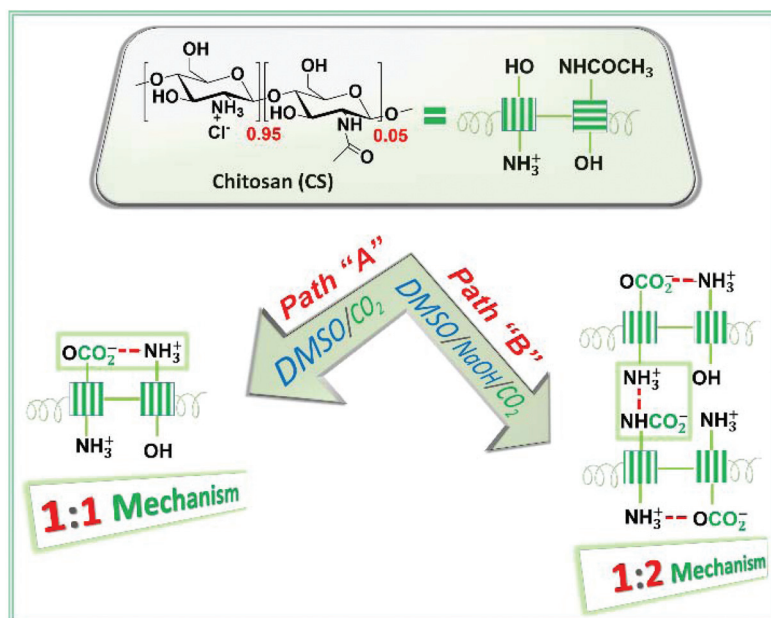


Fig. 1 A. ATR-FTIR Spectra of CS-HCl/NaOH/DMSO before (red) and after bubbling (black) with CO_2 . Absorption profiles of physisorbed carbon dioxide (blue), organic carbonate (green) and carbamate (gray) as a function of time of B. Neat DMSO. C. CS-HCl/DMSO. D. DMSO/NaOH pellet. E. CS-HCl/NaOH pellet/DMSO, obtained from *in situ* ATR-FTIR.



Scheme 2 Schematic diagram illustrating the proposed chemisorption mechanisms for CO_2 capturing upon CS-HCl dissolution in DMSO. Ionic organic alkylcarbonate (RCO_3^-) (Path A) represents a 1 : 1 mechanism. Ionic carbamates ($\text{RNH-CO}_2^- \text{NH}_3^+ \text{-R}$) (Path B) show a 1 : 2 mechanism.

the formation of two new peaks arising at 157.4 and 161.5 ppm, which correspond to the quaternary carbon of RCO_3^- and $\text{RNH-CO}_2^- \text{NH}_3^+ \text{-R}$ ions, respectively. Further,

^1H NMR (Fig. 2B) shows noticeable changes at two different chemical shift regions. First, a new peak evolved at 6.81 ppm, which corresponds to the ammonium counterpart of the car-

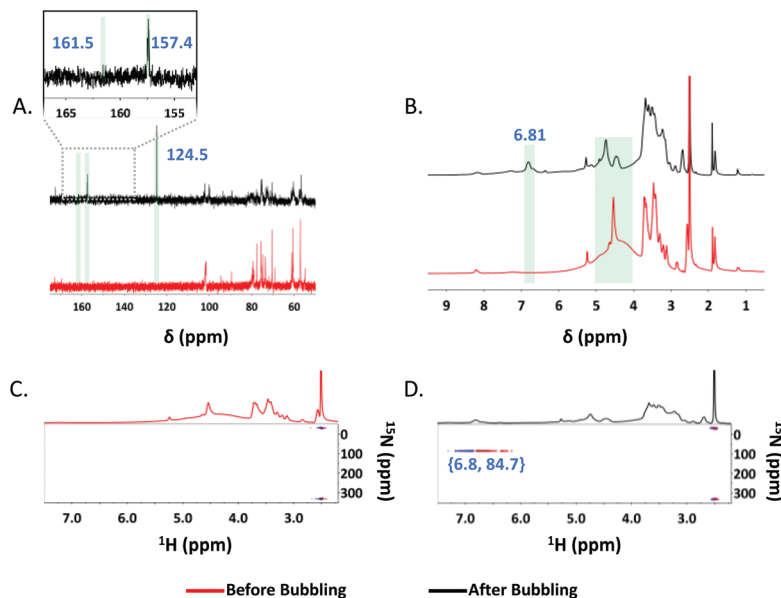


Fig. 2 NMR spectra of CS-HCl/NaOH/DMSO- d_6 before (red) and after (black) bubbling CO_2 . A. ^{13}C NMR. B. ^1H NMR. C. & D. ^1H - ^{15}N HSQC spectra.

bamate ion.³ Second, the methylene group neighboring the hydroxyl at C-6 was down-fielded to 4.75 ppm due to the inductive effect of the organic carbonate.

In addition, ^1H - ^{15}N heteronuclear single quantum coherence (HSQC) NMR (Fig. 2C and D) spectra provided useful information about the formed $\text{RNH-CO}_2^- \text{NH}_3^+-\text{R}$. Cross peaks at 84.7 and 6.8 ppm (correlated to the ammonium counterpart chemical shift, *vide supra*) were recorded to the nitrogen-bound proton resonances upon bubbling CO_2 . The same observation was seen in the monomeric unit of CS-HCl, *viz.* glucosamine hydrochloride (Gln-HCl, Fig. S2, ESI[†]). In ^{13}C NMR, it is noteworthy that doubling of peaks associated with the monomer was due to the 1 : 2 mechanism; the same observation was seen for task-specific ionic liquids as shown by Bates *et al.*⁴⁸ Doubling of peaks was not clearly observed in CS-HCl/NaOH/DMSO filtered solution (pellet-free) due to the presumed macromolecular effect (Fig. S2, ESI[†]). Structural simplicity of a monomeric unit cannot be extended to the oligomeric/polymeric form. This is further reflected over other physical properties such as solubility, viscosity, and crystallinity.

The reversible binding character of CO_2 was achieved by sonicating the DMSO solution at 55 ± 3 °C and confirmed by diminishing the chemical shifts of the sequestered species obtained by ^{13}C NMR spectroscopy (at *ca.* 157 and 161 ppm).

2.2. Computational investigation

In order to attain an in-depth understanding of the interaction between CS and CO_2 , gas phase density functional theory (DFT) calculations were performed using a Gln trimer as a model compound; the optimized structure is shown in Fig. 3. The proton affinity (PA) values for the ionizable amine and

hydroxyl groups of the optimized structure were calculated and are shown in Table 1.

Although the gas phase is considered as the “ultimate” non-polar environment,⁴⁹ solvents play an important role when exploring the acidity/basicity of different compounds. The gas phase calculations provide the intrinsic PA values rather than relative reactivity, which could be exploited to understand the influence of solvation and intermolecular forces on reactivity.^{50,51} The higher the PA values, the stronger is the base and the weaker the corresponding conjugated acid in the gas phase. Results revealed that the deprotonation of the ammonium ($-\text{NH}_3^+$) group is the easiest compared to the other possible ionizable sites, followed by the hydroxyl groups at C-6 and C-3, respectively. This implies that the $-\text{OH}$ group at C-6 is the second most reactive site towards bases and thus, its alkoxide (RO^-) ion counterpart is the most susceptible to form RCO_3^- upon reacting with CO_2 even in the absence of supramolecular stabilization as in the corresponding oligomer (*vide supra*).

Besides the effect of aforementioned electronic parameter on the difference in the acidity between the primary (1°) hydroxyl group at C-6 and its secondary (2°) counterpart at C-3,

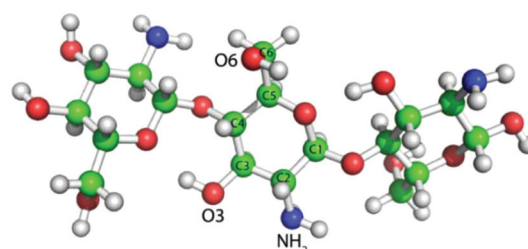


Fig. 3 The optimized structure of Gln trimer, as a model compound.

Table 1 Calculated proton affinities^a (PA) of the amino and the hydroxyl group at the central Gln unit in the trimer; the structure is shown in Fig. 3

Possible protonation active sites	PA (kcal mol ⁻¹)
Gln-Gln(NH ₂)-Gln + H ⁺ → Gln-Gln(NH ₃ ⁺)-Gln	293.4
Gln-Gln(NH ₂)(O ⁻ -6)-Gln + H ⁺ → Gln-Gln(NH ₂)(OH-6)-Gln	329.4
Gln-Gln(NH ₂)(O ⁻ -3)-Gln + H ⁺ → Gln-Gln(NH ₂)(OH-3)-Gln	331.2

^a PA values were calculated using the Gaussian 09 software (B3LYP/6-31+G* level of theory) as the negative of the enthalpy change (ΔH) of the gas phase reaction, $A_{(g)} + H^+_{(g)} \rightarrow AH^+_{(g)}$. Under standard conditions, the value of the enthalpy of the gas-phase proton was taken as 1.48 kcal mol⁻¹.⁵²

the solvation effect might also contribute to higher PA values. It seems that DMSO molecules can easily solvate, and hence stabilize the unhindered RO⁻ anion at C-6 compared to C-3 once formed. This is consistent with the NMR data obtained for Gln·HCl/NaOH/DMSO-*d*₆ upon bubbling CO₂ (Fig. S2 A, ESI[†]), where ¹³C NMR spectra indicated the emergence of two peaks at 157.7 and 159.2 ppm, corresponding to formation of RCO₃⁻ and RNH-CO₂⁻ NH₃⁺-R, respectively. The complexity of the ¹³C NMR of Gln·HCl due to the different organic carbonate/carbamate assemblies, which resulted in peak doubling (*vide supra*), was better resolved by using glucose as an analogous chemical structure (Fig. S3, ESI[†]). The ¹³C-NMR of glucose/NaOH/DMSO indicated that the chemical shift of C-6 was down-fielded from 61.7 ppm to a set of split peaks ranging from (63.4 to 64.8) ppm due to the RCO₃⁻ formation and presumably the inter- and intramolecular interactions after bubbling CO₂. Other hydroxyl groups from C-1 to C-4 were not shifted in the spectrum due to their lower reactivity (2° alcohols).

To fully understand the stability of two possible CO₂ adducts (if present), the optimized structures of RCO₃⁻ (either at C-6 or C-3) and RNH-CO₂⁻ NH₃⁺-R (at C-2) at the central unit of the trimer are shown in Fig. 4. The calculated relative energy values showed that the formation of carbamate and organic carbonate at C-3 (Fig. 4A) is less favorable by 15 kcal mol⁻¹ compared to that formed at C-6 (Fig. 4B), as a result of the strong repulsion between the carbonate at C-3 and the carbamate. This is verified by ¹³C NMR experiments (no C-3 carbonate was observed, *vide supra*). The optimized

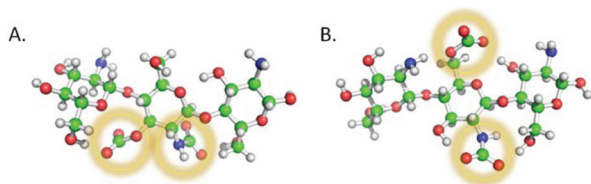


Fig. 4 DFT-optimized structures of carbamate-together with organic carbonate-adducts formed at A. C-3 and B. C-6 of the central unit of the glucosamine trimer.

structures (Fig. S4, ESI[†]) and the calculated relative energy values for the hypothetically formed single CO₂ species, *i.e.*, either carbonate or carbamate, are presented in Table S2, ESI[†].

2.3. Biodegradation study

The biodegradation of the chitosan oligosaccharide in a controlled compost was measured in a 1 L stirred tank bioreactor accompanied with the CO₂ unit (washing, drying and capturing). Fig. 5 shows the biodegradation diagram as a function of incubation time maintained at 58 °C. Within the first 10 days, results showed that less than 10% of CS·HCl was degraded as seen from the minor differences in the amount of evolved CO₂ from the blank and sample vessels. On day 11, the degradation appeared to be more intense until it reached about 80% after 33 days. The high degree of degradation in the relatively short time (according to the ISO protocol, see section 4.1.4) clearly indicated that CS·HCl is well-suited as sustainable and degradable in the presence of DMSO. It also fortified the usage of this solvent and formed a clear-cut evidence that it has no influence on the biodegradation of CS, which encountered concerns presented recently by Clark and coworkers⁴¹ on the guidelines of selecting green solvents. This finding could be of great importance for both the academic and industrial sectors.

2.4. Cytotoxicity results

Fig. 6 presents the percentage cell proliferation determined as (Absorbance of experimental well/Absorbance of negative control well) × 100 as a function of concentration. Statistical analysis was performed by applying the Student's *t*-test using SPSS 10.0 statistical software package (SPSSFW, SPSS Inc., Chicago, IL, USA). A *p*-value <0.05 was considered statistically significant. Each experiment represented the average of a series of three replicates. Notably, cell viability was not significantly changed after exposure of human fibroblasts to CS·HCl using the MTS assay. Cell growth of fibroblast cell cultures was evaluated using the MTS assay after 24 h and 48 h exposure periods. As demonstrated in Fig. 6, there is no statistically significant difference between the cell proliferation rates in wells

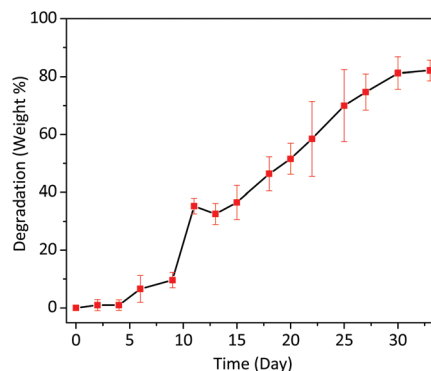


Fig. 5 Biodegradation evaluation method by gravimetric measurement of CO₂ evolved via a laboratory-scale test using DASGIP® benchtop bioreactor in a controlled compost at 58 °C following the standard protocol, ISO/DIS 14855-2:2007/Cor.:2009.

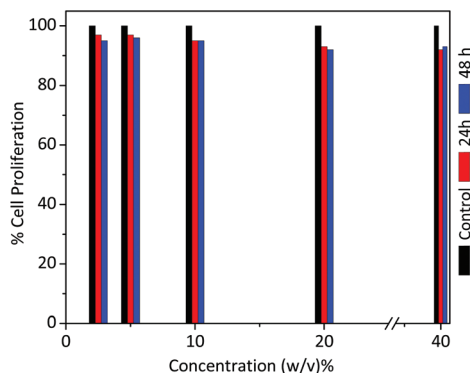


Fig. 6 Percentage of cell proliferation after 24 and 48 hours exposure periods.

Table 2 Antimicrobial activity measured by a zone of inhibition (mm). Results represent the means of three independent readings

Microorganism	CS-HCl/DMSO	Control
<i>Staphylococcus aureus</i>	9 ± 0.7	14 ± 0.9
<i>Escherichia coli</i>	12 ± 0.5	18 ± 1.0
<i>Aspergillus flavus</i>	13 ± 0.9	25 ± 1.0

treated with CS-HCl/DMSO at the concentration ranges used relative to control cells (untreated well) after both exposure periods, indicating a reasonable safety margin of CS-HCl/DMSO.

As shown in Table 2, upon comparison with the antibacterial activity of Norfloxacin, CS-HCl/DMSO exhibited pronounced activities against *Staphylococcus aureus* and *Escherichia coli*. In addition, CS-HCl/DMSO demonstrated a significant antifungal activity against *Aspergillus flavus* relative to Fluconazole.

3. Conclusions

Briefly, a sustainable oligochitosan hydrochloride dissolved in DMSO as a green sorbent for CO₂ capturing is reported. Two different mechanisms are described: the formation of organic carbonate through the 1:1 mechanism in the absence of NaOH, and the formation of novel organic carbonato-carbamato species following a 1:2 mechanism. NMR and ATR-FTIR support the formation of carbonato-carbamato species in the CS-HCl/NaOH/DMSO solution. Absorption profiles indicate that the carbamate is formed faster than carbonate in NaOH/DMSO solution. Further, DFT calculations confirm the formation of the carbonate at the C-6 position together with carbamate formation. Further testing showed that CS-HCl/DMSO had a minor effect (non-toxicity) on cell proliferation after two days of the exposure. Moreover, it was shown to be a biodegradable binary mixture. Also, the CS-HCl/DMSO binary sorbent showed both antibacterial and antifungal characteristics with good activities. This confirms that DMSO usage

within the sorbent system is eco-friendly and it does not have a negative impact on CS-HCl as a non-toxic/biodegradable green sorbent for CO₂ capture. Explicitly, this makes the application of CS-HCl/DMSO to be more suited towards academic and industrial interests upon implementation, which will open new horizons in sustainable green technology. Furthermore, greater focus should be directed towards the dissolution of high molecular weight bio-feedstocks that are able to sequester CO₂ as organic ionic alkylcarbonates and/or carbamates.

4. Experimental

4.1. Materials and methods

4.1.1. Chemicals. Unless otherwise stated, all chemicals were used without further purification. Low molecular weight chitosan hydrochloride (CS-HCl) was prepared by G.T.C. Bio Corporation (1.5 kDa), Qingdao, China. For experimental manipulations, CS-HCl was dried overnight in a Schlenk tube at 50 °C (oil bath, *in vacuo*). CO₂ (99.95%, Food Grade) was purchased from Advanced Technical Gases Co. (Amman, Jordan). Glucosamine hydrochloride (Gln-HCl), DMSO-*d*₆, D₂O, sodium hydroxide (NaOH) and hydrochloric acid (HCl, 37%) were purchased from Sigma-Aldrich and DMSO was purchased from TEDIA.

4.1.2. Instruments. Solution ¹H, ¹³C, and ¹H-¹⁵N heteronuclear single quantum coherence (HSQC -nuclear magnetic resonance (NMR)) spectra were collected at room temperature using (AVANCE-III 400 MHz (¹H: 400.13 MHz, ¹³C: 100.61 MHz, ¹⁵N: 40.560 MHz)) FT-NMR NanoBay spectrometer (Bruker, Switzerland) in either DMSO-*d*₆ or D₂O. Elemental Analysis (EA) was performed using a EURO EA 3000 instrument (Euro Vector, Italy). *In situ* attenuated total reflectance-Fourier transform infrared (ATR-FTIR) measurements were carried out using an MMIR45 m RB04-50 (Mettler-Toledo, Switzerland) with an MCT Detector, with a silicon windows probe connected *via* a pressure vessel. Sampling was done from 3500 to 650 cm⁻¹ at 8 wavenumber resolution; scan option: 64; gain: 1×. *Ex situ* ATR-FTIR spectra were recorded on a Bruker Vertex 70-FT-IR spectrometer at room temperature coupled with a Vertex Pt-ATR accessory. Water content was measured using a Karl-Fischer titrator (TZ 1753 with Diaphragma, KF1100, TitroLine KF). pH measurements were obtained *via* an RL 150-Russel pH meter.

4.1.3. Computational method. Calculations were performed within Gaussian 09.⁵³ The full optimization was performed using the DFT method (B3LYP/6-31+G*). Minima were characterized by the absence of imaginary frequencies.

4.1.4. Biodegradability study. The biodegradability test was conducted in accordance with the standard operating procedure of ISO/DIS 14855-2:2007/Cor.:2009. The controlled composite was collected from a soil of chicken farms in Munich-Germany. The incubation was continued at 58 °C in 1 L stirred tank glass bioreactors (DASGIP® Benchtop Bioreactors, Eppendorf, Germany). Bioreactors were connected to a

designed unit for effective CO₂ washing, drying and capture. The evolved CO₂ was measured gravimetrically using an electronic balance (Sartorius, Germany) with a display reading down to ±1 mg. According to of ISO14855-2:2007, the polymer should reach a 75% degradation ratio after 45 days to be considered as a biodegradable polymer.

4.1.5. Cytotoxicity study. Human skin fibroblasts were maintained in a phenol red-free culture medium DMEM/F12 (Dulbecco's modified essential medium/Ham's 12 nutrient mixture, Gibco), supplemented with 5% (v/v) fetal calf serum (JS Bioscience, Australia), and 1% (v/v) antibiotic (2 mM L-glutamine, 100 U mL⁻¹ penicillin and 0.1 mg mL⁻¹ streptomycin; Gibco). Cultured cells were incubated at 37 °C in a humidified 5% CO₂ incubator. The confluent cell layers were enzymatically removed, using Trypsin/EDTA (Gibco, USA), and resuspended in the culture medium. Cell viability was assessed by vital staining with trypan blue (0.4% (w/v); Sigma, USA), and cell number was determined using a light microscope.

In vitro evaluation of the cytotoxicity was performed using the Promega CellTiter 96® Aqueous Non-Radioactive Cell Proliferation (MTS) assay to determine the number of viable cells in the culture (Promega, 2005). CS-HCl/DMSO was added to the culture media at concentrations of 2.5, 5, 10, 20, and 40% (w/v DMSO) and incubated at 37 °C with 5% CO₂. Two sets of exposure times were carried out. These included 24 h and 48 h exposure periods. At the end of each exposure time, an MTS mixture (20 µL per well) was added. The absorbance of the formazan product was read at 492 nm using a microplate enzyme-linked immunoassay (ELISA) reader. Each experiment was repeated on three independent occasions. Two internal controls were used for each experiment; a negative control consisting of cells only without any treatment; and a positive control consisting of cells treated with vincristine, a microtubulin polymerization inhibitor.

4.1.6. Anti-microbial activity assays. Antibacterial activity of CS-HCl/DMSO was studied against *Staphylococcus aureus* ATCC 6538, and *Escherichia coli* ATCC 29425. Antifungal activity of CS-HCl/DMSO was examined against mycelial fungi (*Aspergillus flavus*). Overnight cultures of microorganisms were freshly prepared for each assay.

The agar diffusion method was used to assess the anti-microbial activities of CS-HCl/DMSO, with a minor modification. Briefly, Trypticase Soy agar (Difco) medium was aseptically inoculated with the bacterial or fungal suspension of the microorganism under examination. Wells were drilled and filled with 25 µL of CS-HCl/DMSO. Bacterial plates were incubated at 37 °C for 24 h whereas fungal plates were incubated at 25 °C for 48 h. After completion of the incubation period, the inhibition zones were observed and measured in mm. A positive control, Norfloxacin 1 mg mL⁻¹ for bacteria and Fluconazole 1 mg mL⁻¹ for fungi, and a negative control of the vehicle (DMSO) were employed. Each assay was repeated in triplicate.

4.1.7. Experimental procedure

4.1.7.1. NMR. In an NMR tube, 30 mg of the substrate was dissolved in 0.5 mL DMSO-*d*₆. Upon dissolution, CO₂ was

bubbled into the NMR tube *via* a long cannula for 20 minutes. CO₂ Saturation was ensured using NMR spectroscopy.

4.1.7.2. *In situ* ATR-FTIR. – Formation of carbonato-terminated oligosaccharide

The addition of 1.0 g CS-HCl together with 10 mL dry DMSO (6.1 ppm H₂O, Karl-Fischer titrator) in a Schlenk flask was performed, and was sonicated till it completely dissolved. This solution was transferred into the IR autoclave, with parameters set at 25 °C, 4 bar CO₂, and then the reaction was run for 4 hours (intervals of 15 seconds, initial and end pressure are to be reported). Initial pressure: 4.0 bar, final pressure: 3.0 bar, organic alkyl carbonate contribution through sorption was 0.6 bar.

– Formation of carbonato-carbamato-terminated oligosaccharide

One gram of CS-HCl together was added to 10 mL dry DMSO (6.1 ppm H₂O, Karl-Fischer titrator) in a Schlenk flask and sonicated till it completely dissolved. Further, 1.0 g of sodium hydroxide pellets was added and stirred for a minute and the solution was filtered in order to prevent any side reactions with the base used. Upon completion, the constituents were transferred into the IR autoclave using the same previous parameters (*vide supra*). Initial pressure: 4.2 bar, final pressure: 2.8 bar; carbamates contribution through sorption process: 0.2 bar; organic alkyl carbonate contribution through sorption was 0.6 bar.

For correction purposes, 10 mL DMSO was added into the IR autoclave; the solvent contribution was 0.4 bar as a result of physisorption (¹³C NMR peak identified at 124 ppm, together with ATR-FTIR peak centered at 2337 cm⁻¹).

Conflicts of interest

There are no conflicts to declare.

Acknowledgements

AFE acknowledges the Deanship of Scientific Research at the Hashemite University. Marina Reiter (TUM, Germany) is acknowledged for performing the volumetric uptake measurements using the *in situ* ATR-FTIR autoclaves. Thanks to Mr Basem R. Nassrallah (HU, Jordan) for performing the EA experiments.

References

- 1 A. K. Qaroush, D. A. Castillo-Molina, C. Troll, M. A. Abu-Daibes, H. M. Alsayouri, A. S. Abu-Surrah and B. Rieger, *ChemSusChem*, 2015, **8**, 1618–1626.
- 2 A. F. Eftaiha, F. Alsoubani, K. I. Assaf, W. M. Nau, C. Troll and A. K. Qaroush, *RSC Adv.*, 2016, **6**, 22090–22093.
- 3 A. F. Eftaiha, F. Alsoubani, K. I. Assaf, C. Troll, B. Rieger, A. H. Khaled and A. K. Qaroush, *Carbohydr. Polym.*, 2016, **152**, 163–169.

- 4 H. Xie, S. Zhang and S. Li, *Green Chem.*, 2006, **8**, 630–633.
- 5 X. Sun, C. Huang, Z. Xue and T. Mu, *Energy Fuels*, 2015, **29**, 1923–1930.
- 6 P. S. Barber, C. S. Griggs, G. Gurau, Z. Liu, S. Li, Z. Li, X. Lu, S. Zhang and R. D. Rogers, *Angew. Chem., Int. Ed.*, 2013, **52**, 12350–12353.
- 7 K. Pohako-Esko, M. Bahlmann, P. S. Schulz and P. Wasserscheid, *Ind. Eng. Chem. Res.*, 2016, **55**, 7052–7059.
- 8 J. J. Gassensmith, H. Furukawa, R. A. Smaldone, R. S. Forgan, Y. Y. Botros, O. M. Yaghi and J. F. Stoddart, *J. Am. Chem. Soc.*, 2011, **133**, 15312–15315.
- 9 Y. Lin, Q. Yan, C. Kong and L. Chen, *Sci. Rep.*, 2013, **3**, 1859.
- 10 Z. Hu, M. Khurana, Y. H. Seah, M. Zhang, Z. Guo and D. Zhao, *Met.-Org. Framew. Emerg. Chem. Technol.*, 2015, **124**, 61–69.
- 11 Q. Zhang, N. S. Oztekin, J. Barrault, K. De Oliveira Vigier and F. Jérôme, *ChemSusChem*, 2013, **6**, 593–596.
- 12 Y. Yang, L. Song, C. Peng, E. Liu and H. Xie, *Green Chem.*, 2015, **17**, 2758–2763.
- 13 P. Anastas and N. Eghbali, *Chem. Soc. Rev.*, 2010, **39**, 301–312.
- 14 C. E. Powell and G. G. Qiao, *J. Membr. Sci.*, 2006, **279**, 1–49.
- 15 N. Du, H. B. Park, G. P. Robertson, M. M. Dal-Cin, T. Visser, L. Scoles and M. D. Guiver, *Nat. Mater.*, 2011, **10**, 372–375.
- 16 S. Supasitmongkol and P. Styring, *Energy Environ. Sci.*, 2010, **3**, 1961–1972.
- 17 R. Dawson, A. I. Cooper and D. J. Adams, *Polym. Int.*, 2013, **62**, 345–352.
- 18 S. Choi, J. H. Drese and C. W. Jones, *ChemSusChem*, 2009, **2**, 796–854.
- 19 N. Yan and X. Chen, *Nature*, 2015, **542**, 155–157.
- 20 E. Stoye, Chitin, Chemistry World Podcast, August 2013, Chitin-Biopolymer-Chitosan.
- 21 T. Heinze and A. Koschella, *Polim.: Cienc. Tecnol.*, 2005, **15**, 84–90.
- 22 A. Pinkert, K. N. Marsh and S. Pang, *Ind. Eng. Chem. Res.*, 2010, **49**, 11121–11130.
- 23 M. T. Clough, K. Geyer, P. A. Hunt, S. Son, U. Vagt and T. Welton, *Green Chem.*, 2015, **17**, 231–243.
- 24 T. P. Thuy Pham, C.-W. Cho and Y.-S. Yun, *Water Res.*, 2010, **44**, 352–372.
- 25 M. Pera-Titus, *Chem. Rev.*, 2014, **114**, 1413–1492.
- 26 P. G. Jessop, D. J. Heldebrant, X. Li, C. A. Eckert and C. L. Liotta, *Nature*, 2005, **436**, 1102–1102.
- 27 P. G. Jessop, S. M. Mercer and D. J. Heldebrant, *Energy Environ. Sci.*, 2012, **5**, 7240–7253.
- 28 Q. Zhang, N. S. Oztekin, J. Barrault, K. De Oliveira Vigier and F. Jérôme, *ChemSusChem*, 2013, **6**, 593–596.
- 29 G. V. S. M. Carrera, N. Jordao, L. C. Branco and M. Nunes da Ponte, *Faraday Discuss.*, 2015, **183**, 429–444.
- 30 K. I. Assaf, A. K. Qaroush and A. F. Eftaiha, *Phys. Chem. Chem. Phys.*, 2017, **19**, 15403–15411.
- 31 A. K. Qaroush, K. I. Assaf, A. Al-Khateeb, F. Alsoubani, E. Nabih, C. Troll, B. Rieger and A. F. Eftaiha, *Energy Fuels*, 2017, **31**(8), 8407–8414.
- 32 D. Wu, J. J. Gassensmith, D. Gouvêa, S. Ushakov, J. F. Stoddart and A. Navrotsky, *J. Am. Chem. Soc.*, 2013, **135**, 6790–6793.
- 33 J. J. Gassensmith, J. Y. Kim, J. M. Holcroft, O. K. Farha, J. F. Stoddart, J. T. Hupp and N. C. Jeong, *J. Am. Chem. Soc.*, 2014, **136**, 8277–8282.
- 34 K. J. Hartlieb, J. M. Holcroft, P. Z. Moghadam, N. A. Vermeulen, M. M. Algaradah, M. S. Nassar, Y. Y. Botros, R. Q. Snurr and J. F. Stoddart, *J. Am. Chem. Soc.*, 2016, **138**, 2292–2301.
- 35 Y. Qin, X. Lu, N. Sun and R. D. Rogers, *Green Chem.*, 2010, **12**, 968–971.
- 36 D. Stoye, in *Ullmann's Encyclopedia of Industrial Chemistry*, Wiley-VCH Verlag GmbH & Co. KGaA, 2000.
- 37 T. W. Pearson, H. J. Dawson and H. B. Lackey, *J. Agric. Food Chem.*, 1981, **29**, 1089–1091.
- 38 *Dimethyl Sulfoxide Producers Association*, United States Environmental Protection Agency, 2003.
- 39 M. Ganguly, C. Mondal, J. Jana, A. Pal and T. Pal, *Langmuir*, 2014, **30**, 348–357.
- 40 M. L. McPherson and N. M. Cimino, *Pain Med.*, 2013, **14**, S35–S39.
- 41 F. P. Byrne, S. Jin, G. Paggiola, T. H. M. Petchey, J. H. Clark, T. J. Farmer, A. J. Hunt, C. Robert McElroy and J. Sherwood, *Sustainable Chem. Processes*, 2016, **4**, 7.
- 42 *A Handbook of Applied Biopolymer Technology: Synthesis, Degradation and Applications*, ed. S. K. Sharma and A. Mudhoo, The Royal Society of Chemistry, 2011.
- 43 *Determination of the Ultimate Aerobic Biodegradability of Plastic Materials under Controlled Composting Conditions-Method by Analysis of Evolved Carbon Dioxide-Part 2: Gravimetric Measurement of Carbon Dioxide Evolved In a Laboratory-Scale Test*, ed. International Organization for Standardization, ISO 14855-2, ISO, Geneva, Switzerland, 2007, <https://www.iso.org/obp/ui/#iso:std:iso:14855:-2:ed-1:v1:cor:1:v1:en>.
- 44 M. Funabashi, F. Ninomiya and M. Kunioka, *J. Polym. Environ.*, 2007, **15**, 245–250.
- 45 M. Kunioka, F. Ninomiya and M. Funabashi, *Int. J. Mol. Sci.*, 2009, **10**, 4267–4283.
- 46 D. J. Heldebrant, C. R. Yonker, P. G. Jessop and L. Phan, *Energy Environ. Sci.*, 2008, **1**, 487–493.
- 47 P. V. Kortunov, M. Siskin, L. S. Baugh and D. C. Calabro, *Energy Fuels*, 2015, **29**, 5940–5966.
- 48 E. D. Bates, R. D. Mayton, I. Ntai and J. H. Davis, *J. Am. Chem. Soc.*, 2002, **124**, 926–927.
- 49 X. Sun and J. K. Lee, *J. Org. Chem.*, 2007, **72**, 6548–6555.
- 50 J. I. Brauman and L. K. Blair, *J. Am. Chem. Soc.*, 1968, **90**, 6561–6562.
- 51 C. A. Deakynne, *Thermochem. Solvation Gas Phase Ions*, 2003, **227**, 601–616.
- 52 A. Moser, K. Range and D. M. York, *J. Phys. Chem. B*, 2010, **114**, 13911–13921.
- 53 M. J. Frisch, G. W. Trucks, H. B. Schlegel, G. E. Scuseria, M. A. Robb, J. R. Cheeseman, G. Scalmani, V. Barone, B. Mennucci, G. A. Petersson, H. Nakatsuji, M. Caricato, X. Li, H. P. Hratchian, A. F. Izmaylov, J. Bloino, G. Zheng,

J. L. Sonnenberg, M. Hada, M. Ehara, K. Toyota, R. Fukuda, J. Hasegawa, M. Ishida, T. Nakajima, Y. Honda, O. Kitao, H. Nakai, T. Vreven, J. A. Montgomery, Jr., J. E. Peralta, F. Ogliaro, M. Bearpark, J. J. Heyd, E. Brothers, K. N. Kudin, V. N. Staroverov, T. Keith, R. Kobayashi, J. Normand, K. Raghavachari, A. Rendell, J. C. Burant, S. S. Iyengar, J. Tomasi, M. Cossi, N. Rega, J. M. Millam, M. Klene,

J. E. Knox, J. B. Cross, V. Bakken, C. Adamo, J. Jaramillo, R. Gomperts, R. E. Stratmann, O. Yazyev, A. J. Austin, R. Cammi, C. Pomelli, J. W. Ochterski, R. L. Martin, K. Morokuma, V. G. Zakrzewski, G. A. Voth, P. Salvador, J. J. Dannenberg, S. Dapprich, A. D. Daniels, O. Farkas, J. B. Foresman, J. V. Ortiz, J. Cioslowski and D. J. Fox, *Gaussian 09*, Gaussian, Inc., Wallingford CT, 2010.

Chemisorption of CO₂ by Chitosan Oligosaccharide/DMSO: Organic Carbamato-Carbonato Bond Formation

Abdussalam K. Qaroush^{a*} Khaleel I. Assaf,^b Sanaa K. Bardaweel,^c Ala'a Al-Khateeb,^d Fatima Alsoubani,^d Esraa Al-Ramahi,^d Mahmoud Masri,^e Thomas Brück,^e Carsten Troll,^f Bernhard Rieger,^f Ala'a F. Eftaiha,^{d*}

^aDepartment of Chemistry, Faculty of Science, The University of Jordan, Amman 11942, Jordan.

^bDepartment of Life Sciences and Chemistry, Jacobs University Bremen, Campus Ring 1, 28759 Bremen, Germany.

^cDepartment of Pharmaceutical Sciences, Faculty of Pharmacy, The University of Jordan, Amman 11942, Jordan.

^dDepartment of Chemistry, the Hashemite University, P.O. Box 150459, Zarqa 13115, Jordan.

^eDivision of Industrial Biocatalysis, Department of Chemistry, Technische Universität München, Lichtenbergstraße 4, 85748 Garching, Germany.

^fWACKER-Lehrstuhl für Makromolekulare Chemie, Technische Universität München, Lichtenbergstraße 4, 85747 Garching bei München, Germany.

* Corresponding Authors: a.qaroush@ju.edu.jo (AKQ)
alaa.eftaiha@hu.edu.jo (AFE)

Electronic Supporting Information (ESI)

Figure S1. Partial ¹H NMR spectrum of CS•HCl dissolved in D₂O and its proposed chemical structure. The degree of deacetylation (DDA) was determined using the integration of the acetyl protons (**H-Ac**) and the sum of the protons attached to **C-2**, till **C-6** according to the following equation¹: $DDA = (1 - [(H-Ac/3)/(H-((C-2)-(C-6))/6)]) \times 100\% \approx 94.8\%$

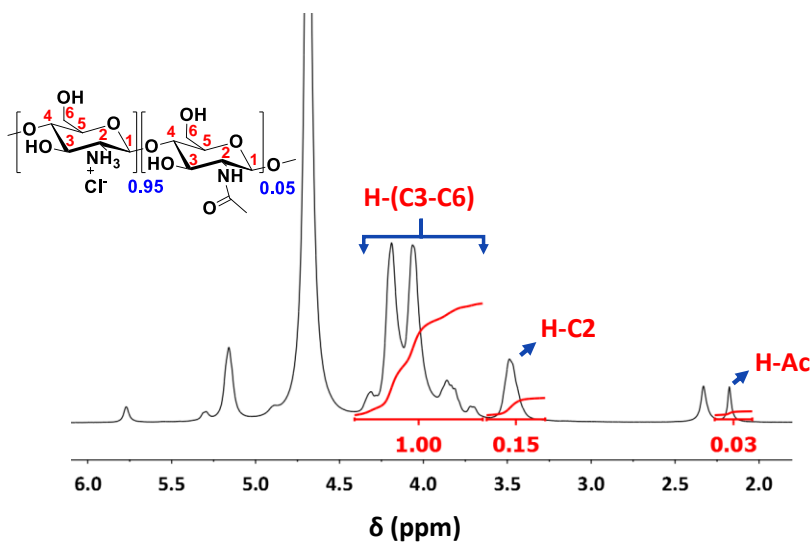


Table S1. CHN results of CS•HCl obtained from EA. DDA was calculated from the weight ratio between carbon and nitrogen ($W_{C/N}$) according to the following equation²:

$$DDA = (4 - (0.583 \times W_{C/N})) \times 100\%$$

C %	H%	N%	$W_{C/N} = 5.228$	$DDA = 95.2\%$
35.60	6.24	6.81		

Figure S2. NMR spectra of Gln•HCl/NaOH/DMSO- d_6 before (red) and after (black) bubbling CO_2 . **A.** ^{13}C NMR, **B.** 1H NMR, **C.** & **D.** 1H - ^{15}N HSQC spectra.

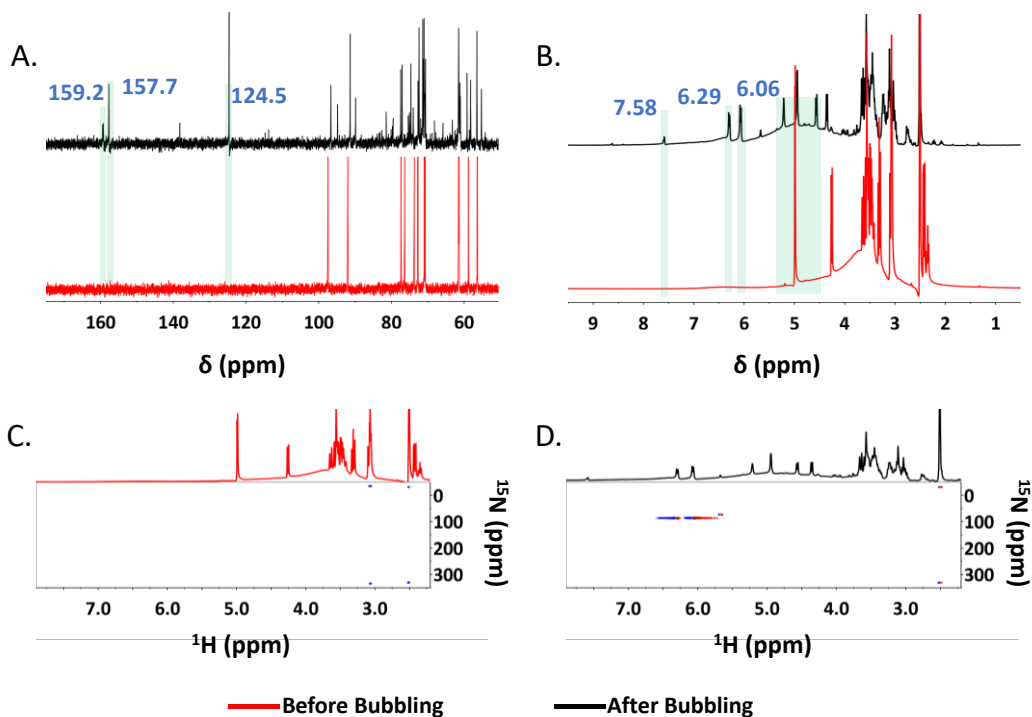


Figure S3. Partial ^{13}C NMR spectra of glucose/NaOH pellet/in $\text{DMSO-}d_6$ obtained before (red) and after bubbling of CO_2 (black). The peak emerged at 167.5 ppm corresponds to inorganic bicarbonate as a result of the side reaction of the NaOH with CO_2 .

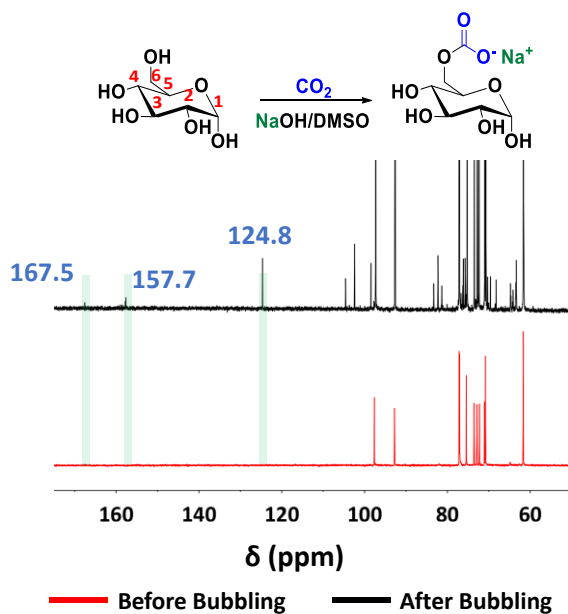
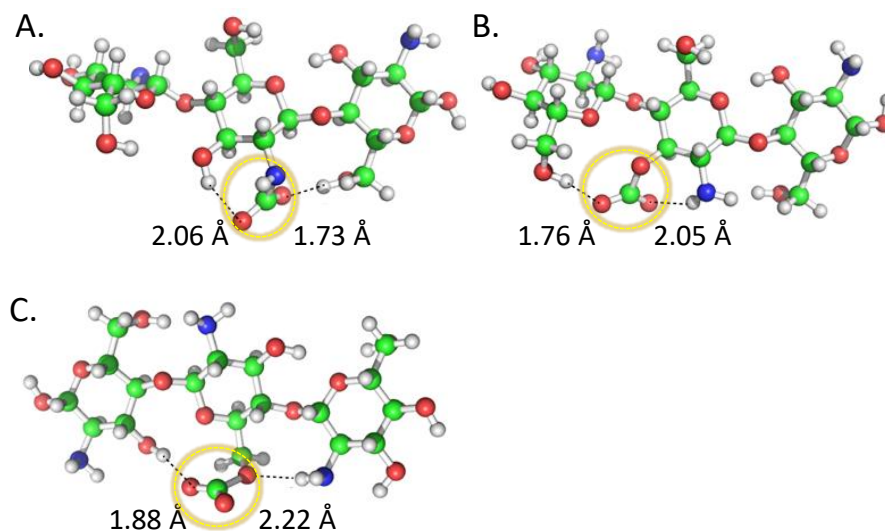


Figure S4. DFT optimized structures of hypothetically-formed single CO_2 species at the central glucosamine unit: **A.** Carbamate. **B.** Ionic organic alkylcarbonate at C-3. **C.** Ionic organic alkylcarbonate at C-6.



In an earlier report, we displayed that the interaction between a CO₂ molecule and the amino group using a glucoseamine trimer was more favorable compared to the interaction with the hydroxyl group at **C-6** by ~2 kcal mol⁻¹.³ In terms of stability, the obtained energy values (Table S2) showed that the formed ionic organic alkylcarbonate product is thermodynamically more favorable. For all cases, the optimized structures (Figure S4) indicated that the organic carbonate/carbamate anion is stabilized through hydrogen bonding with the adjacent hydroxyl and amino groups, in agreement with our previous finding for the carbonate formation in chitin-acetate/DMSO binary system.^{2,3} The calculated relative energy values for the three possible structures showed that the formation of organic carbonate at **C-6** is more favorable over **C-3** by ~ 3 kcal mol⁻¹, which support the reactivity of the alkoxide ions toward CO₂ as anticipated from the proton affinity data (*vide supra*).

Table S1. Relative stability (kcal mol⁻¹) of carbonate and carbamate at the central unit of the glucoseamine trimer. The more negative value, the higher stability.

	ΔE	ΔH	ΔG
Carbamate	0.00	0.00	0.00
Carbonate (C-3)	0.03	-0.82	0.09
Carbonate (C-6)	-3.93	-4.07	-2.97

References:

- 1 A. Hirai, H. Odani and A. Nakajima, *Polym. Bull.*, 1991, **26**, 87–94.
- 2 Z. M. dos Santos, A. L. P. F. Caroni, M. R. Pereira, D. R. da Silva and J. L. C. Fonseca, *Carbohydr. Res.*, 2009, **344**, 2591–2595.
- 3 A. F. Eftaiha, F. Alsoubani, K. I. Assaf, C. Troll, B. Rieger, A. H. Khaled and A. K. Qaroush, *Carbohydr. Polym.*, 2016, **152**, 163–169.